

**DEVELOPMENT OF
NEW ADAPTIVE MATERIALS
BASED ON
SPIROPYRAN MOLECULAR
PHOTOSWITCHES**

Silvia Scarmagnani M.Sc.

Thesis submitted for the Degree of Doctor of Philosophy

Supervisor: Professor Dermot Diamond

Dublin City University

20th January 2010



DECLARATION

I hereby certify that this material, which I now submit for assessment on the programme of study leading to the award of Doctor of Philosophy is entirely my own work, that I have exercised reasonable care to ensure that the work is original, and does not to the best of my knowledge breach any law of copyright, and has not been taken from the work of others save and to the extent that such work has been cited and acknowledged within the text of my work.

Signed: _____

Silvia Scarmagnani

ID No.: 56121997

Date: _____

ACKNOWLEDGEMENTS

First of all I want to thank prof. D. Diamond for giving me the chance to work for his group and for always encouraging and supporting me during my PhD.

I want to thank Zarah and Fernando for their friendship and for contributing with their knowledge and their experience to the realisation of my work and for sharing with me the best and the worst moments of this research project.

Thanks to Conor, Nameer, Emer, Alek, Robert, Martina, Simon, Mercedes, Tanja, Lourdes, Claudio, Michele, prof. B. Paull, Dr. M. Macka and all the people that within Clarity and the NCSR helped me, each one in its own way, during my three years in DCU.

Thanks to Prof. G. Wallace, Michael, Shannon and Lynn for their kindness and for taking care of me during my research visit to IPRI.

Thanks to Danilo, Dario, Francesco, Sinead, Pasquale and Leti for their friendship and their support during my three years in Dublin.

I want to thank my parents for their affection and for giving me the gift of life.

Thanks to Erica and Valentina for sharing with me joys, disappointments, adventures and discoveries, hurts and highs, every bright and dark moment of my life, always holding my hand for better or for worse.

Thanks to my grandparents, my aunties and uncles for the unreserved affection and sustain that they have always given to me.

I want to thank Giuseppe for loving me in every possible way, for being my partner and my best friend and for never stop believing in me, I love you baby.

Thanks to Marzia, Ayla, Gabriel and all my friends indeed for their affection and for helping me with their character and their personality to become what I am.

RINGRAZIAMENTI

Ringrazio inanzitutto il prof. D. Diamond per aver creduto in me, per avermi dato la possibilità di lavorare nel suo gruppo e avermi sempre incoraggiato e supportato durante il mio lavoro di dottorato.

Ringrazio Zarah e Fernando per la loro amicizia e per aver contribuito con le loro conoscenze e la loro esperienza alla realizzazione del mio progetto di tesi e aver condiviso con me i momenti migliori e peggiori di questo lavoro di ricerca.

Ringrazio Conor, Nameer, Emer, Alek, Robert, Martina, Simon, Mercedes, Tanja, Lourdes, Claudio, prof. B. Paull, Dr. M. Macka e tutti coloro che in Clarity e nell'NCSR mi hanno aiutato, ognuno a loro modo, durante i miei tre anni alla DCU.

Ringrazio il Prof. G. Wallace, Michael, Shannon e Lynn per il loro aiuto e per essersi presi cura di me durante la mia visita di lavoro all'IPRI.

Ringrazio Danilo, Dario, Francesco, Sinead, Pasquale e Leti per la loro amicizia e il loro supporto in questi ultimi tre anni dublinesi.

Ringrazio i miei genitori per il loro affetto e per avermi dato il dono della vita.

Ringrazio Erica e Valentina per aver condiviso con me le gioie, le delusioni, i giochi, le avventure, le scoperte, i pianti, le risate, ogni momento bello o brutto della mia vita, tenendomi sempre per mano nel bene e nel male.

Ringrazio i miei nonni, i miei zii, le mie zie per l'affetto incondizionato e il sostegno che mi hanno sempre dimostrato.

Ringrazio Giuseppe per volermi bene in ogni modo possibile, per essere il mio compagno e il mio migliore amico e per non aver mai smesso di credere in me, ti amo piccolo.

Ringrazio Marzia, Ayla, Gabriel e tutti i miei veri amici e amiche per il loro affetto, per avermi aiutato ciascuno con il proprio carattere e la propria personalità a diventare quello che sono e per essere essi stessi parte di me.

PUBLICATIONS

Peer-Reviewed Journal Articles

- 1. Photonic modulation of surface properties: a novel concept in chemical sensing.** Radu, A.; Scarmagnani, S.; Byrne, R.; Slater, C.; Lau, K. T.; Diamond, D., *Journal of Physics D: Applied Physics* **2007**, (23), 7238-7244.
- 2. Wireless Sensor Networks and Chemo-/Biosensing.** Diamond, D.; Coyle, S.; Scarmagnani, S.; Hayes, J., *Chem. Rev.* **2008**, 108, (2), 652-679.
- 3. Polystyrene Bead-Based System for Optical Sensing using Spiropyran Photoswitches.** Scarmagnani, S.; Walsh, Z.; Slater, C.; Alhashimy, N.; Paull, B.; Macka, M.; Diamond, D., *Journal of Materials Chemistry* **2008**, 18, 5063-5071.
- 4. Photoswitchable Stationary Phase based on Packed Spiropyran Functionalized Silica Microbeads.** Scarmagnani, S.; Walsh, Z.; Benito-Lopez, F.; Slater, C.; Macka, M.; Paull, B.; Diamond, D., *e-Journal of Surface Science and Nanotechnology* **2009**, 7, 649 - 652.
- 5. Spiropyran modified micro-fluidic chip channels as photonically controlled self-indicating system for metal ion accumulation and release.** Benito-Lopez, F.; Scarmagnani, S.; Walsh, Z.; Paull, B.; Macka, M.; Diamond, D., *Sensors and Actuators B: Chemical* **2009**, 140, (1), 295-303.
- 6. Spiropyran-based reversible, light-modulated sensing with reduced photofatigue.** Radu, A.; Byrne, R.; Alhashimy, N.; Fusaro, M.; Scarmagnani, S.; Diamond, D., *Journal of Photochemistry and Photobiology A: Chemistry* **2009**, 206, 109-115.

7. Delinquent Sensors & Schizophrenic Materials: Using Molecular Switches to Make Materials with multiple personalities. Byrne, R.; Scarmagnani, S.; Benito-Lopez, F.; Radu, A.; Diamond, D., *Irish Chemical News - Nanotechnology edition* **2009**, 21, (January), 26-28.

8. Structure-activity analysis of 2'-modified cinnamaldehyde analogues as potential anticancer agents. Gan, F. F.; Chua, Y. S.; Scarmagnani, S.; Palaniappan, P.; Franks, M.; Poobalasingam, T.; Bradshaw, T. D.; Westwell, A. D.; Hagen, T., *Biochemical and Biophysical Research Communications* **2009**, 387, (4), 741-747.

9. Photoreversible Ion-Binding using Spiropyran Modified Silica Microbeads. Scarmagnani, S.; Walsh, Z.; Paull, B.; Macka, M.; Diamond, D., *International Journal of Nanomanufacturing* **2010**, 5, 38-52.

10. Chemical Modification of Polyaniline Nanofibres: Towards Broadening Potential Applications. Lahiff, E.; Scarmagnani, S.; Schazmann, B.; Cafolla, A.; Diamond, D., *International Journal of Nanomanufacturing* **2010**, 5, 88-99.

CONFERENCE CONTRIBUTIONS

Conference proceedings

1. Beads-based system for optical sensing using spiropyran photoswitches. Scarmagnani, S.; Walsh, Z.; Alhashimy, N.; Radu, A.; Paull, B.; Macka, M.; Diamond, D., *IEEE Eng. Med. Biol. Soc.*, 23-26 August **2007**, Lyon (France), 4096-4097.

2. Photoswitchable Surfaces: A New Approach to Chemical Sensing. Radu, A.; Scarmagnani, S.; Byrne, R.; Slater, C.; Alhashimy, N.; Diamond, D., *SPIE Europe-Remote Sensing for Environmental Monitoring*, 17 - 20 September **2007**, Florence (Italy), pp. Z7491.

3. Schizophrenic Molecules and Materials with Multiple Personalities - How Materials Science could Revolutionise How we do Chemical Sensing. Diamond, D.; Byrne, R.; Benito-Lopez, F.; Scarmagnani, S.; Radu, A., *Spring MRS Meeting*, 13-17 April **2009**, San Francisco (USA), DOI: 10.1557/PROC-1190-NN08-01.

Oral Presentations

1. Beads-based system for optical sensing using spiropyran photoswitches. Scarmagnani, S.; Walsh, Z.; Alhashimy, N.; Radu, A.; Paull, B.; Macka, M.; Diamond, D., *IEEE Eng. Med. Biol. Soc.*, 23-26 August **2007**, Lyon (France).

2. Photoswitchable Stationary Phase based on Packed Spiropyran Functionalized Silica Microbeads. Scarmagnani, S.; Walsh, Z.; Benito-Lopez, F.; Slater, C.; Macka, M.; Paull, B.; Diamond, D., *International Symposium on Surface Science and Nanotechnology*, 9-13 November **2008**, Tokyo (Japan).

3. Incorporation of Photochromic Spiropyran Compounds and Spiropyran Modified Substrates into Flow Micro-systems. Scarmagnani, S.; Walsh, Z.; Benito-Lopez, F.; Abele, S.; Macka, M.; Paull, B.; Diamond, D., *Analytical Research Forum*, 12-15 July **2009**, University of Kent, Canterbury (UK).

4. Towards the development of adaptive nanostructured platforms. Scarmagnani, S.; Lahiff, E.; Wallace, G.; Diamond, D., *IUPAC*, 2-7 August **2009**, Glasgow, (Scotland).

5. Dye Based and Dye Functionalised Monolithic Materials for Chromatography and Electroosmotic Pumps. Walsh, Z.; Scarmagnani, S.; Norton, M.; Benito-Lopez, F.; Nie, F.-Q.; Abele, S.; Svec, F.; Diamond, D.; Paull, B.; Macka, M., *IICS 2009 - International Ion Chromatography Symposium*, 21-24 September **2009**, Malahide, Co. Dublin (Ireland).

6. Spiropyran modified PDMS micro-fluidic chip device for photonically controlled sensor array detection of metal ions. Benito-Lopez, F.; Scarmagnani, S.; Walsh, Z.; Paull, B.; Macka, M.; Diamond, D., *ICTBSB-2009 - International Conference on Trends in Bioanalytical Sciences and Biosensors*, 26-28 January **2009**, Dublin (Ireland).

Posters

1. Beads-Based System for Optical System using Spiropyran Phoswitches. Scarmagnani, S.; Walsh, Z.; Alhashmi, N.; Slater, C.; Lopez, F. B.; Paull, B.; Macka, M.; Diamond, D., *Pittcon 2008-59th Pittsburgh Conference on Analytical Chemistry and Applied Spectroscopy*, 2-7 March **2008**, New Orleans (USA).

2. Monolithic Photochromic Stationary Phases with Light Switchable Retention. Walsh, Z.; Scarmagnani, S.; Alhashimy, N.; Connolly, D.; Abele, S.; Paull, B.; Diamond, D.; Macka, M., *Analytical Research Forum*, 16-18 July **2007**, Glasgow (UK).

3. Elution by Light: Photochromic Monolithic Stationary Phases with Light Switchable Retention. Walsh, Z.; Scarmagnani, S.; Alhashimy, N.; Connolly, D.; Abele, S.; Paull, B.; Diamond, D.; Macka, M., *HPLC 2007*, 17-21 June **2007**, Ghent (Belgium).

4. Photochromic Monolithic Stationary Phases: Study of Covalent Linkage to the Underlying Monolithic Scaffold. Walsh, Z.; Scarmagnani, S.; Abele, S.; Moyna, Á.; Connolly, D.; Alhashimy, N.; Diamond, D.; Paull, B.; Macka, M., *Pittcon 2008-59th Pittsburgh Conference on Analytical Chemistry and Applied Spectroscopy*, 2-7 March **2008**, New Orleans (USA).

5. Spiropyran Modified Microfluidic Chip Channels for Photonically Controlled Sensor Array Detection of Metal Ions. Benito-Lopez, F.; Scarmagnani, S.; Walsh, Z.; Paull, B.; Macka, M.; Diamond, D., *CIMTEC'08, 3rd International Conference on Smart Materials, Structures and systems*, 9-13 June **2008**, Acireale, Sicily (Italy).

6. Spiropyran Modified Polyaniline Nanofibers. Scarmagnani, S.; Lahiff, E.; Diamond, D., *ACES Electroactive Materials Symposium*, 4-6 February **2009**, Wollongong (Australia).

7. Photo-Controlled Electroosmotic Pumps Based on Spiropyran Polymeric Monoliths for Micro-Fluidic Devices. Walsh, Z.; Scarmagnani, S.; Benito-Lopez, F.; Abele, S.; Diamond, D.; Paull, B.; Macka, M., *HPLC 2009*, 28 June - 2 July **2009**, Dresden (Germany).

8. Immobilisation and incorporation of photochromic spiropyran dyes in polymeric substrates for metal ion sensing and micro-fluidics. Scarmagnani, S.; Walsh, Z.; Benito-Lopez, F.; Macka, M.; Paull, B.; Diamond, D., *IICS 2009 - International Ion Chromatography Symposium*, 21-24 September **2009**, Malahide, Co. Dublin (Ireland).

ABSTRACT

Spiropyran is a family of photochromic compounds that can be reversibly switched between two states: a colourless, non-polar, uncharged spiro form (SP) and a highly coloured, polar, conjugated, zwitterionic merocyanine form (MC), i.e. $SP \rightarrow MC$ (UV light), $MC \rightarrow SP$ (green, white light). Furthermore, the MC form possesses a phenolate group that can reversibly bind metal ions and this ion binding is also photo-reversible, as when the MC-ion complex reverts to the passive SP form (upon green/white light exposure), it releases the bound ions. Using molecular-switches based on spiropyran-like molecules, new materials were produced whose properties such as metal-ion uptake/release and polarity can be controlled under external photonic stimulation.

Spiropyran derivatives were immobilised on polystyrene and silica microbeads and evaluated for their reversible photoswitchable metal ion binding behaviour. When in the MC form, in the presence of metal ions such as Cu^{2+} and Zn^{2+} , further spectral and colour changes occurred that were found to vary according to which metal ion was bound. Subsequent irradiation with white light caused reformation of the SP form and release of the metal ion. This process was shown to be repeatable at least several times. The spiropyran functionalised silica microbeads were packed into a capillary column and the new stationary phase demonstrated to form the basis of a photodynamic system for retention, detection and release of metal ions pumped into the capillary.

In parallel other spiropyran derivatives were incorporated into monolithic stationary phases. The spiropyran-functionalised polymer was switched between a protonated MC form and a neutral SP form upon white light irradiation. The monoliths were encased on a microfluidic chip and the system filled with an acid electrolyte. When a voltage was applied at the two ends of the encased monolith, electro-osmotic flow was generated and the flow rate shown to be variable upon white light exposure as a consequence of the formation of the SP form and the formation/disruption of the surface charge necessary for efficient electro-osmotic pumping.

In this thesis the synthesis and the characterisation of these new materials is described and the switchable optical properties evaluated.

LIST OF ABBREVIATIONS

ABS	Acrylonitrile butadiene styrene copolymer plastic
Acrylated SP	Acryl ester of (1',3',3' triimethyl-6-hydroxyspiro(2H-1)benzopyran-2, 2'-indole)
AFM	Atomic Force Microscopy
AIBN	2,2'-azobisisobutyronitrile
APTES	(3-Aminopropyl)triethoxysilane
BuMA	Butyl methacrylate
DAP	2,2-dimethoxy-2-phenylacetophenone
DCC	Dicyclohexylcarbodiimide
DMANF	2-methylamino7-nitrofluorene
DMAP	4-(Dimethylamino)pyridine
DMF	Dimethylformamide
DVB	Divinylbenzene
EDC	1-ethyl-3-(3-dimethylaminopropyl) carbodiimide hydrochloride
EDMA	Ethylene glycoldimethacrylate
EDTA	Ethylendiamine tetra-acetic acid
EOF	Electro-osmotic flow
EOP	Electro-osmotic pump
FNF	2-fluoro-7-nitrofluorene
FTIR	Fourier Transform Infrared spectroscopy
FTIR-ATR	Fourier Transform Infrared - Attenuated Total Reflectance spectroscopy
HOMO	Highest occupied molecular orbital
HPLC	High Performance Liquid Chromatography
IR	Infrared
ISBP	Indolinespirobenzopyran
ISNBP	Indolinespiro nitrobenzopyran
LED	Light-emitting diode
LCST	Lower critical solution temperature

LOAC	Lab-on-a-chip
LUMO	Lowest unoccupied molecular orbital
MC	Merocyanine form
MC-H ⁺	Protonated merocyanine form
MES	2-(N-morpholino)ethanesulfonic acid
MHA	(16-mercapto)hexadecanoic acid
NIPAAm	N-isopropyl acrylamide
NMR	Nuclear magnetic resonance
8-OMe ISBP	1',3'-dihydro-1',3',3'-trimethyl-8-methoxy [2H-1] benzopyran-2, 2'-(2H)-indoline
ODS	Octadecylsilane
PEEK	Poly ether ether ketone
PMMA	Polymethylmethacrylate
PS	Polystyrene
PSA	Pressure sensitive adhesive
PS(11)SP	Polystyrene microbeads spiropyran functionalised using a 4 carbons diamino linker (11 atoms distance between the spiropyran and the polystyrene bead surface)
PS(15)SP	Polystyrene microbeads spiropyran functionalised using an 8 carbons diamino linker (15 atoms distance between the spiropyran and the polystyrene bead surface)
PS(PA)SP	Polystyrene microbeads with physically adsorbed spiropyran
pSPNIPAAm	hydrogel copolymer of an acrylated SP and poly(N-isopropylacrylamide)
PTFE	Polytetrafluoroethylene
Q-factor	Quality-factor
RGB	Red Green and Blue scale
SAMs	Self-assembled monolayers
SEM	Scanning electron microscopy
Si	silica

Si(10)SP	Silica microbeads functionalized with aminogroups and subsequently with spiropyran (10 atoms distance between the spiropyran and the silica bead surface).
Si(16)SP	Carboxylated silica microbeads functionalised with 4 carbons amino linker and subsequently with spiropyran (16 atoms distance between the spiropyran and the silica bead surface)
Si(20)SP	Carboxylated silica microbeads functionalised with 8 carbons amino linker and subsequently with spiropyran (20 atoms distance between the spiropyran and the silica bead surface)
Si(PA)SP	Silica microbeads with physically adsorbed spiropyran
SP	Spiro form
SP-1	1',3'-dihydro-1',3',3'-trimethyl-6-nitrospiro [2H-1] benzopyran-2, 2'-(2H)-indoline
SPCOOH	1'-(3-carboxypropyl)-3',3'-dimethyl-6-nitrospiro[2H-1]-benzopyran-2,2'-indoline
μTAS	Micro-Total Analysis Systems
TESBN	4-(triethoxysilyl)-butyronitrile
UV	Ultraviolet
Vinyl SP	1'-(9-decenyl)-3',3'-trimethyl-6-nitrospiro [2H-1] benzopyran-2, 2'-(2H)-indoline
Vis	Visible

Table of Contents

CHAPTER 1: INTRODUCTION

1.1 Material science	2
1.2 Chemical sensors and biosensors	2
1.2.1 Controlling liquid movement in surfaces and on channels	4
1.2.2 Controlling binding processes at sensor surfaces.....	9
1.3 Chemichromism	12
1.4 Photochromism	13
1.5 Spirobenzopyrans	15
1.5.1 Structural conformation of spiropyrans and dynamics of the conversion to the merocyanine form.....	18
1.5.2 Synthesis of indolinespirobenzonitropyrans (ISBP)	32
1.5.3 Thermochromism	35
1.5.4 Solvatochromism.....	36
1.5.5 Photodegradation.....	37
1.5.6 Binding of Metal Ions	42
1.5.7 Protonation of the MC form	50
1.5.8 Other application of ISBP derivatives.....	52
1.6 Bead based systems	53
1.7 Monoliths	57
1.8 Microfluidics and lab on a chip devices	58
1.9 Conclusions	59
1.10 Thesis Overview	61
1.11 References	62

CHAPTER 2: PRELIMINARY STUDIES

2.1 Introduction	72
2.2 Solution Studies on SP-1	73
2.2.1 Experimental: Materials and instruments.....	73
2.2.2 Spectroscopic studies on response characteristics of MC-1 in different solvents.....	73
2.2.3 Spectroscopic studies on response characteristics of MC-1 ion complexes in ethanol solutions	74
2.3 Results and discussion	75
2.3.1 Response characteristics of MC-1 in different solvents.....	75
2.3.2 Response characteristics of MC-1 complexes with metal ions in ethanol solution	79
2.3.3 Response characteristics of MC-1 in the presence of H ⁺ in ethanol solution.....	92
2.4 Conclusion	97
2.5 Reflectance measurements using ocean optic spectrometer	98
2.5.1 Experimental: Materials and instruments.....	98
2.5.2 Monolith synthesis	99
2.5.3 Reflectance measurement set-up.....	101
2.5.4 Experimental procedure for diffuse reflectance measurements on vials	104
2.5.5 Experimental procedure for diffuse reflectance measurements on capillaries	105
2.6 Result and discussion	107
2.6.1 Diffuse reflectance measurements on vials.....	107
2.6.2 Diffuse reflectance measurements on capillaries	113
2.7 Conclusions	117
2.8 References	117

CHAPTER 3: POLYSTYRENE BEADS-BASED SYSTEM FOR OPTICAL SENSING USING SPIROPYRAN PHOTOSWITCHES

3.1 Introduction.....	124
3.2 Experimental: Materials and instruments.....	126
3.3 Synthesis and characterisation of spiropyran functionalised polystyrene microbeads.....	127
3.3.1 Covalent immobilisation of spiropyran on the surface of polystyrene microbeads using an eight and four carbon linkers.....	127
3.3.2 Physisorption of spiropyran on the surface of polystyrene Microbeads.....	128
3.3.3 Solvent compatibility evaluation and Scanning Electron Microscopy.....	129
3.3.4 Contact Angle Measurements.....	129
3.4 Optical properties of the spiropyran functionalised polystyrene microbeads.....	129
3.4.1 Reflectance measurements.....	129
3.4.2 Comparison of LEDs for SP \leftrightarrow MC switching.....	131
3.4.3 Evaluation of the spiropyran immobilisation strategies.....	132
3.4.4 Influence of solvents on MC \rightarrow SP kinetics.....	132
3.4.5 Photostability evaluation of the surface immobilised spiropyran.....	133
3.4.6 Evaluation of Ca ²⁺ , Cu ²⁺ , Co ²⁺ , Cd ²⁺ , Zn ²⁺ , Hg ²⁺ interactions with spiropyran functionalised microbeads.....	133
3.5 Results and discussion.....	134
3.5.1 Dispersion evaluation and SEM imaging in different solvents.....	134
3.5.2 Contact angle measurements on spiropyran functionalised polystyrene microbeads.....	137
3.5.3 Optical properties of spiropyran coated microbeads.....	139
3.5.4 Photostability.....	147
3.5.5 Ion-binding behaviour of spiropyran coated microbeads.....	149
3.6 Conclusions.....	156
3.7 References.....	157

CHAPTER 4: PHOTOREVERSIBLE ION-BINDING USING SPIROPYRAN

MODIFIED SILICA MICROBEADS

4.1 Introduction.....	162
4.2 Experimental: Materials and instruments.....	163
4.3 Synthesis and characterisation of spiropyran functionalised silica microbeads.....	164
4.3.1 Amino functionalisation of the silica microbead surface.....	164
4.3.2 Carboxyl functionalisation of the silica microbead surface	165
4.3.3 Covalent immobilization of spiropyran on amino functionalized silica microbeads	165
4.3.4 Covalent immobilization of spiropyran on carboxyl functionalised silica microbeads using 4 and 8 carbon linkers.....	166
4.3.5 Physisorption of spiropyran on silica microbeads.....	167
4.3.6 Elemental analysis.....	168
4.3.7 Contact angle measurements	168
4.3.8 Atomic force microscopy (AFM).....	168
4.3.9 Spiropyran glass slide functionalisation.....	170
4.4 Optical properties of the spiropyran functionalised polystyrene microbeads.....	171
4.4.1 Sample preparation for UV-vis spectroscopic analysis.....	171
4.4.2 Switching properties of the spiropyran functionalised microbeads ..	171
4.4.3 Evaluation of the spiropyran immobilisation strategies	172
4.4.4 Influence of solvents on MC→SP photo-induced kinetics	172
4.4.5 Photostability evaluation of the surface immobilised spiropyran	173
4.4.6 Evaluation of metal ion interactions with spiropyran functionalised microbeads	173
4.5 Results and discussion	174
4.5.1 Elemental Analysis.....	174
4.5.2 Contact angle measurements	177
4.5.3 AFM force curve measurements	180
4.5.4 Optical properties of spiropyran coated microbeads.....	187

4.5.5 Influence of solvents on MC→SP kinetics	195
4.5.6 Photostability evaluation of the surface immobilised spiropyran	202
4.5.7 Photoreversible ion-binding properties	204
4.6 Conclusions.....	210
4.7 References.....	212

CHAPTER 5: INCORPORATION OF PHOTOCROMIC SPIROPYRAN BEADS AND MONOLITHS INTO FLOW MICRO-SYSTEMS

5.1 Introduction.....	215
5.2 Incorporation of spiropyran functionalised silica beads in a flow system for Zn²⁺ detection	216
5.2.1 Experimental: Materials and instruments.....	216
5.2.2 Synthesis of monolithic frits and packing of microcolumn with Si(10)SP microbeads	217
5.2.3 Experimental set-up for continuous flow reflectance measurements on Si(10)SP beads packed capillary	219
5.3 Results and discussion	221
5.3.1 Rreflectance measurements on Si(10)SP beads packed capillary	221
5.3.2 Optical properties of the on Si(10)SP beads packed capillary	222
5.4 Incorporation of Spiropyran monolith on microchip for photo-controlled electro-osmotic flow (EOF)	229
5.4.1 Experimental: Materials and instruments.....	229
5.4.2 Synthesis of spiropyran acrylate monolith	230
5.4.3 Investigation of the photochromic behaviour in the presence of HCl.....	232
5.4.4 Microfluidic chip for electro-osmotic flow measurement.....	233
5.5 Results and discussion	234
5.5.1 Photochromic properties of spiropyran acrylate monolith	234
5.5.2 EOF evaluation.....	239

5.6 Conclusions.....	247
5.7 References.....	249

CHAPTER 6: CONCLUSIONS AND FUTURE WORK

6.1 Conclusions.....	252
6.2 Future work.....	255
6.3 References.....	260

CHAPTER 1

INTRODUCTION

1.1 Material science

Materials science is a very broad interdisciplinary field that spans many areas of scientific research, with recent exciting developments arising from our increasing ability to control the behaviour of bulk materials through manipulation at the molecular level.

The key to large-scale deployments of chem/bio-sensors lies in fundamental materials science. Radically new approaches to low-power transport of water across surfaces, through materials and along microchannels are needed, for example based on light or electrochemical mediated control of surface charge/polarity. In a similar manner, control of surface binding and release of molecular guest targets is another exciting prospect. Accordingly, there is a wonderful opportunity to link research in molecular materials with microsystems engineering, and developing new platforms capable of performing reliable chemo/bio-sensor measurements in scaled-up deployments that will have a major impact on individuals and society.

1.2 Chemical sensors and biosensors

Chemical sensors and biosensors are devices that provide information about binding events happening at the interface between a sensitive platform and a sample phase. The function of the sensitive platform is to ensure that the binding at this interface is as selective as possible and hence the platform usually contains entrapped or covalently bound sites (e.g. ligands, enzymes, antibodies) to impart the selectivity. The binding event is further coupled with a transduction mechanism of some kind; and in optical sensing, this usually involves a change in the colour or fluorescence of the sensing platform.

Clearly, these materials are 'active' in that they must interact with the sample, and binding processes must occur that lead to signal transduction for them to be of any analytical use. However, it is self-evident that these sensitive interfaces will change over time, for example due non-specific binding in real samples that can lead to surface poisoning, or leaching of active components into the sample phase. Consequently, the response characteristics of chemical sensors and biosensors tend to change over time, and there tends to be a gradual decrease in sensitivity, loss of selectivity and drifting of the baseline signal. These effects are well-known to those experienced in using these

devices, and in practice, they may be overcome by regular calibration, until the device deterioration reaches some limiting level.

Currently, there is very significant interest in the deployment of sensor networks, and many important applications require the involvement of chemical sensors and biosensors. However, for this to happen on a large scale, there needs to be a revolution in the way chemical sensors/biosensors are employed, as conventional calibration is inappropriate for large-scale deployments due to the cost of ownership (particularly maintenance) of these rather complex devices^{1,2}.

Chem/bio-sensing involves liquid handling using conventional technologies (pumps, valves, etc.) which are very energy intensive. Furthermore, chem/bio-sensing requires intimate binding events or reactions to occur either in solution (e.g. with reagent based systems) or at the surfaces of sensing devices. Thus chem/bio-sensors are prone to degradation, as they depend on active materials and surfaces that interact with the sample, and therefore they must be regularly calibrated to compensate for changes in their operating characteristics over time. While considerable advances have been achieved, for example, with the move towards microfluidics and lab-on-a-chip devices, the scale of the improvements required to meet the demands of pervasive sensing are such that a complete rethink of how we perform chem/bio-sensing is probably needed.

In this discussion, we consider the use of ‘adaptive’ materials (i.e. materials that can be switched reversibly between two or more different forms with radically different characteristics). This may open the way to the development of materials that can exist in a passive form (non-binding) until a measurement is required, at which point the material is switched to an ‘active’ form. Binding then occurs and a signal is generated, and the material subsequently switched back to the ‘passive’ form. We have demonstrated that binding of metal ions and amino acids at spiropyran modified surfaces can be controlled photonically using LEDs²⁻⁵. It is possible that this may provide a route to more sophisticated materials whose host-guest binding behaviour and signal generation can be activated or deactivated on demand. This effect has important potential applications in sensors, separation science and drug delivery.

1.2.1 Controlling liquid movement in surfaces and on channels

A fundamental issue with all chemo/bio-sensing platforms is how to control the movement of liquids in a way that is virtually energy free, so that functions like calibration can be incorporated. While considerable improvements can be obtained through downscaling analytical instruments using micro-fabrication approaches, for truly pervasive chemo/bio-sensing there is a need to go beyond downscaling of conventionally engineered devices like pumps and valves in order to reach a more widespread deployments of autonomous analytical instruments.

The ubiquitous presence of water in nature makes this study extremely relevant, yet despite the fact that many critical processes in nature, including sensing, occur at surface-aqua interfaces, the fundamental structure of water, and its behaviour at surface interfaces is still not fully understood⁶. Classically, materials are divided into two categories in terms of their degree of interaction with water: hydrophilic and hydrophobic⁷.

Surface tension can enable liquids to move spontaneously over surfaces without any application of external forces⁸. Wetting and adhesion properties between liquids and solids can be described by the measure of the contact angle between the two surfaces: the larger the wetting tendency is, the smaller the contact angle or the surface tension is. Surface tension changes, caused by the evaporation of the alcohol, are responsible for the formation of drops of wine on the surface of a glass⁹. This is generally known as the Marangoni effect¹⁰ and it describes the spontaneous movement of liquid from a low surface tension to a high surface tension environment. Unbalanced surface tension forces can drive liquid motion without any external intervention of any kind. It has been demonstrated that the speed of liquid flow driven by surface tension can be increased by a factor of hundreds or thousand times compared to the typical Marangoni effect by creating a radial surface tension gradient through the deposition of hydrophobic molecules in the centre of a hydrophilic surface and subsequently forming water droplets by condensing steam on the hydrophobic region¹¹. The drops driven by the gradient forces from one side and coalescence forces from the other side were found to move at speeds of up to 1.5 m/s. While the immediate applications of this effect are found in heat exchangers, it has an important role in clinical conditions such as in the treatment of

respiratory distress syndrome (RDS), in which the lungs of prematurely born infants are not sufficiently developed to produce enough surfactant to control liquid distribution and hence effective gas exchange is impaired¹². These phenomena demonstrate that it is possible to use purpose-designed chemistries to control water behaviour (including transport) across or even through surfaces. For example, by generating a spatial surface tension gradient on a surface the movement of a water droplet uphill without the assistance of any external energy has been demonstrated¹³. The gradient surface was created by diffusing decyltrichlorosilane vapour over a silicon wafer; the evaporation of the silane vapour created a gradient of concentration that decreased along the length of the surface. As a consequence, the edge of the wafer surface closest to the vapour source became hydrophobic, and the farthest hydrophilic. When a water droplet is placed on the obliquely positioned silicon wafer, with the hydrophobic part lower than the hydrophilic part, the droplet begins to move spontaneously ‘uphill’ towards the hydrophilic end. This arises because of unbalanced forces acting on the liquid-solid contact line on the two opposite sides of the drop, driving the droplet upwards against gravity towards the hydrophilic end.

Water repellence and in general material wettability are very important properties which depend on a material’s surface free energy and surface roughness. The control of these properties is important for many applications, such as variable focus liquid lens¹⁴ or self-cleaning surfaces¹⁵. Using an electrode, droplet movement can be achieved using direct electrical control of the surface tension^{16,17}. For example, it has been demonstrated that a droplet of a polarizable and conductive liquid can be moved when placed between two parallel plates, the upper consisting of a single continuous ground electrode and the bottom consisting of an array of independently controlled electrodes¹⁷. In another case, controlled droplet motion has been demonstrated on an open surface. A droplet placed on the surface between two dielectric coated coplanar electrodes starts to move towards the more positive electrode when a sufficient current voltage is applied. The greater positive polarity of one electrode relative to the other is responsible of the phenomenon, which is known as asymmetric electrowetting-on-dielectric oscillation (AEWOD). It is claimed that through this effect, unidirectional and oscillatory transport of a droplet on an electrode surface can be performed¹⁶.

Another exciting possibility is light-driven liquid movement on a photoresponsive surface¹⁸. In one example, azobenzene derivatives were switched between the cis- and trans-isomers using light, with corresponding changes from hydrophilic to hydrophobic surface characteristics. For a surface modified with an azobenzene derivative (o-carboxymethylated calixresorcinarene), switching was achieved using UV-irradiation to form the cis-azobenzene (hydrophilic) isomer, and blue-light to form the trans-azobenzene (hydrophobic) isomer¹⁹. When an olive oil droplet was placed on the surface, asymmetrical photoirradiation caused a gradient in the surface polarity that induced droplet motion, whose direction and velocity were found to be tunable by varying the light intensity (figure 1.1).

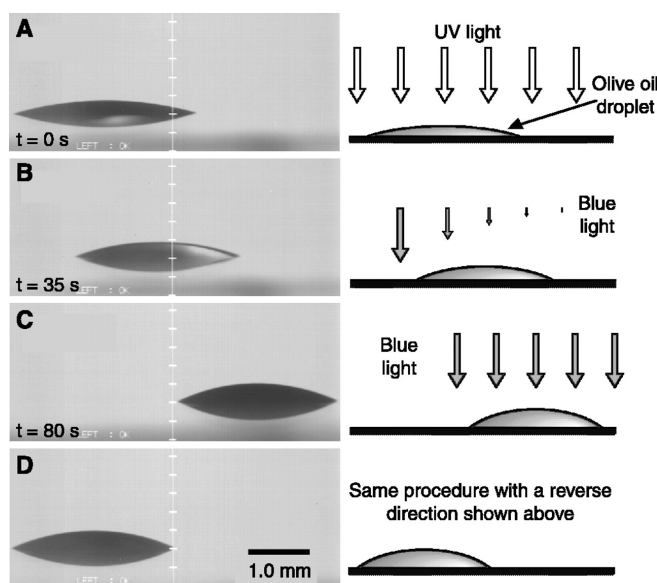


Figure 1.1: Photographs of light-driven motion of an olive oil droplet on a silica plate modified with an azobenzene derivative. The oil droplet moves because of a surface energy gradient generated by asymmetrical irradiation with 436-nm light perpendicular to the surface. (A to C) The sessile contact angles were changed from 18° (A) to 25° (C) confirming photonic modification of the surface polarity. (D) The direction of movement of the droplet could be controlled by varying the direction of the photoirradiation. Reproduced from *Science*, **2000**, 288, 1624-1626.

In the examples reported above, external control of the surface wettability by means of light or electrochemical potential provides a mechanism for controlling liquid transport

on surfaces at relatively high flow rates without the need for high voltages/currents and avoiding the use of conventional pumps, valves or channels. Hence changes in surface tension can provide a driving force to move liquids without the application of an external mechanical force. Another consequence of surface-tension is capillary movement. This depends on the diameter of the channel and on the contact angle between the liquid and the channel. The smaller the radius of the channel and the larger the contact angle, the more a liquid will be affected by capillary forces. When capillary forces become dominant, the flow regime is typically laminar, and the high ratio between area and volume makes the physical and chemical properties of the liquid-surface interface critical for determining the overall characteristics of the system.

Electro-osmotic flow (EOF) has drawn increasing attention in recent years in parallel with the development of micro total analytical system²⁰.

EOF, based on electro-osmosis, is the movement of uncharged liquid relative to a stationary charged surface due to an externally applied electric field (**figure 1.2**).

This type of fluid movement offer a wide range of advantages compared to commonly used pumping systems (such as peristaltic pumps), as it creates a constant pulse-free flows in which the magnitude and the direction of the flow are easy to control and it eliminates the necessity of moving parts.

In order to originate EOF a charged surface need to be generated. Most surfaces such as silica, spontaneously acquire charges when in contact with aqueous solutions, due to the presence of deprotonated silanol groups. The charged surface attracts counter ions and repels ion which has the same charge, creating an electric double layer. When an electric field is applied parallel to the surface, the ions are dragged in the direction of the electric field, causing the motion of the bulk fluid²⁰.

Examples of fabrication of EOF pumps are columns packed with microbeads²¹ and porous monolithic columns²² which are prepared by polymerising inside a capillary a mixture of a monomer, crosslinker, radical initiator and porogen*, to form a single piece of continuous porous polymer.

*Porogen = solvent which allows the formation of a polymeric monolith with a porous structure.

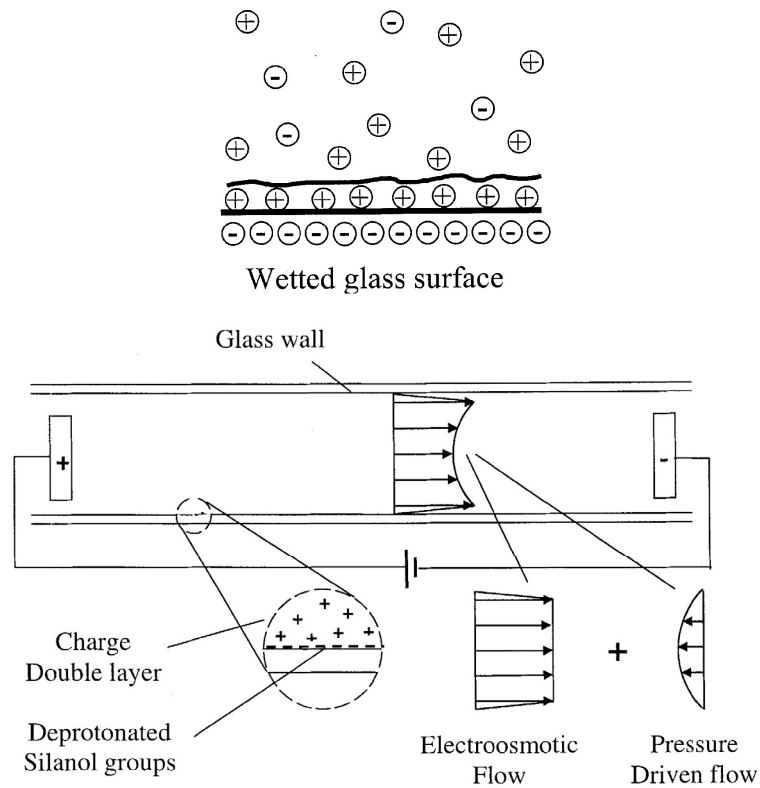


Figure 1.2: (Above) Schematic of the structure of the electric double layer: glass acquires a negative surface charge upon contact with an aqueous solution. The surface charge attracts dissolved counter-ions and repels co-ions, resulting in a charge separation. (Below) Basic flow principle of EOF pumps: In EOF flow, mobile ions in the diffuse counter-ion layer of the electric double layer are driven by an externally applied electrical field. These moving ions drag along bulk liquid through viscous force interaction. Reproduced from *Journal of Microelectromechanical Systems*, **2002**, 11, 672-683.

EOF pumps packed with silica particles can generate flow rate up to 1 μ l per minute and are suitable for applications which require a pressure higher than 10 atm. This kind of system offers a simple, cost-effective way to produce adequate pressure coupled with low flow rate and reduced back-pressure for capillary chromatography separations and micro-flow injection analysis²⁰.

The size, the flow-rates, the pumping pressure and the simplicity of material and fabrication of EOF pumps match extremely well into micro analysis system and are easily integrateable on lab-on-a-chip devices.

1.2.2 Controlling binding processes at sensor surfaces

For all chemo/bio-sensors, control of surface structure at the molecular scale is the ultimate goal, as this in turn determines all observable macroscale behaviour, such as chemo/bio-activity, selectivity, sensitivity, response time. In the past, materials science has focused on the generation of surfaces that had a particular function, for example, very passive, protective surfaces such as Teflon, or very active surfaces generated by the immobilisation of specific binding sites such as synthetic ligands, or bio-receptors such as enzymes or antibodies. More recently, the concept of ‘switchable’ or ‘adaptive’ surfaces has emerged, in which the surface typically can be switched between two or more modes that can have very distinctly different characteristics. Key to this developing area has been ways of immobilising functional molecules on sensor substrates. In the following section, we shall examine strategies for producing functionalised surfaces that can be electrochemically, optically or chemically switched between different modes of behaviour (e.g. passive or non-binding surface, and active or binding surface), using external chemical, electrochemical or photonic stimuli.

Control of binding behaviour can be effected through molecules whose conformational, electron distribution (polarity), charge, wetting properties and optical properties can be changed using light, electrostatic/magnetic field, electrochemical or chemical stimuli²³. For surfaces exhibiting such behaviour, it raises the intriguing possibility of having a material that can be maintained in a passive mode that is relatively unaffected by exposure to the sample environment over time and switched to the active mode only when a measurement is needed, and subsequently switched back to passive mode. In principle, this could open the way to new types of chemo/bio-sensors that can maintain their operating characteristics for much longer times, and hence reducing the need for complex calibration routines.

Electrochemical modulation of host-guest complexes at solid-liquid interfaces has been demonstrated using self-assembled monolayers (SAMs) based on pseudorotaxanes. Pseudorotaxanes are a class of supramolecular compounds composed of a molecular thread, encircled by a molecular bead, typically a macrocyclic cage, free to dissociate from the molecular thread^{24,25} (**figure 1.3**).

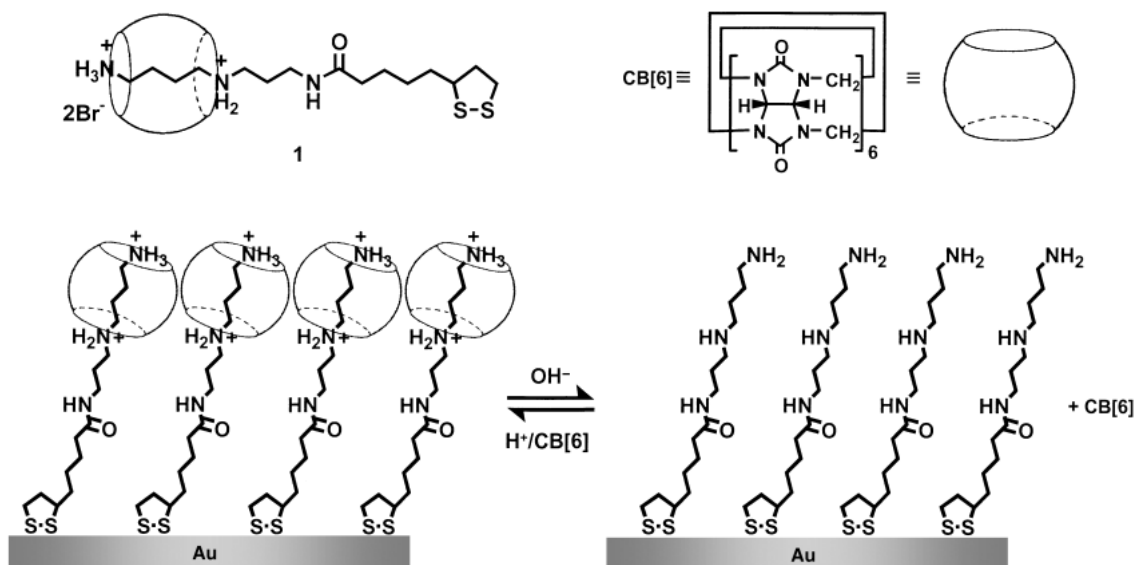


Figure 1.3: Self-assembled monolayer of pseudorotaxane on Au and dethreading and rethreading of the cucurbituril (CB(6)) macrocyclic cage on varying the pH. Reproduced from *Angew. Chem.*, **2003**, 115, 2395-2398.

pH dependent, reversible dethreading and rethreading of the ring has been demonstrated when the thread component of the pseudorotaxanes is anchored to a gold surface by means of a disulfide pentacycle at the end of the chain and the macrocyclic cage is a cucurbituril (CB(6)), a compound comprising six glycoluril units. Under acidic conditions, the macrocyclic cage can bind an appropriate guest to form the pseudorotaxane supramolecular compound, while under alkaline conditions, there is a dethreading of the macrocyclic guest and consequently a dissociation of the pseudorotaxane complex. On the surface of an electrode, depending on the pH, the SAM can block or allow accessibility of electroactive species such as iron hexacyanate (III)²⁵. Apparently, the pseudorotaxane-SAM layer acts as “ion gate”, and its conductance can be changed under pH control. It has also been demonstrated that the complexation properties of a pseudorotaxane functionalised self-assembled monolayer can be electrochemically controlled by adjusting the redox state of the guest species²⁴. In this system the guest is a stable tetrathiafulvalene anchored to a gold electrode and the hosts are electron-deficient and electron-rich macrocyclic compounds. Electrochemical reduction of the tetrathiafulvalene leads to the formation of a pseudorotaxane with the electron-deficient macrocyclic host, while oxidation of the tetrathiafulvalene in the

presence of the electron-rich macrocyclic host leads to the formation of a pseudorotaxane. Although reversibility is still an issue, this system offers the possibility of electrochemical or pH based control of interactions at the molecular scale. In a similar way, a reversible control of the surface properties can be performed with electrical switching. Electrical potential stimulation can be used to control the surface properties of SAMs based on ionisable alkanethiolate on a gold surface²⁶. This is achieved using low density ionizable SAMs (LD-SAM) of (16-mercapto)hexadecanoic acid (MHA) where on one side of the long alkane chain, the thiol groups anchor the molecule to a gold surface, while on the other side the carboxylic function provides an hydrophilic cap over the hydrophobic chain. Upon applying a positive potential, the negatively charged carboxylate groups bend towards the gold surface, exposing the hydrophobic chain of the MHA to the surrounding medium. Otherwise, by applying a negative potential, the negatively charged carboxylate groups undergo electronic repulsion towards the gold surface and the MHA adopts a straight conformation, exposing hydrophilic groups to the surrounding medium (**figure 1.4**). A simple conformation change induced by electronic potential therefore can induce significant changes in the overall surface binding properties.

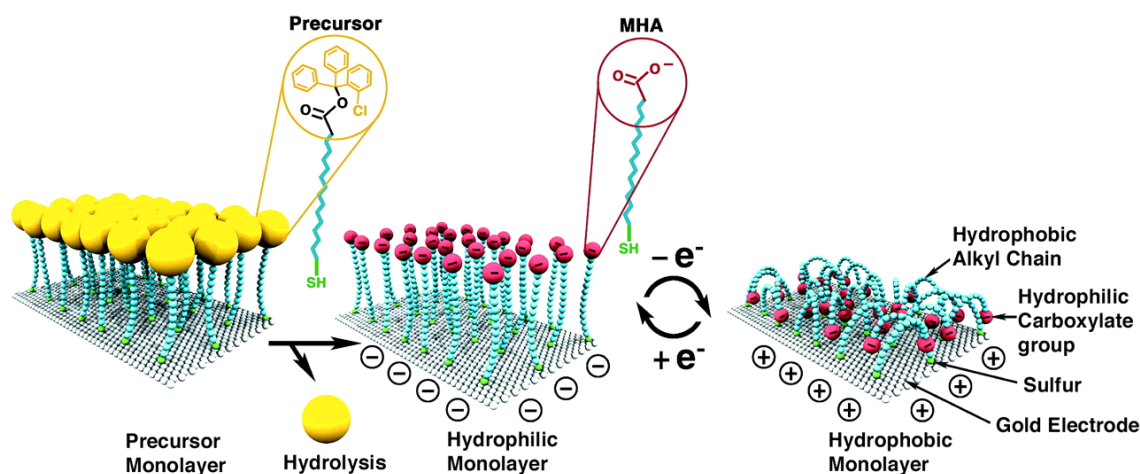


Figure 1.4: Representation of the wrapping–unwrapping step of the alkanethiolate with molecules that can provide a molecular event between to maintain the MHA chains at a certain distance and then the transition of the MHA chains between straight (hydrophilic) and bent (hydrophobic) molecular conformations. Reproduced from *Science*, **2003**, 299, 371-374.

In order to ensure that there is enough space for the MHA chains to bend and lift up, the assembling process of the SAM includes a wrapping–unwrapping step of the alkanethiolate with molecules that can provide a spacer function to maintain the MHA chains at a certain distance. The LD-SAM switchable surfaces have been demonstrated to control protein assembly of two kinds of fluorescent avidin with two different isoelectric points, one positive and one neutral. This could open the way to controlled protein adsorption-release in capillaries, channels or protein chips²⁷.

Light-driven processes accompanied by colour changes can also be used to induce reversible conformational transitions in molecules that can produce surfaces with switchable behaviour. Colour changes (chemichromism) represent an interesting property which can be exploited demonstrating that macroscopic effects are controlled by molecular scale physical and chemical modifications.

If the spectroscopic/molecular change can be externally controlled using light irradiation (photochromism), this represents an interesting means to control macroscopic effects by changes at the molecular level.

1.3 Chemichromism

Chemichromism is a term which refers to a general colour change which can be induced by an external stimulus, which can be chemical or physical²⁸. Many classes of compounds undergo colour changes due to heat, light, electrical current but also pH changes or the presence of metal ions.

The colour change phenomena can be classified according to the different causes which determine them. Some examples are: photochromism, thermochromism, electrochromism, solvatochromism, ionochromism and halochromism where the stimulus is respectively: light irradiation, heat, electrical current, solvent polarity, presence of ions and pH changes²⁹.

Colour changes provide an important signal that can be used to communicate information about the surrounding environment in a fast and effective way. Furthermore, when the colour variation is fully reversible, the possible applications widens significantly, especially in terms of sensors and biosensors.

Conventional chemical and biological sensors and biosensors depend on selective reactions at active surfaces which are directly exposed to the sample. Active surfaces generally tend to change over time and processes like fouling, decomposition or leaching significantly influence chemo/bio-sensor operating characteristics (sensitivity, selectivity and baseline) and consequently devices must be calibrated or in other words, the sensing surface should periodically be removed from the sample and re-characterised. Therefore, accurate in-situ chemical monitoring typically requires relatively complex instrumentation that incorporates pumps, fluidic manifolds, detectors, reagent reservoirs and highly skilled operators³⁰.

Ultimate the possibility of an adaptive material, whose sensing surface, after the sensing process has been performed, can be then restored exploiting the reversibility of the conversion at a molecular level, can lead to a completely different approach to chemical sensing. In principle these devices may be capable of addressing the so called “chemical sensing paradox” of combining the absolute requirement of an active surface to bind the target species, with passive behaviour that minimises changes in the surface binding characteristics over time, in order to reduce the need for calibration².

1.4 Photochromism

Photochromism is the reversible interconversion of a single chemical specie between two states with different absorption spectra when irradiated with light^{28,29,31}

The so-generated isomers differ not only in the absorption spectra but also in various physical and chemical properties such as refractive index, dielectric constant and geometrical structure.

Organic photochromic compounds are molecules of considerable interest as they are expected to offer routes to new functional materials that take advantage of polarity and geometrical changes induced by irradiation. Photochromic molecules can be used to produce platforms with switchable behaviour where light irradiation can be used to induce reversible conformational transitions³². The colour changes induced by photoirradiation leads to their use in various photoresponsive devices such as light sensitive eyewear³³, optical memory³⁴, molecular devices³⁵ and optical sensing applications, such as transport of metal ions³⁶ and metal detection³⁷⁻³⁹.

Well known families of photochromic include the spirobenzopyrans, spiro-naphthooxazine, naphthopyran, diarylethenes and furylfulgides⁴⁰ (**figure 1.5**). They all undergo reversible photochromic behaviour: one isomer can be transformed to the other which then reverts back to the initial form in the dark (thermodynamically) or under a different light irradiation.

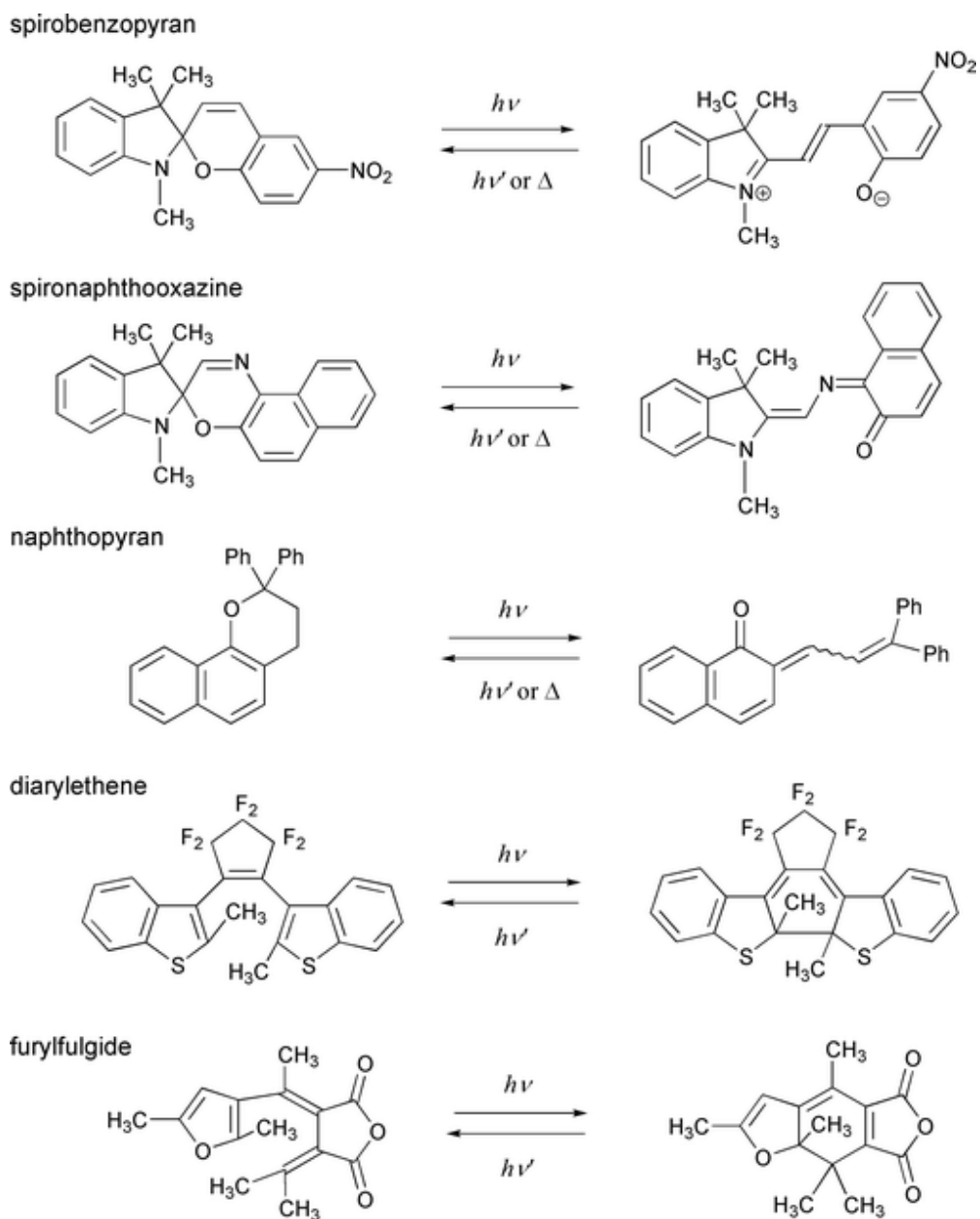


Figure 1.5: Different families of photochromic compounds. Reproduced from *Annual Reports Section "C" (Physical Chemistry) 2003*, 99, 277-313.

There has been an increasing interest in organic photochromic compounds as they represent bistable molecular systems, that exist in two stable molecular forms which can be converted from one to another with a wide range of potential applications in electronic, photonics and computing⁴¹. Molecular sized switches, incorporated into a nanoscaled logic circuit are able to detect events and transmit signals in response to environmental stimulation⁴².

Among the different families of photochromic compounds, spirobenzopyrans are probably the most widely studied⁴¹ due to their high photosensitivity, very clear colour change and rapid switching kinetics between the two isomers, one of which has a guest binding site for certain metal ions⁴³. When the photochromic behaviour is combined with the possibility of switchable guest binding, in principle the binding behaviour can be switched “on” and “off” using external light irradiation. In the “off” state, binding sites are passivated hence the active surface is deactivated whereas in the ‘on’ state, the surface binding sites are activated and available. The use of this family of compounds could form the basis of new approaches to photoswitchable uptake and release of molecular guests or photocontrolled separations.

This new concept for chemical sensing is based on the following principles:

- The sensor surface should be in an inactive or passive state when a measurement is not being conducted;
- The surface is converted into an active state under an external light stimulus;
- The active surface binds with the target species and generates a signal that enables the analytical measurement to be made;
- After the measurement is completed, the target species is expelled by an external light stimulus and the surface returns to its inactive form.

1.5 Spirobenzopyrans

The photochromic properties of spirobenzopyrans were first discovered by Fischer and Hirshberg in 1952⁴⁴ where they observed that irradiation of several solutions of spirobenzopyrans with UV-light (not exceeding 450nm) were producing colour modifications that could be reversed by exposing the same solutions to yellow light (containing no radiation below 500 nm).

Spirobenzopyrans refer in general to (substituted) *2H-1-benzopyrans* having a second ring system, usually (but not necessarily) heterocyclic, attached to the 2-carbon atom of the pyran in a spiro manner with a common tetrahedral carbon atom⁴⁵. The two halves of the molecule are in two orthogonal planes (**figure 1.6**).

The benzopyran part is the common structure to all spiropyrans, except for different substitutions on the aromatic ring, while the heterocyclic part is variable and often is built upon mono or bi-heteroatomic azaheterocycles saturated or benzofused³¹.

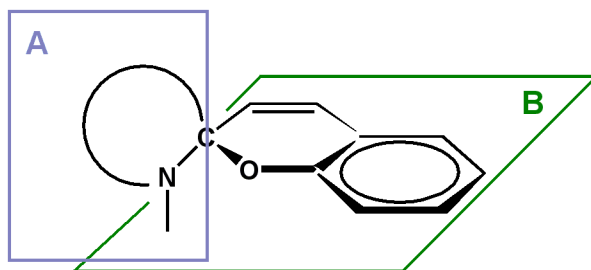


Figure 1.6: Schematic representation of the structure of spirobenzopyrans, showing the two orthogonal planes formed by the two halves of the molecule: the heterocyclic (A) and the benzopyran (B).

Spirobenzopyrans photochromism can only be observed in solutions, not in solid state.

Spiropyran exist in a closed, unpolar, orthogonal and colourless “spiro” form (SP) (leuco dye) which is converted by exposure to ultraviolet (UV) light to an open, planar, conjugated, highly coloured “merocyanine” form (MC).

Upon irradiation, the C-O spiro bond in the SP form is cleaved heterolytically and the "spiro" carbon which was sp^3 -hybridized achieves sp^2 hybridization and becomes planar (**figure 1.7**). The aromatic group rotates, aligns its π -orbitals with the rest of the molecule, and it forms the conjugated system of the merocyanine form, with ability to absorb photons of visible radiation, and therefore are strongly coloured.

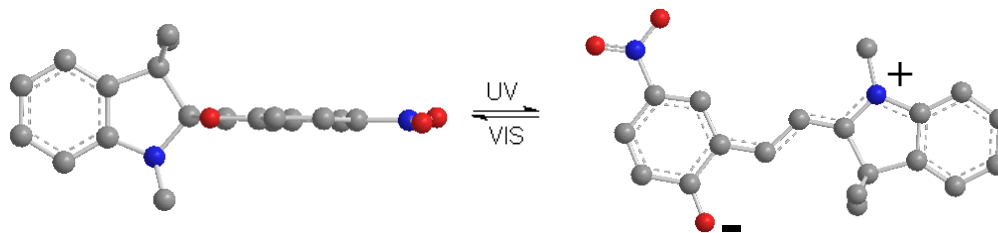


Figure 1.7: Indolinespiro nitro-benzopyran (ISNBP) conversion of the SP (left) to the MC form (right), by exposure to UV light and the reversible switching from the MC to the SP form, by exposure to visible light or thermodynamically.

When the UV source is removed, the molecules thermodynamically relax to their ground state, the carbon-oxygen bond reforms, the spiro carbon atom becomes sp^3 hybridised again, and the molecule returns to its colourless state.

In solution the SP form presents an absorption spectrum in the UV range (200-400nm) with an actinic band situated between 320-380 nm. The absorption around this band causes conversion to the MC form, in which the conjugation between the two halves of the molecule results in a shift the absorption band from the UV to the visible region of the spectrum³¹.

Generally spirobenzopyrans undergo “positive” photochromism, as the thermodynamically less stable state is the more deeply coloured. Upon UV irradiation the solution acquires a strong coloration which then fades thermally back to the original colourless SP state. A few spirobenzopyrans, especially those bearing free hydroxyl, carboxyl and amine groups, exhibit so called “negative” photochromism as their solutions appear moderately coloured in the dark and reversibly fade under UV light irradiation.

Besides photochromism, many benzospiropyrans also exhibit thermochromism, and their solutions become coloured when heated. In general the photochromic property of spirobenzopyrans depends on the structure of the derivative, the solvent and the temperature.

In this work we will focus our attention on indolinespirobenzopyran (ISBP), where the spiro carbon atom links together a benzoindoline and a benzopyran part, as this family of compounds is the basis for the development of our new adaptive materials.

1.5.1 Structural conformation of spiropyrans and dynamics of the conversion to the merocyanine form

As mentioned above, spiropyrans have two perpendicular π electron systems linked through a spiro tetrahedral carbon atom. Molecules having such a structural feature can be subjected to spiroconjugation; i.e. there could be an overlap between the π orbitals accompanied by electronic delocalization which leads to the appearance of a characteristic band in the visible region of the spectrum, due to intermolecular charge transfer between the two halves of the molecule⁴⁶.

Spiroconjugation is verified when the two halves of the spirocompound, linked by the spiro atom, consist of an electron-donor and electron-acceptor part, whose frontier orbitals (the LUMO of the acceptor and the HOMO of the donor) are antisymmetric with respect to the two planes generated by the two halves of the molecule separated by the spiro carbon (**figure 1.8**).

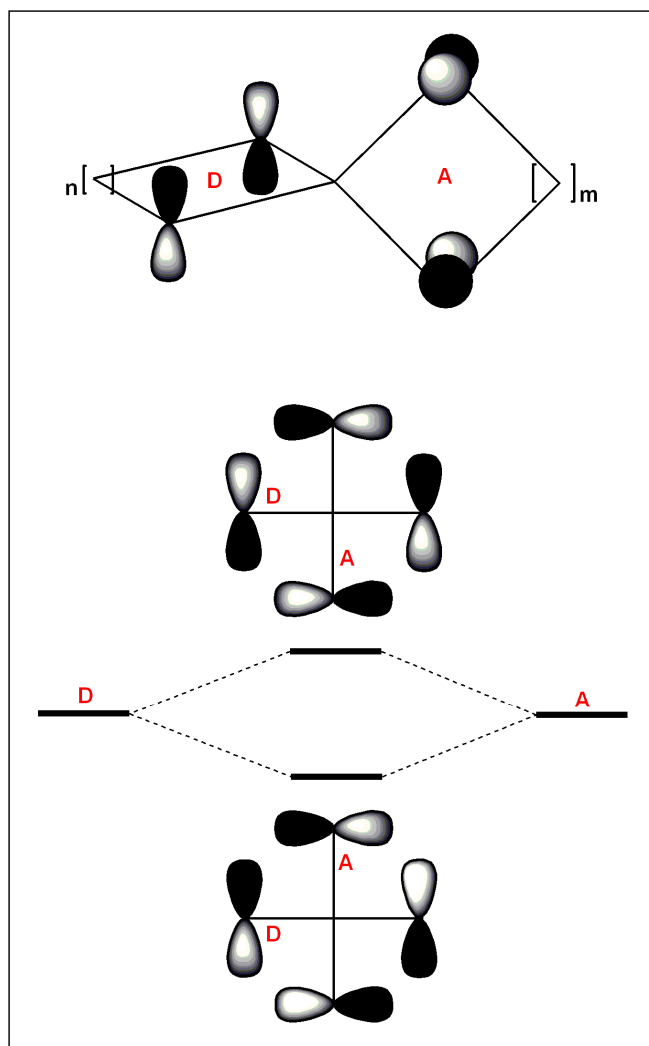


Figure 1.8: Scheme representing the π orbitals of two allyl systems connected through a tetrahedral spiro carbon center. In this spiroconjugated system D is the donor part (substituted diamines) and A is the acceptor part (indandione moiety).

Below the symmetry of the π orbitals of the HOMO and the LUMO are represented for both A and D. Spiroconjugation is verified when the symmetry of the HOMO and the LUMO is asymmetric versus both molecular planes.

This symmetry leads to a non-zero overlap which is required for intramolecular interactions⁴⁷ and the electronic transition between these two orbitals correspond to a charge transfer transition⁴⁷.

Maslak et al. have studied a series of spiroconjugated compounds which differ in the structure of the π systems of the two halves of the molecule connected through the common insulating tetrahedral carbon^{47,48}.

They named one half “the donor” (substituted diamines, **D**) and the other “the acceptor”, (indandione moieties, **A**) and they synthesized a series of spirocompounds formed by combinations of different diamines and indandione units in order to study the influence of the molecular structure of the two π arrangements in the spiroconjugation effect.

The donor and the acceptor part have been chosen on the basis of the determination of the energy and the symmetry of their orbitals using MOPAC calculations.

Only acceptor with an antisymmetric LUMO and donors with antisymmetric HOMO will generate interactions which will give rise to new spiroconjugated orbitals spanning the entire spiromolecule. The new lower energy orbital (the new HOMO) corresponds to the bonding combination between the two halves and the higher energy one (the new LUMO) correspond to the antibonding combination.

They have demonstrated that spiroconjugation occurs most readily when the symmetry of the LUMO of the acceptor and the one of the HOMO of the donor are antisymmetric versus both molecular planes of the spiro orthogonal structure. When this condition is satisfied, the HOMO energy is lowered compared to isolated donor part and the LUMO energy is increased compared to the isolated acceptor. Orbital overlap then occurs and new bands in the visible region of the absorption spectra appear, while when considering the two isolated molecules that correspond to the two halves of the spiro-compound they don't show any appreciable band above 370 nm.

The intramolecular nature of the charge transfer is confirmed by the fact that the new bands in the visible region follows the Lambert-Beer law and that the λ_{max} value and the extinction coefficient remain constant over dilution.

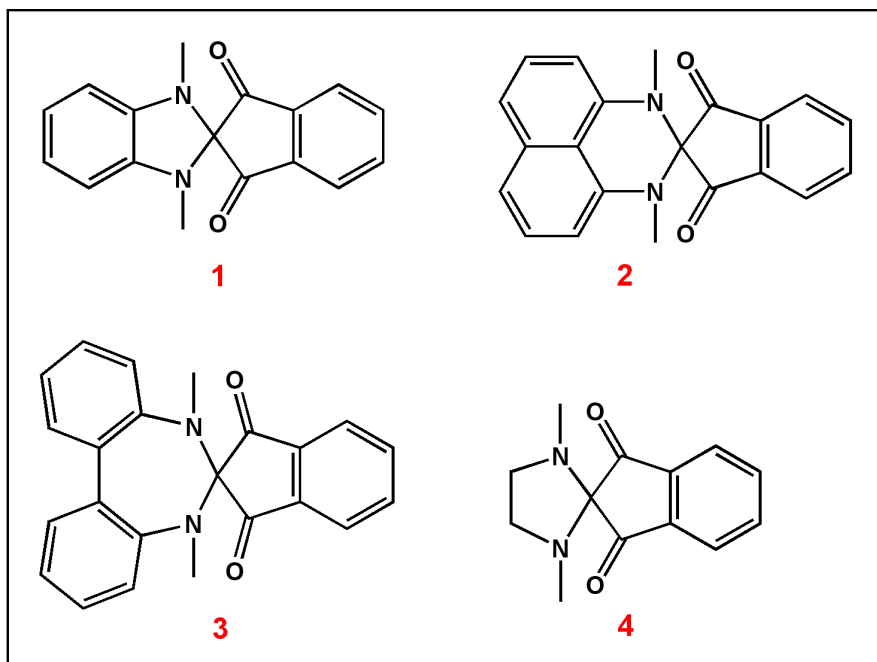


Figure 1.9: Structures of four spirocompounds synthesized by Maslak and al. with different interactions between the donor (1,3-indandione) and acceptor moiety (different *N,N*-dimethyl amines).

The spirocompounds synthesized by Maslak and al.⁴⁸ are composed by a 1,3-indandione moiety as a acceptor (kept constant) in which the π -system has an antisymmetric LUMO, and different aromatic and non-aromatic *N,N*-dimethyl amines as donor (**figure 1.9**). The so generated compounds present a new absorption band in the visible region, although the presence and the entity the charge transfer phenomenon due to spiroconjugation varies, depending on the symmetry of the orbital of the donor and acceptor part.

In **1**, the *N,N*-dimethyl-1,2-phenylenediamine donor present a symmetrical HOMO. The interaction between the two halves of the molecule is very weak, as the transition HOMO-LUMO is forbidden by geometrical reasons and its extinction coefficient is very low (**figure 1.10**).

On the contrary the 1,8-bis (methylamino) naphthalene donor of **2** present an antisymmetric HOMO which strongly conjugate with the antisymmetric LUMO of the indandione acceptor. As a result charge transfer is highly favored and the compounds present the highest extinction coefficient among the others.

In **3**, the dimethyl-2,2'-diaminobiphenyl donor, present the correct symmetry, with an antisymmetric HOMO, which is though lower in energy when compared to the donor in **2** as the seven-membered ring may not allow the perfect overlap between the HOMO and the LUMO orbitals. Thus, spiroconjugation is weaker.

Similarly the HOMO of the donor in **4** presents the correct symmetry to conjugate with the LUMO of the acceptor, but the energy gap between the two orbitals is the largest among the other compounds and the spiroconjugation as well as the extinction coefficient is even weaker than **3** (**figure 1.10**).

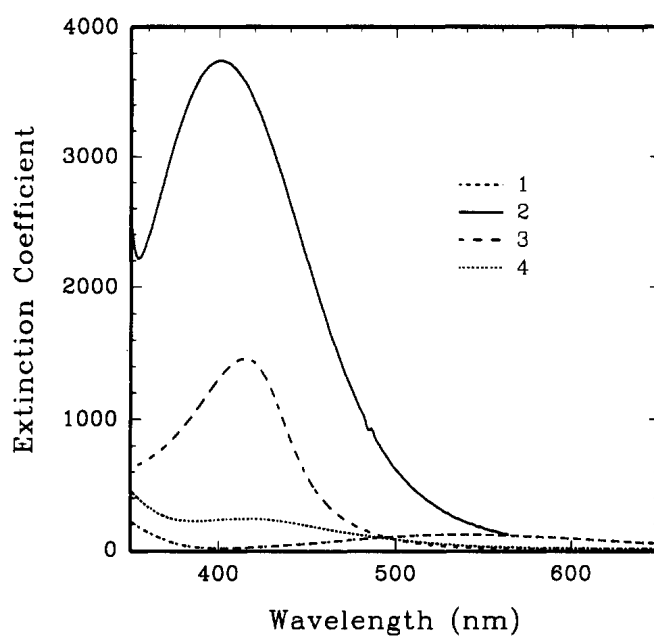


Figure 1.10: Extinction coefficients (in $M^{-1} cm^{-1}$) of the charge-transfer bands of **1-4** in acetonitrile. Only the visible part of the spectrum is shown. The indandione and the diamines alone or in mixtures do not have any detectable transitions in this spectral region. Reproduced from *Journal of the American Chemical Society* **1993**, 115, 9331-9332.

These experiments demonstrate how in spirocompounds the charge transfer phenomenon depends both on the symmetry of the orbitals and on the strength of the donor and the acceptor.

For the specific purpose of this discussion, attention will be focused on a particular class of spiropyrans: indolinespirobenzopyran (ISBP) (**figure 1.11**).

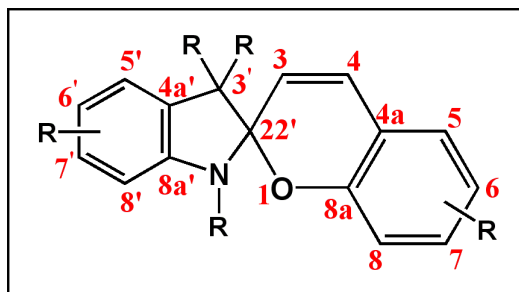


Figure 1.11: Schematic representation of indolinespirobenzopyran moiety.

In the case of the ISBP family of compounds the LUMO of the 2H-pyran fragment is antisymmetric whereas the HOMO of the indoline part is symmetric⁴¹ (**figure1.12**). This combination does not meet the requirement for spiroconjugation and the two orthogonal π systems do not allow interaction between the two halves of the spiro molecule. Thus, the absorption spectra of the closed spiro form is the sum of the spectra of the individual fragments, with absorption band between in the UV region and no band in the visible region⁴⁹.

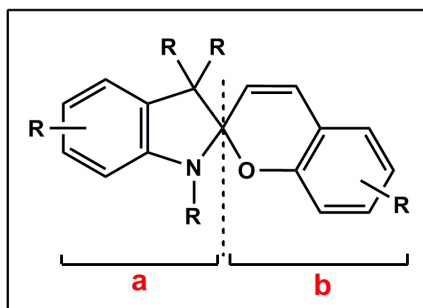


Figure 1.12: Schematic representation of the spirobenzopyran indoline moiety. The structure of the molecule consists in indoline part (**a**) attached in a spiro manner through an insulating tetrahedral carbon to a 2H-benzopyran ring (**b**).

Upon UV-irradiation of the ring-closed spiro form, the C-O bond breaks causing molecular unfolding and the previously isolated π electrons become extensively conjugated in the MC form and a strong absorption band appears in the visible region of the spectrum, between 500-600 nm⁵⁰.

In the case of the indoline spirobenzopyran family, important stereoelectronic effects, rather than spiroconjugation (which is not allowed due to incompatibility of the HOMO-LUMO symmetry) dominates their behaviour.

In general, the photochemical activity of spiropyrans depends on: the polarity of the $C_{\text{spiro}}\text{-O}$ bond, the charge distribution on the benzopyran ring (in particular the presence of electronegative group on the benzene ring) and the degree of interactions between the indoline and the benzopyran sections.

Ground state interactions between the two halves of the spiropyran molecule around the spiro carbon occur as a consequence of stereo electronic phenomena arising from negative hyperconjugation and the anomeric effect.

Negative hyperconjugation is the effect of donation of electron density from filled n_{π} orbitals (non-bonding orbitals) containing a lone pair electron to a σ bond or σ^* antibonding orbital, resulting in building a π character into bonds that nominally possesses only σ character⁵¹.

The anomeric effect was initially used to explain the tendency of the heteroatomic substituents to prefer an axial instead of the equatorial orientation in a cyclohexane ring. Generally speaking this conformational phenomenon occurs in a system wherein a carbon is linked to an heteroatom with a lone electronic pair on one side, and to an electronegative atom on the other.

In spiropyran, the spiro carbon is covalently joined to the indoline nitrogen and to the benzopyran oxygen. The nitrogen orbitals have a pyramidal structure with the lone electron pairs perpendicular to the plane formed by C_{8a} and C_{spiro} (C_{22} , **figure 1.11**), with the plane formed by $\text{N-C}_{\text{spiro}}\text{-C}_3$, forming a dihedral angle around 23-30°. This structure reduces the conjugation between the lone pair electron of the N and the π system of the benzene ring⁵².

On the other side, the electron density of the lone pair electron on the oxygen occupies a *trans* position relative to that of the unshared electron pair of the nitrogen. This conformation causes specific interactions between the lone pair electron orbital on the nitrogen (n_{N}) and the antibonding orbital between the C_{spiro} and the electronegative oxygen atom ($\sigma^*_{\text{C-O}}$), and defines the anomeric effect.

Considering that the electronegativity of the oxygen is greater than that of the nitrogen, the energy level of the electron pair in the n_{O} is lower than the one in the n_{N} and the antibonding orbital $\sigma^*_{\text{C-O}}$ is lower in energy than the $\sigma^*_{\text{C-N}}$.

As a result, interaction between the n_N electrons and the σ^*_{C-O} occurs, leading to a strengthening of the $C_{\text{spiro}}-N$ bond and a weakening of the $C_{\text{spiro}}-O$ bond⁵² (**figure 1.13**). Studies on the length of these bonds shows that the $C_{\text{spiro}}-N$ bond is in the range of 1.432-1.453 Å, shorter than the normal length of a general $C_{\text{sp}^3}-N_{\text{sp}^3}$ bond (1.47-1.48 Å), while the $C_{\text{spiro}}-O$ bond is remarkably longer than usual, being in the range of 1.452-1.497 Å, instead of 1.41-1.43 Å.

This variation in the $C_{\text{spiro}}-O$ bond length is critical in determining the overall photobehaviour of the molecule, as it has been found that under continuous irradiation of their solutions, all spiropyrans with $C_{\text{spiro}}-O$ bond length longer than 1.42 Å undergo photochromism, while spiropyrans with $C_{\text{spiro}}-O$ bond shorter than 1.42 Å do not⁴¹.

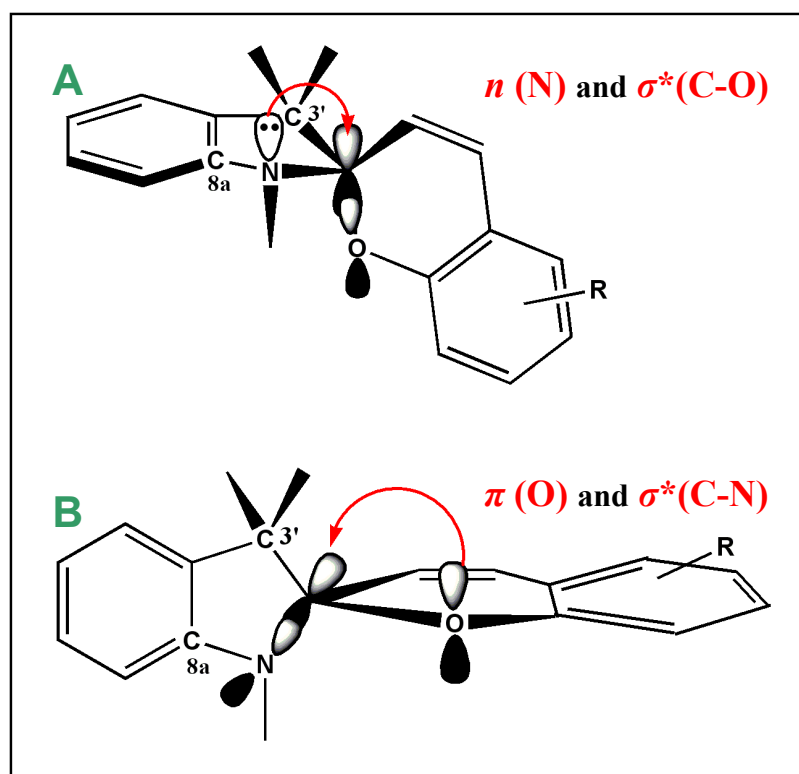


Figure 1.13: Scheme representing the two spatial interactions which may occur between the lone pair electrons on the nitrogen and oxygen and the σ^* antibonding between the C_{spiro} and the two heteroatoms. As the electronegativity of the oxygen is greater than one of the nitrogen, the energy of the unshared electron pair in the n_N is greater than the one in the n_O and the energy level of the σ^*_{C-O} is lower than the σ^*_{C-N} . For these reasons, the interaction between the n_N electrons and the σ^*_{C-O} (**A**) is favoured compared to the lone pair n_O electrons interactions with the σ^*_{C-N} (**B**), determining a weakening of the the $C_{\text{spiro}}-O$ bond and a strengthening of the $C_{\text{spiro}}-N$ bond.

Photoexcitation of the molecule induced by UV light irradiation causes the cleavage of the already weakened and elongated C_{spiro}-O bond.

The presence of electronegative substituents on the benzene ring linked to the pyran cycle further increase the photochromic properties of the spiropyran molecule.

For example, the presence of electron accepting substituents on the benzopyran ring, such as nitro groups (NO₂) leads to an increase in delocalisation due to charge transfer from the lone pair electrons of the O to the π system of the benzene ring, thus further weakening the C_{spiro}-bond. The stabilisation effect of the MC form is also verified once the C_{spiro}-O bond has been cleaved by vibrational excitation as the electronegative nitro group enhances delocalisation by resonance of the negative charge on the oxygen, when cleavage occurs^{31,52,53}.

The position of the NO₂ on the benzene attached to the pyran ring is crucial for the stabilisation of the open MC form. Only *para* and *ortho* nitro substituted benzene rings show this stabilisation effect of the MC form due to mesomeric effect.

The cleavage of the C_{spiro}-O due to photoexcitation leads to the formation of an opening excited state in a time scale of femtoseconds while a small fraction re-forms the broken C_{spiro}-O bond (also in the femtoseconds time scale), its major fraction vibrationally relaxes with a time constant of picoseconds (depending on the medium), undergoing subsequent isomerisation which leads to the formation of the coloured isomer, a conjugated MC form, which strongly absorbs in the visible region due to delocalization of the π -electronic system⁵⁴. These transient isomers can be represented as different resonance forms of a twisted cisoid (which appears just after the C_{spiro}-O bond breaks) and planar transoid stereoisomers, which are more stable, as it minimize the non-bonding interactions³¹ (**figure 1.14**).

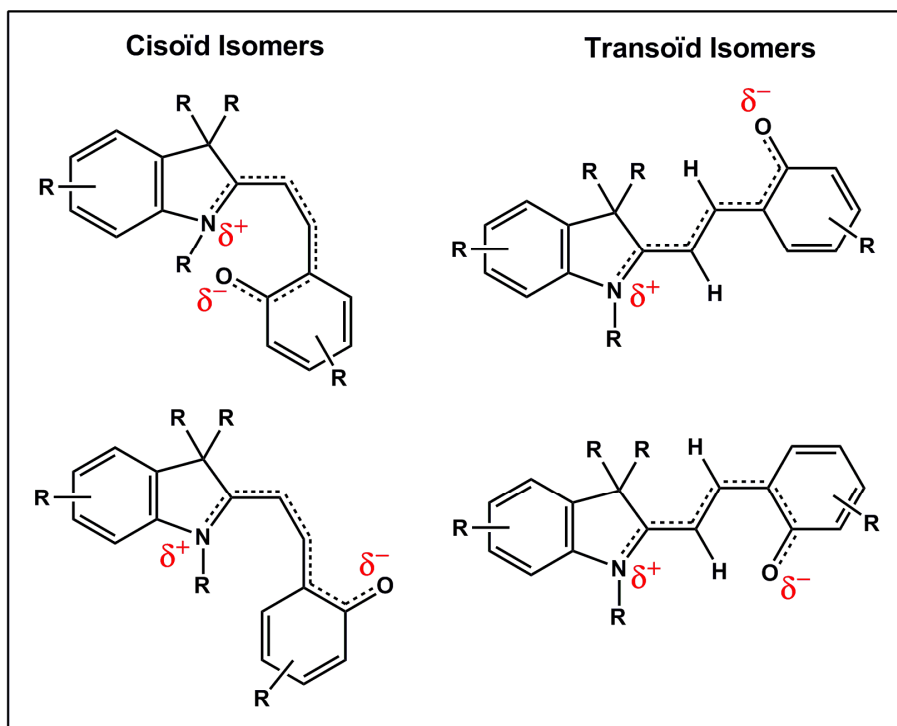


Figure 1.14: Examples of possible cisoid and transoid isomers of the ISBP MC form.

As the structure of the transoid stereoisomers is similar to the one of the Brooker's merocyanine dye⁵⁵, the ring-open form of indolinespirobenzopyrans has been named after it.

Brooker's merocyanine dye exists in two forms, a covalent quinone form and a zwitterionic form, and the equilibrium between these two isomeric forms depends on the surrounding environment. In a similar way, the spiropyran photomerocyanine in the more stable transoid isomers can be described as a resonance hybrid between a quinonic and a dipolar zwitterionic form (**figure 1.15**).

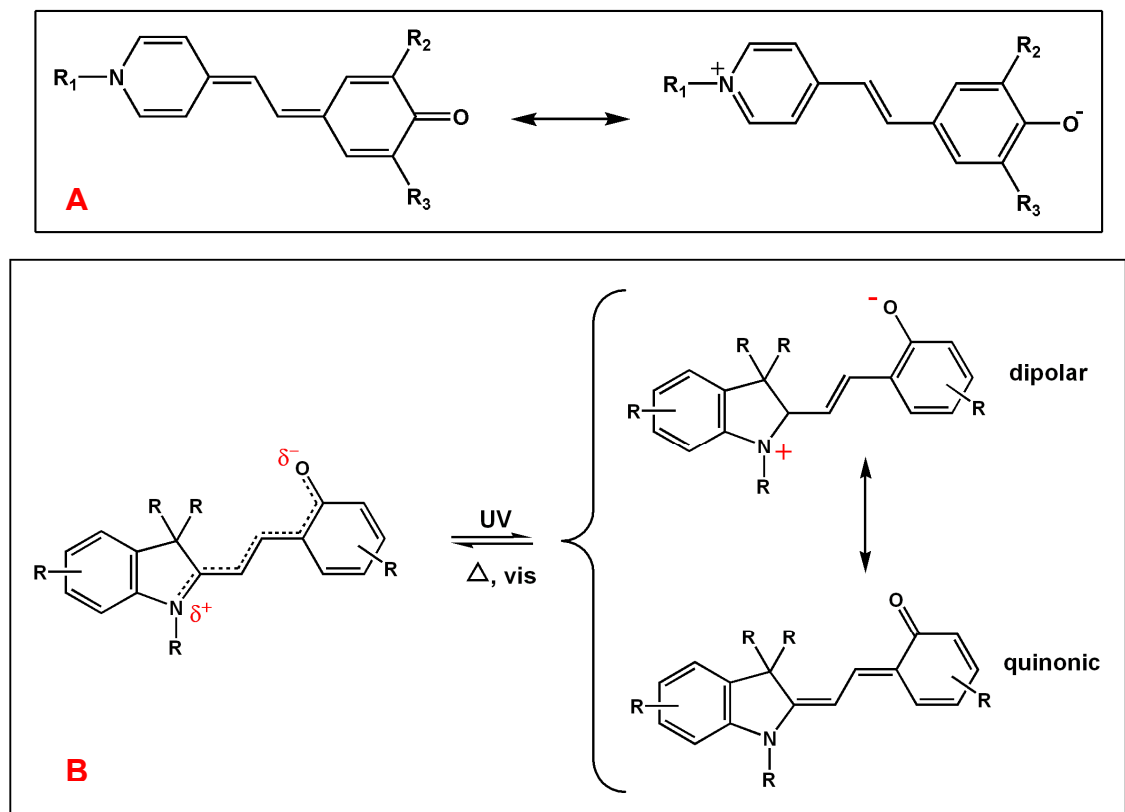


Figure 1.15: (A) Brooker's merocyanine equilibrium isomers; (B) Quinonic and dipolar resonance hybrids of a transoid structure of the ring-open ISBP merocyanine form.

The ring opening reaction which starts with a cleavage of the $C_{\text{spiro}}\text{-O}$ bond initially leads to the formation of a sterically strained intermediate which is higher in energy as the two halves of the molecule are still orthogonal to each other. This rapidly converts to the more stable, planar transoid isomers⁴¹.

Different MC isomers have been identified using transient spectroscopy methods. They all differ for the geometrical arrangements along the central chain of the three conjugated C-C bonds ($C_{22'}\text{-}C_3\text{-}C_4\text{-}C_{4a}$), defining three dihedral angles. All the three carbon bonds have a partial double-bond character, and their dihedral angles can be closer either to 0° or to 180° , which correspond to cisoid and transoid configurations.

These cisoid or transoid configurations have been labeled by a sequence of three C or T letters indicating the setting of the three dihedral angles.

Only the isomers having a central transoid segment represent a local energy minimum and are stable MC isomers. The other cisoid configurations are at a relatively higher energy level due to internal steric hindrance⁵⁰.

The structure of the most stable isomers have been reported as TTC and CTC conformers as these possess a larger dipole moment according to theoretical modelling calculations⁴¹.

Upon light excitation, C_{spiro}-O bond cleavage is induced with formation of a cisoid intermediate, which through subsequent rotation around the C_{spiro}-N bond leads to the MC isomer CTC which undergoes isomerisation through rotation of the C-C bond leading to the formation of the more stable TTC isomer (**figure 1.16**).

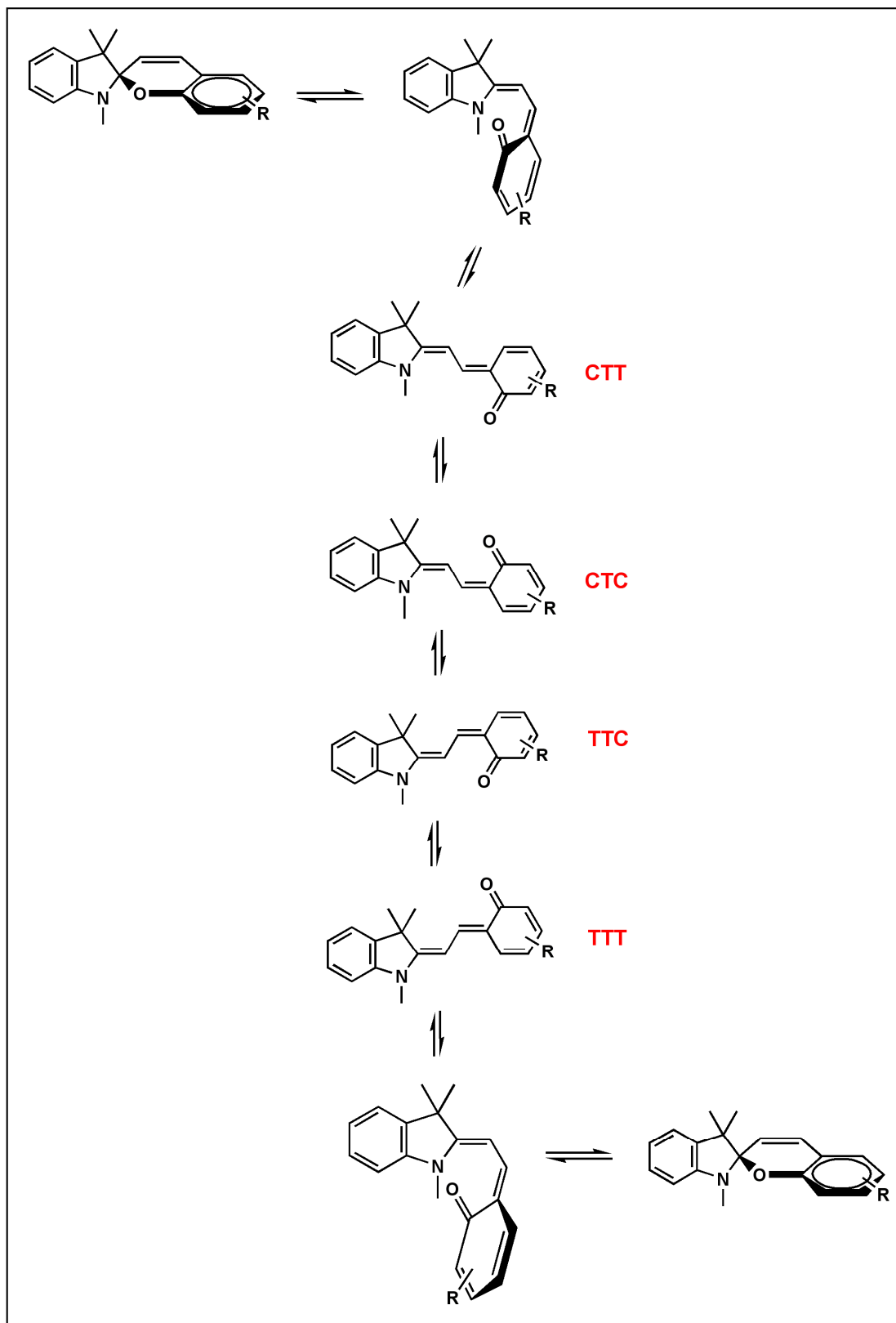


Figure 1.16: Schematic representation of different possible intermediate isomers induced by photoexcitation of the ring closed ISBP spiro form.

The nature of the excited states is strongly dependent on substitution of the parent spirobenzopyran ring^{41,56}.

For compounds containing a nitro group in position 6 studies performed using resonance raman spectroscopy, laser photolysis and quenching have shown that the ring-opening mechanism follow a triplet state pathway, with the excitation inducing the formation of an open cisoid singlet state which converts by intersystem crossing to a triplet state (enhanced by the presence of the nitro group). This is precursor of a triplet MC, which is quenched in the presence of oxygen to more stable CTC and TTC transoid conformers (**figure 1.17**). In contrast the excitation of spiropyran without a nitro group follows a singlet pathway.

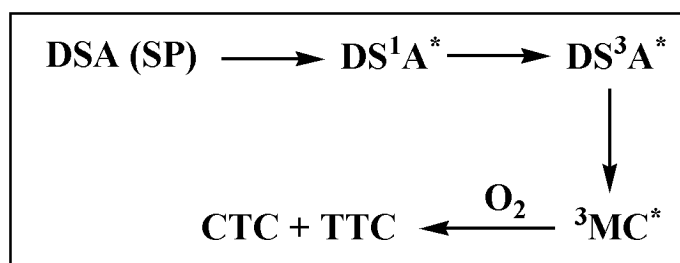


Figure 1.17: Schematic representation of the triplet excitation pathway followed by nitro substituted spiropyran. DSA represent a general spiropyran with a nitro group in the benzopyran ring (A) which is linked to a D indoline ring through a spiro carbon atom (S).

After removal of UV-light irradiation, the enhanced colouration slowly reverts back to the original ring closed colourless spiro form. The relaxation time at room temperature depends significantly on the structure of the spiropyran and on the solvent polarity. This thermal decolouration of the MC has been demonstrated to follow a first order decay rate⁵⁷. The reversion to the closed uncoloured spiro form can be also photochemically induced by white light irradiation³¹.

In summery, indolispiro nitro-benzopyran derivatives (ISNBP) are in general strongly affected by solvent polarity and by the presence of oxygen. Upon UV irradiation they undergo strong colour changes and they will be the main focus of our discussion in this thesis.

1.5.2 Synthesis of indolinespirobenzopyran (ISBP)

ISBP are generally prepared from a fisher base (heterocyclic ammonium salt in basic medium) and 2-hydroxysalicylaldehyde derivatives. The fisher base is generally a 2-ethylene-1,3,3-substituted indoline. The solvent is generally anhydrous ethanol, or benzene when a substrate in the reaction is labile or possess other reactive functions (**figure 1.18**).

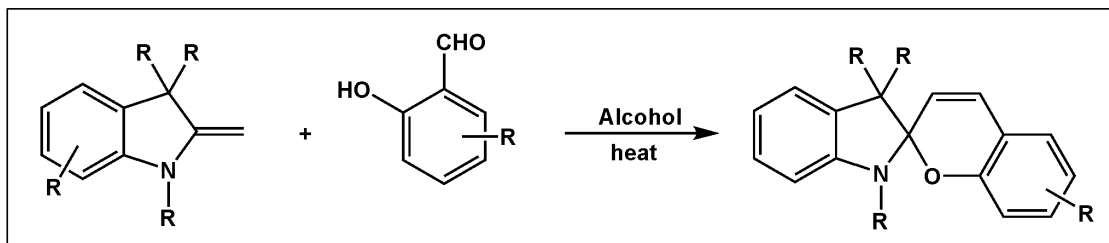


Figure 1.18: General reaction scheme for the synthesis of indoline spirobenzopyrans.

The reaction mechanism involves the formation of a carbanion by the mesomeric effect from the fisher base, and this species carries out a nucleophilic attack to the carbonyl group of the substituted 2-hydroxysalicylaldehyde. This is followed by ring closure through intramolecular addition of the phenolic oxygen to the ammonium group which gives, under elimination of water, the spiro-compound⁸ (**figure 1.19**).

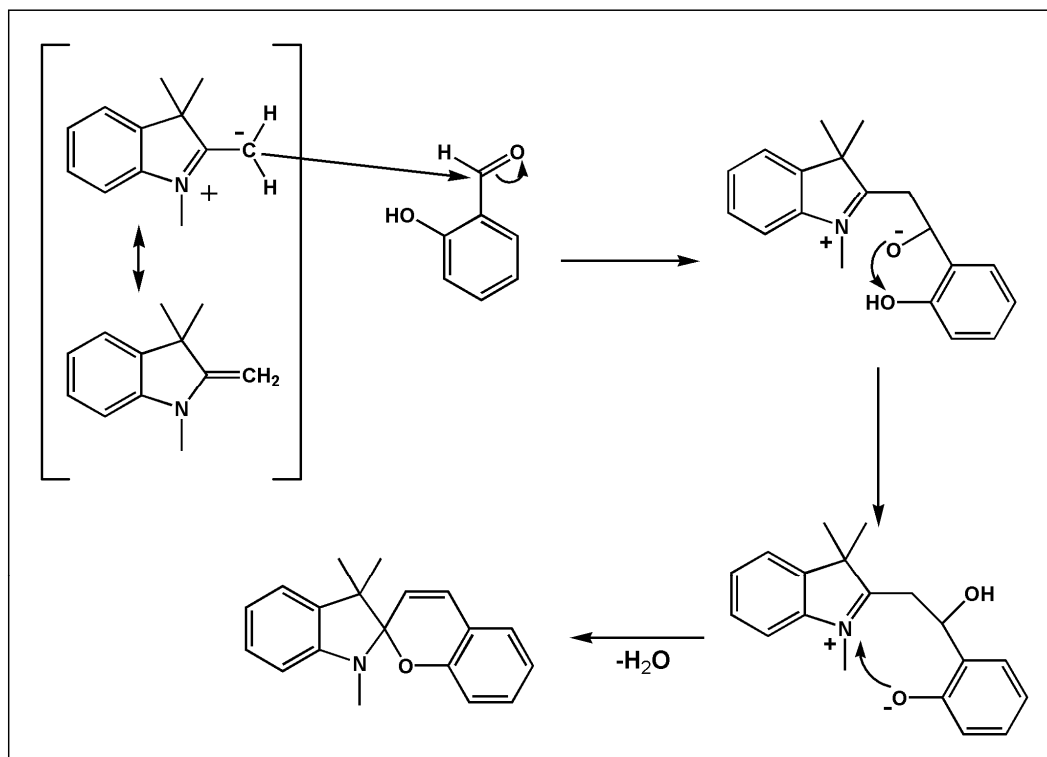


Figure 1.19: Schematic representation of the reaction mechanism between the fisher base and the 2-hydroxysalicylaldehyde derivatives to produce a general indoline benzopyran molecule.

Three different spiroopyran derivatives have been synthesised in order to use them as a template for the functionalisation of different materials to obtain adaptive surfaces with photochromic behaviour. They all contain reactive groups that can be used to promote coupling reactions for material covalent functionalisation (**figure 1.21**).

For the purpose of this research two particular indolispiro nitro-benzopyran derivatives (ISNBP) derivatives and one ISBP derivative have been synthesized. The two ISNBP derivatives present a nitro group in position 6, and differing aliphatic substituents on the indoline nitrogen in order to allow the attachment of the photochromic unit on different substrates. As previously explained, the presence of the nitro group promotes fast and effective switching, stabilizes the open form and generates strongly coloured MC forms. The ISBP derivative instead presents a reactive acrylate group in position 6 and no substituents on the indoline nitrogen.

A spiroopyran containing a carboxylic acid side chain (1'-(3-carboxypropyl)-3',3'-dimethyl-6-nitrospiro(2H-1)benzopyran-2,2'-(2H)-indole (**SPCOOH**) (**figure 1.21**) was synthesised as described elsewhere⁵⁸. This derivative can easily react with primary

aminogroups present on previously modified materials using 1-Ethyl-3-[3-dimethylaminopropyl] carbodiimide hydrochloride (EDC) (**figure 1.20**).

EDC is a crosslinking agent used to couple carboxyl groups to primary amines⁵⁹. If this intermediate does not encounter an amine, it will hydrolyze and regenerate the carboxyl group.

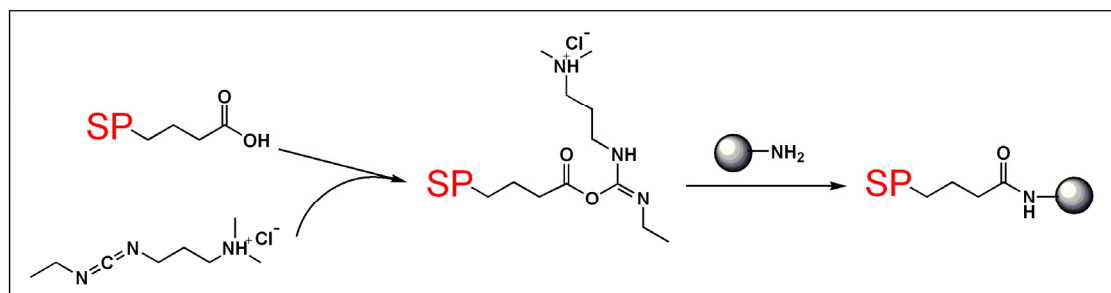


Figure 1.20: EDC reacts with a carboxyl group on a spiropyran modified with the addition of a carboxyl side chain (SPCOOH), forming an amine-reactive O-acylisourea intermediate. This intermediate can react with the amine group of a molecule of an amino modified substrate yielding a conjugate of the two molecules joined by a stable amide bond.

A monomeric spiropyran, 1', (9-decenyl)-3,3'-dimethyl-6-nitrospiro[2H-1]-benzopyran-2,2'-indoline (**vinyl SP**) (**figure 1.21**), containing an eight carbon vinyl chain at the R position (Fig.1, main text) was synthesised according to the procedure described by McCoy et al⁶⁰ from a two steps process (a previous N-alkylation of the 2,3,3-trimethylindoline with a 10-bromoalkene followed by a coupling with 5-nitrosalicylaldehyde). This derivative is an inherently polymerisable spiropyran with photochromical properties, suitable for subsequent copolymerisation with vinyl monomers.

The other monomeric spiropyran, the acryl ester of (1',3',3' triimethyl-6-hydroxyspiro(2H-1)benzopyran-2, 2'-indole) (**Acrylated SP**) (**figure 1.21**) was synthesised in our group by Dr. Robert Byrne according to a previously reported procedure⁶¹. This derivative is suitable for subsequent copolymerisation with other acrylated monomers.

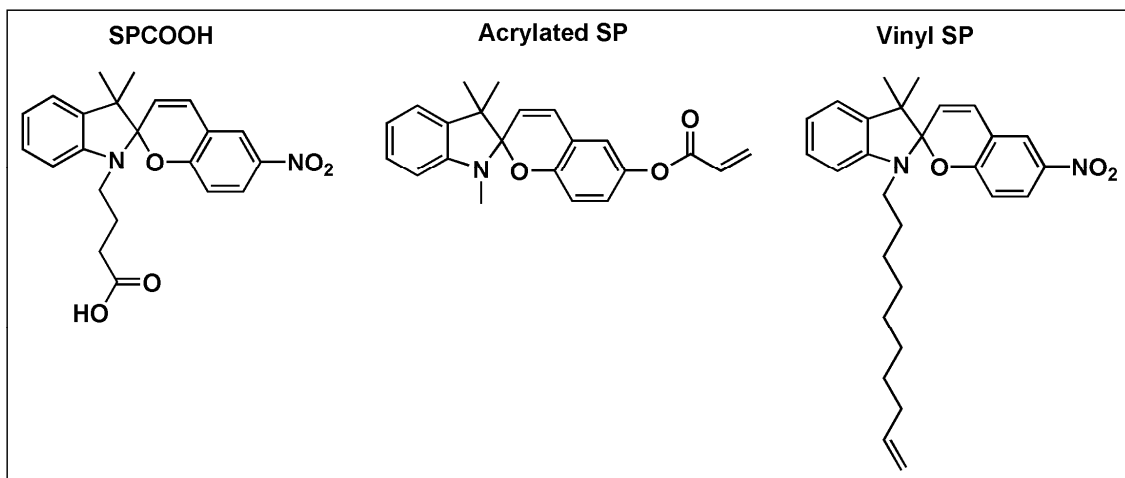


Figure 1.21: Molecular structure of the three different spiroopyran derivatives which have been synthesised in order to be used as a template for the functionalisation of different material and polymeric substrates.

1.5.3 Thermochromism

Prior to the discovery of their photochromic behaviour, the thermochromic nature of ISBP had been reported as early as 1921³¹ (**figure 1.22**).

The rearrangement between the two thermodynamically stable states can be thermally induced and is accompanied by a reversible colour change.

However, not all the photochromic spirobenzopyran derivatives are thermochromic. Thermochromism occurs only in those compounds where the energy potential barrier of the thermal reaction colourless \rightarrow coloured form is equal or lower to the energy transferred to the system by an increase in temperature⁴⁴.

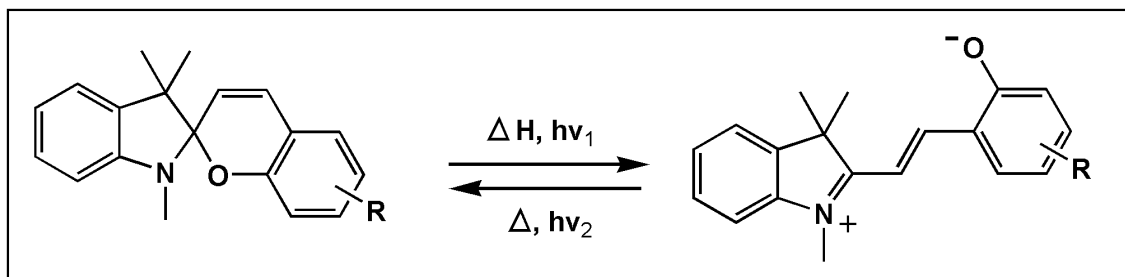


Figure 1.22: Thermochromism and photochromism of ISBP.

1.5.4 Solvatochromism

The solvatochromic effect occurs where there is a strong dependence of the UV-vis absorption bands of a compound on variations in the polarity of the solvent medium.

It involves a change in the position and sometimes in the intensity of the absorption bands of the molecule when measured in different solvents. These changes are caused by intermolecular interactions between the solute and solvent that modify the energy gap between the ground and excited state of the absorbing species^{31,41}. Consequently, variations in the position, intensity, and shape of the absorption spectra can be direct measures of the specific interactions between the solute and solvent molecules.

The family of spiropyran compounds undergoes solvatochromism, as the equilibrium between the ring closed spiro (SP) form and the ring open merocyanine (MC) form is influenced by the external medium in which the molecule is dissolved.

The solvatochromism of spiropyrans depends on three main factors: 1) solvent polarity 2) nature of the substituent groups, 3) concentration of the solution and it is governed by two mechanisms. The first is related to the shifting of the equilibrium between the SP and the MC form when the molecule is placed in solvent with different polarity. This effect is manifested by a shift in the absorption bands.

The second is governed by the interactions which may occur between solvent and solute in solvents with different physical and chemical properties.

In general for ISNBP as the polarity of the solvent increases, the maximum absorbance shifts to shorter wavelengths, higher frequency (*hypsochromic* or blue shift), while as the polarity decreases the maximum absorbance shifts to longer wavelengths, lower frequency (*bathochromic* or red shift).

The coloured MC form is highly conjugated and characterised by a strong polar character, due to its zwitterionic character which strongly contributes to the electronic distribution of the ground state. As a consequence it is stabilized by polar solvents, which decrease the thermal relaxation rate constant and the reconversion MC→SP.

The colour of the MC form depends on the difference in polarity between the photo-excited MC form and the conjugated zwitterionic ground state. In polar solvents, the ground state of the MC form is stabilised relative to the excited state, leading to a blue shift in the visible absorption band. In non-polar solvents, the energy difference between

the ground and the excited state is much lower, because of the high energy level of the ground state.

As a result the stabilisation of the conjugated zwitterionic MC form in polar solvents leads to a larger energy of activation and a slower conversion back to the ring closed spiro form when compared to non-polar solvents (**figure 1.23**).

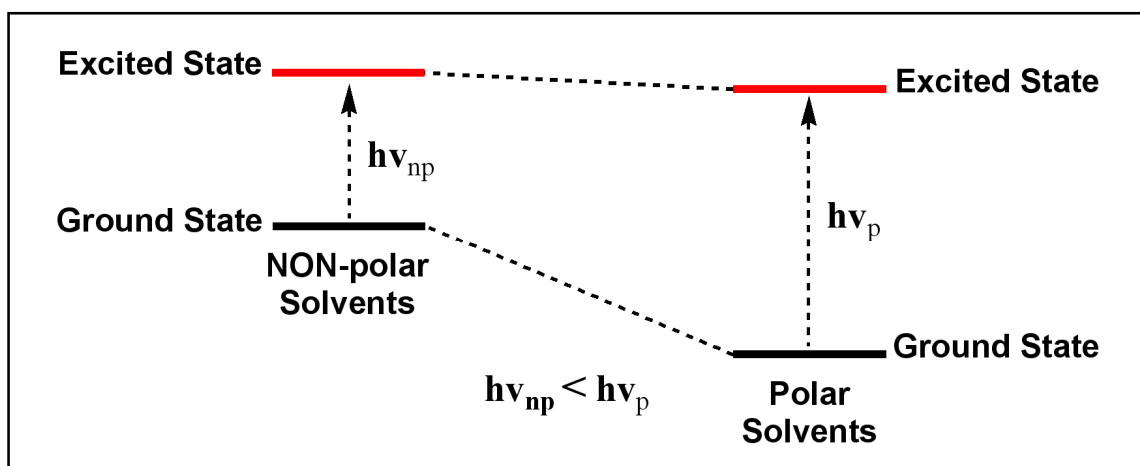


Figure 1.23: Schematic representation of the energy difference between the ground and the excited state of the MC form in polar and non-polar solvents.

1.5.5 Photodegradation

Photodegradation of MC is a well-known phenomenon that limits application of spiropyran in reversible, self-regenerated sensing devices. It occurs when the photochromic compounds are repeatedly switched between the two forms over a certain number of times and is mainly due to prolonged exposure to UV incident radiation.

It has been demonstrated that the photostability of spiropyrans depends on factors such as oxidative degradative processes which occur in the presence of singlet or free radical oxygen⁶²⁻⁶⁵ and MC aggregation^{64,66}. It is generally accepted that interaction of MC form with singlet and triplet oxygen leads to photodecomposition of MC⁶⁷. Therefore, by putting together films containing different photochromic compounds such as fulgides and spiropyran and sealing them air-tight, Matsushima et al. were able to significantly reduce the photodegradation of fulgimides.⁶⁴ Interestingly, this approach did not provide any improvement in photo-fatigue of spiropyrans. On the other hand, they noticed that reducing the concentration of SP in the film had beneficial effect on the reduction of

photodegradation, implying that aggregation of MC also has an important role in their photodegradation. A similar conclusion was drawn by Arai et al. and Tork et al. while studying photodegradation of MC in solution⁶⁸ and in polymer matrixes,⁶⁹ respectively. The work of these research groups indicates that reducing the degree of motion of MC reduces the possibility of interaction between MC molecules and has beneficial effects on reducing the photo-fatigue.

Therefore, the addition of antioxidant agents, the immobilisation of antioxidant pendant groups as a side chain to spiropyran compounds or reduction of MC aggregation by for example covalent immobilization of spiropyran derivatives within polymeric matrixes, should significantly reduce the degradation process.

Since covalent attachment drastically limits the movement of MC, it should result in films showing improved photo-fatigue. To further study this hypothesis Radu et al.⁷⁰ prepared PMMA films containing non-immobilised SPCOOH which is not covalently attached to the surface and monitored its absorbance at 560 nm while continuously switching between the SP and MC forms relatively to a film containing covalently attached SPCOOH. The loading of SPCOOH in both films was approximately 1% w/w.

Figure 1.24 depicts the comparison of the signals obtained for the two films measured at 560 nm.

As expected, the loss of signal in the case of non-attached SPCOOH is dramatic. The difference in absorbance between SP and MC forms at the 12th cycle is only 43% of the 2nd cycle. On the other hand, the signal in the case of covalently immobilized SPCOOH is significantly more stable and the signal of the 12th cycle is 73% of the 2nd cycle. Therefore, the covalent immobilization of SPCOOH indeed improved the stability of the signal and reduced its photodegradation.

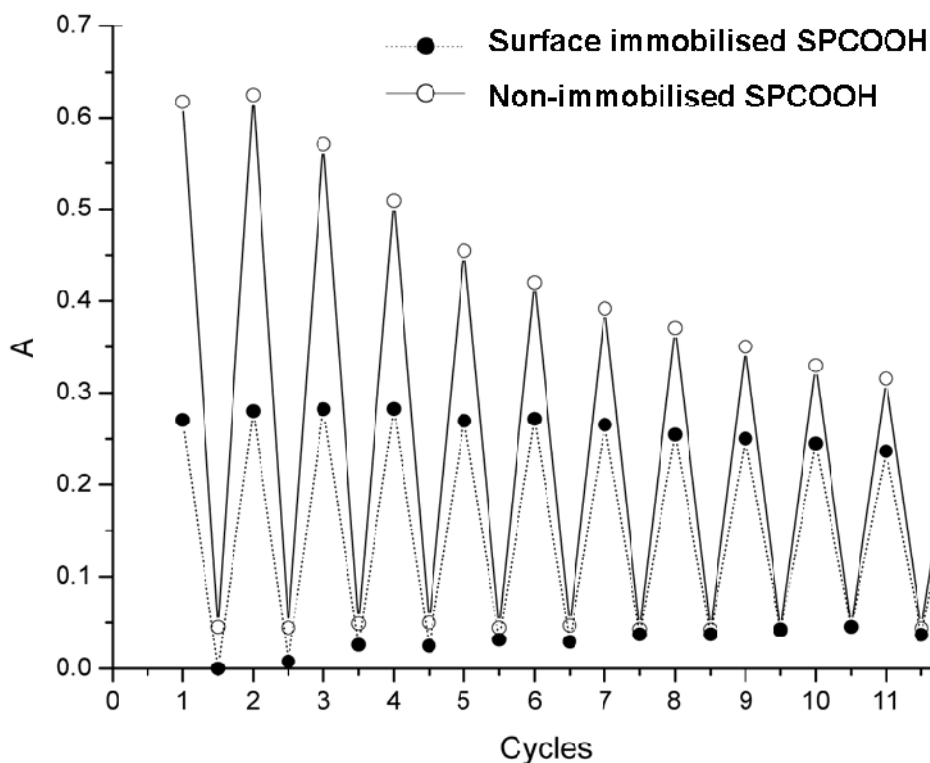


Figure 1.24: Absorbance measured at 560 nm for cyclical switching between SP and MC when for surface immobilized (full circles) and non-immobilized (open circles) SP-1. Reproduced from *Journal of Photochemistry and Photobiology A: Chemistry* **2009**, 206, 109-115.

Recently another important factor involved in the photostability has been identified. The use of LEDs instead of strong power light sources such as commonly used mercury lamps has turned out to significantly reduce the rate of photodegradation^{3,5}. Typically used LEDs present ca. 1 mW/cm² power compared to the power of arc lamp light sources reported in most papers, which are typically 50-100 W. The reduction in the relative photon intensity of the LEDs compared to arc lamp-sources is thus reduced of a 10⁵ factor. Despite the lower power of LEDs they are perfectly suitable for switching the equilibrium between the SP and the MC forms. It has been demonstrated that green and UV LEDs can be easily used to cycle spiropyran doped PMMA (polymethylmethacrylate) film between the SP and MC forms³.

Further investigation on the photostability of a similar polymeric film with covalently attached SPCOOH^{5,32} (figure 1.25) has demonstrate that using an appositely designed

LED-cluster⁷¹ (**figure 1.26**) which incorporates UV (365 nm) and green (565 nm) LEDs to perform the SP \leftrightarrow MC switching as well as LEDs for performing reflectance colorimetry at 660 nm, 560 nm and 425 nm (red, green, and blue respectively) along with a photodiode to measure reflected light intensity, the photostability can be remarkably increased.

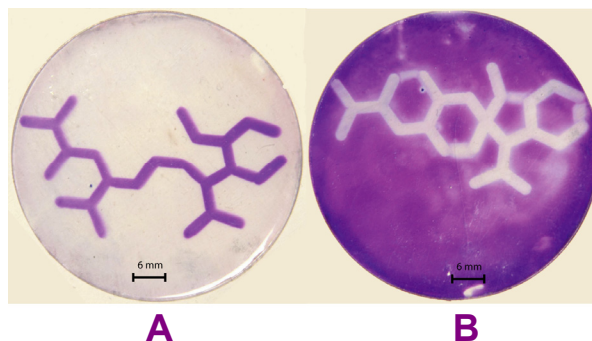


Figure 1.25: Spatial control of SP-modified film. **A)** Film in passive mode irradiated with UV through a MC shaped-mask. **B)** Film in active mode irradiated with white light through a SP shaped-mask. Reproduced from *Journal of Physics D: Applied Physics* **2007**, 40, 7238-7244.

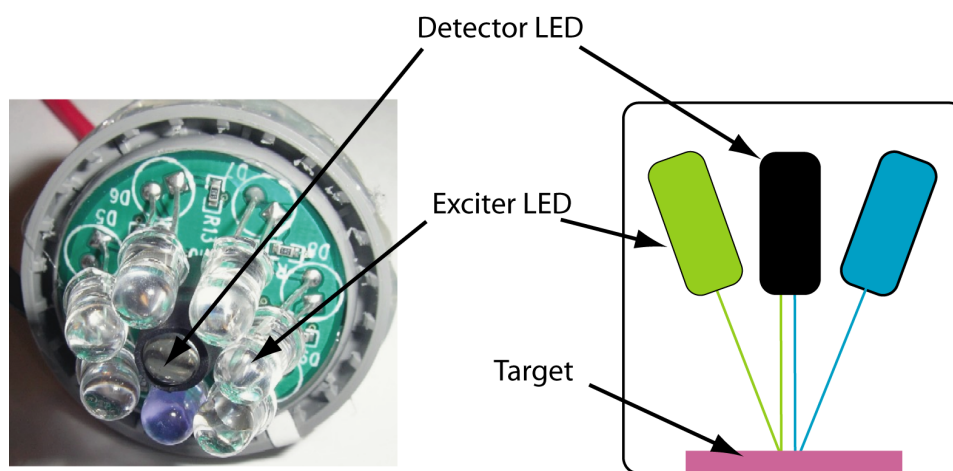


Figure 1.26: Left – picture of LED array. Right – scheme depicting diffuse reflectance measurement. Reproduced from *Sensors and Actuators B: Chemical* **2006**, 114, 819-825.

After more than 380 cycles, there is a loss of 14% of the original intensity of the signal at c.a. 560 nm.⁵ (**figure 1.27**), which is really low compared to the best value achieved in solution by the introduction of antioxidant pendant group which is 1% after 13 cycles⁶⁵, which at this rate translate in roughly 30% loss of photostability after the same number

of cycles, using a high pressure mercury lamp. Adding to this the LEDs array is programmed so that the matrix is exposed to the UV-LED light for 60 seconds every cycle, while in the second case the exposure is 30 seconds per cycle, making the photostability value achieved using LEDs even more impressive.

In conclusion, the use of LEDs as a light source to perform photochromic reactions in spiropyran derivatives, combined to polymeric immobilisation, strongly increases the stability of the compounds, without affecting the efficiency of the switching, making them suitable for chemical sensing application.

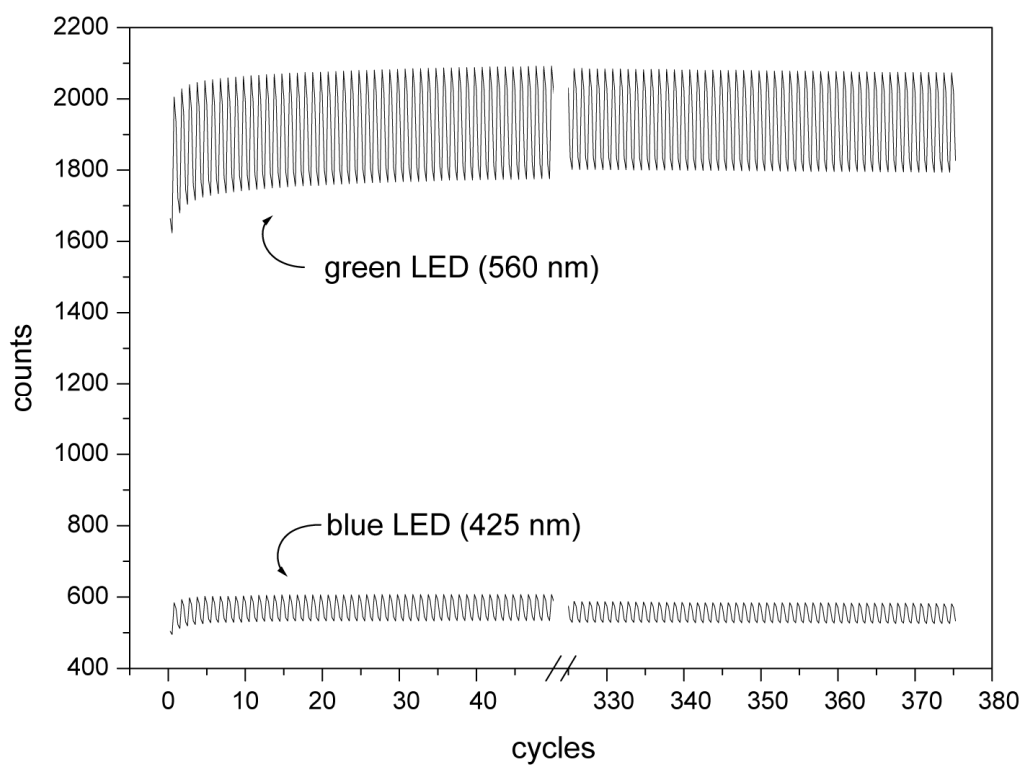


Figure 1.27: Multiple optical switching and monitoring of a single location on a SP-modified PMMA film using LED cluster. Despite an overall reduction of ~25% (425 nm) and ~14% (560 nm) in the signal, a remarkable number of cycles can be achieved. Reproduced from *Journal of Physics D: Applied Physics* **2007**, *40*, 7238-7244.

1.5.6 Binding of metal ions

Metallochromic ligands are molecules that interact with metal ions to form coloured complexes. Colour changes are crucial recognition events in analytical chemistry as a tool to gather information from molecular-scale events.

When metallochromic ligands are also photochromic compounds the possibilities from an analytical point of view are even more interesting, as it is possible to externally control using light the presence of the active or passive state of the ligand.

ISNBP derivatives are known to form chelates with metal ions in solvents of medium polarity and complex formation is accompanied by drastic changes in the spectral properties of the MC active metal-binding form^{43,57}.

As previously described, spiropyran derivatives can be photoswitched to isomerise between an non-polar ring closed SP form (by irradiation with white light) and a more polar ring open MC form (by UV exposure). The exciting feature of this system is the ability of the MC to form complexes with certain d- and f- metal ions in solution, and the complexation causes a blue shift in the MC visible absorption band⁴³. On binding the metal ion, the absorbance maximum shifts to lower wavelength and the absorbance of the MC within the visible region decreases. Hence, the system is inherently self-indicating, as the colour changes between the free MC and the MC-metal ion complex.

Bidentate transition elements have been shown to induce the most striking spectral changes upon complex formation whose structure depend on the ISNBP derivative type (**figure 1.28**).

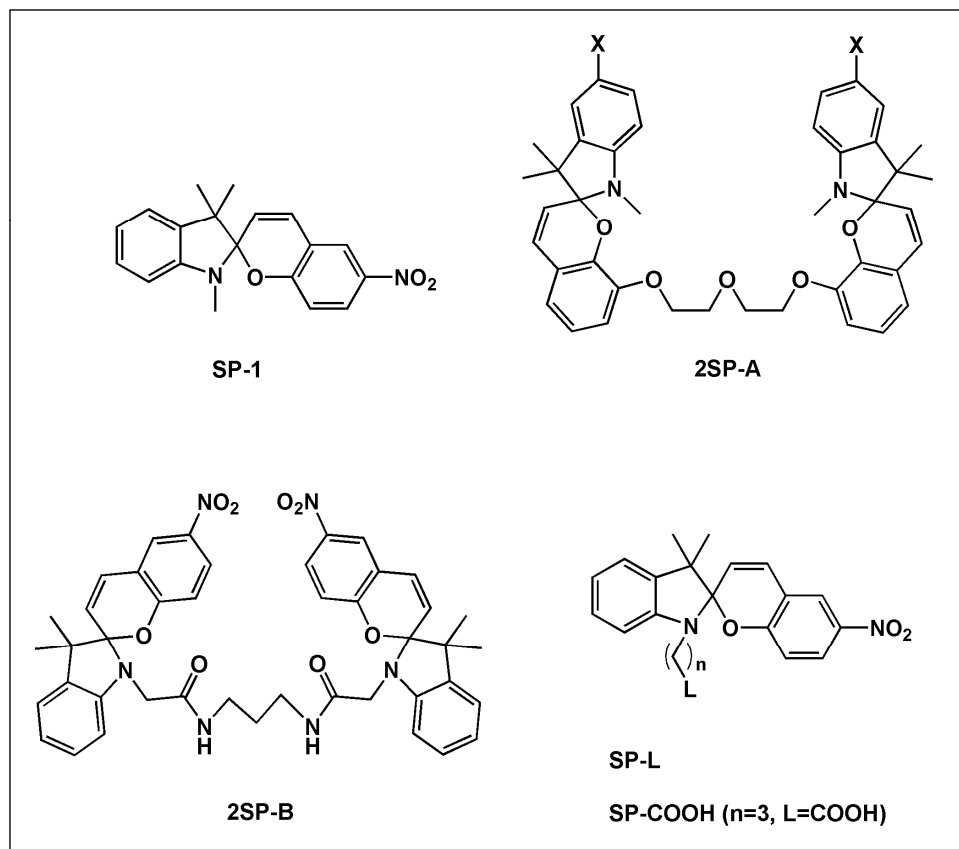


Figure 1.28: Scheme showing four kinds of ISBP derivatives with different metal complexation ability.

SP-1 derivative types (**figure 1.28**) have shown to reversibly bind metal ions through the negatively charged phenolate group with 2:1 MC form to metal binding ratio^{5,32,72} with the phenolate groups of two MC forms complexing one metal ion (**figure 1.29**).

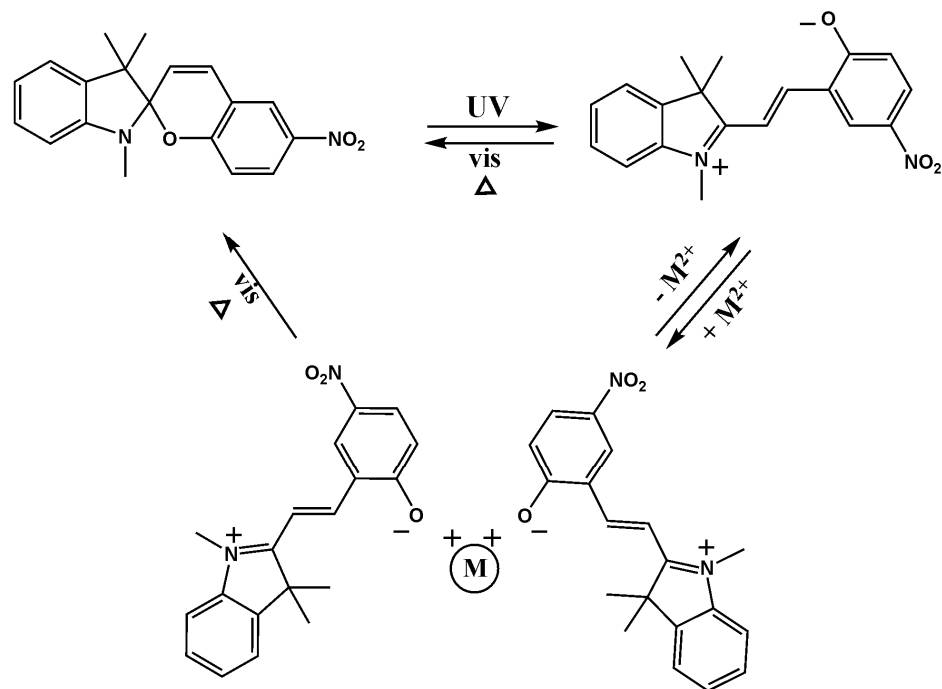


Figure 1.29: SP-1 reversible conversion between a closed, uncharged, inactive, non-planar and colourless SP form, by exposure to visible light, and open, planar, active, highly conjugated, highly coloured MC form by exposure to ultraviolet (UV) light. The MC form can bind metal ions through the phenolate anionic site. The guests can be subsequently expelled by irradiation with visible light and the spiropyran reverts to the closed form. Light modulated control of ion-binding at spiropyran modified surfaces is therefore possible

It also has been demonstrated that when SPCOOH derivatives (**figure 1.28**) are covalently immobilised on a PMMA polymeric film (through an amide involving the carboxyl group), the complex formation happens only when spacers of a certain length are placed between the surface and the spiropyran unit so to give enough freedom to two proximal merocyanines to adjust in order to complex the metal ion³².

Free SP-L derivative types, presenting an additional binding group linked to the photochromic moiety are thought to form metal complexes wherein the MC form interacts with a bidentate metal ion through the negatively charged phenolate group and the additional group, such as a negatively charged carboxyl group (in the case of SPCOOH)^{73,74}.

More complex spiropyran based photochromic systems such as 2SP-A⁷⁵ and 2SP-B⁷⁶ (**figure 1.28**) are particularly effective metal ligands, as the two MC binding units are pre-arranged in the molecular structure. These pre-arranged systems have also shown to be sensitive to alkaline earth metals such as Ca²⁺ and Mg²⁺. In the case of 2SP-B it has been demonstrated that the binding constant of the bis-spiropyran system is eight times higher when compared to the binding constant of the mono-spiropyran unit.

Even though in a pre-arranged system the binding ability is strongly enhanced some of them, such as 2SP-B type, don't show any light-induced photochromism and the SP form only converts to the MC in the presence of certain metal ions. This unfortunately negates any external control over the complex formation which is also not reversible.

In the literature the complex formation of many MC derivatives have been evaluated in different solvents with a wide range of transition metals^{43,77} and in particular with Copper (II)^{74,78} and Zinc (II)⁷²⁻⁷⁴.

Interesting approaches have been carried out to demonstrate light driven metal ion transport between two liquid phases using different spiropyran derivatives.

Photoswitchable metal transport between a water-chloroform interface inside a U shaped tube has been demonstrated using different ISNBP derivatives dissolved in chloroform. Successful photodynamic metal transport was achieved with Zn²⁺, Cd²⁺ and Hg²⁺³⁶.

Transport of metal ions through membranes has also been reported. Phosphate unilamellar vesicles containing small amount of an Amphiphilic-SP (**figure 1.30**) shows a decrease in K⁺ release when the SP was photoisomerised to its MC form by exposure to UV light. Subsequent exposure to visible light causes reformation of the spiro compound with a corresponding increase in the leak rate⁷⁹. These effects have been demonstrated to be fully reversible over several photoisomerisation cycles, suggesting that the SP form is located relatively deeply within the aqueous/organic interface where it disrupts the alkyl chain bilayer arrangement, increasing the electrolyte permeability. Conversion to the more polar MC form is accompanied by relocation of the molecule away from the membrane interior, decreasing the inner lipophilic chain disorder and restoring the normal ion impermeability of the bilayers.

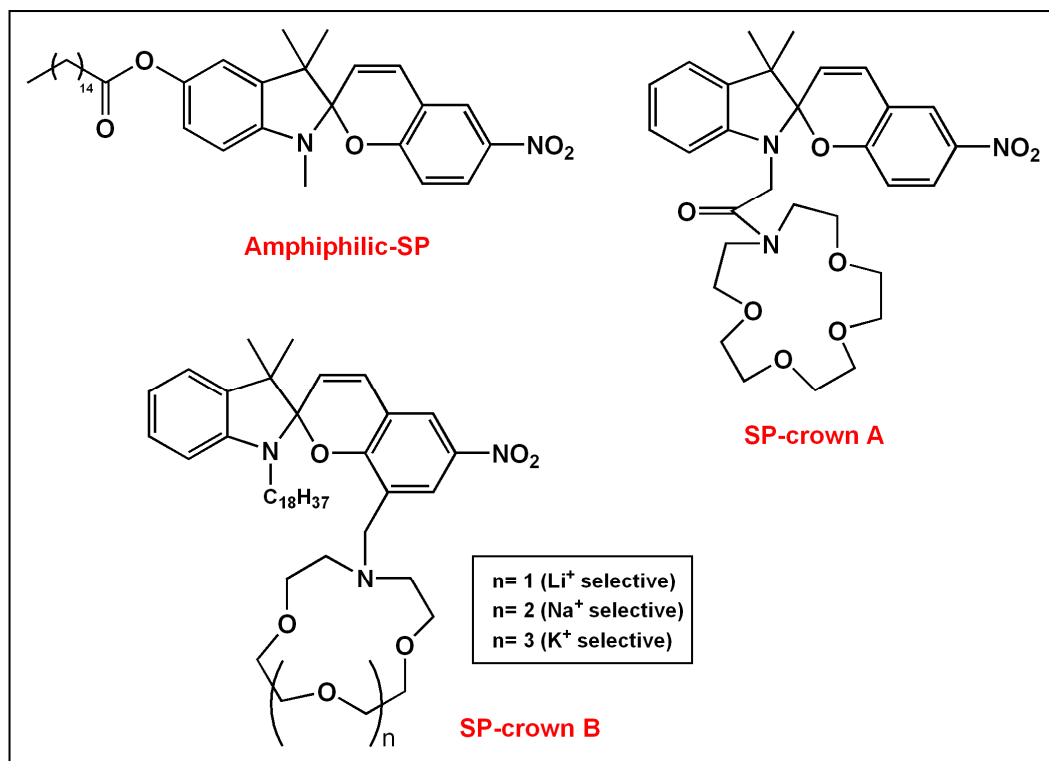


Figure 1.30: ISNBP derivatives used for different types of photocontrolled membrane transports.

The same experiment was repeated using phosphatidylcholine unilamellar vesicles containing K⁺ selective crown ether attached to spiropyran (SP-crown A, **figure 1.30**).

UV-induced photoisomerisation of the SP was accompanied by a strong enhancement of K⁺ leakage and the effect was fully reversible, with K⁺ leak rates returning to their basal levels upon irradiation with visible light⁸⁰.

Metal ion transport using liquid membranes was also demonstrated using other type of ISNBP derivatives modified with crown ether⁸¹ (SP-crown B, **figure 1.30**). The passive transport was performed on a U-shaped glass cell in which three phases were present: 1) a source phase containing water solutions of alkali metals, 2) an organic phase containing crown selective-spiropyran derivatives for Li⁺, Na⁺ and K⁺ and 3) a receiving phase containing aqueous tetramethylammonium hydroxide.

The transport of the alkali metal from the source phase to the receiving aqueous phase through the spiropyran liquid membrane was accelerated by UV-light irradiation and retarded under visible light exposure. Uphill transport of metal ions was achieved when the source phase was irradiated with UV light and the receiving phase with white light.

Photoreversible metal binding studies have been reported for different spiropyran derivatives immobilised on different matrixes such as gold electrode surfaces⁸², synthetic copolymers based on N-isopropyl acrilamide³⁹ or PMMA films³².

When thiol functionalised spirpyran units are immobilised on gold electrodes, the electronic potential can be photomodulated in the presence of Zn^{2+} ions⁸² (**figure 1.31**). The variation of the electrode potential was due to a membrane potential change of the modified electrode as a result of the reversible transformation of the SP and MC forms and the uptake and release of metal ions by MC upon alternating UV and visible light irradiation.

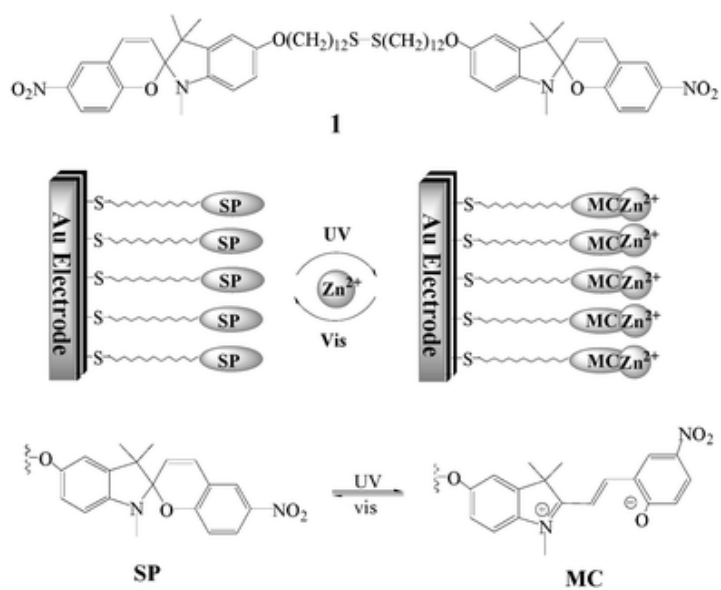


Figure 1.31: Structure of thiol functionalised spiropyran units immobilised on gold electrode and illustration of the transformation of SP into MC as well as MC coordination with Zn^{2+} on the electrode surface. Reproduced from *Chemical Communication* **1999**, 321-322.

Photoreversible Pb^{2+} complexation was also achieved using a synthetic copolymer composed of N-isopropyl acrylamide and a spiropyran acrylate³⁹ (**figure 1.32**).

This polymer was found to be thermosensitive in water, showing a lower critical solution temperature (LCST) around 29°. Below this temperature the co-polymer was water soluble while above the LCST, the aqueous solution generated a solid polymer and separated into two phases.

Below the LCST in aqueous solution, the soluble polymer has an absorption band in the visible region around 533 nm, suggesting that the polar environment strongly favoured isomerisation to the MC form. Upon addition of Pb^{2+} ions, the 533 nm band disappeared almost completely and a new band appeared at 433 nm, associated with the MC- Pb^{2+} complex. When the temperature was raised above the LCST, the solid polymeric phase contained the bound metal and this can be easily separated from the solution. Conversely, upon decreasing the temperature, the metal was released through dissolution of the polymer and irradiation with white light to re-convert the MC back to the non-binding SP form, and thereby release free metal ions.

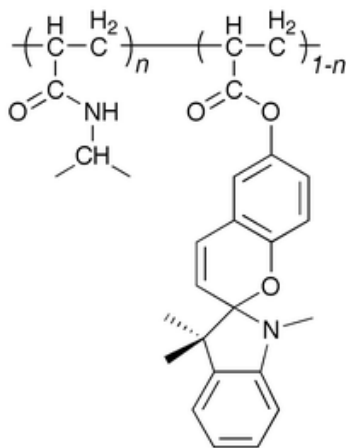


Figure 1.32: Structure of the synthetic thermosensitive copolymer composed of N-isopropyl acrylamide and a spirocyclic spiro[chromene]acrylate. Reproduced from *Chemical Communication* **2004**, 2036-2037.

It was also suggested that the same photo-reversible metal-complexation and release could be applied to Cu^{2+} , Ni^{2+} , Zn^{2+} and Mn^{2+} .

Another example of photoreversible metal binding using a spirocyclic spiro[chromene]acrylate functionalised polymer was reported for SPCOOH (**figure 1.28**) derivatives covalently immobilized onto an optically transparent PMMA (polymethylmetacrylate) surface³².

The polymer was functionalised with spirocyclic spiro[chromene]acrylate using couplers of varying chain length. It was found that the polymer could be reversibly switched between the SP and MC forms. The UV activated MC form presented a binding site for Co^{2+} ions. Complexation

resulted in an absorbance shift from 560 nm to 460 nm and a corresponding visual colour change. Upon irradiation of the MC-Co²⁺ complex with visible light, the cation was released and the MC reverted back to the passive SP form. The complexation behaviour of the functionalised PMMA film was found to be highly dependent on the tether length between the photochromic unit and the polymeric surface. A minimum tether length of 8-CH₂ groups was demonstrated to be required to facilitate switching efficiency of the photochromic spiropyran and ion-complex formation on the polymer surface.

Further studies on the same modified PMMA film showed that the spiropyran fatigue resistance on the polymer surface could be improved by using LEDs as light sources. The reversible SP↔MC switching and photoswitchable uptake and release of Cu²⁺ and Co²⁺ ions (**figure 1.33**) was successfully achieved using an LED array for diffuse reflectance measurements⁵ (**figure 1.26**).

It was also found that the polymeric film could be activated and deactivated at a selected location using LEDs. When the complex was formed between the MC and metal ions, irradiation with a green (or white) LED caused release of the bound ions and reversion of the MC form to the inactive SP form. This cycle was repeated multiple times using UV and green LEDs to control the surface binding of a range of metal ions, such as Co²⁺ and Cu²⁺. In principle, therefore, these are surfaces that can be switched reversibly between active and passive states. Furthermore the system is inherently self-indicating, due to the colour changes that accompany switching between SP and MC isomers and the formation of the MC-metal ion complexes. Furthermore, the bound species can be reversibly expelled on demand, simply by illumination of the surface with green or visible light, and the system once again indicates its status through return to the colourless SP form.

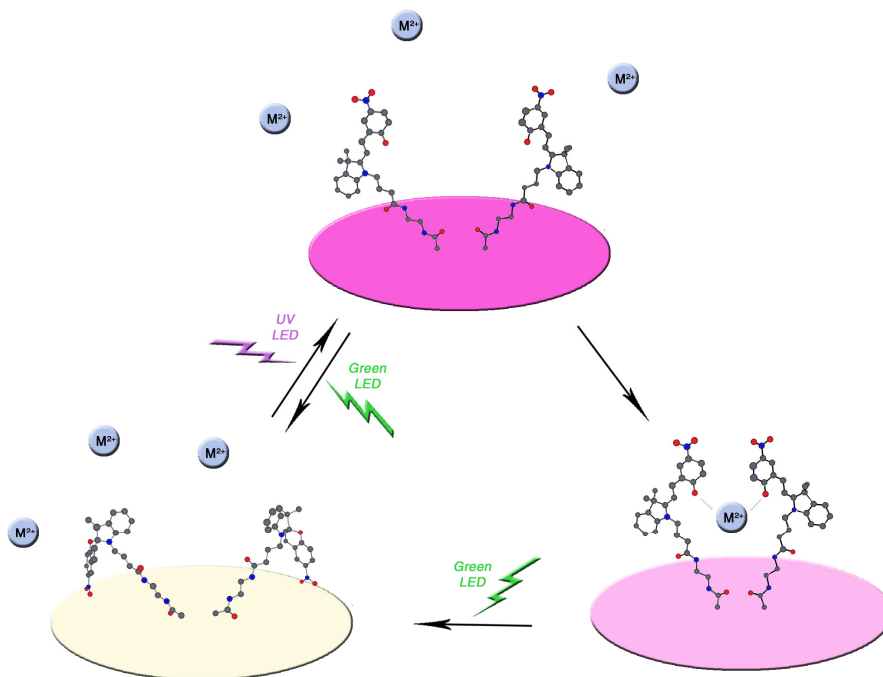


Figure 1.33: Schematic representation of a spiropyran derivative covalently immobilized onto an optically transparent polymeric surface of PMMA (polymethylmetacrylate). The colourless inactive SP form (top) can be reversibly switched using UV light/green LEDs to the pink zwitterionic MC active form (bottom). The negatively charged phenolate group of the MC form provides a binding site for Cu^{2+} and Co^{2+} (M^{2+}).

1.5.7 Protonation of the MC form

In addition to metal ion interactions the phenolate group of the MC form can be easily protonated⁸³⁻⁸⁵.

The formation of the protonated MC form has been followed by addition of strong acids to organic solutions of spiropyran. The protonation results in a blue-shift of the MC band to a lower wavelength, just above 400 nm.

The protonation of the phenolate group stabilizes the polar MC by a non-thermal, non-photochemical route, and create a stable positive charge upon the molecular unit at the phenolate group.

This feature is of particular interest from the material science point of view as through protonation, it is possible to create a stable charge which can be easily cancelled by reverting the MC back to the non-polar SP form *via* white light irradiation.

Exploiting this property, it has been demonstrated that the volume of a hydrogel copolymer of an acrylated spiropyran and poly(N-isopropylacrylamide) (pSPNIPAAm) can be reversibly reduced and increased when the gel is alternatively exposed to blue light or kept in the dark⁶¹ (**figure 1.34**).

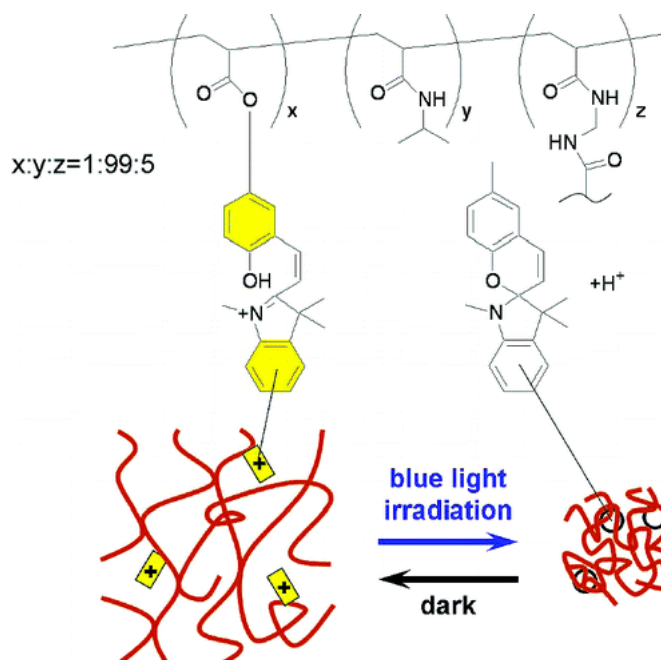


Figure 1.34: Chemical structure of the cross-linked poly(N-isopropylacrylamide) hydrogel functionalized with SP and a schematic illustration of the photoinduced shrinking of pSPNIPAAm hydrogel. Reproduced from *Chemistry of Materials*, **2007**, *19*, 2730-2732.

In addition to switchable micro-relief formation properties, the hydrogel exhibits changes in its electrostatic properties. When the hydrogel is placed on a slightly acidic bath, the spiropyran moiety is neutral when irradiated with blue light (because of the prevalence of the SP form) and positively charged when kept in the dark (because of the prevalence of the MC form, in which the phenolate is protonated). After micro-relief formation, negatively charged fluorescent nanoparticles are adsorbed on the non-irradiated region, to demonstrate the presence of an overall positive charge due to protonation of the photochromic compound.

Photoreversible MC protonation will be further discussed for other uses in microfluidic related techniques (**chapter 5**).

1.5.8 Other applications of ISBP derivatives

Indolinespirobenzopyran derivatives have found a wide range of applications when incorporated within different substrates to create new platforms whose function and properties can be radically changed and controlled using external stimuli. Applications include not only sensing, separation science and controlled sampling and release as previously described, but also optical memories⁸⁶, microfluidics⁵⁸ and optoelectronic systems⁸⁷.

The discovery of spiropyran photochromic behaviour initiated research into photochemical erasable memory⁸⁸. Different spiropyran derivatives, homogeneously dispersed in different polymeric matrices were successfully tested for writing and reading information in 3D storage memory³⁴.

More recently the reversible photoregulation of the electrical conductivity of spiropyran doped polyaniline was demonstrated⁸⁹. The electrical conductivity of polyaniline strongly depends on its degree of protonation. When a polyaniline thin film doped with spiropyran is prepared, the photoreversible protonation of the MC form results in a reversible photoregulation of the electrical conductivity of the film. Upon UV irradiation the film conductivity was reduced to around 40% of the initial value due to MC protonation, while subsequent white light irradiation increase the conductivity to 95% due to release of the protons to the polyaniline conducting polymer. This material may find potential application in information recording and processing where the information retrieval can be performed in a non-destructive manner (polymer electronic devices).

The incorporation of photoswitchable units on certain proteins or enzymes may induce photostimulation of their biocatalytic activity⁸⁷. For example concanavalin A is a lectin that specifically binds α -D-mannopyranose and α -D-glucopyranose. Upon light irradiation the binding affinity of the protein for the two substrates can be modulated as upon UV light exposure, the formation of the MC form induces complex dissociation resulting in a decrease of the binding ability of the lectin.

Similarly when a nitrospiropyran flavoenzyme glucose oxidase was assembled as a monolayer on a Au electrode, in the presence of the SP form, the enzyme actively catalysed the oxidation of glucose, while in the MC form it captures the protons

belonging to the acidic electron transfer mediator species, resulting on inhibition of the catalytic activity.

The physical properties of materials can also be highly influenced by the presence of spiropyran photochromic compounds.

It has been demonstrated that coating spiropyran derivatives onto a glass slide results in photoresponsive surfaces which wettability can be externally controlled using light with 11°-14 ° difference in contact angle between the SP and the MC form⁵⁸.

Applying the same chemistry to obtained spiropyran functionalised glass capillaries causes light induced changes in the equilibrium rise of water vertically inside the capillary.

Water in the capillary tubes has been demonstrated to rise when the light source was switched from vis to UV. For a 500 µm diameter capillary the rise due to UV irradiation was 2.8 mm greater than the rise under vis irradiation.

Clearly this work shows that by employing photochromic molecules, both physical and chemical properties of different substrates can be externally controlled by means of external light irradiation.

The photoswitchable SP ↔ MC equilibrium associated with different substrates opens up the exciting prospect of control of materials properties (conductivity, viscosity, surface energies, permeability, host-guest binding, actuation, etc.) using light.

1.6 Bead-based systems

Bead-based systems are a particular kind of bi-phase system in which solid particles in suspension can be moved as a fluid but easily separated from the liquid-phase. Beads provide a higher surface area than flat surfaces for chemical reactions and bead-based analytical approaches offer significant advantages for techniques that require reactions on surfaces⁹⁰. The low density of the polymer matrix allows binding kinetics that are comparable to those of solution based systems and their large surface area and greater density permit rapid and highly efficient binding of target species.

Micro- or nano-particles can be chemically derivatised with a wide range of specific ligands, or specific recognition groups. General specificity particles are largely produced as substrates to attach a variety of affinity ligands which allow a broad range of direct

applications, such as fluid flow-cytometry analysis ⁹¹, immunoassay-diagnostics ^{92,93}, cell biology ^{94,95}, and controlled release ⁹⁶. They are also generating increasing interest in the photonics community due to their high quality-factor (Q-factor) morphology dependent resonances and their sensitivity to refractive index and size changes. When biomolecules are adsorbed on their surface, a change in their effective size and refractive index occurs and it has been claimed that a biosensor based on this phenomenon can detect a single molecule⁹⁷.

A variety of materials, including organic and inorganic polymers, have been used as the substrate for micro and nanospheres. Common organic substrates are polystyrene or polymethacrylate. Polystyrene microspheres are often used for protein binding, due to the high degree of nonspecific protein adsorption (hydrophobic interaction is the most likely mechanism involved in adsorption of proteins). Inorganic substrates include metals, silica or alumina. Silica microspheres are naturally hydrophilic, so relatively little non-specific protein absorption should occur. Chromophore modified microspheres are available in a wide variety of colors, as are beads modified with fluorochromes and fluorophors. Superparamagnetic or radioactive microspheres are available with a range of different mean magnetic and radio activities.

The application of beads to different fields has led to the development of bead-based systems for separations, sample extraction, analyte detection and controlled release. Silica beads coated with octadecylsilane (ODS) packed in a microfluidic system enabled an on-chip solid-phase electrochromatography for the extraction of analytes with different polarity to be developed. The ODS coated beads were mobilized in the cavity of a chromatography bed as a part of a microfluidic system using electro-osmotic flow. Two weirs within a sample channel formed a cavity in which the beads were trapped. Beads were similarly packed in a chamber and reversed-phased mode capillary electrochromatography performed. A fluorescent non-polar analyte and fluorescein were loaded on the chromatographic bed and a complete separation was achieved after 20 seconds⁹⁸.

Bead-based techniques have been successfully adopted also for miniature bio-samplers, such as filter-less bio-separators, that allow the separation of target biomolecules or bacteria from a liquid ⁹⁹. Super-paramagnetic particles have been coated with antibodies

and controlled in a microfluidic channel with a planar electromagnet⁹⁹. When the magnetic field is applied, beads are held in the channel, and when antigens are injected, the bound antigens are retained while others are washed out with the flow. In the end magnetic beads are released to the sensing chamber for detection and the filterless bio-separator is ready for another separation.

Immunoassay, thanks to its high specificity, is one of the most important detection methods for clinical diagnosis and biochemical studies. Employing mobile beads in an immunosorbent assay leads to a very flexible system with attractive characteristics compared to conventional approaches¹⁰⁰. For example, a bead-based system provides simple and effective separation of the free and bound forms and allows heterogeneous immunosorbent assays to be performed within a microchannel. Polystyrene beads pre-absorbed with s-IgA (antigen) were introduced in a microchannel, reacted with colloidal gold conjugated anti-s-IgA (antibody) and detected by a thermal lens microscope. With this method the overall analysis time was reduced from 24 hours for the conventional homogeneous liquid phase immunoassay to 1 hour, avoiding numerous washing and solution removal procedures.

A bead system has also been employed for gene expression analysis. A so-called 'nanobarcode' based microbead assay has been developed to give an accurate and reproducible gene expression profile¹⁰¹. Four different quantum dot nanocrystal fluorescence emitters with different emission were mixed with a polymer and coated in magnetic microbeads to generate nanobarcode beads called Qbeads. Gene specific oligonucleotide probes were conjugated to the surface of each Qbead to create a panel which was able to decode an RNA target on the basis of the spectral profiles and intensity ratios of the four Qbeads. Unbound RNA can be easily washed out when the beads are exposed to a magnetic field. The gene expression data obtained with the beads was found to have a high correlation with reference Affymetrix Genechip microarray data. This nanobarcode system opens the way for a huge variety of applications in biology, chemistry and medical diagnosis and can potentially code more than one million combinations.

Similarly, a bi-functional system based on mesoporous silica beads embedded with both a semiconductor quantum dots for optical encoding and iron oxide for magnetic

separation has been developed¹⁰². Quantum dots have attractive properties such as size-tunable light emission, resistance against photobleaching and simultaneous excitation properties, while beads embedded with iron-oxide have been used for biological separation, capture of rare cells, proteins and nucleic acids. Functionalised magnetic nanoparticles have also been successfully used to control and switch the hydrophilicity/hydrophobicity of an electrode surface¹⁰³. A two-phase system, made up of water and toluene as the liquid phase and magnetic nanoparticles embedded with hydrophobic alkyl chains as a suspended solid phase, was placed in contact with an Au-electrode. Applying an external magnetic field on the electrode surface induced physical attraction of the particles to the electrode surface turning the surface hydrophobic. On the other hand, applying a magnetic field to the upper toluene phase induces the migration of the particles to this layer, generating a hydrophilic surface at the gold electrode (**figure 1.35**). Electrochemical switching of the conductive support surface has been demonstrated by performing magnetoswitchable bioelectrocatalytic oxidation of glucose in the presence of glucose oxidase and ferrocene dicarboxylic acid.

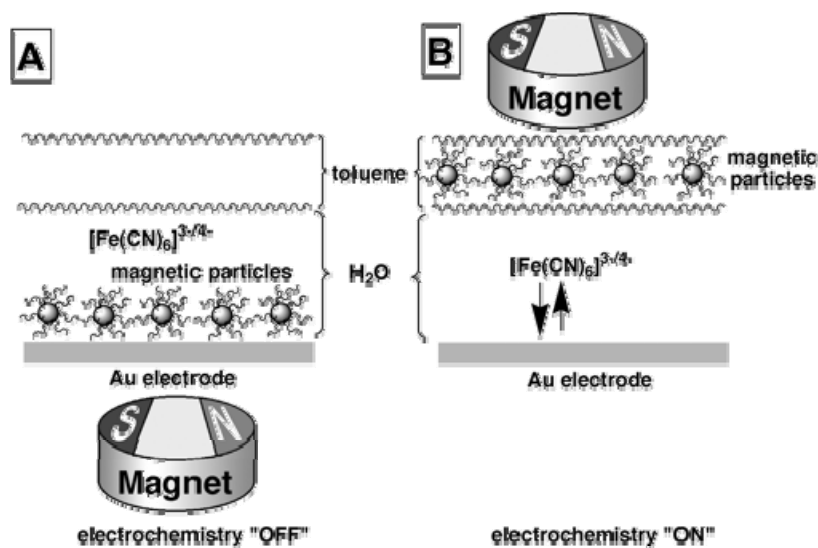


Figure 1.35: Magneto-controlled reversible translocation of the functionalized magnetic particles between the organic phase above the aqueous electrolyte and the electrode surface (A). The electrode surface is blocked with functionalized magnetic particles attracted to the electrode by the external magnet. (B) The magnetic particles are retracted from the electrode surface, and the electrode surface is electrochemically active. Reproduced from *Langmuir*, **2004**, 20, 9714-9719.

The removal of the magnetic particles from the electrode surface allows the oxidation of ferrocene dicarboxylic acid at the electrode surface and the bioelectrocatalyzed oxidation of glucose by glucose oxidase. This process is blocked by the attraction of the particles to the electrode. Hence, by means of a physical change (bead movement) it is possible to control a reactive interface using the chemical and mobility properties of a bead-based system.

Light-excitation is another mechanism for controlling the properties of microparticle systems. Light-modulation of spiropyran coated gold nanoparticles provides a potential system for the controlled release of aminoacids⁹⁶. A spiropyran modified derivative with a thiol chain was self-assembled onto a gold nanoparticle surface and the photoswitching of the Au-SP nanoparticles in the presence of various amino acid derivatives was investigated. The SP was excited with UV-light and converted to the MC form. Subsequently, it was demonstrated that the presence of certain amino acid derivatives stabilised the MC form, due to the formation of a stable complex between MC and the amino acid derivatives. Furthermore irradiation of the complex with visible-light triggers the reversion of the MC to the SP form, and releases of the guest species.

Following these exciting results the synthesis and the characterisation of the light-modulated properties of polystyrene and silica microbeads functionalised with spiropyran will be carried out in terms of photoswitchable metal binding ability.

1.7 Monoliths

The term “monolith” in separation science first appeared in 1992 and it was associated with a continuous rod of macroporous polymer used for protein separation¹⁰⁴. Later on this term was related to rigid macroporous polymers prepared by bulk polymerisation on a closed mold. The mold was typically a tube (fused silica capillary for example) sealed at one end, filled with the polymerisation mixture and sealed at the other end. The reaction is a free radical polymerisation usually triggered by light or UV irradiation

The so-formed monolith typically exhibits a well defined macroporous structure which consists of numerous interconnected cavities of different sizes, with a structural rigidity due to extensive cross linking. The formation of the porous structure is secured by the

addition of a porogen to the polymerisation mixture that can be for example a non-solvating solvent for the polymer.

Monoliths have found extensive applications in separation science as stationary phases to separate different type of analytes, such as mixtures of aromatic compounds, peptides and protein^{105,106}. Their use is an alternative to microparticles packed columns, commonly used in standard chromatography¹⁰⁷.

Monoliths and packed microparticles are interesting platforms for the fabrication of separation devices on chips which are an important step forward towards new approaches to high throughput chemical and biological analysis.

1.8 Microfluidics and lab on a chip devices

The concept of ‘micro-total analysis systems’ or μ TAS was introduced by Manz et al. around 1990¹⁰⁸ and in the USA it rapidly became known as lab-on-a-chip (LOAC). At its core, the concept involved integrating multiple separate operations (sampling, sample processing, reagent addition, calibration, detection, etc.) into a compact, integrated, microfluidic manifold, which had channel dimensions typically in the range 10-500 μ m, to both speed up sample throughput and improve precision. Since then, this has become a huge area of research¹⁰⁹⁻¹¹¹.

One of the main limitations of LOAC devices arises from difficulties in finding liquid handling/transport approaches that are truly compatible with scaled down microfluidic manifolds. Most published work involves the use of bench-scale pumps and external valves, with the emphasis being on the improved sample handling capabilities of the integrated microfluidics system, and reduced reagent consumption/waste generation. Furthermore, attempts to produce integrated systems typically involve the use of scaled-down conventional pumps/valves produced by micromachining. While this has produced some very elegantly engineered systems, there is a growing realisation that the next evolution of these devices requires completely new approaches to integration of liquid handling functions, and that the solution to this issue lays in fundamental materials science, and new ways of thinking about microfluidics. For example, Whitesides and coworkers have demonstrated valve-effects using distortions in soft polymers¹¹², while others propose more biomimetic solutions, in which the microfluidic

manifold is regarded as a primitive mimic of a biological circulation system, and biologically inspired routes to generation fluid circulation are employed, for example, using the ‘artificial muscle’ function exhibited by some redox active soft polymers. Wallace et al. produced a pump based on the expansion/contraction cycle accompanying oxidation/reduction of polypyrrole deposited on a water permeable tube. Application of an oxidising potential at one end of the tube generated a peristalsis-type expansion-wave that migrated along the surface, carrying water with it¹¹³. Recently, a biomimetic soft polymer pump was demonstrated based on polypyrrole nafion actuators compressing a soft-walled polyurethane/polydimethylsiloxane chamber¹¹⁴. These pumps offer advantages in terms of relatively low energy requirements, and are ultimately more compatible with microfluidics as their soft nature makes them much less prone to physical malfunction due to, for example, ingress of microparticulates, than conventional micro-engineered pumps and valves. For an introduction to biomimetics related to sensors, actuators and artificial muscles¹¹⁵.

LOAC devices, in principle, offer a route to the incorporation of sophisticated chemo/bio processing steps in a compact, low-power platform, which is attractive for remote sample processing (phase extraction, separation steps, reagent additions, calibration etc.). Therefore these devices offer a compromise between existing lab-based instruments, and the vision of tiny, completely self-sustaining sensors capable of massive scale up. The limiting factor is now probably the need for reagents and waste storage/disposal. Ideally, these devices should be able to generate their own reagents on demand (e.g. electrochemical generation of protons or hydroxide ions to provide localized control of pH), but we are still a long way from this ideal vision of completely self-sustaining chemo/bio sensing devices.

1.9 Conclusions

Molecules which respond to different external stimuli and exhibit macroscopic changes due to variation in their molecular structure can be exploited for the realisation of new adaptive material that can found a wide variety of applications in chemical and biological sciences.

In the literature there are many reported examples on how, through the modification of different substrates using “smart molecules”, it is possible to operate an external control over the surface structure at a molecular level in order to move liquid across a surface, to operate a control over the binding process or to modulate its electrochemical properties. When the molecular rearrangement corresponds to a colour change which is induced by light exposure, the phenomenon is called photochromism and it allows external manipulation of physical or chemical properties of a compound simply using light irradiation.

Photochromic molecules such as spiropyrans has the ability of reversibly switch between a strongly coloured MC form, which forms as a consequence of UV-light irradiation and a leuco SP form and, by exposure to white light. The two isomers present different physical and chemical properties and the equilibrium is also influenced by solvent medium and temperature. In the presence of certain metal ions, the characteristic MC visible absorption band shifts, making possible an additional level of recognition. This allows visual identification of the complex with particular metal guests, so that the the SP, MC and MC-M²⁺ complex can be spectroscopically distinguished and monitored and the three states can be externally controlled using light.

Integrating spiropyran photoswitches within a sensing platform, this can be switched between a strongly coloured, polar, guest binding form and a colourless, non-polar form on demand. This has found a wide range of applications in material and analytical science which ranges from optical memories to the control over biomolecules activity.

This particular research is focused on their application to the reversible binding of guest species and to changes in polarity induced by light exposure.

On this purpose, the functionalisation and characterisation of polystyrene and silica microbeads together with molithic stationary phases with different *ad hoc* synthesised spiropiran derivatives will be further discussed.

Solution studies will be initially performed to study the photoswitchable activity of the photochromic molecule that will be then compared to the results obtained for the characterisation of the same molecule after substrate immobilisation using new set-ups to characterise the adaptive materials.

Microbeads are high surface area bi-phase system which offers interesting possibilities for sensing and analytical applications. Combining spiropyran photochromic derivatives into microbeads-based systems it is possible to generate a versatile, externally controlled, high surface area platform which can be switched between two states with different physical and chemical properties and binding abilities and eventually incorporated into flow-systems.

Together with packed microbeads, polymeric organic monoliths provide another platform which can be functionalised to acquire new properties and can be easily incorporated into microscale devices towards the development of analytical or sensing units which combine adaptive material with multiple functionalities, able to perform the analytical or sensing activity on a microscale without the necessity for high-power consumption pumping, valve or calibrating devices which limits their employment on a large scale.

Incorporating the spiropyran functionalised beads and monoliths into flow systems it possible to exploit their new photochromic properties to obtain reversibly photoswitchable metal binding and light tunable electro-osmotic flow (EOF).

Fundamental research on new adaptive material is the key for the future development of new autonomous analytical and sensing devices.

1.10 Thesis Overview

In the following chapter the photochromic behaviour in solution of an ISNBP is discussed in terms of solvatochromism, ionochromism and halochromism, in order to provide a series of reference studies for the further characterisation of spiropyran functionalised materials.

In parallel a new set-up for reflectance measurements using ocean optic spectrophotometer is evaluated for recording colour and spectral changes on polystyrene microbeads and monolith, in which a strong light scattering effect prevent the use of absorption methods.

In chapter three and four, the synthesis and the characterisation of silica and polystyrene microbeads is discussed and their photo-reversible metal binding behaviour evaluated towards a range of metal ions.

In chapter five the incorporation of spiropyran functionalised silica microbeads on capillary columns was performed. This packed column behaviour is described as an example of photodynamic system for retention, detection and release of metal ions pumped into the capillary. Together with the silica bead-based stationary phase a microfluidic chip for electro-osmotic flow measurement is produced. On the microchip are encased polymeric spiropyran monoliths that can be photo-reversibly protonated. Once a voltage is applied to the microchip, electro-osmotic flow is generated and the presence of spiropyran allows reversible photo-modulation of the flow due to photo-reversible protonation of the spiropyran derivatives which is co-polymerised in the monolith. In the final chapter conclusions are drawn and future work discussed.

1.11 References

- (1) Diamond, D. *Analytical Chemistry* **2004**, *76*, 278A-286A.
- (2) Byrne, R.; Diamond, D. *Nature Materials* **2006**, *5*, 421-424.
- (3) Stitzel, S.; Byrne, R.; Diamond, D. *Journal of Materials Science* **2006**, *41*, 5841-5844.
- (4) Scarmagnani, S.; Walsh, Z.; Slater, C.; Alhashimy, N.; Paull, B.; Macka, M.; Diamond, D. *Journal of Materials Chemistry* **2008**, *18*, 5063-5071.
- (5) Radu, A.; Scarmagnani, S.; Byrne, R.; Slater, C.; Lau, K. T.; Diamond, D. *Journal of Physics D: Applied Physics* **2007**, 7238-7244.
- (6) Gopalakrishnan, S.; Liu, D.; Allen, H. C.; Kuo, M.; Shultz, M. J. *Chemical Reviews* **2006**, *106*, 1155-1175.
- (7) Verdaguer, A.; Sacha, G. M.; Bluhm, H.; Salmeron, M. *Chemical Reviews* **2006**, *106*, 1478-1510.
- (8) Grunze, M. *Science* **1999**, *283*, 41-42.

- (9) Gugliotti, M. *Journal of chemical education* **2004**, *81*, 67-68.
- (10) Scriven, L. E.; Sterling, C. V. *Nature* **1960**, *187*, 186-188.
- (11) Wasan, D. T.; Nikolov, A. D.; Brenner, H. *Science* **2001**, *291*, 605-606.
- (12) Bull, J. L.; Grotberg, J. *Exp. Fluids* **2003**, *34*, 1.
- (13) Chaudhury, M. K.; Whitesides, G. M. *Science* **1992**, *256*, 1539-1541.
- (14) Kuiper, S.; Hendriks, B. H. W. *Applied Physics Letters* **2004**, *85*, 1128-1130.
- (15) Cheng, Y. T.; Rodak, D. E.; Wong, C. A.; Hayden, C. A. *Nanotechnology* **2006**, *17*, 1359-1362.
- (16) Tsu-Te, W.; Po-Wen, H.; Shih-Kang, F. International Conference on Micro Electro Mechanical Systems (MEMS) Istanbul, 2006; p 174-177.
- (17) Pollack, M. G.; Fair, R. B.; Shenderov, A. D. *Applied Physics Letters* **2000**, *77*, 1725-1726.
- (18) Ichimura, K.; Oh, S.-K.; Nakagawa, M. *Science* **2000**, *288*, 1624-1626.
- (19) Sekkat, Z.; Wood, J.; Geerts, Y.; Knoll, W. *Langmuir* **1995**, *11*, 2856-2859.
- (20) Wang, X.; Cheng, C.; Wang, S.; Liu, S. *Microfluidics and Nanofluidics* **2009**, *6*, 145-162.
- (21) Zeng, S.; Chen, C.-H.; Mikkelsen, J. C.; Santiago, J. G. *Sensors and Actuators B: Chemical* **2001**, *79*, 107-114.
- (22) Nie, F.-Q.; Macka, M.; Paull, B. *Lab on a Chip* **2007**, *7*, 1597-1599.
- (23) Liu, Y.; Baohong, L. M.; Kong, L. J. *Chemistry - A European Journal* **2005**, *11*, 2622-2631.
- (24) Bryce, M. R.; Cooke, G.; Duclairoir, F. M. A.; John, P.; Perepichka, D. F.; Polwart, N.; Rotello, V. M.; Stoddart, J. F.; Tseng, H.-R. *Journal of Materials Chemistry* **2003**, *13*, 2111-2117.

- (25) Kyunpil Kim; Jeon, W. S.; Kang, J.-K.; Lee, J. W.; Jon, S. Y.; Kim, T.; Kim, K. *Angewandte Chemie* **2003**, *115*, 2395-2398.
- (26) Lahann, J.; Mitragotri, S.; Tran, T.-N.; Kaido, H.; Sundaram, J.; Choi, I. S.; Hoffer, S.; Somorjai, G. A.; Langer, R. *Science* **2003**, *299*, 371-374.
- (27) Liu, Y.; Mu, L.; Liu, B.; Zhang, S.; Yang, P.; Kong, J. *Chemical Communications* **2004**, 1194-1195.
- (28) Christie, R. M. *Colour Chemistry*; RSC Paperbacks, 2001.
- (29) Bamfield, P. *Chromic Phenomena - Technological Applications of Colour Chemistry*; RSC Paperbacks, 2001.
- (30) Johnson, R. D.; Gavalas, V. G.; Daunert, S.; Bachas, L. G. *Analytica Chimica Acta* **2008**, *613*, 20-30.
- (31) Dürr, H.; Bouas, L. H. *Photochromism - molecules and systems*; Elsevier: Amsterdam, Boston, 2003.
- (32) Byrne, R. J.; Stitzel, S. E.; Diamond, D. *Journal of Materials Chemistry* **2006**, *16*, 1332-1337.
- (33) Crano, J. C.; Flood, T.; Knowles, D.; Kumar, A.; Van Gemert, B. *Pure and Applied Chemistry* **1996**, *68*, 1395-1398.
- (34) Dvornikov, A. S.; Malkin, J.; Rentzepis, P. M. *J. Phys. Chem.* **1994**, *98*, 6746-6752.
- (35) Willner, I.; Rubin, S.; Shatzmiller, R.; Zor, T. *Journal of the American Chemical Society* **2002**, *115*, 8690-8694.
- (36) Winkler, J. D.; Deshayes, K.; Shao, B. *Journal of the American Chemical Society* **1989**, *111*, 769-770.

- (37) Collins, G. E.; Morris, R. E.; Wei, J.-F.; Smith, M.; Hammond, M. H.; Michelet, V.; Winkler, J. D.; Serino, P. M.; Guo, Y. *Energy & Fuels* **2002**, *16*, 1054-1058.
- (38) Evans, L.; Collins, G. E.; Shaffer, R. E.; Michelet, V.; Winkler, J. D. *Analytical Chemistry* **1999**, *71*, 5322-5327.
- (39) Suzuki, T.; Kato, T.; Shinozaki, H. *Chemical Communication* **2004**, 2036-2037.
- (40) Kobatake, S.; Irie, M. *Annual Reports Section "C" (Physical Chemistry)* **2003**, *99*, 277-313.
- (41) Minkin, V. I. *Chemical Reviews* **2004**, *104*, 2751-2776.
- (42) Raymo, F. M.; Giordani, S. *Journal of the American Chemical Society* **2001**, *123*, 4651-4652.
- (43) Görner, H.; Chibisov, A. K. *Journal of the Chemical Society, Faraday Transactions* **1998**, *94*, 2557-2564.
- (44) Fischer, E.; Hirshberg, Y. *Journal of the Chemical Society* **1952**, 4522-4524.
- (45) Crano, J. C.; Guglielmetti, R. J. *Organic photochromic and thermochromic compounds*; Kluwer Academic/Plenum Publishers: New York, 1999.
- (46) Simmons, H. E.; Fukunaga, T. *Journal of the American Chemical Society* **2002**, *89*, 5208-5215.
- (47) Maslak, P.; Chopra, A.; Moylan, C. R.; Wortmann, R.; Lebus, S.; Rheingold, A. L.; Yap, G. P. A. *Journal of the American Chemical Society* **1996**, *118*, 1471-1481.
- (48) Maslak, P.; Chopra, A. *Journal of the American Chemical Society* **1993**, *115*, 9331-9332.
- (49) Celani, P.; Bernardi, F.; Olivucci, M.; Robb, M. A. *Journal of the American Chemical Society* **1997**, *119*, 10815-10820.

- (50) Ernsting, N. P.; Arthen-Engeland, T. *The Journal of Physical Chemistry* **1991**, *95*, 5502-5509.
- (51) *IUPAC Compendium of Chemical Terminology - the Gold Book*; International Union of Pure and Applied Chemistry, 2009
- (52) Aldoshin, S. M. *Russian Chemical Reviews* **1990**, 663-684.
- (53) Kholmanskii, A. S.; Dyumaev, K. M. *Russian Chemical Reviews* **1987**, 136-151.
- (54) Zhang, J. Z.; Schwartz, B. J.; King, J. C.; Harris, C. B. *Journal of the American Chemical Society* **2002**, *114*, 10921-10927.
- (55) Morley, J. O.; Morley, R. M.; Docherty, R.; Charlton, M. H. *Journal of the American Chemical Society* **1997**, *119*, 10192-10202.
- (56) Aramaki, S.; Atkinson, G. H. *Journal of the American Chemical Society* **2002**, *114*, 438-444.
- (57) Görner, H. *Physical Chemistry Chemical Physics* **2001**, *3*, 416-423.
- (58) Rosario, R.; Gust, D.; Hayes, M.; Jahnke, F.; Springer, J.; Garcia, A. A. *Langmuir* **2002**, *18*, 8062-8069.
- (59) Nakajima, N.; Ikada, Y. *Bioconjugate Chemistry* **2002**, *6*, 123-130.
- (60) McCoy, C. P.; Donnelly, L.; Jones, D. S.; Gorman, S. P. *Tetrahedron Letters* **2007**, *48*, 657-661.
- (61) Szilagyi, A.; Sumaru, K.; Sugiura, S.; Takagi, T.; Shinbo, T.; Zrinyi, M.; Kanamori, T. *Chemistry of Materials* **2007**, *19*, 2730-2732.
- (62) Baillet, G.; Campredon, M.; Guglielmetti, R.; Giusti, G.; Aubert, C. *Journal of Photochemistry and Photobiology A: Chemistry* **1994**, *83*, 147-151.
- (63) Baillet, G.; Giusti, G.; Guglielmetti, R. *Journal of Photochemistry and Photobiology A: Chemistry* **1993**, *70*, 157-161.

- (64) Matsushima, R.; Nishiyama, M.; Doi, M. *Journal of Photochemistry and Photobiology A: Chemistry* **2001**, *139*, 63-69.
- (65) Li, X.; Li, J.; Wang, Y.; Matsuura, T.; Meng, J. *Journal of Photochemistry and Photobiology A: Chemistry* **2004**, *161*, 201-213.
- (66) Bilski, P.; McDevitt, T.; Chignell, C. F. *Photochemistry and Photobiology* **1999**, *69*, 671-676.
- (67) Demadrille, R.; Rabourdin, A.; Campredon, M.; Giusti, G. *Journal of Photochemistry and Photobiology A: Chemistry* **2004**, *168*, 143-152.
- (68) Monjushiro, H.; Hirai, A.; Watarai, H. *Langmuir* **2000**, *16*, 8539-8542.
- (69) Tork, A.; Boudreault, F.; Roberge, M.; Ritcey, A. M.; Lessard, R. A.; Galstian, T. V. *Applied Optics* **2001**, *40*, 1180-1186.
- (70) Radu, A.; Byrne, R.; Alhashimy, N.; Fusaro, M.; Scarmagnani, S.; Diamond, D. *Journal of Photochemistry and Photobiology A: Chemistry* **2009**, *206*, 109-115.
- (71) Lau, K.-T.; Yerazunis, W. S.; Shepherd, R. L.; Diamond, D. *Sensors and Actuators B: Chemical* **2006**, *114*, 819-825.
- (72) Collins, G. E.; Choi, L.-S.; Ewing, K. J.; Michelet, V.; Bowen, C. M.; Winkler, J. D. *Chemical Communication* **1999**, 321-322.
- (73) Wojtyk, J. T. C.; Buncel, E.; Kazmaier, P. M. *Chemical Communications* **1998**, 1703 - 1704.
- (74) Wojtyk, J. T. C.; Kazmaier, P. M.; Buncel, E. *Chemistry of Materials* **2001**, *13*, 2547-2551.
- (75) Yagi, S.; Nakamura, S.; Watanabe, D.; Nakazumi, H. *Dyes and Pigments* **2009**, *80*, 98-105.

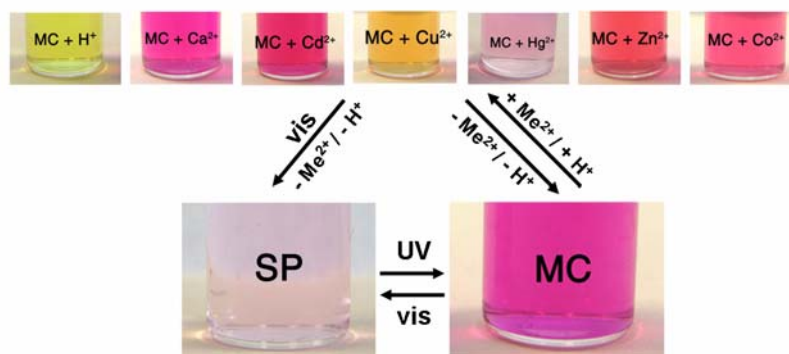
- (76) Filley, J.; Ibrahim, M. A.; Nimlos, M. R.; Watt, A. S.; Blake, D. M. *Journal of Photochemistry and Photobiology A: Chemistry* **1998**, *117*, 193-198.
- (77) Chibisov, A. K.; Gorner, H. *Chemical Physics* **1998**, *237*, 425-442.
- (78) Zhou, J.-W.; Li, Y.-T.; Song, X.-Q. *Journal of Photochemistry and Photobiology A: Chemistry* **1995**, *87*, 37-42.
- (79) Khairutdinov, R. F.; Hurst, J. K. *Langmuir* **2001**, *17*, 6881-6886.
- (80) Khairutdinov, R. F.; Hurst, J. K. *Langmuir* **2004**, *20*, 1781-1785.
- (81) Sakamoto, H.; Takagaki, H.; Nakamura, M.; Kimura, K. *Analytical Chemistry* **2005**, *77*, 1999-2006.
- (82) Wen, G.; Yan, J.; Zhou, Y.; Zhang, D.; Mao, L.; Zhu, D. *Chemical Communications* **2006**, 3016-3018.
- (83) Drummond, C. J.; Furlong, D. N. *Journal of the Chemical Society, Faraday Transactions* **1990**, *86*, 3613 - 3621.
- (84) Roxburgh, C. J.; Sammes, P. G. *Dyes and Pigments* **1995**, *27*, 63-69.
- (85) Chernyshev, A. V.; Chernov'yants, M. S.; Voloshina, E. N.; Voloshin, N. A. *Russian Journal of General Chemistry* **2002**, 1468-1472.
- (86) Berkovic, G.; Krongauz, V.; Weiss, V. *Chem. Rev.* **2000**, *100*, 1741-1754.
- (87) Willner, I. *Accounts of Chemical Research* **1997**, *30*, 347-356.
- (88) Hirshberg, Y. *Journal of the American Chemical Society* **1956**, *78*, 2304-2312.
- (89) Guo, X.; Zhang, D.; Yu, G.; Wan, M.; Li, J.; Liu, Y.; Zhu, D. *Advanced Materials* **2004**, *16*, 636-640.
- (90) Kim, K.; Jeon, W. S.; Kang, J.-K.; Lee, J. W.; Jon, S. Y.; Kim, T.; Kim, K. *Angew. Chem. Int. Edit.* **2003**, *115*, 2395.
- (91) Wedemeyer, N.; Potter, T. *Clinical Genetics* **2001**, *60*, 1-8.

- (92) Haukanes, B.-I.; Kvam, C. *Nat Biotech* **1993**, *11*, 60-63.
- (93) Sinha, V. R.; Goyal, V.; Bhinge, J. R.; Mittal, B. R.; Trehan, A. *Critical Reviews™ in Therapeutic Drug Carrier Systems* **2003**, *20*, 431-460.
- (94) Margel, S.; Beitler, U.; Ofarim, M. *J Cell Sci* **1982**, *56*, 157-175.
- (95) Windler-Hart, S.; Chen, K.; Chenn, A. *BMC Cell Biology* **2005**, *6*.
- (96) Ipe, B. I.; Mahima, S.; Thomas, K. G. *Journal of the American Chemical Society* **2003**, *125*, 7174-7175.
- (97) Demir, A.; Serpenguzel, A. *IEE Proceedings - Nanobiotechnology* **2005**, *152*, 105-108.
- (98) Oleschuk, R. D.; Shultz-Lockyear, L. L.; Ning, Y.; Harrison, D. J. *Anal. Chem.* **2000**, *72*, 585-590.
- (99) Choi, J.-W.; Ahn, C. H.; Bhansali, S.; Henderson, H. T. *Sensors and Actuators B: Chemical* **2000**, *68*, 34-39.
- (100) Sato, K.; Tokeshi, M.; Odake, T.; Kimura, H.; Ooi, T.; Nakao, M.; Kitamori, T. *Anal. Chem.* **2000**, *72*, 1144-1147.
- (101) Eastman, P. S.; Ruan, W.; Doctolero, M.; Nuttall, R.; deFeo, G.; Park, J. S.; Chu, J. S. F.; Cooke, P.; Gray, J. W.; Li, S.; Chen, F. F. *Nano Lett.* **2006**, *6*, 1059-1064.
- (102) Sathe, T. R.; Agrawal, A.; Nie, S. *Anal. Chem.* **2006**, *78*, 5627-5632.
- (103) Katz, E.; Sheeney-Haj-Ichia, L.; Basnar, B.; Felner, I.; Willner, I. *Langmuir* **2004**, *20*, 9714-9719.
- (104) Svec, F.; Frechet, J. M. J. *Analytical Chemistry* **1992**, *64*, 820-822.
- (105) Yu, C.; Svec, F.; Fréchet, J. M. J. *Electrophoresis* **2000**, *21*, 120-127.
- (106) Belenkii, B. *Russian Journal of Bioorganic Chemistry* **2006**, *32*, 323-332.

- (107) Unger, K. K.; Skudas, R.; Schulte, M. M. *Journal of Chromatography A* **2008**, *1184*, 393-415.
- (108) West, J.; Becker, M.; Tombrink, S.; Manz, A. *Analytical Chemistry* **2008**, *80*, 4403-4419.
- (109) Paik, P.; Pamula, V. K.; Pollack, M. G.; Fair, R. B. *Lab on a Chip* **2003**, *3*, 28-33.
- (110) Terray, A.; Oakey, J.; Marr, D. W. M. *Science* **2002**, *296*, 1841-1844.
- (111) Vestad, T.; Marr, D. W. M.; Oakey, J. *Journal of Micromechanics and Microengineering* **2004**, *14*, 1503-1506.
- (112) Weibel, D. B.; Kruithof, M.; Potenta, S.; Sia, S. K.; Lee, A.; Whitesides, G. M. *Analytical Chemistry* **2005**, *77*, 4726-4733.
- (113) Wu, Y.; Zhou, D.; Spinks, G. M.; Innis, P. C.; Megill, W. M.; Wallace, G. G. *Smart Materials and Structures* **2005**, 1511-1516.
- (114) Ramirez-Garcia, S.; Diamond, D. *Journal of Intelligent Material Systems and Structures* **2007**, *18*, 159 - 164.
- (115) Myers, R.; Vickers, M.; Kim, H.; Priya, S. *Applied Physics Letters* **2007**, *90*, 054106.

CHAPTER 2

PRELIMINARY STUDIES



2.1 Introduction

Polymeric and inorganic microbeads have been widely used the past few decades for different biological and chemical sensing applications¹⁻⁴ due to their high surface area and their versatility. They provide a solid support that can be moved as a solution and easily separated as a solid phase from the suspension medium by sonication. They also can be used as stationary phases in separation science as they can be incorporated into separation columns^{5,6}.

The incorporation of spiropyran on microparticle systems offers the interesting possibility of combining the photochromic properties of spiropyran and the advantage of having it on such a flexible solid support.

Before the functionalisation was performed, solution studies were carried out, as a reference for further characterisation of the spiropyran modified microbeads.

Among the different spiropyran derivatives, 1',3'-dihydro-1',3',3'-trimethyl-6-nitrospiro [2H-1] benzopyran-2, 2'-(2H)-indole (**SP-1**, **figure 2.1**) was chosen because of the rapid switching, dramatic colour change induced by UV irradiation (due to the presence of a nitro electron withdrawing group on the benzopyran ring) and the ability of its MC to form complexes with metal ions⁷⁻⁹ as described in the **Chapter 1 (Introduction)**. Upon UV irradiation of SP-1 the coloration is strongly and rapidly enhanced and this photochemical ring opening occurs in the sub-ns range¹⁰.

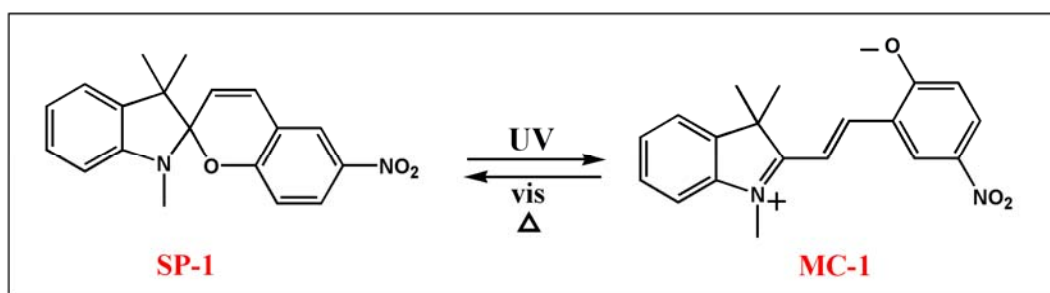


Figure 2.1: Structures and photochromic equilibrium between SP-1 and MC-1.

In parallel, studies on the new experimental set-up for optical measurements on microbeads were necessary. Polymeric microbeads such as polystyrene, present very

strong scattering effects which can impede the use of absorbance and transmittance based methods.

Reflectance presents an interesting alternative to transmittance and absorbance spectroscopic measurements and can be evaluated using optic fibres and a miniature diode array spectrometer¹¹. Using different *ad hoc* prepared experimental designs, reflectance measurements technique has been applied to evaluate the colouration of microbead suspensions, and monolith filled capillaries which are used in separation techniques.

2.2 SOLUTION STUDIES ON SP-1

2.2.1 Experimental: Materials and instruments

1',3'-dihydro-1',3',3'-trimethyl-6-nitrospiro [2H-1] benzopyran-2, 2'-(2H)-indole (**SP-1**, **figure 2.1**), calcium nitrate hydrate, copper(II) nitrate trihydrate, calcium chloride hexahydrate, mercury(II) chloride, zinc chloride, cadmium nitrate tetrahydrate, cobalt(II) nitrate hexahydrate were purchased from Sigma Aldrich (Ireland).

Hydrochloric acid 32%, density 1.16 g/cm³ was purchased from Fisher Scientific. BONDwand UV-365 nm was purchased from Electrolite Corporation. As a white light source a Lloytron 60W desk lamp was used.

Absorbance spectra were recorded using an Absorbance Plate Reader (BioTek Instruments, Inc., USA) for the ion-binding evaluation experiments and a Perkin Elmer UV-vis Spectrometer Lambda 900 for the absorbance measurement of spiropyran in different solvents.

2.2.2 Spectroscopic studies on response characteristics of MC-1 in different solvents

10⁻³ M Stock solution of SP-1 in ethanol, acetonitrile, toluene, acetone, DMF and chloroform were prepared by dissolving 3 mg of SP-1 in 10 ml of the corresponding solvent and stored in the dark at room temperature.

Then 3 ml of each solution were exposed to 1 minute UV light irradiation and the absorbance spectra were recorded. Then the absorbance value at the MC λ_{\max} in each solvent was monitored every second for 180 seconds in order to evaluate the ring closing kinetic over time.

2.2.3 Spectroscopic studies on response characteristics of MC-1 ion complexes in ethanol solutions

10^{-2} M, 10^{-3} M, 5×10^{-2} M, 5×10^{-3} M, 5×10^{-4} M standard solutions of Ca^{2+} , Hg^{2+} , Cd^{2+} and H^{+} and 10^{-2} M, 10^{-3} M, 10^{-4} M, 5×10^{-3} M, 5×10^{-4} M, 5×10^{-5} M standard solutions of Co^{2+} , Cu^{2+} , Zn^{2+} were prepared by dissolving the corresponding chloride and nitrate salts in ethanol by serial dilutions of 10^{-1} M stock solutions of each salts. 10^{-3} M stock solutions of SP-1 in ethanol were prepared and stored in the dark at room temperature.

Solution studies were performed using ethanolic solutions of spiropyran which were irradiated with UV light and then added with the previously prepared guest solutions. Absorbance spectra were recorded using a plate well reader with the following procedure:

- Aliquots of 1.5 ml of SP-1 10^{-3} M stock solution were placed in plate wells.
- The solutions were irradiated for 1 minute with UV light and the spectra were recorded immediately after.
- In all the plate wells, except for one, 0.05 ml of each metal ion solution at differing concentrations was added at the same time using a multi channel automatic pipette. Final concentrations: 3.2×10^{-3} M (from 0.05 ml of 10^{-1} M metal stock solution), 1.6×10^{-3} M (from 0.05 ml of 5×10^{-2} M stock solution), 3.2×10^{-4} M (from 0.05 ml of 10^{-2} M stock solution), 1.6×10^{-4} M (from 0.05 ml of 5×10^{-3} M stock solution), 3.2×10^{-5} M (from 0.05 ml of 10^{-3} M stock solution), 1.6×10^{-5} M (from 0.05 ml of 5×10^{-4} M stock solution), 3.2×10^{-6} M (from 0.05 ml of 10^{-4} M stock solution), 1.6×10^{-6} M (from 0.05 ml of 5×10^{-5} M stock solution). In the last well 0.05 ml of ethanol was added and the sample kept as a reference.
- The absorbance spectra of the solutions were taken immediately after the addition.

2.3 Results and discussion

2.3.1 Response characteristics of MC-1 in different solvents

As previously described, the spiropyran photomerocyanine is well known to undergo solvatochromism. Solvatochromism refers to a strong dependence of the UV-vis absorption bands of a compound on the polarity of the solvent medium which typically involves changes in the position and intensity of the absorption bands of the molecule when measured in different solvents. These changes are caused by intermolecular interactions between the solute and solvent that modify the energy gap between the ground and excited state of the absorbing species¹⁰.

Spectroscopic studies were carried out on MC-1 dissolved in different solvents (**figure 2.2**).

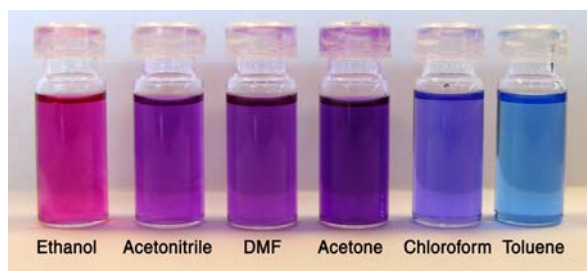


Figure 2.2: Picture showing the colour changes of MC-1 (10^{-3} M) in six different solvents.

The λ_{\max} of MC-1 undergoes red and blue shifts depending on the solvent type (**table 2.1**). Among the solvents analysed, the lowest λ_{\max} value is found with ethanol (540 nm). This value increases to 558 nm in acetonitrile, 560 nm in acetone and 562 nm in DMF. The highest values are observed for chloroform (578 nm) and toluene (605 nm) (**figure 2.3**).

In the absorbance spectra of the MC in toluene a shoulder around 565 nm is clearly defined. This can be attributed to the presence of aggregates which are well known to form for MC forms in non-polar solvents under UV-irradiation¹²⁻¹⁴. In general two types of aggregates have been identified: J-aggregates which have parallel arrangement are shifted to longer wavelengths, while H-aggregates have a head to tail arrangement of the MC dipoles and the spectra are shifted to shorter wavelengths.

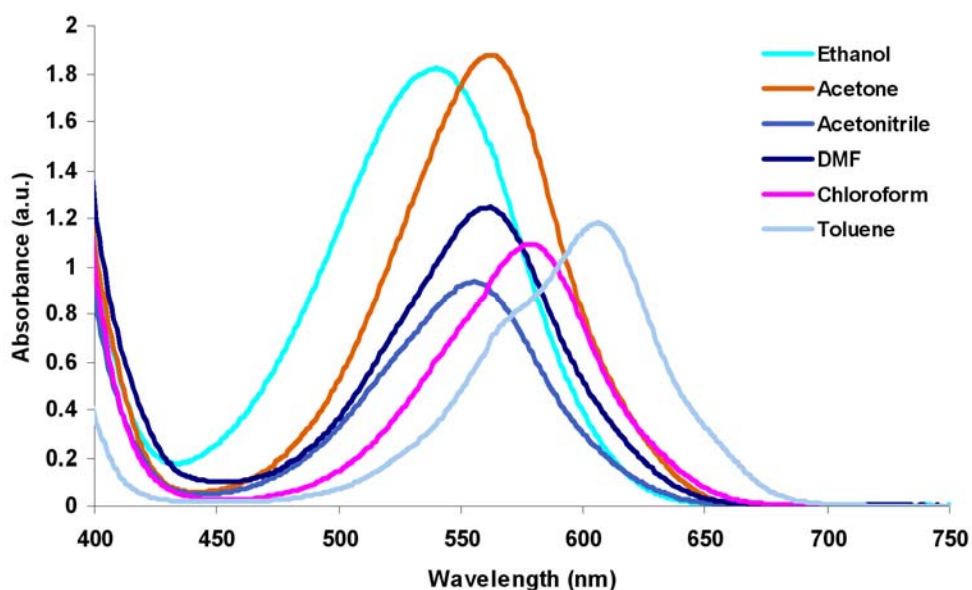


Figure 2.3: Absorbance spectra of MC-1 in six different solvent (concentration 10^{-3} M). MC-1 λ_{\max} undergoes blue shift as the solvent polarity increases (the lowest MC-1 λ_{\max} is 540 nm in ethanol) and red shift as the solvent become more unpolar (the highest MC-1 λ_{\max} is 605 nm in toluene).

According to the solvent polarity scale described on the “Handbook of Solvents” (SPP scale)¹⁵, based on two ideal molecular probes (DMANF and FNF, respectively 2-methylamino-7-nitrofluorene and 2-fluoro-7-nitrofluorene, **figure 2.4**) DMF is the more polar solvents (0.939), followed by acetonitrile (0.895), acetone (0.881), ethanol (0.853), chloroform (0.786) with toluene being the more non-polar (0.786).

Analysing the absorbance shifts happening with the MC-1 isomer in different solvents, they are in agreement with the SPP scale, except for DMF and ethanol.

DMF according to the SPP scale is the most polar among the six solvents, with a value of 0.939, while ethanol has an intermediate polarity value of 0.853, after acetonitrile and acetone. Contrary to expectations MC-1 shows the lowest λ_{\max} in ethanol and an intermediate λ_{\max} for DMF, after acetonitrile and acetone.

This is probably due to MC-1 structural changes by effect of the solvent nature (for example transition among different tautomeric forms) which affects the equilibrium between the different MC isomers. This does not occur with DMANF and FNF, which

have been chosen for their high sensitivity to solvent polarity without undergoing structural changes due to the solvent nature.

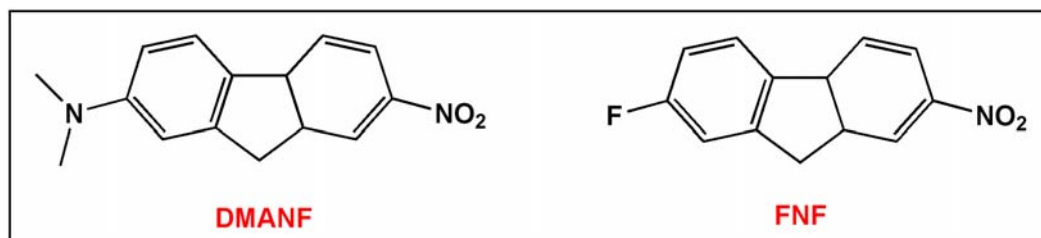


Figure 2.4: Structures of DMANF and FNF molecular probes which are used to determine the SPP solvent polarity scale.

Kinetic studies were performed in order to evaluate how the solvents affect the ring closing kinetics of the MC-1 form, which is known to follow first order kinetics¹⁶.

This involved inducing the formation of the MC-1 state by exposure to the UV light for 1 minute, and recording the absorbance value of the MC-1 at the λ_{max} in each solvent at fixed time intervals (every 1 s for 180 s) as equilibrium is re-established between the SP and MC forms. During these measurements, the sample is kept in the dark to avoid the influence of the ambient light on the reversion to the SP-1 form (**figure 2.5** and **figure 2.6**).

The first order rate constants were estimated by fitting the normalised reflectance values at 560 nm using Microsoft Excel Solver^{17,18} using the following equation (**table 2.1**):

$$y = ae^{k_R t} + b \quad [2.1]$$

where y is the normalised absorbance value at the MC-1 λ_{max} on each solvent, a is the pre-exponential factor, k_R is the rate constant and b is the asymptotic value.

Our results show that the ring closing kinetic of the MC towards the SP form strongly depends on the solvent type and the calculated values are in accordance with the relaxation times reported by Görner¹⁶.

In toluene, the ring closing is extremely fast and within 100 sec the MC-1 is completely reconverted back to SP-1 form with a k_R value of $4.0 \times 10^{-2} \text{ s}^{-1}$.

In chloroform the k_R value increases to $1.4 \times 10^{-2} \text{ s}^{-1}$ and the complete conversion to the SP form is not verified within 180 s. In comparison, the relaxation time kinetics of more polar solvents such as ethanol, DMF, acetonitrile and acetone are noticeably lower. For toluene and chloroform the k_R value for MC-1 \rightarrow SP-1 conversion is respectively 7.7 and 22 times faster than in ethanol.

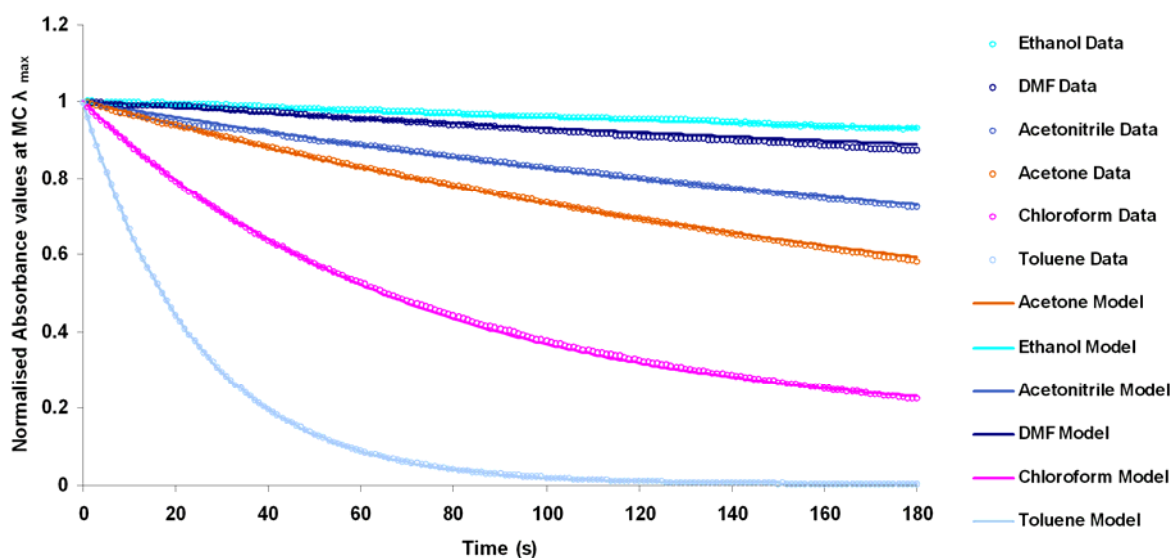


Figure 2.5: First order kinetic curves obtained plotting time against the normalised absorbance values at the MC-1 λ_{\max} in each solvent (10^{-3} M). The residual error calculated between the data and the model in between does not exceed 3% at any point in the fitted curve (figure 2.6).

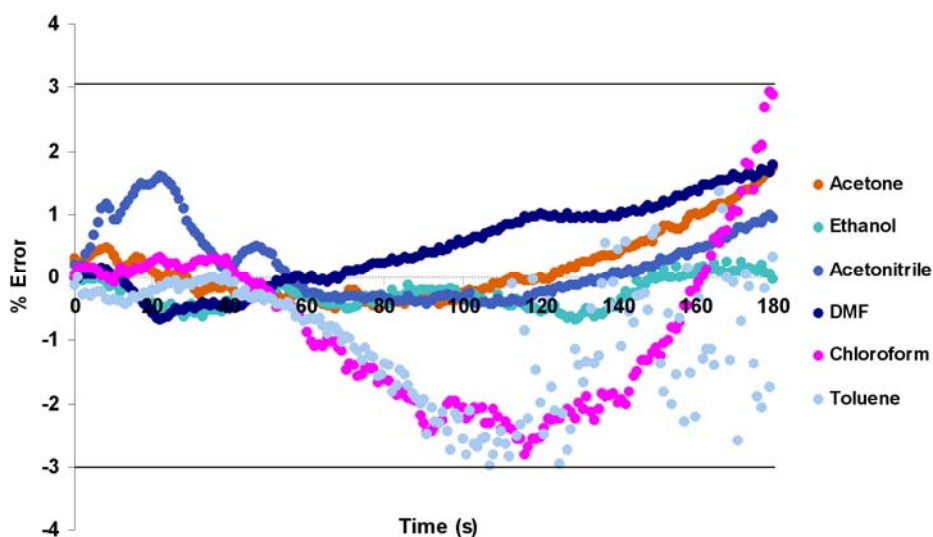


Figure 2.6: The residual error calculated between the data and the model does not exceed 3% at any point in the fitted curve.

SOLVENT	MC-1 λ_{\max}	SPP polarity scale	k_R (s^{-1})	Ratio to Ethanol
Ethanol	540 nm	0.853	1.8×10^{-3}	1
Acetone	560 nm	0.881	4.6×10^{-3}	2.5
Acetonitrile	558 nm	0.895	4.5×10^{-3}	2.5
DMF	562 nm	0.939	3.1×10^{-3}	1.7
Chloroform	578 nm	0.786	1.4×10^{-2}	7.7
Toluene	605 nm	0.655	4.0×10^{-2}	22

Table 2.1: MC-1 λ_{\max} values in different solvents reported together with the SPP polarity scale which defines the polarity of each solvent using DMANF and FNF molecular probes.

These values are followed by the rate constants for the ring closing and ring opening equilibrium obtained from the best-fit curves of the normalised absorbance values in figure 2.5, recorded at MC-1 λ_{\max} in each solvent. The rate constants are compared in terms of ratio to ring closing kinetic in ethanol.

As previously reported the increasing solvent polarity stabilizes the ground state of the MC-1 form relative to the excited state, enlarging the energy gap between the spirocyan ground state and the merocyanine (**figure 1.23, Chapter 1**).

As a result the stabilisation of the conjugated zwitterionic MC-1 form in polar solvents leads to a slower conversion back to the ring closed spiro form when compared to unpolar solvents^{12,19}.

Ethanol has the slowest relaxation time ($k_R = 1.8 \times 10^{-3} s^{-1}$), meaning that the ring closing process is highly inhibited, as the MC-1 form is stabilized in the polar ethanol environment, creating a higher energy gap between the two isomeric forms.

Then DMF, acetonitrile and acetone has slightly higher kinetic values (k_R $3.1 \times 10^{-3} s^{-1}$, $4.5 \times 10^{-3} s^{-1}$ and $4.6 \times 10^{-3} s^{-1}$) and this is probably due to a corresponding slight decrease in the stabilisation energy of the polar MC-1 form relatively to the SP-1 form.

2.3.2 Response characteristics of MC-1 complexes with metal ions in ethanol solutions

In ethanol solution, upon irradiation of the colourless SP-1 form with UV light, conversion to MC-1 form occurred, which was accompanied by the appearance of the characteristic strong absorbance band in the UV-VIS spectrum around 540 nm.

When placed in contact with increasing concentrations of certain metals, particularly transition metals^{7,20}, the band around 540 nm decreases, accompanied by an increase in absorbance towards the blue end of the spectrum.

The response characteristics of MC-1 complexes with metal ions in ethanol solutions have been evaluated for the following metals: Cu²⁺ (from Cu(NO₃)), Co²⁺ (from Co(NO₃)), Zn²⁺ (from ZnCl₂), Hg²⁺ (from HgCl₂), Cd²⁺ (from Cd(NO₃)) and Ca²⁺ (from Ca(NO₃) and CaCl₂).

During the experiments the MC-1 concentration was kept constant (10⁻³ M) while increasing concentrations of metal ions in the same volume were added.

Ethanol was chosen as the solvent as it has been demonstrated to be very efficient in stabilising the MC-1 form and it is also effective at solvating both the MC-1 ligand and the metal guest salts.

In order to obtain consistent results, the experiments were performed by placing 1.5 ml 10⁻³ M of SP-1 in seven wells. The solution had been previously irradiated for one minute, in order to ensure the SP-1 ↔ MC-1 equilibrium was preferentially on the MC - 1 side, and there was approximately equal concentration of MC-1 in each of the seven samples. Large variation in the total MC-1 concentration obviously leads to an alteration of the equilibrium of the complex, making comparisons between the complexes generated from different metal concentrations difficult to do.

To facilitate a further homogenization of the measurements, the different metal ions concentrations were added simultaneously using an automatic pipette loaded with the seven different solutions. This was done with the purpose of avoiding different effect on the MC-1 concentration arising from variations in exposure to ambient light as a consequence of delays with the addition of the metal ion samples that would have occurred if the solutions were added with different timing.

When the solutions were simultaneously added to the seven wells containing the MC form, the absorbance were recorded in the dark inside a plate well reader in order to avoid additional interference from ambient light on the photochromic equilibrium.

The interaction between the phenolate group of the MC-1 form and these metal ions is not particularly selective, but according to our solution studies, Cu²⁺ ions in ethanol cause the most appreciable colour change. In the presence of Cu²⁺, the 540 nm

absorbance band decreases, and a new absorbance band at 420 nm increases, resulting in a clear colour change from purple to orange-yellow (**figure 2.7**).

The concentration range analysed ranges from 1.6×10^{-6} M to 3.2×10^{-4} M, at which point the MC-1 band at 540 nm is completely disappeared and the 420 nm band reaches its maximum.

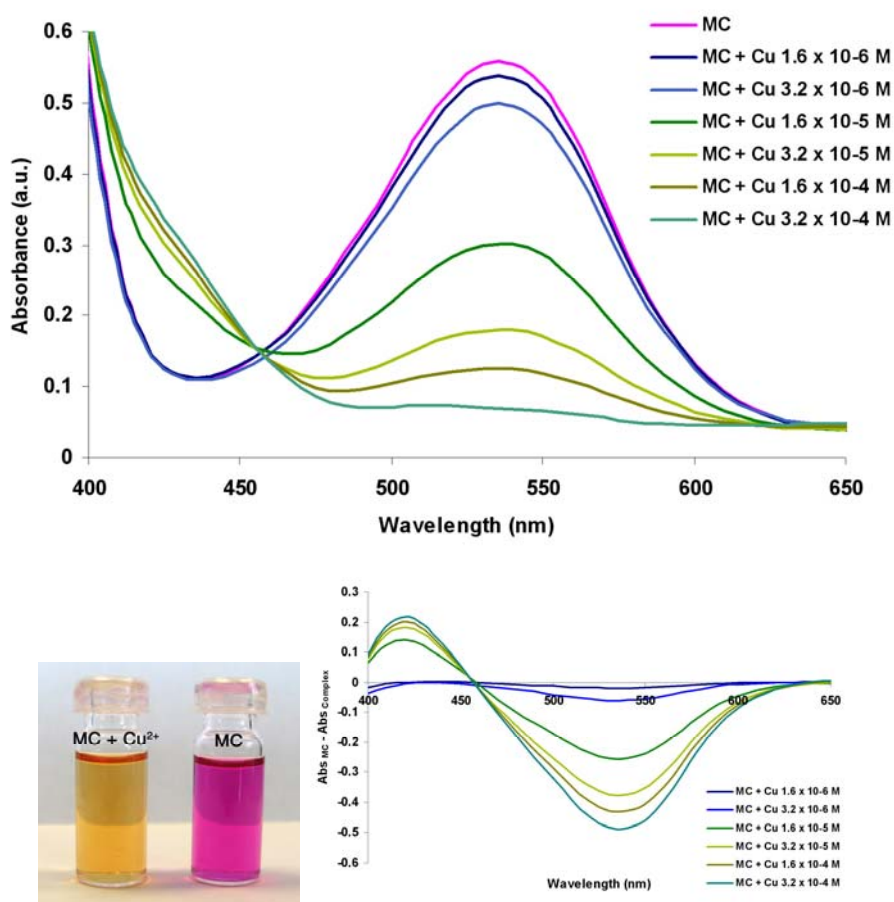


Figure 2.7: (Above) Absorbance changes in the spectra of the MC form (10^{-3} M in ethanol) when placed in contact with increasing concentrations of Cu^{2+} ions in ethanol.

(Below, left) Picture showing the visual colour difference between the MC- Cu^{2+} complex (MC-1 10^{-3} M with 3.2×10^{-4} M Cu^{2+} in ethanol solution) and the MC-1 form (10^{-3} M in ethanol). (Below, right) Graph where the absorbance differences between the MC and the MC- Cu^{2+} complex have been plotted against wavelength (nm).

These effects are in accordance with literature reports of UV-vis absorbance changes accompanying MC-Cu²⁺ complexation^{7,9,20,21} and it is generally agreed that these effects are caused by the formation of a 2:1 mole ratio complex, with two MC molecules bound to each Cu²⁺ ion⁹.

As for Cu²⁺, Co²⁺ has been recently reported to induce spectral changes as a consequence of complexation by the MC form when this is covalently immobilised on a PMMA film⁸. As with Cu²⁺, the molar ratio in this case has been also demonstrated to be 2:1, MC to metal guest^{8,9}. In solution when increasing concentrations of Co²⁺ are added to the photoinduced MC form, the MC absorbance at 540 nm decreases and a new band appears around 430 nm (**figure 2.8**). The concentration range evaluated goes from 1.6 x 10⁻⁶ M to 3.2 x 10⁻⁴ M but in contrast to Cu²⁺, at the highest Co²⁺ concentration the MC band doesn't disappear but rather shifts from 540 nm to 530 nm as the Co²⁺ concentration increases. Simultaneously the colour of the solution changes from purple to a red-pink colour.

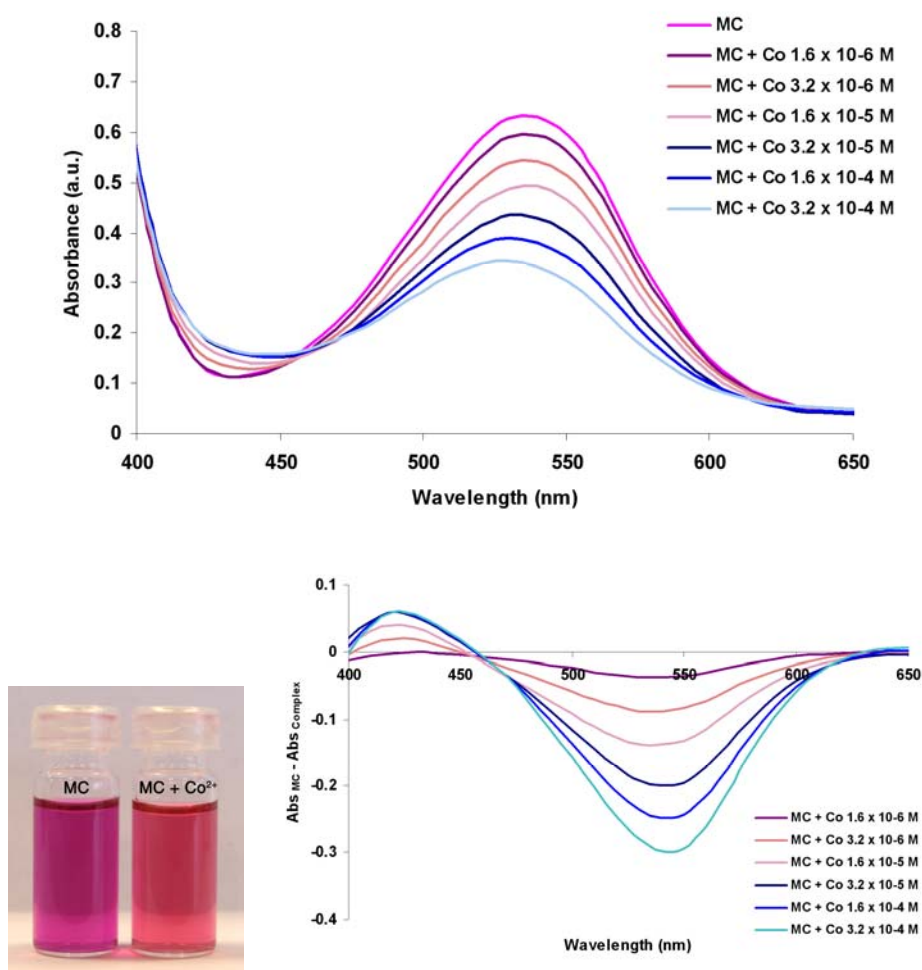


Figure 2.8: (Above) Absorbance changes in the spectra of the MC form (10^{-3} M in ethanol) when placed in contact with increasing concentrations of Co^{2+} ions in ethanol.

(Below, left) Picture showing the visual colour difference between the MC- Co^{2+} complex (MC-1 10^{-3} M with 3.2×10^{-4} M Co^{2+} in ethanol solution) and the MC-1 form (10^{-3} M in ethanol). (Below, right) Graph where the absorbance differences between the MC and the MC- Co^{2+} complex have been plotted against wavelength (nm).

Zinc is another metal whose complexation by the MC form have been widely reported^{22,23} and the complex have been demonstrated to be 2:1 ligand to guest molar ratio.

Our experiments on MC complexation of Zn^{2+} in ethanol solution (**figure 2.9**), shows that increasing the metal concentration induces the appearance of a new band around 450 nm and a MC absorbance shifts from 540 nm to 510 nm, when the Zn^{2+}

concentration reaches 3.2×10^{-4} M. The visual colour observed is from purple to a reddish colour.

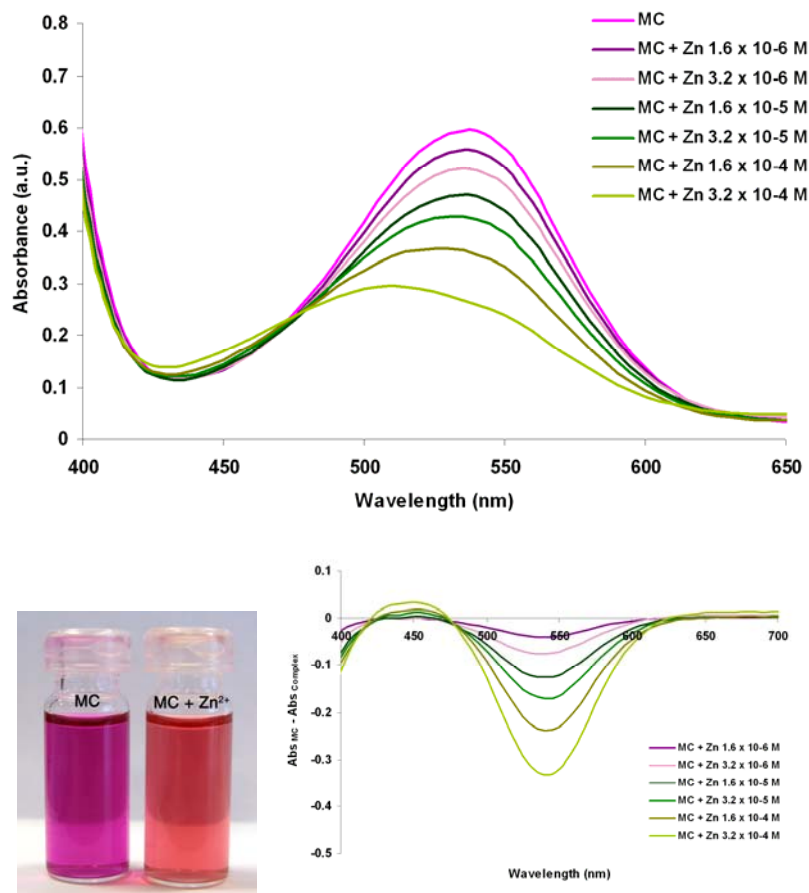


Figure 2.9: (Above) Absorbance changes in the spectra of the MC form (10^{-3} M in ethanol) when placed in contact with increasing concentrations of Zn^{2+} ions in ethanol.

(Below, left) Picture showing the visual colour difference between the MC- Zn^{2+} complex (MC-1 10^{-3} M with 3.2×10^{-4} M Zn^{2+} in ethanol solution) and the MC-1 form (10^{-3} M in ethanol). (Below, right) Graph where the absorbance differences between the MC and the MC- Zn^{2+} complex have been plotted against wavelength (nm).

Mercury is another transition metal which have been chosen for its importance in toxicology, as an ubiquitous environmental toxin that causes a wide variety of adverse health effects²⁴. Studies on nitroquinoline spirocyanine show that the relative fluorescent emission of these compounds is highly affected by the presence of Hg^{2+} ions²⁵. Our solution studies on absorbance changes due to complexation of the MC-1 form with

Hg^{2+} in ethanol solution shows that the metal concentration range analysed has to be increased by one order of magnitude (from 1.6×10^{-5} to 3.2×10^{-3} M) when compared to other transition metals such as Cu^{2+} , Co^{2+} and Zn^{2+} , in order to have an appreciable effect on the MC absorbance. By increasing the Hg^{2+} concentration added, a new band appears around 420 nm while the MC band decreases significantly without changes to its λ_{max} value (**figure 2.10**). Simultaneously, a visual colour change from purple to light purple could be observed.

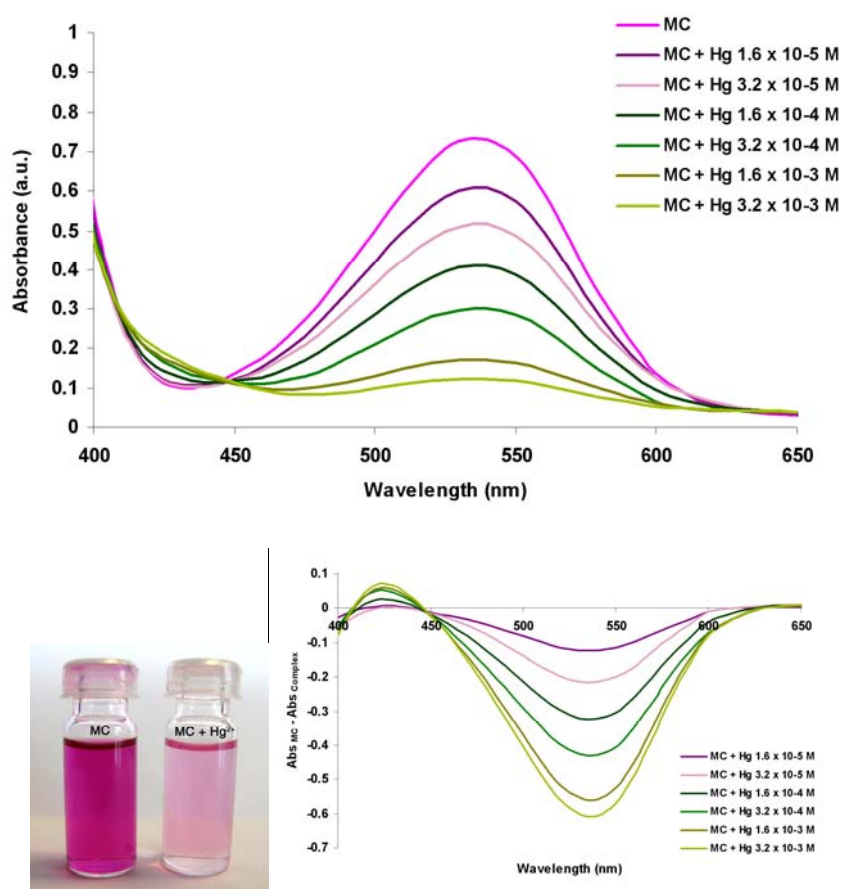


Figure 2.10: (Above) Absorbance changes in the spectra of the MC form (10^{-3} M in ethanol) when placed in contact with increasing concentrations of Hg^{2+} ions in ethanol.

(Below, left) Picture showing the visual colour difference between the MC- Hg^{2+} complex (MC-1 10^{-3} M with 3.2×10^{-3} M Hg^{2+} in ethanol solution) and the MC-1 form (10^{-3} M in ethanol). (Below, right) Graph where the absorbance differences between the MC and the MC- Hg^{2+} complex have been plotted against wavelength (nm).

Another transition metal which was analysed for its importance as a pervasive environmental contaminant is Cadmium²⁶. Complexation studies on MC-1 and Cd²⁺ were carried out in acetone solution by Görner and Chibsov^{7,16} showing an extent of complex formation lower than Cu²⁺, Co²⁺ and Zn²⁺. Other studies on quinoline and nitroquinoline spiropyran show a significant increase of relative fluorescence emission due to the presence of Cd²⁺ ions. Our preliminary solution studies on SP-1 in ethanol shows that in the presence of Cd²⁺ the MC-1 undergoes absorbance decreasing at 540 nm with a progressive shift in λ_{max} towards 530 nm and the simultaneous appearance of a new band around 430 nm (**figure 2.11**). Also in the case of Cd²⁺ the metal concentration range analysed had to be increased by one order of magnitude (from 1.6×10^{-5} to 3.2×10^{-3} M) compared to other ions such as Cu²⁺, Co²⁺ and Zn²⁺, in order to have an appreciable effect on the MC-1 absorbance.

In the presence of Cd²⁺ concentrations of the order of 10^{-3} M, the colour of the MC-1 solution changes from purple to a pink colour.

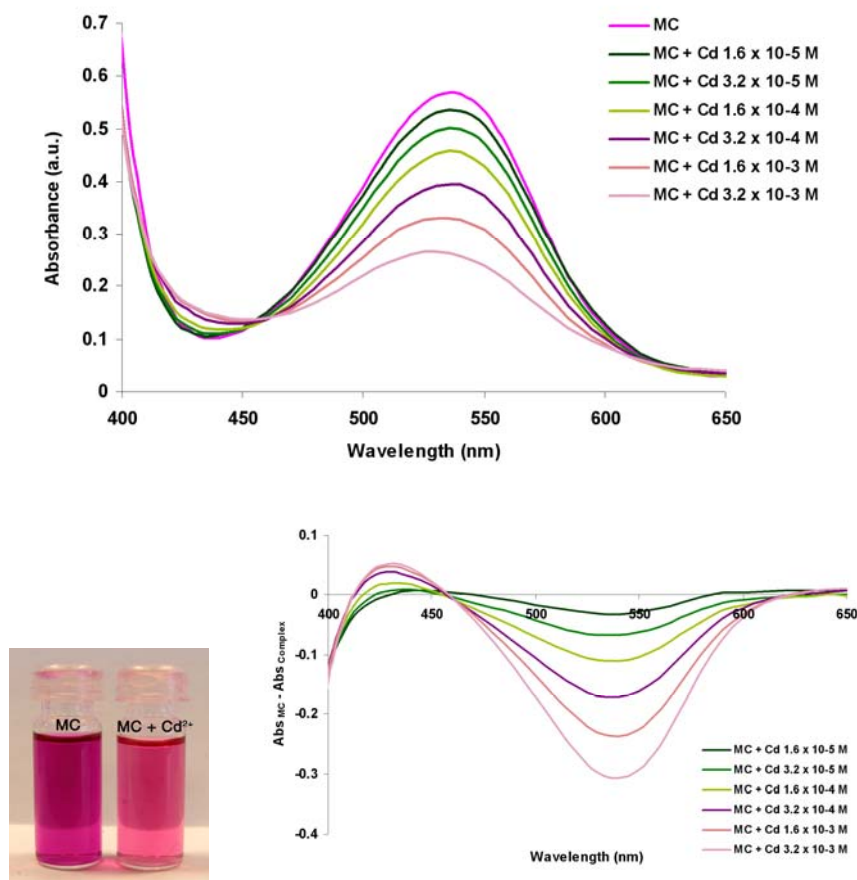


Figure 2.11: (Above) Absorbance changes in the spectra of the MC form (10^{-3} M in ethanol) when placed in contact with increasing concentrations of Cd^{2+} ions in ethanol. (Below, left) Picture showing the visual colour difference between the MC- Cd^{2+} complex (MC-1 10^{-3} M with 3.2×10^{-3} M Cd^{2+} in ethanol solution) and the MC-1 form (10^{-3} M in ethanol). (Below, right) Graph where the absorbance differences between the MC-1 and the MC- Cd^{2+} complex have been plotted against wavelength (nm).

In parallel to the evaluation of MC-1 complexes with transition metals, the interactions with Ca^{2+} , an alkaline earth metal, was evaluated.

Solution studies show that the addition to the MC-1 solution of increasing Ca^{2+} ions in the concentration range 1.6×10^{-5} M to 3.2×10^{-3} M does not cause any appreciable visual colour or spectral change. The MC-1 peak slightly decreases but no spectral shift of the MC-1 absorbance max occurs and no new lower wavelength band is observed.

For this reason both the nitrate and the chloride salt of Ca^{2+} were evaluated in order to investigate any possible effect of the counter ions on the complexation (**figure 2.12**).

In contrast to the dramatic spectral and colour changes occurring in the presence of transition metal such as Cu^{2+} , in the case of Ca^{2+} ions, the only effect observed is a slight decrease in the absorbance of the MC-1 form at λ_{max} (540 nm) which is probably indicative of a general change in the local environment (such as increasing ionic strength) rather than a specific interaction. The same effect is recorded for both the nitrate and chloride calcium salts, showing that the counter ion has no particular effect on the interaction with the MC-1.

However, it is suggested that a relatively strong MC- Ca^{2+} interaction occurs when two MC units belonging to benzospiropyran amide derivative are linked by an acetamidopropane linker to form a bis-benzospiropyranindoline bidentate ligand²⁷. The binding is eight times higher than that achieved with a single spiropyran amide derivative obtained from the separation of the two units.

This result again demonstrates the importance of pre-organisation of the ligand to form sandwich-type bidentate complexes with doubly charged cations.

The simplest example is EDTA (ethylenediamine tetra-acetic acid) with its incredible ability to form very stable complexes with most metal ions in solution, known also as “complexones”²⁸. The complexes present 1:1 ligand-guest ratio with the metal interacting with the phenolate of the four carboxylate groups and coordinate to the two nitrogen atoms, arranging in a 3D structure which present at least three five membered rings, the greater the member of the rings formed the higher the stability of the complex.

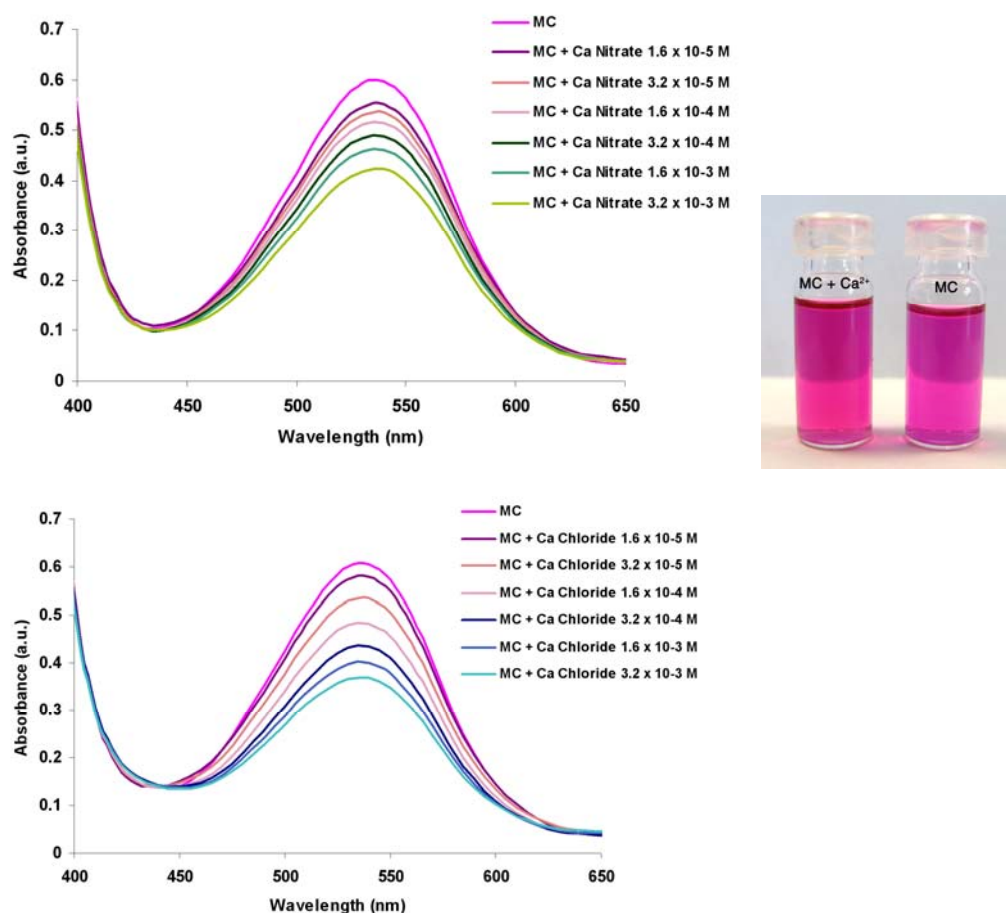


Figure 2.12: (Above) Absorbance changes in the spectra of the MC form (10^{-3} M in ethanol) when placed in contact with increasing concentration of $\text{Ca}(\text{NO}_3)_2$ ions in ethanol. (Below, left) Absorbance changes in the spectra of the MC form (10^{-3} M in ethanol) when placed in contact with increasing concentration of $\text{Ca}(\text{NO}_3)_2$ ions in ethanol. (Below, right) Picture showing the colours of MC- Ca^{2+} complex (MC-1 10^{-3} M with 3.2×10^{-3} M Ca^{2+} in ethanol solution from $\text{Ca}(\text{NO}_3)_2$) and the MC-1 form (10^{-3} M in ethanol).

Other examples of enhanced metal binding have been achieved by attaching crown ether moieties²⁹ to the spiropyran unit. However, in the case of the unmodified benzospiryran unit used in these studies, there is no evidence of any significant MC-1- Ca^{2+} formation.

In the attempt to compare the metal binding behaviour of the MC-1 towards Cu^{2+} , Co^{2+} , Zn^{2+} , Hg^{2+} and Cd^{2+} , the association constant were determined from the absorption data.

If a 1: 2 metal-ligand complex is formed between the metal ions (M^{2+} and the MC-1), the equilibrium can be described by: $L + M^{2+} \leftrightarrow ML^+ + L \leftrightarrow ML_2$ where L denotes the MC-1 ligand and M stands for ion of interest of charge 2+. The corresponding association constant (K) can be approximated as follows:

$$K = \frac{[ML_2]}{[M^{2+}][L]^2} \quad [2.2]$$

where $[ML_2]$, $[M^{2+}]$ and $[L]$ are the concentration of respective species. According to the derivation reported elsewhere^{30,31} with the introduction of the parameter α , as the ratio between the free ligand concentration $[L]$ and the initial ligand concentration (C_t), α can be defined as:

$$\alpha = \frac{[L]}{C_t} \quad [2.3]$$

$$1 - \alpha = 2 \left(\frac{[ML_2]}{C_t} \right) \quad [2.4]$$

According to α definition, the association constant can be expressed as follows:

$$K = \frac{1 - \alpha}{2 [M^{2+}] C_t \alpha^2} \quad [2.5]$$

Where K is the complex equilibrium constant and α is the ratio of the concentration of non-complexated MC-1 to the total concentration of MC-1 present in the system which can be determined from the absorbance changes in the presence of the ion guest as follows:

$$\alpha = \frac{(A - A_0)}{(A_1 - A_0)} \quad [2.6]$$

Where A_0 and A_1 are the absorbance value for $\alpha = 0$ (when all the ligand is complexed) and $\alpha = 1$ (when no metal is present) respectively and A is the absorbance value at the complex λ_{\max} for each solution where the metal guest have been added.

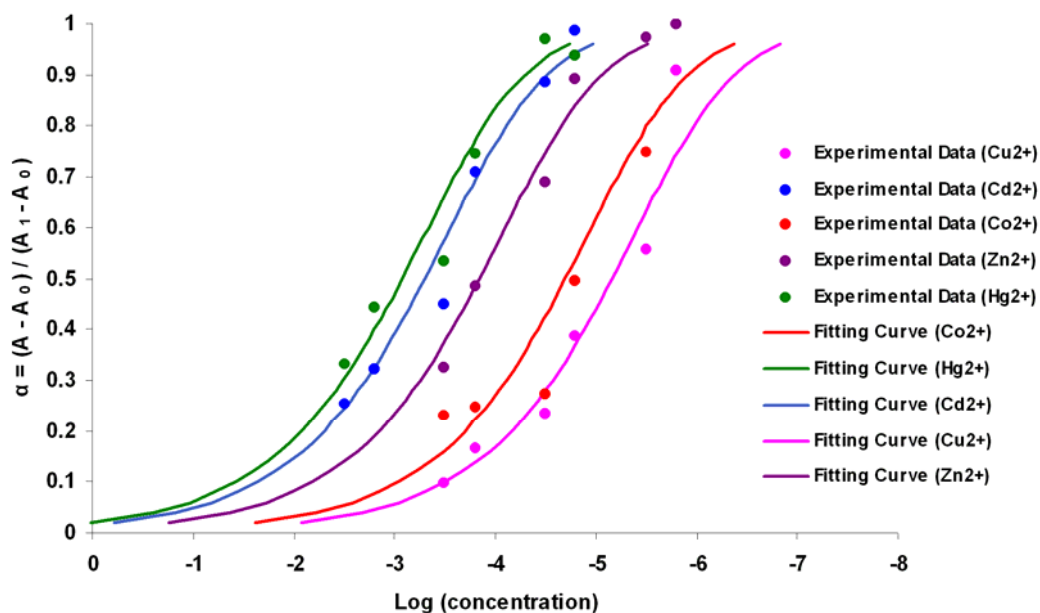


Figure 2.13: Response curves where α is plotted as a function of the logarithm of metal concentration for the experimental data (*dots*) and for the fitting curve calculate form equation [2.5] (*lines*).

By fitting the curve to experimental points using equation [2.5] (**figure 2.13**), the value for complex formation constant has been estimated* as $\log K = 6.0$ for Hg^{2+} , $\log K = 6.3$ for Cd^{2+} , $\log K = 6.8$ for Zn^{2+} , $\log K = 7.7$ for Co^{2+} and $\log K = 8.2$ for Cu^{2+} . The increase of the complex formation constant from Hg^{2+} to Cu^{2+} demonstrates that Cu^{2+} shows the most significant affinity for the MC-1 form, followed by Co^{2+} and Zn^{2+} while Hg^{2+} and Cd^{2+} with lower binding constants appear to have the weakest affinity for complexation by the MC-1 form.

In view of these results, Cu^{2+} , Co^{2+} , Zn^{2+} , Hg^{2+} and Cd^{2+} were tested for MC-1 complex formation when the ligand is immobilised on the surface of polystyrene and silica microbeads, while Ca^{2+} was tested as an example of a non-binding species.

*The estimated average error for the fitting model of the experimental data is 10%.

2.3.3 Response characteristics of MC-1 in the presence of H⁺ in ethanol solution

The phenolate group of merocyanine is also known to be subject to protonation³²⁻³⁴.

The protonation of MC-1 in ethanol solution was evaluated by adding increasing concentrations of HCl in ethanol solution to a 10⁻³ M solution of MC-1 in the same solvent. Spectroscopic studies show a dramatic decreasing of the 540 nm peak of the MC-1 form as the H⁺ concentration increases with a strong increase in a new absorption band around 420 nm (figure 2.14).

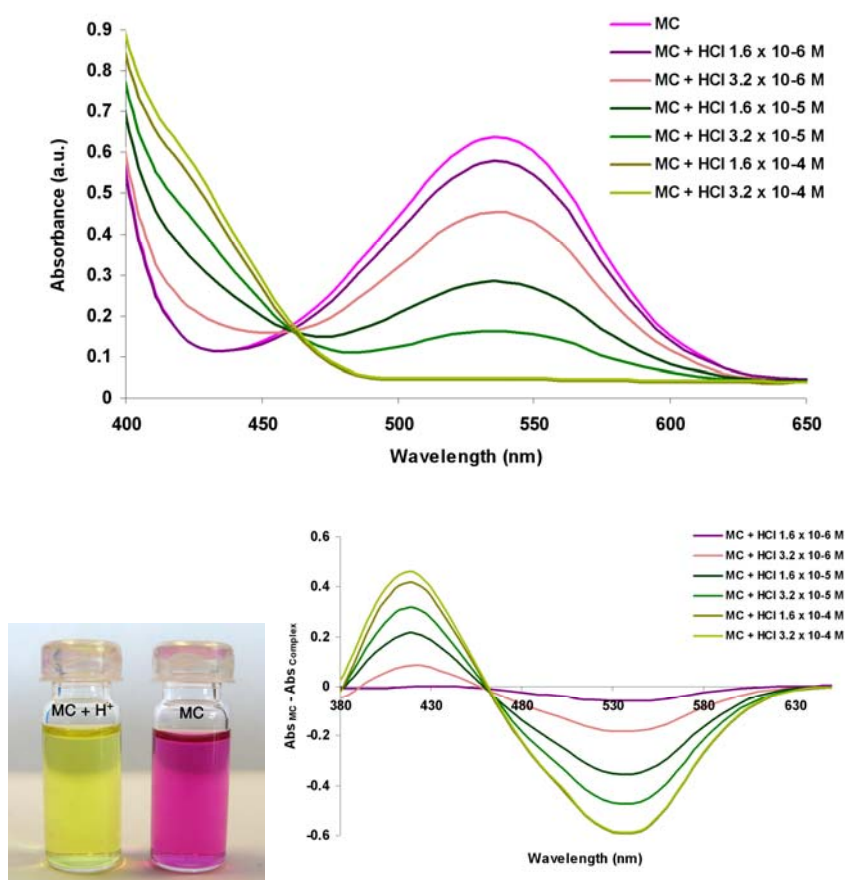


Figure 2.14: (Above) Absorbance changes in the spectra of MC-1 (10⁻³ M in ethanol) when placed in contact with increasing concentrations of H⁺ ions in ethanol.

(Below, left) Picture showing the visual colour difference between the MC-1-H⁺ (MC-1 10⁻³ M with 3.2 x 10⁻⁴ M H⁺ in ethanol solution) and the MC-1 form (10⁻³ M in ethanol). (Below, right) Differential absorbance graph where the differences between MC-1 and the protonated MC-1 absorbance have been plotted against wavelength (nm).

The transition from MC-1 to the protonated MC-1 form is accompanied by a visual colour change from purple to yellow.

Assuming that the all the HCl diluted in ethanol is dissociated, the estimated pKa (as no water is present in the system) of the MC-1 has been evaluated from the spectroscopic data.

Considering the protonation equilibrium: $MC-1 + H^+ \leftrightarrow MC-1-H^+$, the relationship between the concentration of H^+ and the amount of MC-1 and MC-1- H^+ present in the system can be described with dissociation constant Ka:

$$K_a = \frac{[MC-1-H^+]}{[H^+][MC-1]} \quad [2.7]$$

As the $[H^+]$ is normally expressed as pH, equation [2.7] can be re-write as follows:

$$-\log K_a = -\log [H^+] - \log \frac{[MC-1]}{[MC-1-H^+]} \quad [2.8]$$

$$pK_a = pH - \log \frac{[MC-1]}{[MC-1-H^+]} \quad [2.9]$$

Considering the Lambert Beer's law it is possible to correlate the absorbance to the concentration. When no proton is present, all the MC-1 form is in the non-protonated form and therefore:

$$[MC-1] = C_t \quad [2.10]$$

where C_t is the total concentration of dye present in the system.

When the $[H^+]$ is at its highest value, it can be approximated that the all the MC-1 is in the protonated form:

$$[MC-1-H^+] = [H^+] = C_t \quad [2.11]$$

Taking into account these considerations, the ratio between the absorbance values at 540 nm (A_{540nm}) and the absorbance value of the MC-1 form at its maximum ($A_{540nm MAX}$, when no proton is present) at the same wavelength, can be written as follows:

$$\frac{A_{540\text{nm}}}{A_{540\text{nm MAX}}} = \frac{\varepsilon b [\text{MC-1}]}{\varepsilon b [C_t]} \quad [2.12]$$

In the same way, the ratio between the absorbance values at 420 nm ($A_{420\text{nm}}$) and the absorbance value of the MC-1- H^+ complex at its maximum ($A_{420\text{nm MAX}}$, when the proton concentration is at its highest value) at the same wavelength, can be similarly described as:

$$\frac{A_{420\text{nm}}}{A_{420\text{nm MAX}}} = \frac{\varepsilon b [\text{MC-1-H}^+]}{\varepsilon b [C_t]} \quad [2.13]$$

Combining together the two equations the ratio between $[\text{MC-1}] / [\text{MC-1-H}^+]$ at any proton concentration can be calculated from the absorbance values using the following formula:

$$\frac{[\text{MC-1}]}{[\text{MC-1-H}^+]} = \frac{A_{540\text{nm}} / A_{540\text{nm MAX}}}{A_{420\text{nm}} / A_{420\text{nm MAX}}} \quad [2.14]$$

Once the ratio $[\text{MC-1}] / [\text{MC-1-H}^+]$ is calculated, the logarithm of this value can be plotted against pH and considering equation [2.9], the line intersect of this plot is equal to pKa (**figure 2.15**). By fitting the experimental data to a trend line the obtained pKa value is 5.05 (± 0.1). Full regression analysis shows that the F-statistic is greater than the reported F-statistic critical value for the same degrees of freedom, meaning that the regression analysis on experimental values is justified with 95% certainty.

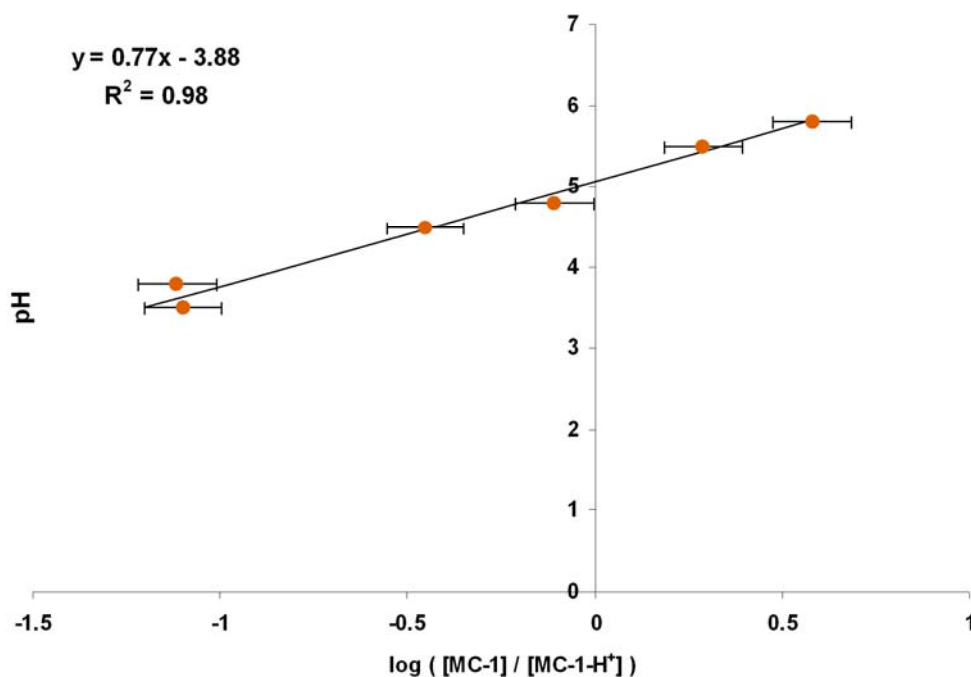


Figure 2.15: Plot of pH as a function of $\log [\text{MC-1} / [\text{MC-1-H}^+]]$. The pKa of the MC-1 corresponds to the intersection of the fitting line with the pH axis. Error bars at \pm standard deviation of the regression equation.

The estimated pKa value is within the range of pKa values previously calculated using a spectroscopic method for a series of 8-OMe ISBP derivatives³² (**figure 2.16**). In this case the pKa values range from 4.37 to 5.72 for derivatives **I**, **II** and **III** and from 3.30 to 3.94 for **IV** and **V**. The pKa of **I**, where only a methoxy group is present, is 5.72; when an additional aldehyde group is introduced in position 6, the pKa drop to 4.37 and 5.00 (for **II** and **III** respectively). When a much stronger withdrawing group such as nitro or bromide are present in position 6, in addition to the methoxy in position 8, the pKa decrease is even more significant, with values of 3.94 and 3.30 for **IV** and **V** respectively.

In the case of SP-1, the estimated pKa is 5.05; this value is very close to derivative **III**, where a methoxy group in position 8 and an aldehyde group in position 6, are present.

We can conclude that the major effect on the pKa is determined by the presence of electron-withdrawing groups in position 6 and 8 of the benzopyran ring (meta and para

in respect of the pyran oxygen), due to stabilisation of the phenolate group of the MC form, for mesomeric reasons (**Chapter 1**).

In general the $pK_a > 4$ when one strong electron-withdrawing group is present in position 6 or when a weak electron-withdrawing group is occupying position 6 and a strong one is present in position 8. When two strong electron-withdrawing groups are present both in position 6 and 8, $pK_a < 4$.

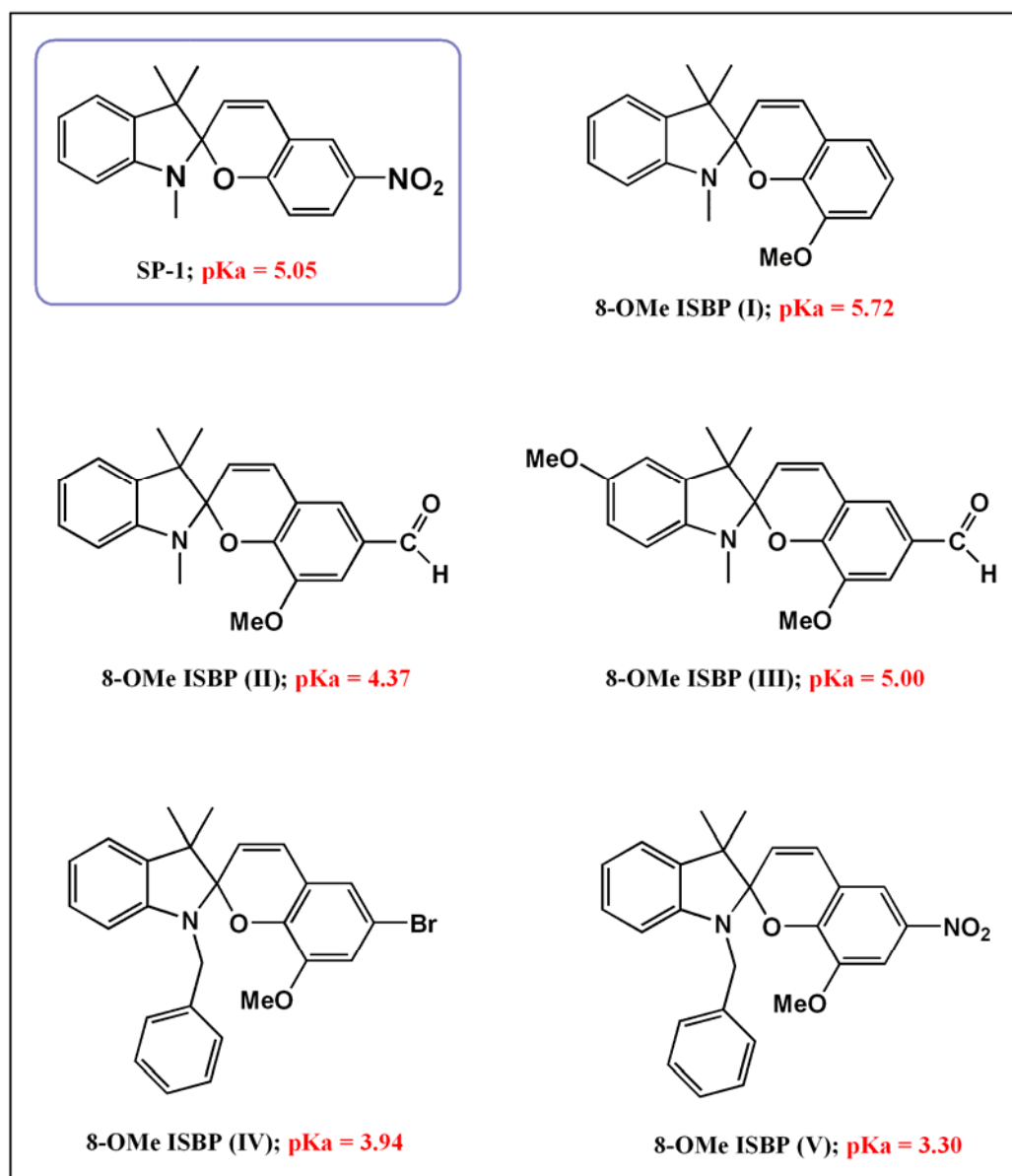


Figure 2.16: Structures of different ISBP derivatives followed by the spectroscopically estimated pK_a values.

The protonation of the MC form is another important equilibrium to be considered as it opens up the possibility of creating systems with the important properties of light-switchable protonation, where the proton can be captured and released using external light irradiation on demand (i.e. photocontrolled buffering of pH).

2.4 Conclusions

The solvatochromic behaviour of MC-1 has been investigated showing that its absorbance spectroscopy and colour is affected by the polarity, as solvent and so is the ring closing relaxation time. The energy gap between the ground SP-1 state and the MC-1 form is elevated in polar solvents, and the thermal relaxation of the MC-1 towards the SP-1 form is much quicker in non-polar solvents, while in polar solvents the MC-1 isomer is stabilised and the re-conversion to the SP-1 form is inhibited.

The ion complexation behaviour of MC-1 has been investigated towards a range of metals in ethanolic solution. Clear colour and associated spectral change occur when certain transition metal ions are added to the MC-1 form. Among the evaluated transition metals, Cu^{2+} , Co^{2+} and Zn^{2+} ions appear to have the greatest affinity towards the MC form. Alkaline metal ions, such as Ca^{2+} , do not cause any appreciable visual or spectroscopic changes to MC-1 form. MC can also be protonated, with the pKa of MC-1 being estimated to be 5.05 (± 0.1) and the visual and spectral changes being similar in effect to the metal ion complexation.

We can conclude that even though the interactions between MC-1 and the evaluated ions are not specific, as no pre-arranged specific binding site is present on the MC form, there are significant differences in the complexation behaviour of MC-1 with different transition metals from a visual and spectroscopical point of view.

Therefore the equilibrium between the SP and the MC forms could provide a system wherein the active MC form preferably binds certain metal ions, especially the transition series ions, whereas the inactive SP form does not have any complexation properties. These results underline the importance of the photoswitchable behaviour of the $\text{SP} \leftrightarrow \text{MC}$ equilibrium and the enhanced properties that a material can acquire when the photochromic spiropyran is incorporated within a substrate. Hence the functionalisation

of different substrates with spiropyran sets the basis for the creation of new “adaptive” materials whose properties can be externally modulated by light.

2.5 REFLECTANCE MEASUREMENTS USING OCEAN OPTIC SPECTROMETER

2.5.1 Experimental: Materials and instruments

Polybead carboxylate microbeads 2.035 μm diameter, were purchased from PolySciences Inc. and they were further modified with spiropyran using the procedure reported in **Chapter 3** to obtain an PS(15)SP sample.

Malachite Green, Nitrazine Yellow, Prussian Blue, Mordant Orange, Vitamine B12, Brilliant Green, Methylene Blue, Methyl Violet 2B, Neutral Red, ethylene dimethacrylate, 2,2'-azobisisobutyronitrile (AIBN), ethylene dimethacrylate (EDMA) and 1',3'-dihydro-1',3',3'-trimethyl-6-nitrospiro [2H-1] benzopyran-2, 2'-(2H)-indole (SP-1, **figure 2.1**) were purchased from Sigma Aldrich (Ireland).

Polymicro transparent polytetrafluoro ethylene (PTFE) coated fused silica capillaries (100 μm internal diameter, 375 μm external diameter) were purchased from Composite Metal Services Ltd (United Kingdom).

Reflectance spectra were recorded using a miniature diode array spectrophotometer (S2000[®]) combined with an FCR-7UV200-2 Reflection probe 7 X 200 micron cores (**figure 2.17**) and a DH-200-FSH Deuterium Halogen light source (Ocean Optics Inc., Eerbeek, Netherlands).

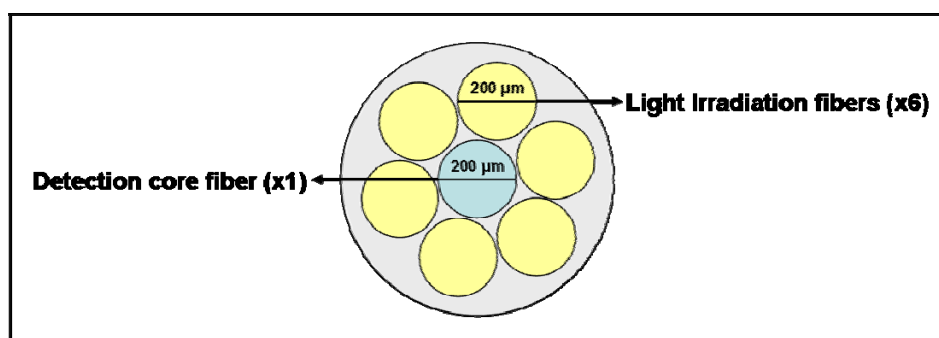


Figure 2.17: Reflectance fiber cross section: it includes 6 external illumination fibers of 200 μm diameter and a central recording fiber of 200 μm diameter.

A white reflectance standard WS-1-SL (Ocean Optic) was used to standardize the measurements, calibrating for 100% reflectance^{35 36}.

UV (375 nm), white (430-760 nm), green (575 nm) LEDs were purchased from Roithner Laser Technik, Austria.

The purposely designed vial and capillary holder for reflectance and fluorescence measurements were fabricated in a 3D printer (Stratasys). This machine prints parts in acrylonitrile butadiene styrene copolymer plastic (ABS) in a variety of colours. For the specific intent of this case the holders were specifically printed in black ABS plastic in order to avoid any interferences coming from ambient light. The holders were designed using the ProEngineer CAD/CAM software package.

Sample spinning was carried out using a ROTOFIX 32 centrifuge (Global Medical Instrumentation, USA.)

Absorbance spectra of spiropyran modified polystyrene microbeads were recorded using a Perkin Elmer UV-vis Spectrometer Lambda 900.

2.5.2 Monolith synthesis

Monoliths containing different dyes copolymerised with ethylene dimethacrylate were synthesised inside transparent polytetrafluoroethylene (PTFE) coated fused silica capillaries with internal diameter of 100 μm and outer diameter of 375 μm .

The dyes chosen were Brilliant Green, Methylene Blue, Methyl Violet 2B and Neutral Red (**figure 2.18**). The choice was based on possible application of these dyes to the selective retention for chemo-bio sensing. Brilliant green is a well known stains for bacteria and yeasts³⁷ and it has been recently reported as a chelating agent for the pre-concentration and separation of mercury in environmental samples³⁸. Methylene Blue is particularly effective as a nerve cells staining agent³⁷ and it is reported in the literature as the active component of biosensor for DNA detection³⁹. Methyl Violet 2B has been reported as a non-competitive ligand for biological receptor⁴⁰. Neutral red electro-polymerised films on platinum showed high selectivity for citrate anion and were used for its determination on soft drinks⁴¹. All these dyes offer potential applications for the separation of chemical and biological species.

Before polymerisation of the monolithic frit the walls of the capillaries were pre-treated with a silanising agent, following a previously reported procedure⁴², to ensure that the monolith would be well anchored to the walls.

Then a solution containing 40 μ l of ethylene dimethacrylate (cross-linker) and 4.4 mg of dye was prepared and subsequently added with a solution of 0.93 mg of AIBN (radical initiator) in 160 μ l of 2-propanol. The resulting mixture was then sonicated for 40 min to dissolve all the components and remove dissolved oxygen from the pre-polymer solution as this can affect the action of the initiator.

Afterwards the solution was flushed into the pre-silanised capillaries whose ends are then capped with rubber septa and placed in a water bath at 60 °C for 24 hours. Following this, the capillaries were removed and washed with methanol until the eluent was clear and all the non-reacted species had been removed.

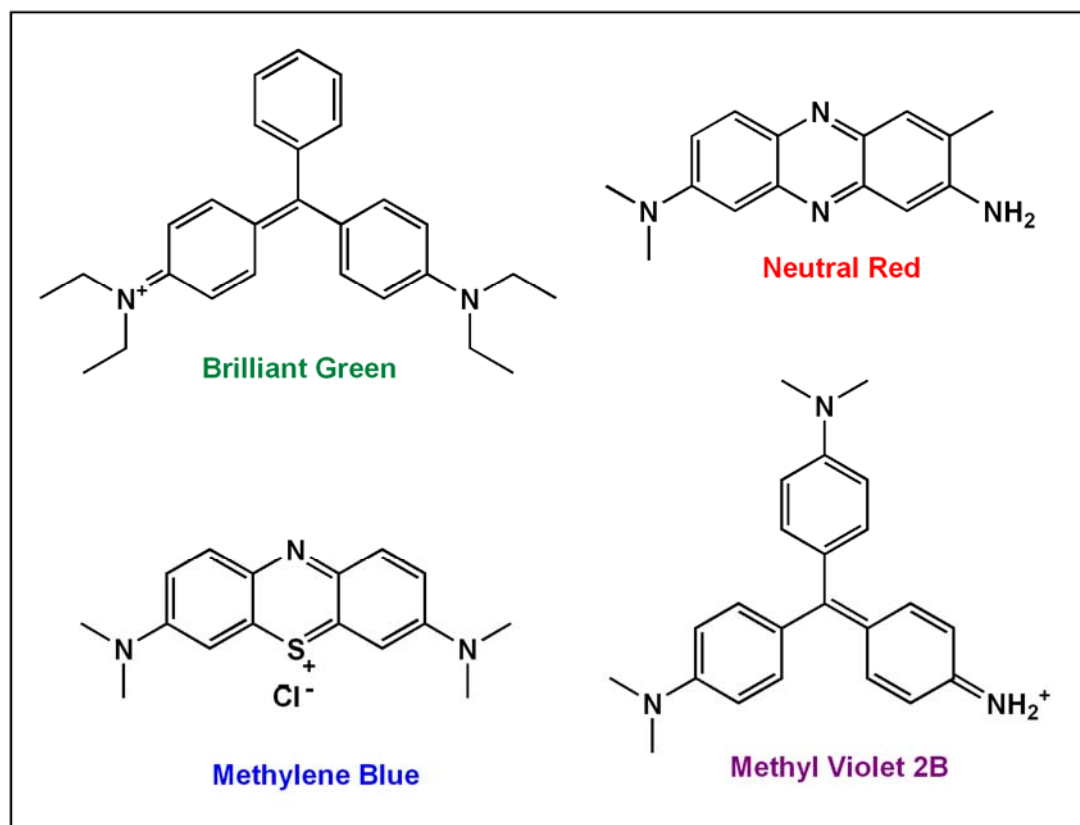


Figure 2.18: Molecular structure of Brilliant Green, Neutral Red, Methylene Blue and Methyl Violet 2B .

2.5.3 Reflectance measurement set-up

Polystyrene microspheres, although they are individually transparent and colourless, present a white milky appearance in bulk suspension due to light scattering⁴³.

Light scattering is a process by which small particles suspended in a medium having different refraction index diffuse a portion of the incident radiation in every direction, in contrast to transparent material that transmits all wavelength of light. Light-scattering changes the direction of the light, without changing its wavelength, by dispersing the photons in all directions as they penetrate the sample.

The white appearance is a consequence of multiple scattering at the bead surface combined with the one of the medium.

When the medium refractive index doesn't match the refractive index of the suspended material the suspension results in a milky white colour⁴⁴. In the case of polystyrene microbeads, their refractive index is 1.59, while the refractive index of water, ethanol, acetonitrile and methanol (solvents from which polystyrene microbeads originate stable suspensions, see **Chapter 3**) is 1.33, 1.36, 1.34 and 1.32 respectively⁴⁵.

Light scattering effect can be eliminated when the refraction at the boundary between two substances is matched. In this case light can propagate in a single medium and the suspension appears transparent.

The same phenomenon can be observed for the fat micelles of milk in water: their refractive index goes from 1.43 to 1.50⁴⁶, while for water the index is equal to 1.33. Light undergoes refraction off the particle surface, at the boundary between the particles and internally according to water's refractive index. As a consequence milk in water appears white. On the contrary when milk fat micelles are dispersed in syrup, whose refractive index is 1.45, the suspension is transparent⁴⁴.

In these particular studies, the functionalisation of polystyrene microbeads with spiropyran (**Chapter 3**) requires evaluation of colour changes at the bead surface.

Due to the different refractive indexes of the microbeads and the suspension medium, when the spiropyran functionalised microbeads turned purple due to the presence of the MC form when illuminated with UV light, the high degree of light scattering inhibits absorbance or transmittance measurements.

The refractive index of the limited number of solvents that can be used to suspend the beads (water, ethanol, acetonitrile and methanol) don't match the refractive index of the particles, therefore the suspension appears white as a consequence of the intense light scattering and the light cannot pass through the sample.

As an alternative to transmittance based spectroscopic technique, reflection spectroscopy is an important method for analysing powder and crystalline materials which are not transparent and whose colouration cannot be evaluated using transmission or absorbance spectroscopy. Surface reflection spectroscopy is an alternative powerful instrument to study dyes and colours and it has been used for a wide range of applications such as determining chromic behaviour of thermochromic organic compounds in crystalline powders⁴⁷, measuring physically adsorbed colorimetric reagents on polystyrene beads for solid phase extractions⁴⁸, developing fibre optic sensors based on the immobilisation of a coloured chelating agent on a cellulose membrane⁴⁹, reflection studies on the surface of spiropyran monolayers for detection of the formation of aggregates from the merocyanine form⁵⁰ and pigment detection in biological samples^{51 11 52 53 35}.

Reflectance in general is the return of radiation by a surface, without a change in wavelength and can be defined as diffuse or specular.

Diffuse reflectance occurs when the angle of incidence is not equal to the angle of reflection while specular reflectance occurs when the angle of incidence is equal to the reflection angle.

Every surface returns both diffuse and specular reflectance, some of them may return mostly specular reflectance other more diffuse reflectance: the glossier the surface, the greater degree of specular reflection.

Reflectance is expressed as a percentage (% R_λ) relative to the reflection from a standard surface which is 100% reflective (in this case the ocean optic WS-1 white reference for reflection measurement):

$$\% R_\lambda = \frac{S_\lambda - D_\lambda}{R_\lambda - D_\lambda} \times 100\% \quad [2.15]$$

where S_λ is the sample intensity at a certain wavelength λ , D_λ is the dark intensity at wavelength λ , R_λ is the reference intensity at wavelength λ .

Optic fibers are widely used as a tool for measuring reflectance. A reflectance fibre comprises three components (**figure 2.19**). One component (A) is linked to a light source and provides the necessary irradiation of the sample. A second component (B) is connected to the detector and collects the reflected light from the sample. The detector is then linked to a computer (D) where software is responsible for the signal processing. These two components are jointed together in the mid-point of the fiber to form a third component (C) (**figure 2.17**) that is placed directly in contact with the sample whose reflectance is to be measured (**figure 2.19**).

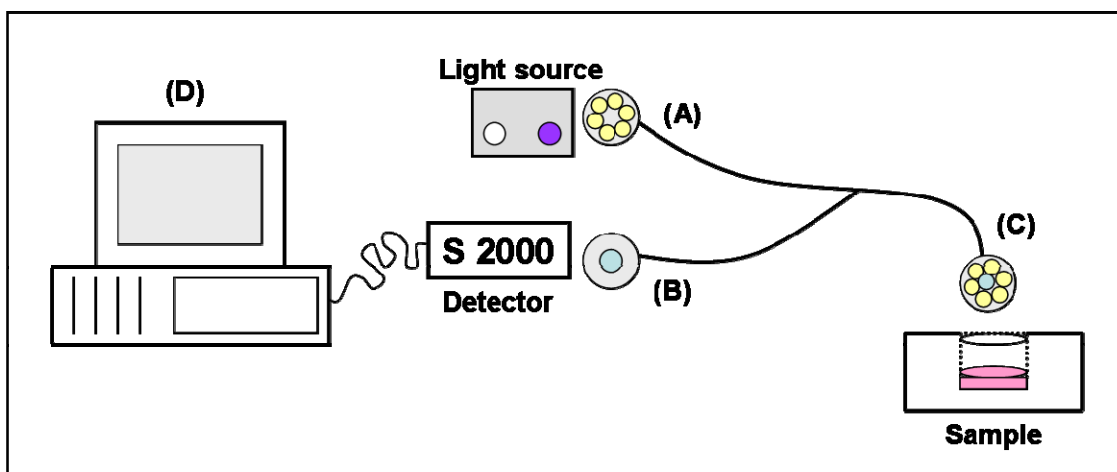


Figure 2.19 Configuration for a reflectance measurement experiment.

When light is shone perpendicularly in close proximity to a non-transparent material, the sample reflects the entire wavelength range that it has been exposed to, in a specular or diffuse way according to its nature, except the particular wavelengths that the material has absorbed because of its particular physical or chemical properties.

From the evaluation of the light reflected from the sample it is possible to estimate its absorption range.

In the case of spiropyran modified polystyrene microbeads, their colour can be evaluated using reflectance when the beads are settled on the bottom of a vial forming a compact layer. Measurements were performed using optically transparent glass vials and an appropriately designed vial and fibre optic probe holder (**figure 2.20**).

The vial holder consists of hollow cylinder in which the vial can be inserted. There is a recess at the bottom for inserting the probe. The probe is held in place by the friction forces generated by the diameter of the recess being slightly smaller than the probe diameter, preventing the probe from slipping out. The second part is the lid that fits over the holder. It has a recess on the underside for securing a vial by its cap. This allows for the vial to be easily inserted and removed. The lid also blocks any ambient light from reaching the probe. Both parts were fabricated in black ABS plastic using a 3D printer to prevent interferences coming from daylight that can affect the probe detection.

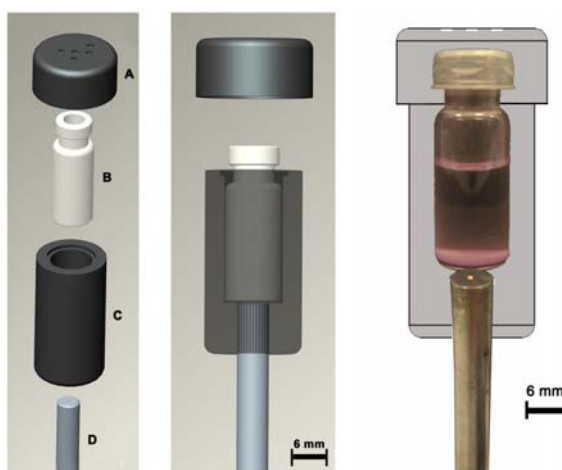


Figure 2.20: *In house* designed reflectance measurement set-up for the evaluation of the reflectance spectra of deposited microbeads on the bottom of a glass vial.

(Left) A) Lid; B) Glass vial containing the sedimented layer of microbeads; C) Main body; D) Reflectance probe.

2.5.4 Experimental procedure for diffuse reflectance measurements on vials

The vial containing the beads was placed into the holder while the reflectance probe was positioned perpendicularly to the thin microsphere layer which settled at the bottom of the vial after spinning procedure (centrifugation of the suspension for 3 minutes at 4000 rpm). When the six external light-irradiation fibres illuminated the beads with halogen light, the reflectance from the sample was detected by the central detection fibre. For the purpose of this measurement, only the halogen lamp was used as it emits primarily in the visible-near infrared region, while the deuterium lamp, which emits in the ultraviolet, was kept off. This done is for three reasons. The first is that the spiropyran immobilised

on the surface of the beads is very sensitive to the UV beam and when this light is on the microbeads are converted to the MC form, even though the halogen lamp is emitting white light. This means that when both the light (UV and visible) are irradiating the beads surface the UV light is the predominant having the strongest effect on the sample that is completely converted to the MC form, making the detection of the SP form impossible. Secondly when recording the spectra of the MC form, a few seconds of exposure to the white beam doesn't affect the equilibrium as strongly, and the spectra can be easily detected without a fast reconversion to the SP form. Finally, since the MC peak appears around 560 nm and this wavelength falls into the visible region the spectrum can simply be detected using just this part of the spectra.

The recorded spectra were then processed using the Ocean Optics software, against a previously recorded reference spectrum of a totally reflective Ocean Optic standard, taken in the dark, at the same distance from the reflectance probe^{35 54 55}.

As a comparison, the spiropyran modified microbeads (0.01 g of a PS(15)SP sample in 3 ml ethanol) were analysed using both absorbance spectroscopy (with a Perkin Elmer UV-vis Spectrometer Lambda 900) and the *in house* designed reflectance set-up.

2.5.5 Experimental procedure for diffuse reflectance measurements on capillaries

The previously described reflectance measurements can be similarly performed on capillaries containing monoliths and packed beads, which are commonly used as stationary phases in separation sciences.

Transparent capillaries with an inner diameter typically ca 100 µm can be filled with polymeric materials grown from the capillary inner walls (monoliths) or packed with different type of beads in order to create new stationary phases for separation of various chemical and biochemical species.

Part of this research is focused on the incorporation of spiropyran modified beads and monoliths on capillaries in order to create new stationary phases that can be reversibly switched between an “off” SP state and an “on” MC state.

When dealing with packed microbeads or monoliths which are modified with spiropyran for example, there is a necessity for a rapid and reliable method to compare and evaluate

the different colours, as these provide a self-indicating function (white = SP = “off”; purple = MC = “on”).

Reflectance spectroscopy combined with fiber optics provides a reliable route to validate the column status. The central recording fibre which is present on the reflectance probe has a diameter of 200 μm making it a good fit to measure the reflectance of the capillary whose inner diameter is 100 μm .

In order to be able to perform a real time reflectance measurement on the capillaries an *ad hoc* designed holder was created (**figure 2.21**).

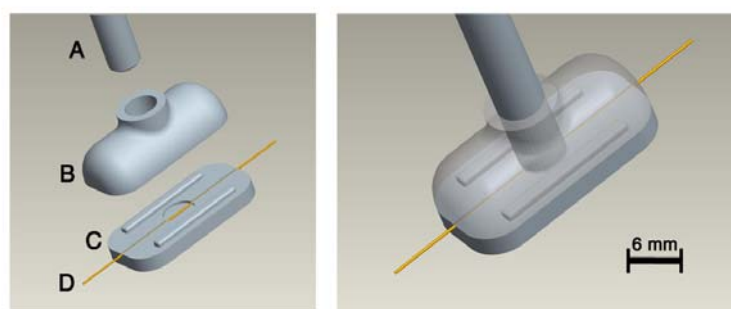


Figure 2.21: In-house designed set up for reflectance measurements on microbead packed columns or monoliths. (A) Reflectance optic fibre. (B) Lid presenting an aperture for the insertion of the optic fibre. (C) Base where a 500 μm deep open channel allows the insertion of the capillary for reflectance measurement. (D) Capillary (100 μm inner diameter) used for separation techniques.

The capillary holder consists of a probe case in which the reflectance fibre can be inserted. The reflectance probe is held effectively in place by its tight fit to the specially designed upper part of the holder. The lower part has a narrow hole of 500 μm diameter in the middle and extrusions at each side of the hole for securing the attachment to the probe case. When the two parts are attached together the capillary can simply be inserted by threading it in the orifice of the capillary case, while the optical fiber is positioned perpendicularly to the capillary.

2.6 Results and discussion

2.6.1 Diffuse Reflectance measurements on vials

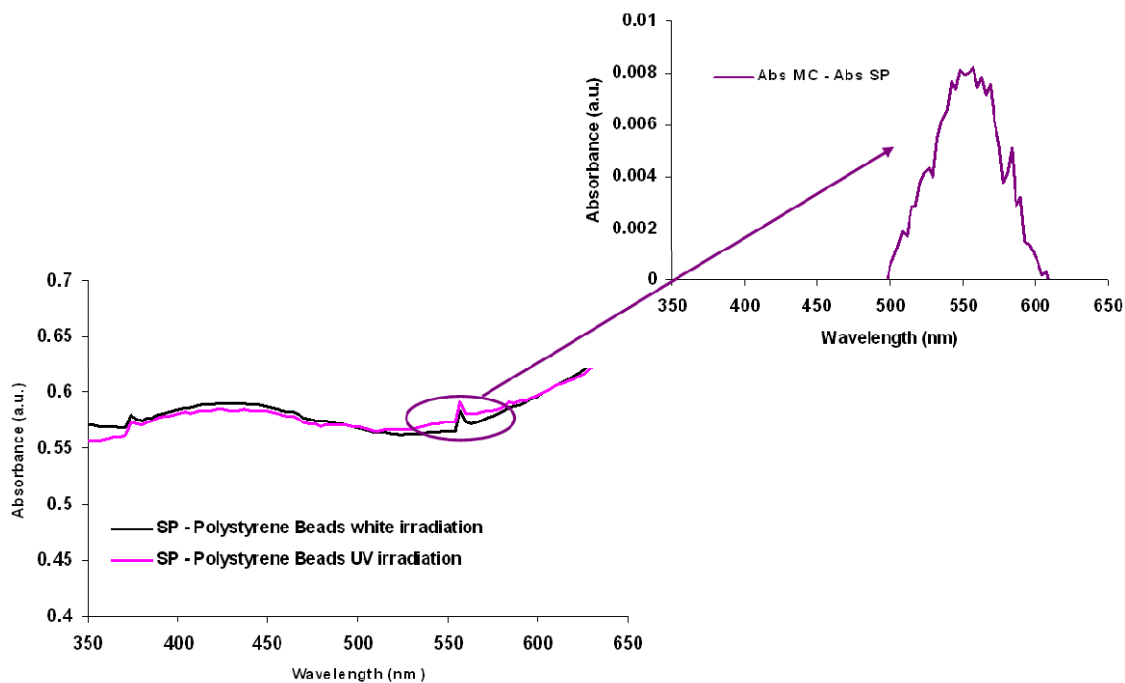
The spiropyran microbeads absorption and reflectance spectra were recorded in parallel when the polystyrene microbeads were both in the SP form (under 1 min white LED irradiation) and MC form (after 1 min UV LED exposure) (**figure 2.22**).

The difference between the SP and the MC absorption spectra using the UV-vis spectrometer can hardly be observed and no actual MC absorbance peak can be detected. Only when the SP spectrum is subtracted from the MC one, a small and noisy peak can be seen at ca 556 nm, with a relative intensity of 0.008 a.u. (**figure 2.22 A**).

In contrast when the same amount of spiropyran modified microbeads (0.01 g of a PS(15)SP in 1.3 ml of supernatant ethanol) are sedimented on an optically transparent vial and the reflectance spectra recorded using the previously described approach (**figure 2.20**) a clear peak at 560 nm is obtained and the two forms can be clearly be distinguished from a spectroscopic point of view without having to use spectral subtraction (**figure 2.22 B**).

This markedly shows the effectiveness of the reflectance method in comparison to the absorbance method to evaluate and detect colours in highly light-scattering microbeads such as polystyrene. This reflectance measurement approach was therefore used to characterise the photoswitchable ion-retention and release behaviour of the spiropyran modified microbeads (**Chapter 3**).

A)



B)

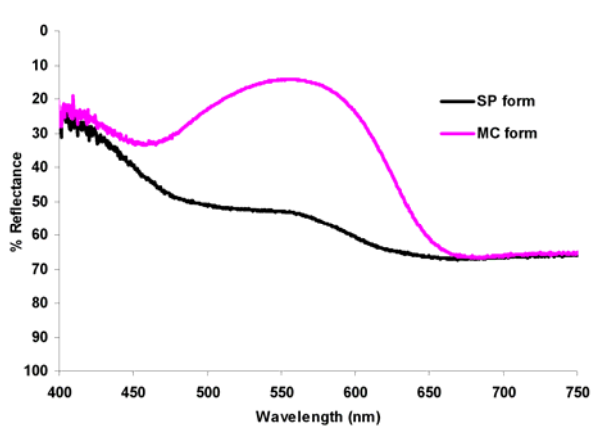


Figure 2.22: (A, *left*) Absorbance spectra of the SP and MC form measured on a spiropyran modified polystyrene bead suspension (0.01 g of a PS(15)SP sample in 3.5 ml ethanol) (A, *right*) Graph showing the result of the subtraction of the SP to from the MC absorption spectra. (B) Reflectance spectra of the SP and the MC form recorded on the sedimented layer of modified polystyrene beads (0.01 g of a PS(15)SP sample in 1.3 ml ethanol) using the *in house* designed vial and fibre holder combined to a miniature diode array spectrophotometer.

An evaluation of the effectiveness of the reflectance measurements upon a broader range of wavelengths was carried out using six different colours which were chosen on the basis of their purity according to the RGB scale and printed on paper (**figure 2.23**). In order to record the reflectance spectra, the reflectance probe has been placed in direct contact with the printed colours in the dark.

The reflectance spectra of a series of colours printed on paper (red, orange, yellow, green, pink and blue) were obtained and the resulting spectra were evaluated in order to validate the method.

For the measurements the previously described miniature diode array spectrophotometer was used along with the reflection probe, UV and visible light sources (Deuterium and Halogen lamps) and a white reflectance standard to standardize the measurements to 100% reflectance.

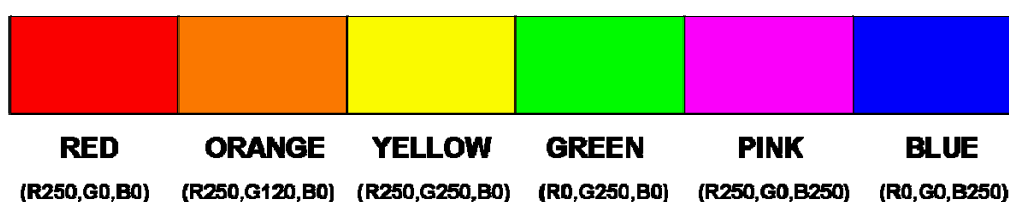


Figure 2.23: Picture showing the six colours chosen for the evaluation of reflectance measurements. Below each colour the RGB numbers are reported.

The reflectance spectra obtained for the colours present very broad ranges and ill-defined peaks. This could be due to the presence of different absorbing dyes that are mixed together in the liquid ink to generate each colour. On the other side this effect might also be caused by different reflectance processes happening on the surface which depend on the material where the colours are present. For different matrices the amount of specular reflection and diffuse reflection varies. When measuring the reflectance spectra of a material to evaluate its colour on the base of light absorption, the presence of specular reflection (or surface reflection) generates distortion in the spectrum and band changes⁵⁶. The distorted reflectance spectra which are recorded for the colours on paper are probably due to a superimposition of surface reflection upon diffuse reflection.

The spectral broadening can be corrected using Kubelka-Munk theory which describes the total diffuse reflectance from a material in terms of its absorption coefficient (K) and scattering properties (S)⁵⁷. In general diffuse reflectance is the light energy that is reflected in all directions from the surface as a result of absorption and scattering processes. Reflectance can be related to transmittance as follows:

$$R = \frac{J}{I} \quad [2.16]$$

Where J is the intensity of the diffusely reflected light collected from the sample and I is the intensity of the incident light.

I is decreased by both absorption and scattering processes while J is only increased by scattering processes, in this way reflectance is dependent both on the absorption coefficient (K) and the scattering coefficient (S). On the base of the Kubelka-Munk mathematical differential transformations⁵⁸⁻⁶⁰ the absolute diffuse reflectance of a sample can be defined as :

$$F(R_{\infty}) = \frac{(1 - R_{\infty})^2}{2 R_{\infty}} = \frac{K}{S} \quad [2.17]$$

Where $F(R_{\infty})$ is the absolute diffuse reflectance and R_{∞} are the recorded reflectance values converted from a percentage scale to a 0 to 1 range.

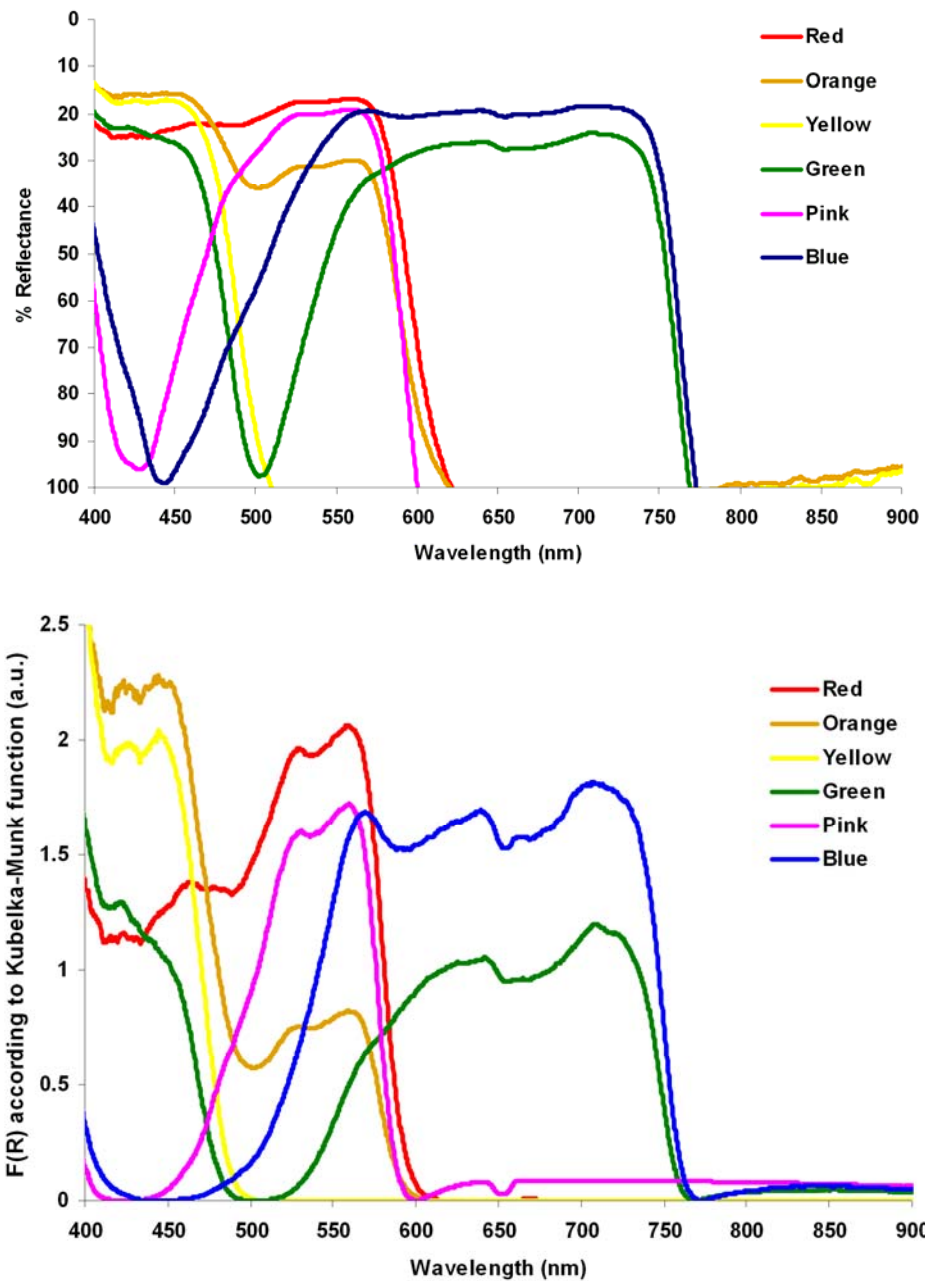


Figure 2.24: (Above) Graph showing the reflectance spectra of the six colours in terms of percentage reflectance recorded by the diode array spectrophotometer. (Below) Graph showing the reflectance spectra of the six colours after mathematical conversion of the data using the Kubelka-Munk equation.

This model was successfully used by Jozwiakowski et al⁶⁰ in order to evaluate the diffuse reflectance spectra of coloured powders of different materials.

Calculating the absolute reflectance according to the Kubelka-Munk equation for each wavelength from the percentage reflectance values recorded it is possible to obtain corrected spectra where the band broadening is highly reduced and the peaks are better defined (**figure 2.24**).

The multiple smaller peaks present on each colour band probably correspond to the absorption peak of the different dyes which are mixed in the ink in order to achieve the colouration.

In the corrected reflectance spectra each colour presents a different absorption range and they can be spectroscopically distinguished from one to the other.

This method can be therefore used for the analysis of colour changes within non-transparent substrates.

The correction of the reflectance spectra with the Kubelka-Munk equation generates interesting improvement also for the spiropyran functionalised polystyrene microbeads on a vial.

When the reflectance spectra of the MC from immobilised on polystyrene beads is compared with a spectrum where the same reflectance values are converted using the Kubelka-Munk theory the resulting spectra appear more regular and the baseline is greatly improved, even though there is no difference in the λ_{\max} of the peak (**figure 2.25**). This is probably due to the presence of specular reflectance, which is the cause of spectral distortion on diffuse measurements.

A considerable improvement in the reflectance spectra occur when applying the Kubelka-Munk equation, but as there is no variation in the peak λ_{\max} and if a real time measurement is required, the reflectance measurements recorded with the miniature diode array spectrophotometer can be directly used without any further processing, allowing direct and comparable instantaneous measurements.

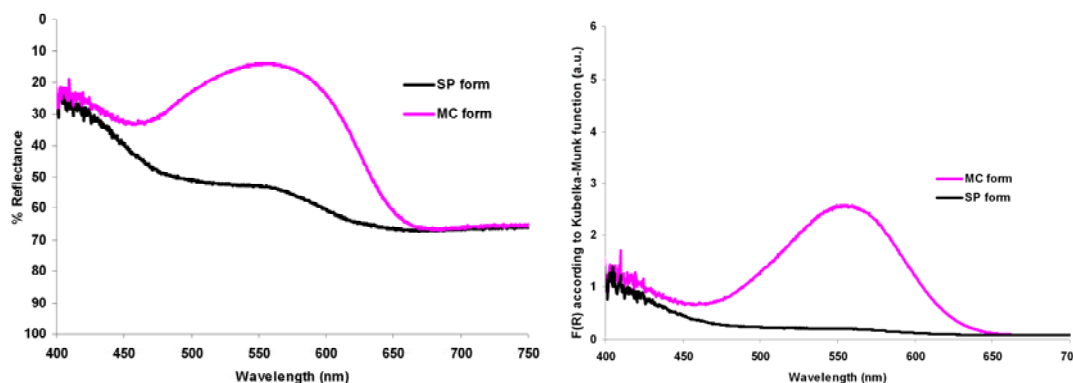


Figure 2.25: (Left) Reflectance spectra of the MC form when immobilised on polystyrene beads (0.01 g of a PS(15)SP sample in 1.3 ml ethanol (**Chapter 3**)) recorded using the *in house* designed vial and fibre holder combined to a miniature diode array spectrophotometer. (Right) Graph showing the conversion of the same reflectance spectra using the Kubelka-Munk equation.

2.6.2 Diffuse Reflectance measurements on capillaries

The reflectance measurement set-up for capillaries using the *ad hoc* designed holder previously described were initially tested by measuring the reflectance spectra of monoliths where four different dyes (brilliant green, methyl violet, methylene blue and neutral red) were copolymerised with ethylene dimethacrylate.

The colouration of each monolith due to the presence of the dye within the polymeric structure was successfully recorded using the capillary reflectance set-up. Each spectrum could be correlated to the absorbance spectra of the dye in solution. Small improvement in terms of peak sharpness and baseline occurs when the data are converted using the Kubelka-Munk equation, probably due to some specular reflectance happening at the capillary surface (**figure 2.26** and **figure 2.27**).

An aqueous brilliant green solution has two absorption maxima, one at 427 nm and another around 626 nm⁶¹. The reflectance spectra of the copolymer brilliant green-ethylene dimethacrylate shows the same absorption peaks: one at 630 nm and another at 430 nm (**figure 2.26**).

Similarly methyl violet in solution shows an absorption peak at 590 nm with a shoulder around 540nm⁶² and the reflectance spectra of the ethylene dimethacrylate copolymer exhibits a peak around 590 nm with a shoulder around 540 nm (**figure 2.26**).

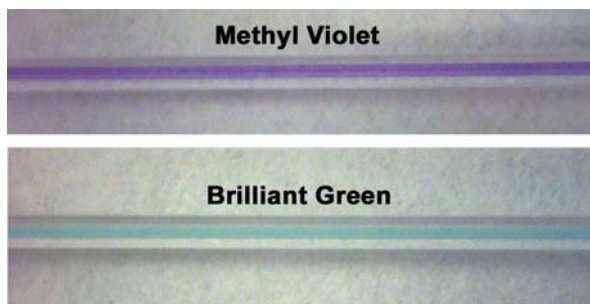
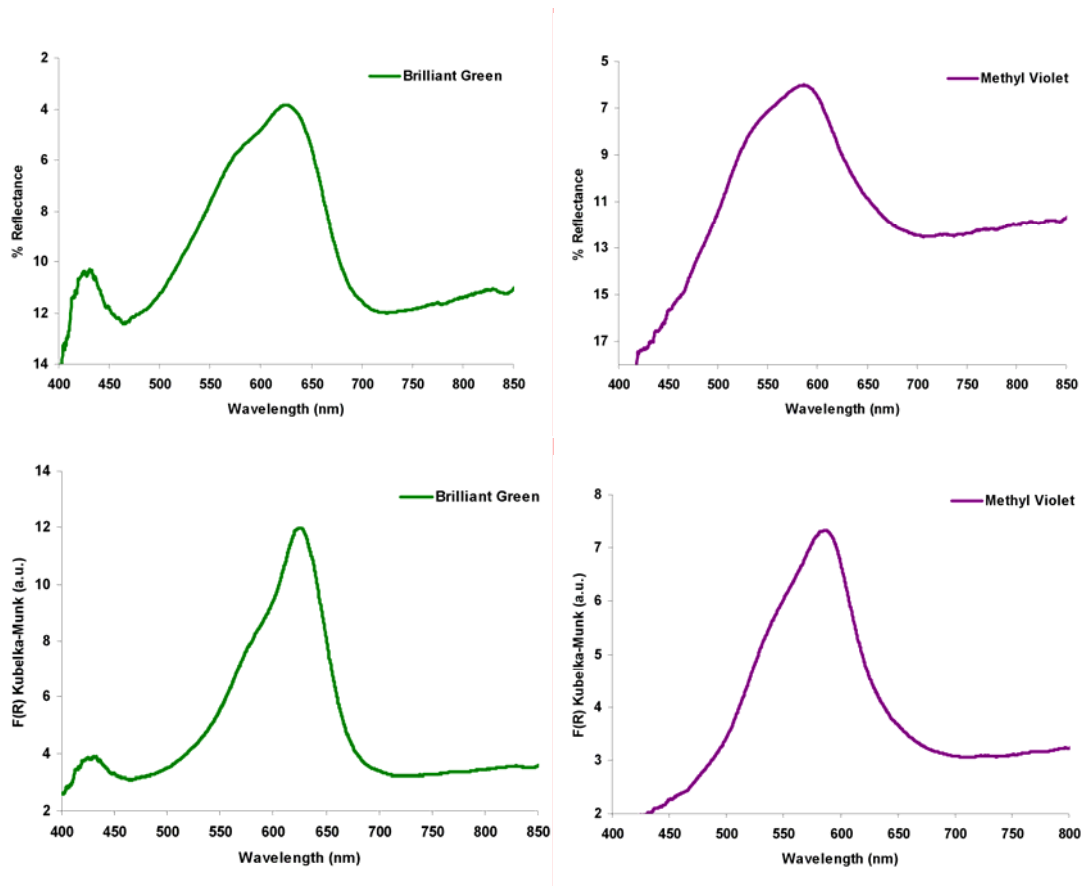


Figure 2.26: (Above) Graph showing the reflectance spectra of two copolymers: brilliant green-ethylene dimethacrylate and methyl violet-ethylene dimethacrylate with on the side the corresponding graph showing the conversion of the same reflectance spectra using the Kubelka-Munk equation. (Below) are photos of the two monolith sections.

Methylene blue in water solution has a λ_{max} at 650 nm with a shoulder around 600 nm⁶³. The same spectrum is observed when recording the reflectance percentage of the copolymer with ethylene dimethacrylate: a main band around 650 nm with a shoulder around 600 nm (**figure 2.27**). On the contrast, Neutral Red which is a well known pH indicator, undergoes a consistent absorbance shifting when copolymerised with ethylene dimethacrylate. The basic and acid form of Neutral Red in solution has λ_{max} at 450 nm and 545 nm, respectively⁶⁴. The reflectance spectrum of the copolymer exhibits two bands, one at 543 nm and another around 630 nm, which are 100 nm red shifted when compared with the dye in solution (**figure 2.27**). This is probably caused by a structure change in the chemical structure of the absorbing unit arising from the copolymerisation procedure.

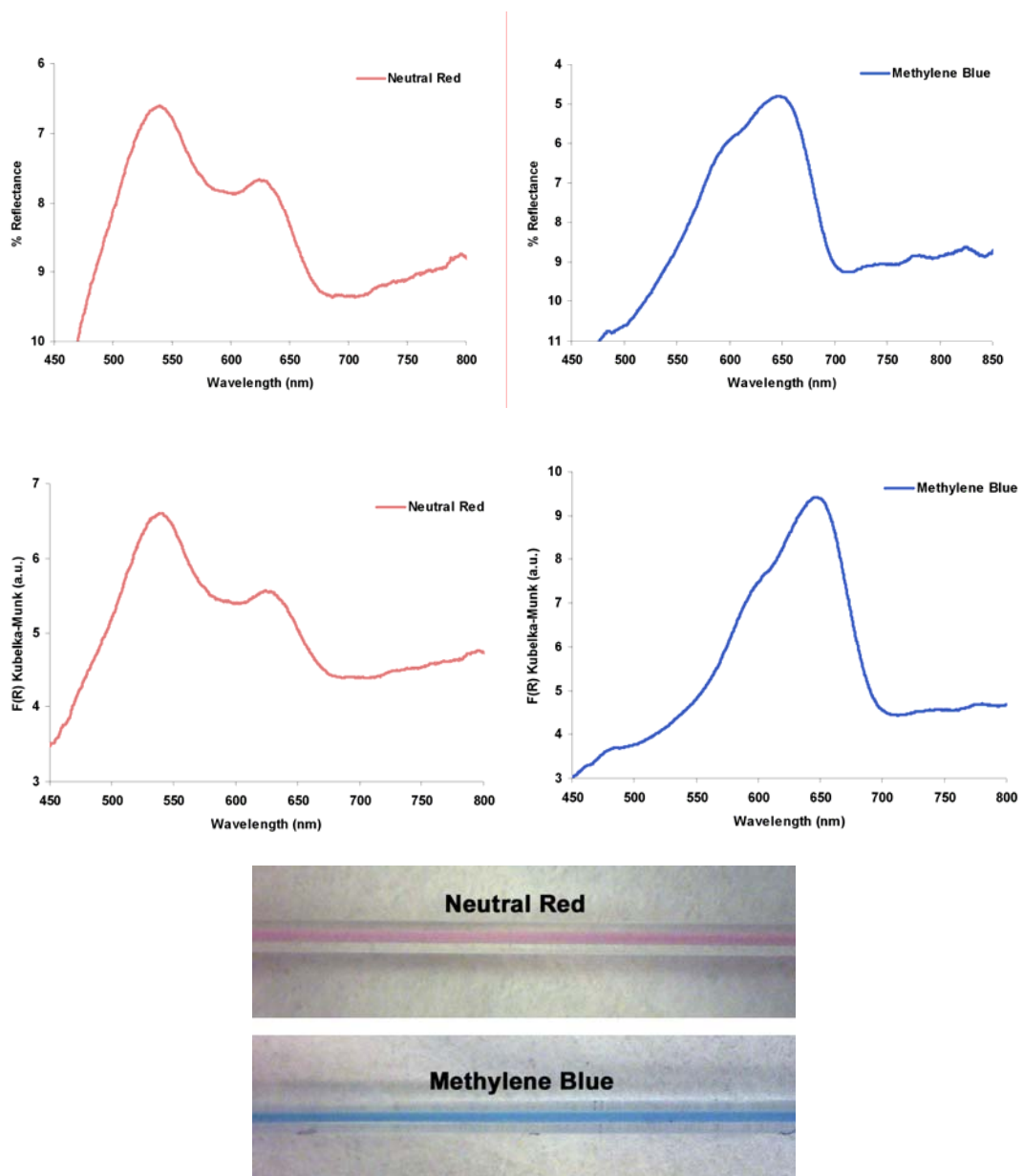


Figure 2.27: (Above) Graph showing the reflectance spectra of the two copolymers: neutral red-ethylene dimethacrylate and methylene blue-ethylene dimethacrylate with on the side the corresponding graph showing the conversion of the same reflectance spectra using the Kubelka-Munk equation. (Below) are photos of the two monolith sections.

2.7 Conclusion

The creation of new set-ups for the characterisation of the spectroscopic properties of highly light scattering microbeads has been successfully achieved.

Reflectance spectroscopy has been demonstrated to be a consistent alternative to absorbance spectroscopy to evaluate colours on non-transparent matrix. On this purpose new set-ups have been tested to measure reflectance using optic fibers combined diode array spectrophotometer and *ad hoc* printed black holders. Using two different holders the reflectance of coloured microbeads and dye-copolymerised monoliths has been successfully measured. Solid state fluorescence can also be monitored using the same diode array spectrophotometer combined with wider measuring fiber and LEDs.

Using these new validated set-ups, the photoswitchable behaviour of spiropyran functionalised polystyrene and silica microbeads could be further characterised.

2.8 References

- (1) Mukhopadhyay, R. *Analytical Chemistry* **2006**, 78, 4247-4247.
- (2) Rosi, N. L.; Mirkin, C. A. *Chemical Reviews* **2005**, 105, 1547-1562.
- (3) Wosnick, J. H.; Liao, J. H.; Swager, T. M. *Macromolecules* **2005**, 38, 9287-9290.
- (4) Asiaie, R.; Huang, X.; Farnan, D.; Horváth, C. *Journal of Chromatography A* **1998**, 806, 251-263.
- (5) Xie, R.; Oleschuk, R. *Analytical Chemistry* **2007**, 79, 1529-1535.
- (6) Qishu, Q.; Xiaoqing, T.; Chengyin, W.; Gongjun, Y.; Xiaoya, H.; Xiao, L.; Yin, L.; Chao, Y. *Journal of Separation Science* **2006**, 29, 2098-2102.
- (7) Görner, H.; Chibisov, A. K. *Journal of the Chemical Society, Faraday Transactions* **1998**, 94, 2557-2564.

- (8) Byrne, R. J.; Stitzel, S. E.; Diamond, D. *Journal of Materials Chemistry* **2006**, *16*, 1332-1337.
- (9) Radu, A.; Scarmagnani, S.; Byrne, R.; Slater, C.; Lau, K. T.; Diamond, D. *Journal of Physics D: Applied Physics* **2007**, 7238-7244.
- (10) Kalisky, Y.; Orłowski, T. E.; Williams, D. J. *J. Phys. Chem.* **1983**, *87*, 5333-5338.
- (11) Gade, J.; Palmqvist, D.; Plomgård, P.; Greisen, G. *Physics in Medicine and Biology* **2006**, *51*, 121-136.
- (12) Minkin, V. I. *Chemical Reviews* **2004**, *104*, 2751-2776.
- (13) Onai, Y.; Mamiya, M.; Kiyokawa, T.; Okuwa, K.; Kobayashi, M.; Shinohara, H.; Sato, H. *J. Phys. Chem.* **1993**, *97*, 9499-9505.
- (14) Uznanski, P. *Synthetic Metals* **2000**, *109*, 281-285.
- (15) Wypych, G. *Handbook of Solvents*; William Andrew, ChemTec Publishing, 2001.
- (16) Görner, H. *Physical Chemistry Chemical Physics* **2001**, *3*, 416-423.
- (17) Diamond, D.; Hanratty, V. C. A. *Spreadsheet Applications in Chemistry using Microsoft Excel*; Wiley: New York, 1997.
- (18) Stitzel, S.; Byrne, R.; Diamond, D. *Journal of Materials Science* **2006**, *41*, 5841-5844.
- (19) Dürr, H.; Bouas, L. H. *Photochromism - molecules and systems*; Elsevier: Amsterdam, Boston, 2003.
- (20) Chibisov, A. K.; Gorner, H. *Chemical Physics* **1998**, *237*, 425-442.
- (21) Zhou, J.-W.; Li, Y.-T.; Song, X.-Q. *Journal of Photochemistry and Photobiology A: Chemistry* **1995**, *87*, 37-42.

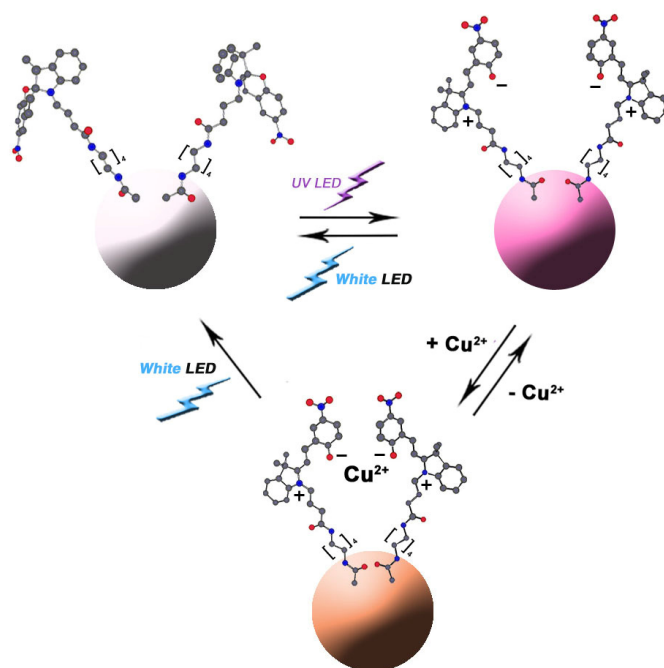
- (22) Collins, G. E.; Choi, L.-S.; Ewing, K. J.; Michelet, V.; Bowen, C. M.; Winkler, J. D. *Chemical Communication* **1999**, 321-322.
- (23) Wojtyk, J. T. C.; Kazmaier, P. M.; Buncel, E. *Chemistry of Materials* **2001**, *13*, 2547-2551.
- (24) Goldman, L. R.; Shannon, M. W. *Pediatrics* **2001**, *108*, 197-205.
- (25) Winkler, J. D.; Bowen, C. M.; Michelet, V. *Journal of the American Chemical Society* **1998**, *120*, 3237-3242.
- (26) Leffel, E. K.; Wolf, C.; Poklis, A.; White, K. L. *Toxicology* **2003**, *188*, 233-250.
- (27) Filley, J.; Ibrahim, M. A.; Nimlos, M. R.; Watt, A. S.; Blake, D. M. *Journal of Photochemistry and Photobiology A: Chemistry* **1998**, *117*, 193-198.
- (28) West, T. S. *Complexometry with EDTA and related reagents*; BDH Chemicals Ltd, 1969.
- (29) Alfimov, M. V.; Fedorova, O. A.; Gromov, S. P. *Journal of Photochemistry and Photobiology A: Chemistry* **2003**, *158*, 183-198.
- (30) Yang, R.; Li, K.; Wang, K.; Zhao, F.; Li, N.; Liu, F. *Anal. Chem.* **2003**, *75*, 612-621.
- (31) Shao, N.; Zhang, Y.; Cheung, S.; Yang, R.; Chan, W.; Mo, T.; Li, K.; Liu, F. *Analytical Chemistry* **2005**, *77*, 7294-7303.
- (32) Chernyshev, A. V.; Chernov'yants, M. S.; Voloshina, E. N.; Voloshin, N. A. *Russian Journal of General Chemistry* **2002**, 1468-1472.
- (33) Roxburgh, C. J.; Sammes, P. G. *Dyes and Pigments* **1995**, *27*, 63-69.
- (34) Radu, A.; Byrne, R.; Alhashimy, N.; Fusaro, M.; Scarmagnani, S.; Diamond, D. *Journal of Photochemistry and Photobiology A: Chemistry* **2009**, *206*, 109-115.

- (35) Yoshioka, S.; Kinoshita, S. *Journal of the Optical Society of America A* **2006**, *23*, 134-141.
- (36) MacLaren, D. C.; White, M. A. *Journal of Materials Chemistry* **2003**, *13*, 1701-1704.
- (37) Lillie, R. D. *Biological Stains*; The Williams & Wilkins Company: Baltimore, 1977.
- (38) Hashemi-Moghaddam, H.; Panahi, H. A.; Nezhati, M. N. *Analytical Letters* **2009**, *42*, 1911 - 1922.
- (39) Zhu, N.; Zhang, A.; Wang, Q.; He, P.; Fang, Y. *Analytica Chimica Acta* **2004**, *510*, 163-168.
- (40) Lurtz, M. M.; Pedersen, S. E. *Mol Pharmacol* **1999**, *55*, 159-167.
- (41) Broncová, G.; Shishkanova, T. V.; Matejka, P.; Volf, R.; Král, V. *Analytica Chimica Acta* **2004**, *511*, 197-205.
- (42) Okanda, F. M.; El Rassi, Z. *Electrophoresis* **2006**, *27*, 1020-1030.
- (43) Ohshima, H.; Furusawa, K. *Electrical Phenomena at Interfaces: Fundamentals, Measurements, and Applications* Marcel Dekker, 1998.
- (44) Gratton, L. M.; López-Arias, T.; Calzá, G.; Oss, S. *Physics Education* **2009**, 411-414.
- (45) *Refractive Indices of Pure Liquids and Binary Liquid Mixtures (Supplement to III/38)*; Springer Berlin Heidelberg, 2008.
- (46) Cheong, C.; Xiao, K.; Grier, D. G. *J. Dairy Science* **2009**, *92*, 95-99.
- (47) Fujiwara, T.; Harada, J.; Ogawa, K. *Journal of Physical Chemistry B* **2004**, *108*, 4035-4038.
- (48) Paradkar, R. P.; Williams, R. R. *Applied Spectroscopy* **1996**, *50*, 753-758.

- (49) Paleologos, E. K.; Prodromidis, M. I.; Giokas, D. L.; Pappas, A. C.; Karayannis, M. I. *Analytica Chimica Acta* **2002**, *467*, 205-215.
- (50) Koji, S.; Toshihiko, N. *Journal of Photopolymer Science and Technology* **2001**, *14*, 233-238.
- (51) Hughes, V. K.; Ellis, P. S.; Burt, T.; Langlois, N. E. I. *Journal of Clinical Pathology* **2004**, *57*, 355–359.
- (52) Balkenius, A.; Kelber, A. *Journal of Experimental Biology* **2004**, *207*, 3307-3316.
- (53) Hofmann, C. M.; Cronin, T. W.; Omland, K. E. *Evolution* **2006**, *60*, 1680-1691.
- (54) Pauw, A. *American Journal of Botany* **2006**, *93*, 917-926.
- (55) Mäthger, L. M.; Hanlon, R. T. *Biology Letters* **2006**, *2*, 494-496.
- (56) Kortüm, G.; Braun, W.; Herzog, G. *Angewandte Chemie International Edition in English* **1963**, *2*, 333-341.
- (57) Abdul-Rahman, A.; Chen, M. *Computer Graphics Forum* **2005**, *24*, 413-422.
- (58) Christy, A. A.; Kvalheim, O. M.; Velapoldi, R. A. *Vibrational Spectroscopy* **1995**, *9*, 19-27.
- (59) Szalay, A.; Antal, I.; Zsigmond, Z.; Marton, S.; Eros, I.; Regdon, G. J.; Pintye-Hódi, K. *Particle & Particle Systems Characterization* **2005**, *22*, 219-222.
- (60) Jozwiakowski, M. J.; Connors, K. A. *Journal of Pharmaceutical Sciences* **1988**, *77*, 241-246.
- (61) Khan, H. M.; Anwer, M.; Chaudhry, Z. S. *Radiation Physics and Chemistry* **2002**, *63*, 713-717.
- (62) Ganesh, P.; Ganesh, S.; Amar, T.; Sanjay, G. *Journal of Basic Microbiology* **2009**, *49*, S36-S42.

- (63) Singhal, G. S.; Rabinowitch, E. *The Journal of Physical Chemistry* **2002**, *71*, 3347-3349.
- (64) Dutta, R. K.; Subray, N. B. *Canadian Journal of Chemistry* **1993**, *71*, 1785-1791.

Polystyrene Beads-Based System for Optical Sensing using Spiropyran Photoswitches



3.1 Introduction

In science, control of interactions at the molecular scale is the ultimate goal, as this in turn determines all macro scale behaviour. For example, switchable or adaptive surfaces can be externally controlled at a molecular level by changing the state of switchable molecule between an active (binding) or passive (non-binding) state, enabling or inhibiting its capability to bind target molecules. Organic photochromic compounds are particularly interesting in this regard, as they offer a potential route to new multifunctional materials that take advantage of photo-reversible interconversion between two thermodynamically stable states with different polarities and geometries¹. Among these, spiropyran derivatives are a useful starting point, as they have been very well studied for many years, and exhibit a striking colour change when switched between the spiropyran (SP) and merocyanine forms (MC); i.e. they are inherently self-indicating.

The colourless, uncharged, passive (i.e. non ion-binding) SP form exhibits an absorption spectrum with an actinic band in the UV range 320-380 nm. Exposure to UV radiation in this range leads to the formation of the strongly coloured, zwitterionic, active MC form, in which the extended conjugation leads to a dramatic shift in the UV-absorption, with a maximum wavelength around 560 nm (depending on the polarity of the immediate environment)². Upon irradiation, the C-O spiro bond in the SP form is cleaved heterolytically and the "spiro" carbon adopts the planar MC configuration. When the UV source is removed, the molecules gradually relax to their ground state³, the carbon-oxygen bond reforms and the molecule returns to the colourless SP form. From this discussion, it is clear that molecular-switches based on spiropyran-like molecules, open the possibility of generating surfaces whose physico-chemical properties can be controlled under an external photonic stimulation.

It has been demonstrated that low-power light sources such as UV and green light emitting diodes (LEDs) can switch spiropyran-modified surfaces between the SP and MC forms⁴. Furthermore, the MC form possesses a phenolate group which is a rather weak binding site for certain cations, such as cobalt⁴. Upon binding, the colour changes again, and afterwards the guest can be expelled using a white or green LED to reform

the original inactive SP. The binding of many metals with spiropyran and various spiropyran derivatives has been abundantly evaluated, either when the photochromic dye is in solution⁵⁻⁷ or within a polymeric matrix^{4,8-11}. Using spiropyran moieties therefore it should be possible to generate ‘adaptive’ or switchable surfaces that bind guest species only when irradiated with UV-light⁴.

Bead-based systems are attractive for many applications, as they are essentially bi-phase systems that combine many of the advantages of solids and liquids, such as providing surfaces that can be readily functionalised using well-established chemistry, while also being highly mobile in suspension like a fluid, yet easily separated from a true liquid-phase.

Although polystyrene beads on the micron range diameter are individually transparent and colourless, their suspension has a strong opaque milky-white colour in natural light as they are very effective light scatterers¹². Polystyrene microbeads with diameter greater than 1 μm tend to be relatively easy to separate from the suspending solution by centrifugation which greatly simplifies purification stages during multi-step synthetic procedures. In this particular study, although the SP functionalised 2 μm diameter microbeads appeared coloured when in the MC form, the high degree of light scattering inhibits transmittance measurements.

Surface reflection spectroscopy is an alternative powerful technique to study dyes and colours and it has been used for a wide range of applications such as determining chromic behaviour of thermochromic organic compounds in crystalline powders¹³, measuring physically adsorbed colorimetric reagents on polystyrene beads for solid phase extractions¹⁴, developing fibre optic sensors based on the immobilisation of a coloured chelating agent on a cellulose membrane¹⁵, reflection studies on the surface of spiropyran monolayers for detection of the formation of aggregates from the MC form¹⁶ and pigment detection on biological samples¹⁷⁻²¹.

These functionalised beads therefore should exhibit switchable binding of certain ions, which could have interesting potential for photo-controlled retention and release of bound species. Furthermore, this behaviour can also be easily location and time specific, depending on where and when the microbeads are irradiated.

3.2 Experimental: Materials and instruments

Polybead carboxylate microbeads 2.035 μm diameter, 2.79% solid contents, were purchased from PolySciences Inc., N-(3-dimethylaminopropyl)-N'-ethylcarbodiimide hydrochloride (EDC hydrochloride), 2-(N-morpholino)ethanesulfonic acid hydrate (MES hydrate), 1,8-diaminooctane, 1,4-diaminobutane, calcium nitrate hydrate, copper(II) nitrate trihydrate, mercury(II) chloride, zinc chloride, cadmium nitrate tetrahydrate, cobalt(II) nitrate hexahydrate were purchased from Sigma Aldrich (Ireland) and 1'-(3-carboxypropyl)-3',3'-dimethyl-6-nitrospiro(2H-1)benzopyran-2,2'-(2H)-indole (SPCOOH, Chapter 1, figure 1.21) was synthesised as described elsewhere²².

Homogeneous suspensions of microbeads were generated using a Branson Ultrasonic Cleaner 5510 from Branson Ultrasonics Corporation, USA. Sample spinning was carried out using a ROTOFIX 32 centrifuge (Global Medical Instrumentation, USA.)

SEM image were captured using an S-3000N VP SEM, Hitachi, Japan.

Contact angle measurements were conducted on "DataPhysics OCA20 Goniometer" which utilises "SCA21 Software".

Circular Glass Coverslips (diameter 30 mm) were purchased from ProSci Tech, Australia.

UV (375 nm), white (430-760 nm), blue (430 nm), green (525 nm), red (630 nm) LEDs were purchased from Roithner Laser Technik, Austria. The UV light source used for contact angle evaluations was a BONDwand UV-365nm obtained from Electrolyte Corporation, USA while as a white light source a Lloytron 60W desk lamp was used.

Reflectance spectra were recorded using a miniature diode array spectrophotometer (S2000®) combined with an FCR-7UV200-2 reflection probe (7 X 200 micron cores) and a DH-2000-FSH deuterium halogen light source (215-1700 nm, Ocean Optics Inc., Eerbeek, Netherlands). A white reflectance standard WS-1-SL was used to standardise the measurements at 100% reflectance^{21 23} (Ocean Optics Inc., Eerbeek, Netherlands).

An in-house designed vial holder (**figure 3.2**) was fabricated using a 3D printer (Stratasys, USA) in black acrylonitrile butadiene styrene co-polymer (ABS) plastic in order to minimise interferences from ambient light. The two parts of the holder (lid and the main body) were designed using ProEngineer CAD/CAM software package.

3.3 Synthesis and characterisation of spiropyran functionalised polystyrene microbeads

3.3.1 Covalent immobilisation of spiropyran on the surface of polystyrene microbeads using an eight and four carbon linkers

A sample of a 0.5 ml suspension of polystyrene carboxylated microbeads (0.01 g) in water was diluted with 3 ml of a 1 M solution of MES in deionised water and stirred at room temperature for 5 minutes. 1 ml of a 45 mg ml⁻¹ aqueous solution of EDC was then added and the mixture stirred for 1 hour at room temperature.

After 1 ml of 35 mg ml⁻¹ of aqueous solution of 1,8-diaminooctane (or 1 ml of a 20 mg ml⁻¹ aqueous solution of 1,4-diaminobutane) was added and the reaction mixture was stirred for 24 hours at room temperature. The microbeads were then washed 3 times with water and 6 times with ethanol.

The washing procedure consists of a four step process:

- Centrifugation of the suspension for 3 minutes at 4000 rpm.
- Removal of the supernatant, addition of 4 ml of fresh solvent.
- Sonication of the suspension for 5 minutes.
- Subsequent further centrifugation.

Separately, 2 ml of an 18 mg ml⁻¹ solution of SPCOOH in ethanol was prepared and added to 1 ml of 15 mg ml⁻¹ solution of EDC in ethanol. The reaction mixture was stirred for half an hour at room temperature in the dark. A 1 ml suspension of the microbeads in ethanol which were previously functionalised with the amino linker was added to the spiropyran/EDC solution and the reaction mixture was stirred for 72 hours at room temperature in the dark (**figure 3.1**). Finally, the spiropyran functionalised microbeads (PS(11)SP and PS(15)SP) were profusely washed 10 times with ethanol following the above reported procedure and stored at 4 °C in the dark.

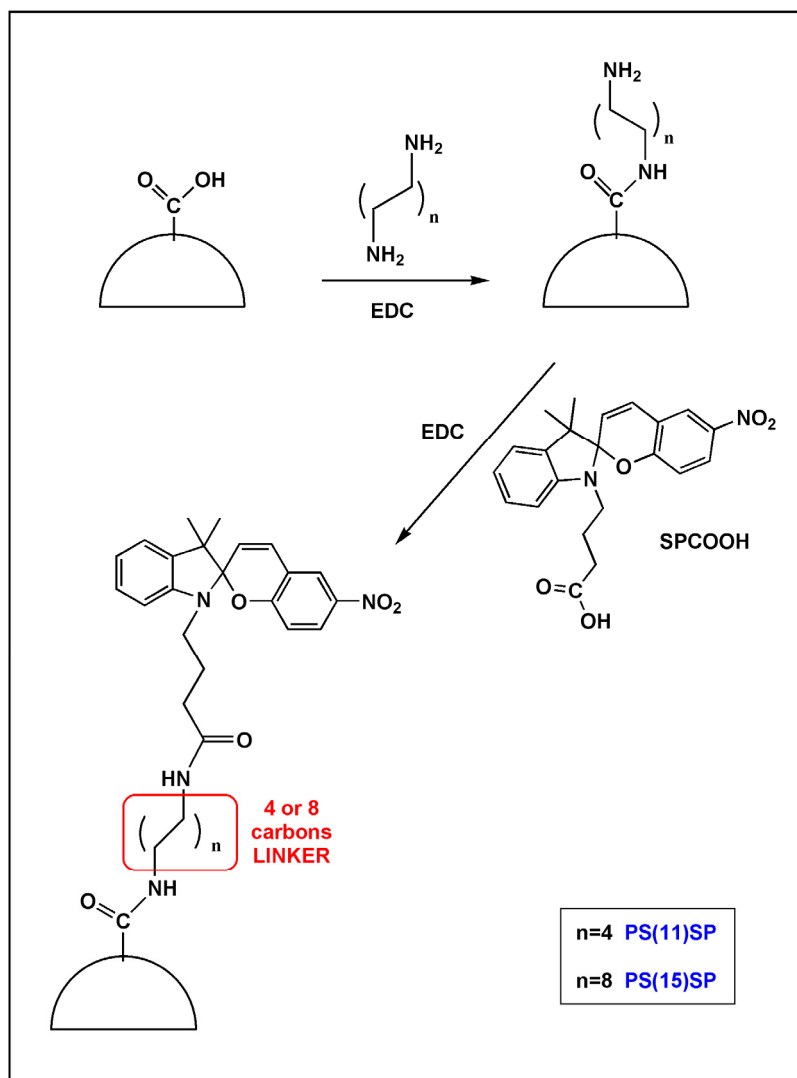


Figure 3.1: Scheme for the covalent immobilisation of SPCOOH on the surface of the polystyrene microbeads.

3.3.2 Physisorption of spiropyran on the surface of polystyrene microbeads

In order to compare the characteristics of covalently functionalised beads, a sample of polystyrene beads with physically adsorbed SPCOOH was prepared.

An aliquot of a 0.5 ml suspension of polystyrene carboxylated microbeads (0.01 g) in water was diluted with 3 ml of ethanol and added to 2 ml of an 18 mg ml^{-1} ethanolic solution of SPCOOH and the mixture was stirred for 72 hours in the dark at room temperature. The beads were then washed 10 times with ethanol following the above reported procedure and stored at $4 \text{ }^\circ\text{C}$ in the dark (PS(PA)SP bead sample).

3.3.3 Solvent compatibility evaluation and Scanning Electron Microscopy

The compatibility of polystyrene microbeads with different solvents was evaluated by immersing the non-functionalised polystyrene microbeads in ethyl acetate, ethanol, chloroform, acetone and acetonitrile. Microbeads samples of 1 mg were immersed in 3 ml of the corresponding solvent and the microscopic features of the suspensions were evaluated.

SEM images were captured on plain polystyrene and PS(15)SP bead samples dispersed in ethanol, acetonitrile, acetone and water.

The sample preparation for SEM imaging was carried out by washing an aliquot of 1 mg of plain polystyrene and PS(15)SP beads 5 times in 3 ml of the corresponding solvent and then placing 0.1ml of the suspensions on SEM carbon disc and finally letting the solvent to dry overnight in the dark.

3.3.4 Contact Angle Measurements

Contact angle measurements were carried out on PS(15)SP bead sample.

The sample preparation was carried out by placing 1 ml of a 1mg/ml solution of microbeads in ethanol on circular glass coverslips (30 mm diameter) which were then dried overnight in the dark.

The samples were then alternatively irradiated with UV and white light for 3 minutes and the contact angle measurement was taken soon after each irradiation.

3.4 Optical properties of the spiropyran functionalised polystyrene microbeads

3.4.1 Reflectance measurements

Measurements were performed using optically transparent glass vials and a specially designed vial and fibre optic probe holder (**Figure 3.2**).

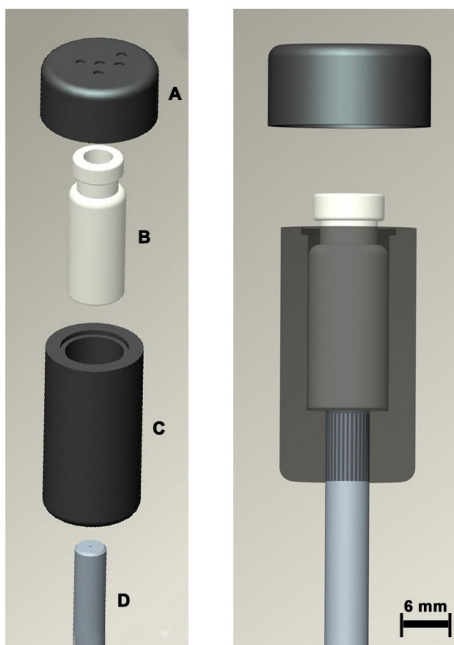


Figure 3.2: In-house designed vial holder with a recess at the bottom for inserting the probe. The lid blocks any ambient light from reaching the probe. Both parts were printed in black ABS. A) Lid; B) Glass vial containing the sedimented layer of polystyrene microbeads; C) Main body; D) Reflectance probe.

The sample was prepared for analysis by centrifugation of a 1.3 ml suspension containing 0.01g of PS(15)SP in ethanol for 5 minutes at 4000 rpm to form a homogeneous thin layer of microbeads in the bottom of a glass vial. The vial holder consists of a hollow cylinder in which the vial can be inserted, with a recess at the bottom for inserting the reflectance probe. The unit is completed with a lid that snaps over the holder which has a recess on the underside for securing a vial by its cap. This design allows the vial to be easily inserted and removed, and is very effective at blocking any ambient stray light. Both parts were printed in black ABS plastic.

The vial is placed into the holder, while the reflectance probe is positioned perpendicularly to the microsphere layer. For reflectance measurements, the halogen lamp is used (400-1700 nm). Illumination with the deuterium lamp (215-400 nm) should be avoided as the SP-functionalised beads are very UV sensitive and will switch to the MC form, and therefore affecting the SP \leftrightarrow MC equilibrium during measurements. In contrast, recording spectra of the MC form over a few seconds using the tungsten lamp doesn't affect the equilibrium as strongly, and the spectra can be easily detected

without a rapid reversion to the SP form. Finally, since the MC peak appears around 560 nm and this wavelength falls in the visible region, the spectra can simply be detected using just this part of the spectrum.

The recorded spectra were processed by the Ocean Optics software against a previously recorded reference spectrum of a totally reflective Ocean Optics standard in the dark at the same distance from the reflectance probe^{21,24,25}.

For the kinetic studies, normalised reflectance values at 560 nm were generated according to the formula:

$$N = \frac{(R - R_{MC})}{(R_{SP} - R_{MC})} \quad [3.1]$$

where N is the normalised reflectance value at time t, R is the reflectance value at time t and R_{MC} and R_{SP} are the initial reflectance values of the SP and MC forms, respectively.

As it was previously demonstrated, interesting improvement occur when applying the Kubelka-Munk equation to the recorded reflectance spectra on the functionalised polystyrene beads in the vial (**Chapter 2**). For this reason, all the recorded reflectance spectra will be presented reporting both the % reflectance data recorded in real time and the corresponding spectra corrected according the Kubelka-Munk equation.

3.4.2 Comparison of LEDs for SP↔MC switching

The thin layer of PS(15)SP sedimented microbeads (0.01 g in 1.3 ml of ethanol) was exposed to different LEDs in order to evaluate their capabilities for switching the surface immobilised spiropyran in a series of parallel experiments.

First SP→MC switching was induced by one minute exposure of the bead layer to a 375 nm LED.

Following this, the MC form was irradiated for 1 minute with white (430-760 nm), blue (430 nm), green (525 nm), and red (630 nm) LEDs in order to compare the effectiveness of each LED to induce MC→SP switching. After each irradiation the sample vials were placed in the holder to measure the reflectance spectrum.

3.4.3 Evaluation of the spiropyran immobilisation strategies

The influence of the different immobilisation strategies on the spiropyran switching efficiency was evaluated by repeatedly cycling three different spiropyran functionalised microbead samples (0.01 g in 1.3 ml of ethanol) between the SP and MC forms using UV and white LEDs according to the following procedure:

- The microbead layer was irradiated for 1 min with a white LED.
- The reflectance spectrum was immediately captured by placing the vial into the specially constructed holder.
- The microbead layer was then irradiated with a UV LED for 1 min.
- The reflectance spectrum was again captured using the same procedure as in (2), above.

Each cycle was repeated ten times for the three different spiropyran immobilisation strategies:

- Physical adsorption (no covalent binding): PS(PA)SP bead sample;
- Covalent immobilisation: PS(11)SP bead sample;
- Covalent immobilisation: PS(15)SP bead sample;

3.4.4 Influence of solvents on MC→SP kinetics

The kinetics of ring closing (i.e. MC→SP conversion) of the PS(15)SP sample was investigated in four different solvents: water, ethanol, methanol and acetonitrile. Other solvents, such as acetone, ethyl acetate and chloroform were found to destroy the polymeric matrix. In each kinetic evaluation experiment the bead sample was washed 6 times with the corresponding solvent. Each washing stage included:

- Centrifugation of 1.3 ml suspension of 0.01g of functionalized microbeads for 3 min at 4000 rpm.
- Removal of the supernatant solvent and addition of 1.3 ml of fresh solvent.
- Sonication of the suspension for 5 min.
- Further centrifugation.

The resulting thin sedimented layer was subsequently exposed for 1 minute to a white LED followed by irradiation with a 375 nm UV LED for 1 minute. Then the sample

was placed in the vial holder and reflectance measurements taken at 0, 1, 5, 15, 30, 60, 100, 140, 180, 220, 260, 300 minutes. During the experiment, the vial was kept in the dark inside the holder and measurements were taken manually at the above fixed time intervals, turning the halogen light on just for the few seconds needed to capture the spectrum, in order to minimise re-conversion to the SP form by the spectrometer white light source.

3.4.5 Photostability evaluation of the surface immobilised spiropyran

The photostability of the surface immobilised spiropyran was evaluated by repeatedly cycling two PS(15)SP freshly prepared samples (0.01 g in 1.3 ml of ethanol) between the SP and MC forms using UV and white LEDs. Cycles were performed according to the procedure reported for the evaluation of the spiropyran immobilisation strategies. Each cycle was repeated 50 times monitoring the reflectance values at 560nm.

3.4.6 Evaluation of Ca^{2+} , Cu^{2+} , Co^{2+} , Cd^{2+} , Zn^{2+} , Hg^{2+} interactions with spiropyran functionalised microbeads

Spiropyran functionalised beads (PS(15)SP) suspended in ethanol and converted to the MC form were exposed to the same concentration of Ca^{2+} , Cu^{2+} , Co^{2+} , Cd^{2+} , Zn^{2+} , Hg^{2+} ethanolic solutions and to increasing concentration of Cu^{2+} and in order to evaluate the complex formation at the bead surface.

Each experiment was carried out using the following procedure:

- Centrifugation of a suspension of 0.01g of functionalised microbeads in 1.3 ml of ethanol for 3 minutes at 4000 rpm.
- Exposure of the resulting thin bead layer to a white LED for 1 minute (promotes MC conversion to the SP form)
- Recording of the reflectance spectrum of the colourless SP form.
- Exposure of the thin layer to a UV LED for 1 minute (promotes SP conversion to the MC form).
- Recording of the reflectance spectrum of the coloured MC form.

- Addition of 0.1 ml of 10^{-2} M Ca^{2+} , Cd^{2+} , Zn^{2+} , Hg^{2+} , Co^{2+} ethanolic solutions (final concentration 7.1×10^{-4} M) and 0.1 ml of 10^{-4} M, 10^{-3} M and 10^{-2} M of Cu^{2+} and (final concentrations 7.1×10^{-6} M, 7.1×10^{-5} M and 7.1×10^{-4} M respectively) followed by sonication for 5 minutes.
- Centrifugation of the microbeads for 3 min at 4000 rpm.
- Recording of the reflectance spectrum.
- Exposure of the thin bead layer to a white LED for 1 minute (promotes metal expulsion and MC conversion to the SP form)
- Copious washing (x 6 times) with fresh ethanol

3.5 Results and discussion

3.5.1 Dispersion evaluation and SEM imaging in different solvents

In order to evaluate the dispersion properties of polystyrene microbeads in different solvents, plain polystyrene bead samples of 1mg each have been suspended in 3 ml of ethyl acetate, ethanol, chloroform, acetone and acetonitrile (**table 3.1**). Solvents such as tetrahydrofuran and toluene were not tested as it is well known that aromatic solvents have good solubility properties towards polystyrene due to the chemical and physical affinity with the polymer²⁶.

Ethyl acetate, chloroform and acetone dissolved or partially dissolved (acetone) the microbeads, leaving clear solutions (ethyl acetate) or opaque solutions (chloroform and acetone) and this is probably due to the unpolar nature of these solvents.

Acetonitrile and ethanol instead originate stable microbeads dispersions. For this reason they were chosen together with water and methanol to evaluate the influence of the solvents on the relaxation kinetic of the MC towards the SP form.

SOLVENTS	EFFECT
Ethyl Acetate	Polystyrene microbeads are completely dissolved and the resulting solution is clear
Ethanol	Polystyrene microbeads are stable and well dispersed
Chloroform	Polystyrene microbeads are completely dissolved and the resulting solution is opaque
Acetone	Polystyrene microbeads are partly dissolved forming a transparent glue-like material surrounded by an opaque solution
Acetonitrile	Polystyrene microbeads are stable and well dispersed

Table 3.1: Effect of different solvents on the dispersion of plain polystyrene microbeads.

SEM images of the spiropyran functionalised (PS(15)SP) and plain polystyrene microbeads were captured from microbead samples dried from acetone, acetonitrile, ethanol and water (**table 3.2**).

Ethyl acetate and chloroform completely destroy the polymeric matrix without leaving any solid residue to be analysed.

SEM images show how the polystyrene microbeads retain their spherical shape in ethanol, acetone and water. After the spiropyran functionalisation the surface coating at a molecular level is probably partly lost and the particle disposition on the carbon disc is less regular and the beads appear to arrange themselves into 3D aggregates rather than flat 2D regular disposition.

Both the functionalized and non-functionalized microbeads undergo partial dissolution in acetone, and the resulting residues appear as a transparent glue-like material, slightly pinkly coloured in the case of the spiropyran functionalised beads (PS(15)SP).

In the residue no trace of spherical-like shapes are present and the microbeads are partially dissolved generating a material which presents small pores on the surface.

These solvent studies provide some background on the compatibility of the polystyrene microbeads with different solvents and enable us to select the more appropriate solvents for further studies on the kinetics of the MC→SP ring closing process on the microbeads surface.

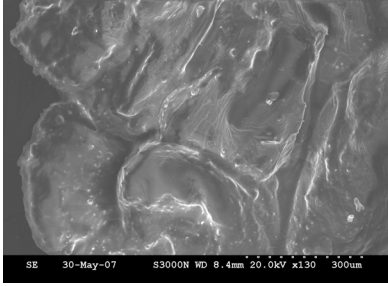
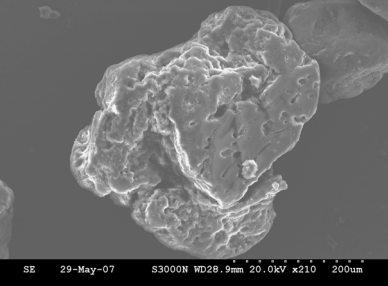
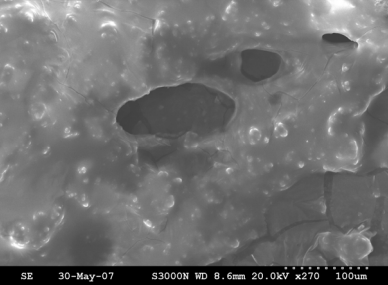
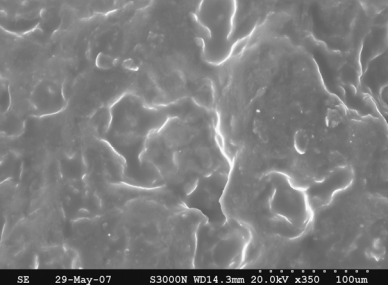
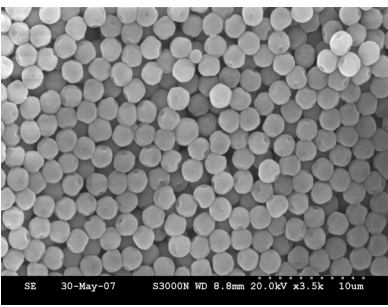
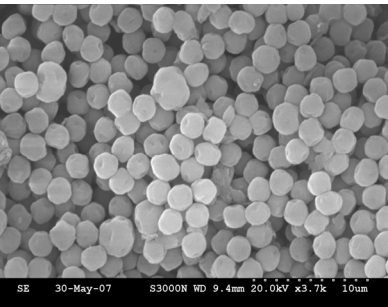
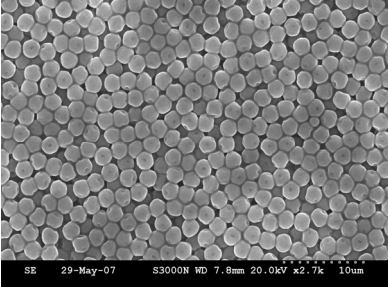
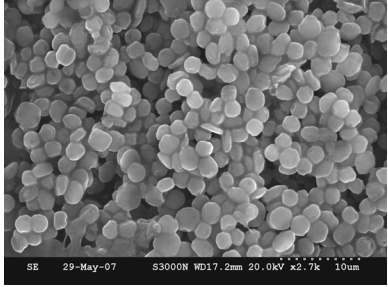
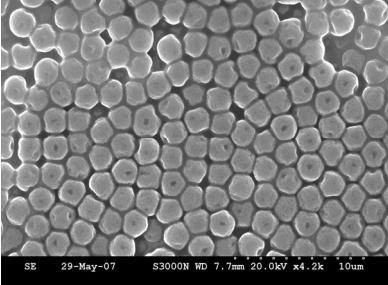
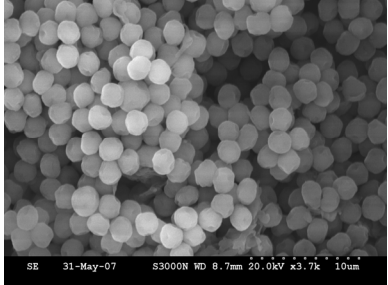
SOLVENT	Plain polystyrene beads	PS (15)SP
ACETONE	 <p>SE 30-May-07 S3000N WD 8.4mm 20.0kV x130 300um</p>	 <p>SE 29-May-07 S3000N WD28.9mm 20.0kV x210 200um</p>
	 <p>SE 30-May-07 S3000N WD 8.6mm 20.0kV x270 100um</p>	 <p>SE 29-May-07 S3000N WD14.3mm 20.0kV x350 100um</p>
ACN	 <p>SE 30-May-07 S3000N WD 8.8mm 20.0kV x3.5k 10um</p>	 <p>SE 30-May-07 S3000N WD 9.4mm 20.0kV x3.7k 10um</p>
ETHANOL	 <p>SE 29-May-07 S3000N WD 7.8mm 20.0kV x2.7k 10um</p>	 <p>SE 29-May-07 S3000N WD17.2mm 20.0kV x2.7k 10um</p>
WATER	 <p>SE 29-May-07 S3000N WD 7.7mm 20.0kV x4.2k 10um</p>	 <p>SE 31-May-07 S3000N WD 8.7mm 20.0kV x3.7k 10um</p>

Table 3.2: SEM images of spiropyran functionalised (PS(15)SP) and plain polystyrene microbeads in different solvents.

3.5.2 Contact angle measurements on spiropyran functionalised polystyrene microbeads

Spiropyran functionalised microbead suspension (PS(15)SP) of 1mg in 1ml of ethanol were deposited on a circular glass coverslip and dried from ethanol overnight in the dark. Contact angle measurements were carried out on the beads layer using a water droplet to investigate the effect of light irradiation on the microspheres due to the presence of the SP and the MC forms on the surface (**figure 3.3**).

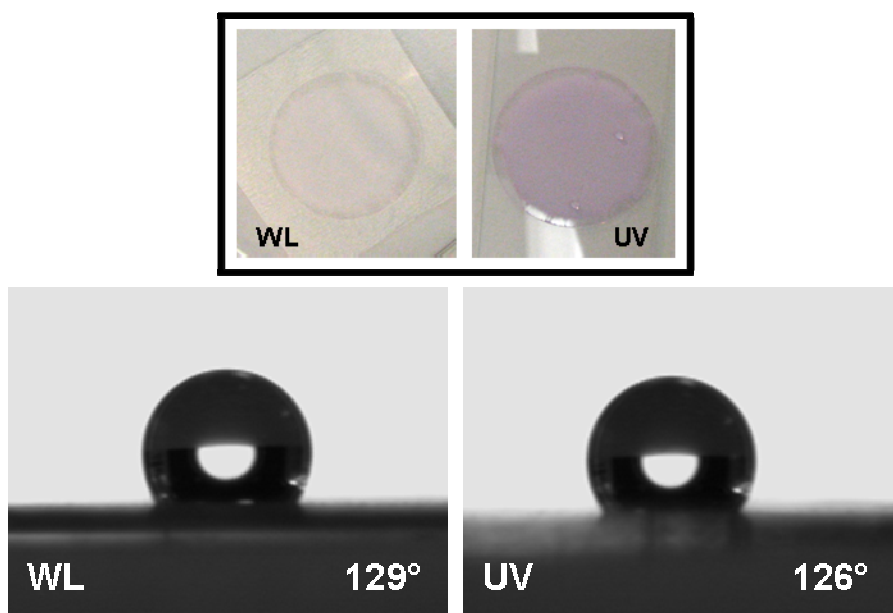


Figure 3.3: (Above) Picture showing the colour changes of the spiropyran microbeads layer (PS(15)SP) from the SP (white light irradiation, WL) and the MC form (UV irradiation) in dry state. (Below) Contact angles measurements acquired when a water droplet is placed on the surface of the spiropyran microbeads layer when irradiated with the two different light sources.

When irradiated with white light the beads layer appears white because of the presence of the unpolar SP form. The contact angle of a water droplet on the surface is 129° . Upon UV light irradiation the beads layer turn violet, because of the conversion of the spiropyran to the more polar MC form and the contact angle decreases by 3° . It is a very small decrease, but repetitions of these contact angle measurements along the sample show consistency (**table 3.3**).

After 3 minutes of white light irradiation three contact angle measurements in three different part of the sample were recorded and the average value calculated is 129.6° (\pm 0.8). When the measurements are repeated after 3 minutes UV light irradiation the average value calculated is 125.7° (\pm 0.2). The average difference in terms of contact angle between the SP and the MC form immobilised on polystyrene beads is 3.9°, demonstrating that even though the difference between the two forms is relatively small, it shows consistency.

PS(15)SP deposited on glass slide	LEFT angle	RIGHT angle
Drop n. 1 white light irradiation	129.0	129.3
Drop n. 2 white light irradiation	129.0	130.7
Drop n. 3 white light irradiation	129.0	130.7
Drop n. 4 UV light irradiation	125.8	126.0
Drop n. 5 UV light irradiation	125.3	125.6
Drop n. 6 UV light irradiation	125.7	125.9

Table 3.3: Contact angle values for the droplet left and right angle recorded after white light and UV irradiation.

The small contact angle change between the two forms is probably due to the unpolar nature of the polystyrene bead matrix, which in the absence of a stabilizing solvent for the MC form such as ethanol, it partly inhibits the conversion to a more polar molecular isomers.

A clear difference in the colour of the MC form which originates from the dry beads (**figure 3.3**) and the ethanol suspended beads (**figure 3.4**) can be noticed, with a greatly enhanced colouration in the presence of ethanol, underlining the importance of the surrounding environment for an efficient photochromic conversion.

3.5.3 Optical properties of spiropyran coated microbeads

The covalently bound spiropyran on the microbeads can be effectively switched between the MC and SP forms. Upon irradiation with a UV-LED (375nm) the beads become purple in colour, and the characteristic large absorption band around 560 nm appears (figure 3.4).

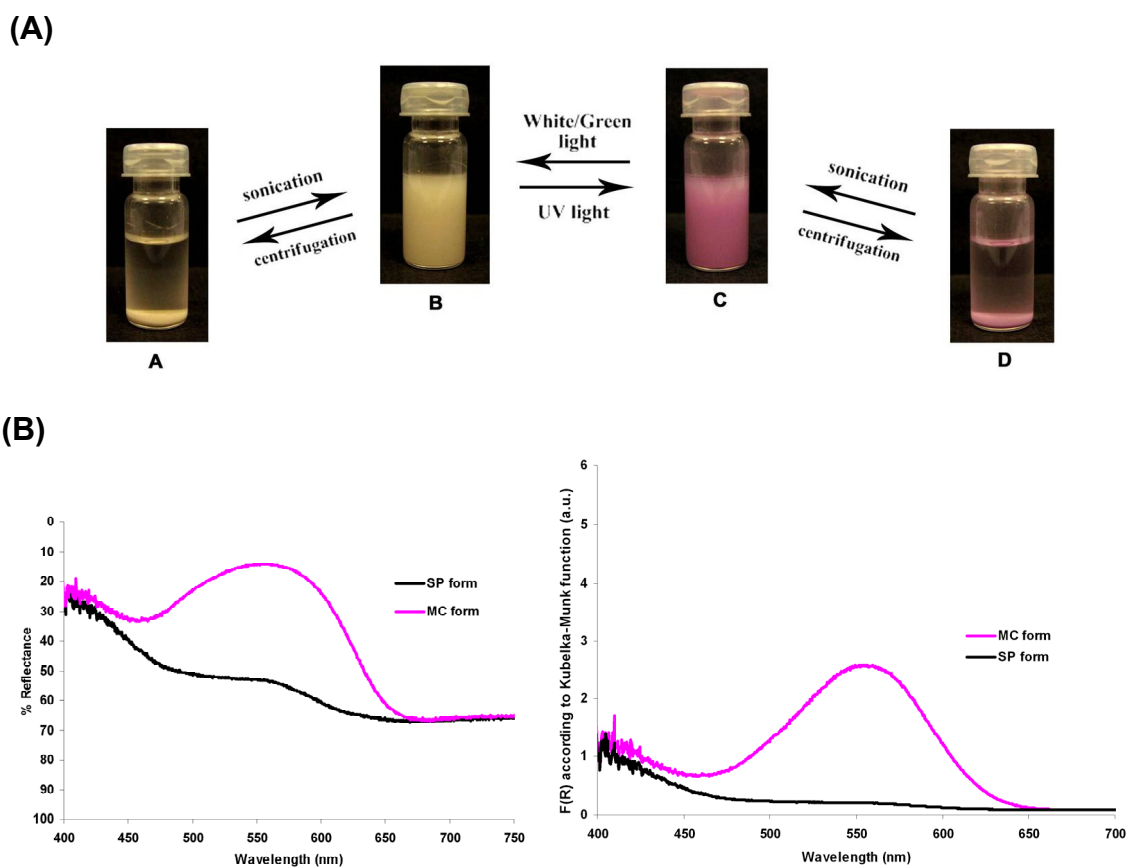


Figure 3.4: (A) A sample of spiropyran functionalised microbeads (PS(15)SP), 0.01 g in 1.3 ml ethanol) in a glass vial is switched between the colourless SP form and the purple MC form. From the left: (A) Sedimented white spiropyran functionalised microbeads layer after centrifugation; (B) Microbeads suspension exposed to one minute of white light; (C) Microbeads suspension exposed to one minute of UV light; (D) Sedimented purple beads layer after centrifugation (all the samples are in ethanol).

The centrifugation process demonstrates that the colour change is happening on the microbead surface and not in the solution medium. (B) (Left) Reflectance spectra of the MC and the SP forms on the microbead surface obtained using the in-house designed holder. (Right) Graph showing the same reflectance spectra after mathematical conversion of the data using the Kubelka-Munk equation.

We have previously demonstrated that the use of LEDs instead of more powerful light sources substantially reduces the well known photobleaching process that occurs when the switching equilibrium between the SP and the MC form is performed extensively over time²⁷. For example, the LEDs we are using are typically ca. 1 mW/cm² compared to the power of arc lamp light sources reported in most papers, which are typically 50-100 W. Despite this large reduction in emission power, the switching efficiency is relatively unaffected and repeated switching can be successfully performed.

We have also investigated how the LEDs emission wavelength affects their ability to switch the immobilised spiropyran. UV LEDs at 375 nm exhibit fast and efficient SP→MC switching, with the initial response occurring within a few seconds, reaching full conversion to the MC form in 60 s (**figure 3.5**).

The first order rate constants for the SP → MC conversion induced by UV-LED irradiation was estimated by fitting the normalised reflectance values at 560 nm using Microsoft Excel Solver^{28, 27} using the following equation:

$$y = ae^{k_R t} + b \quad [3.2]$$

where y is the normalised reflectance value at 560 nm, a is the pre-exponential factor, k_R is the rate constant and b is the asymptotic value.

Fitting the experimental data into the model described by **equation 3.2**, the rate constant for the MC formation under UV-LED exposure was determined to be $7 \times 10^{-2} \text{ s}^{-1}$ with all the experimental values not exceeding the 3% error from the estimated model (**figure 3.5**).

We can conclude that the opening process occur within seconds from the beginning of UV-LED irradiation with a rate constant of $7 \times 10^{-2} \text{ s}^{-1}$ and is completed within 60 s.

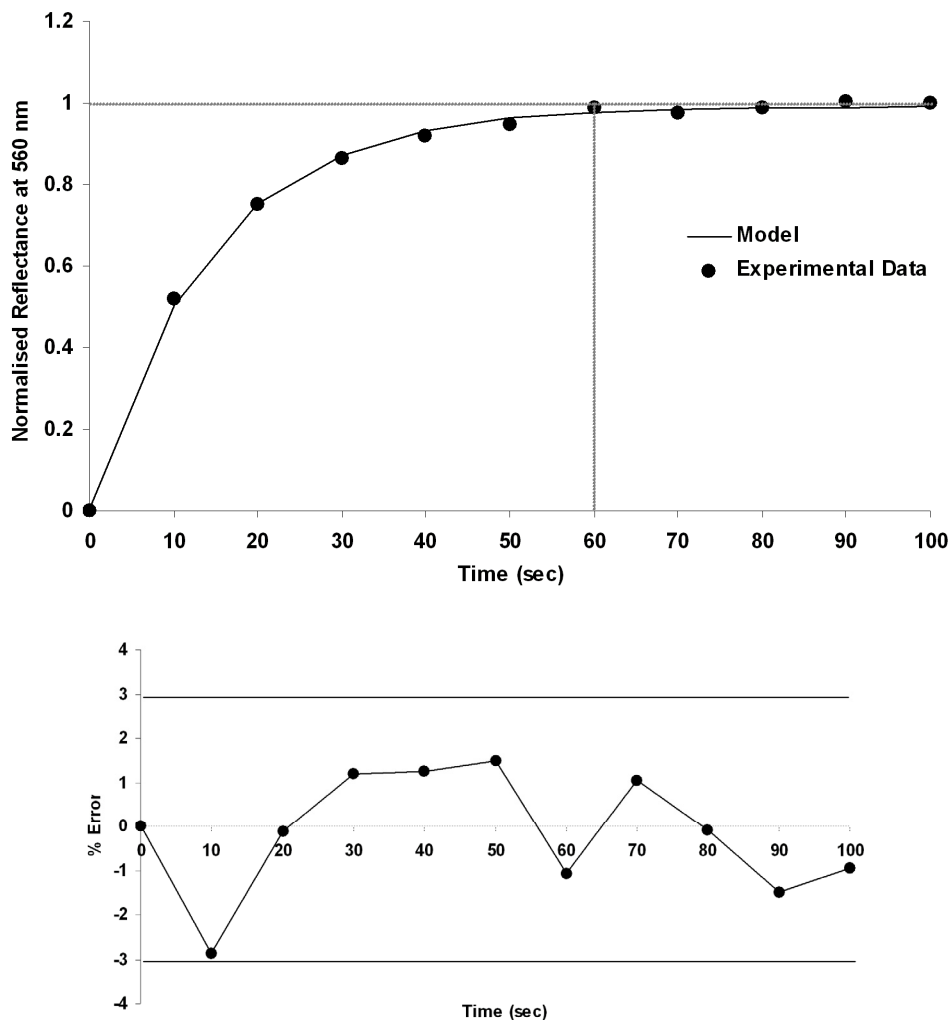


Figure 3.5: (Above) Normalised reflectance values recorded during UV LED irradiation (375 nm) of an PS(15)SP microbead sample (0.01g in 1.3 ml of ethanol) showing that the maximum reflectance value at 560 nm for the conversion to the MC form (plateau) is reached in 60 s. (Below) The residual error calculated between the data and the model does not exceed 3% at any point in the fitted curve.

Green (525 nm), red (630 nm), blue (430 nm) and white (430 -760 nm) LEDs have also been tested for MC \rightarrow SP switching. It was found that after 1 minute irradiation of the MC form with red or blue LEDs, the corresponding reflectance spectra exhibit a consistent 560 nm band, indicating that the coloured MC is still the predominant form. However, after 1 minute exposure to green and white LEDs the MC peak decreases significantly, indicating a much more efficient conversion to the SP form (**figure 3.6**).

Comparing the green and white LEDs, the white is clearly the more efficient: after 60 s exposure of the purple MC form on the bead surface to the white LED, the SP form is fully regenerated, while after 1 minute irradiation with the green LED a small band around 560 nm is still present, although much reduced compared to equivalent exposures using the red and the blue LEDs. It was previously demonstrated⁴ that the green region is the more active region of the visible spectrum for the back-conversion of MC to the SP form.

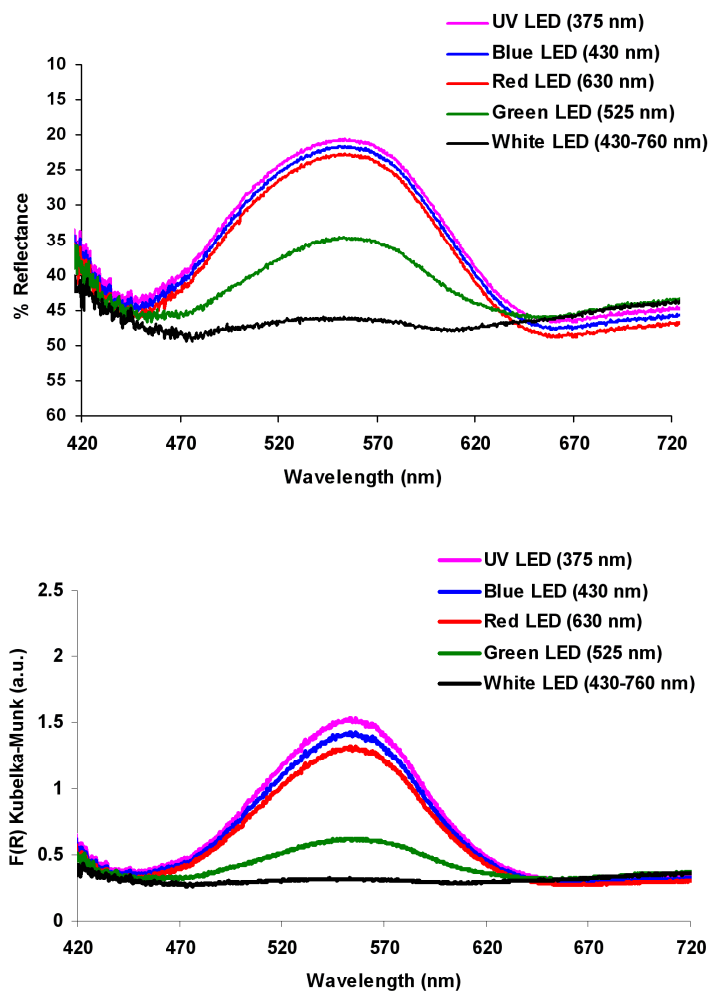


Figure 3.6: (Above) Reflectance spectra of an PS(15)SP microbead sample (0.01g in 1.3 ml of ethanol) after one minute irradiation with UV LED (to promote the conversion to the MC form) and subsequent exposure to blue, red, green and white LED to promote the reconversion to the SP form. (Below) Graph showing the same reflectance spectra after mathematical conversion of the data using the Kubelka-Munk equation.

From these results, it can be concluded that effective SP→MC switching on the microbeads can be achieved through 1 minute irradiation with a UV LED, while the reverse MC→SP switching can be achieved through 1 minute irradiation with a white LED.

The switching efficiency of the surface immobilised spiropyran is also strongly influenced by the presence of a spacer group between the active SP unit and the bead surface. When the spiropyran derivative is simply physically adsorbed on the surface of the beads (after 72 hours of continuous stirring, PS(PA)SP), UV LED irradiation generates almost no colour change. After 1 minute exposure, a faint pink colour appears on the beads and in the supernatant, indicating that SP→MC switching is not effective, and that there is a degree of leaching of SP from the beads, even after repeated washing. Ethanol suspensions of two types of covalently functionalised microbeads (PS(11)SP and PS(15)SP) were also examined.

PS(11)SP, PS(15)SP and PS(PA)SP bead samples were repeatedly exposed (x 20 times) alternatively to 1 minute exposure with a UV-LED followed by 1 minute with a white-LED (figure 3.7).

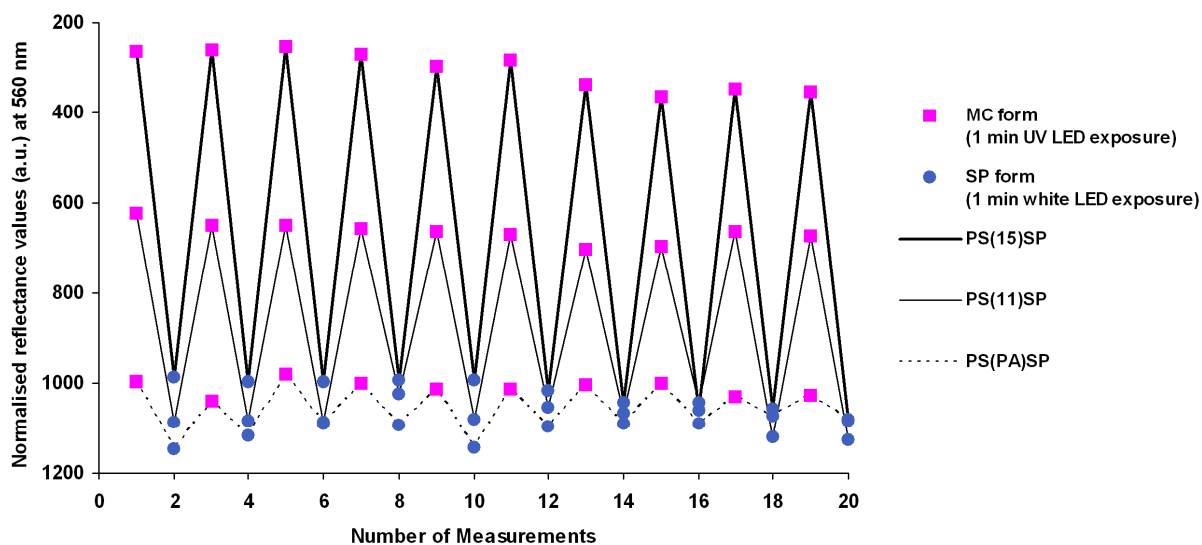


Figure 3.7: Reflectance intensity at 560 nm of the bead surface functionalised with different immobilisation strategies after repeated switching cycles consisting of 1 minute UV-LED irradiation followed by 1 minute white-LED irradiation.

The percentage reflectance values at 560 nm were recorded and the plot clearly shows a high efficiency switching of the beads with the covalently bonded spiropyran while almost no conversion to the MC form is observed on the beads where spiropyran is physically adsorbed.

In contrast, the covalently bound spiropyran appears to be free enough from the surface to be well solvated by the ethanol, which allows the degree of conformational flexibility required for efficient switching between the MC and SP forms. It was previously demonstrated that the use of spacers between a polymeric surface and spiropyran units can dramatically improve the switching efficiency and binding ability, as the molecular re-arrangement that accompanies $SP \leftrightarrow MC$ photoswitching is inhibited if the spiropyran molecule is too close to the surface⁴.

It seems therefore, that when the spiropyran is physically adsorbed onto the microbead surface it is too conformationally restricted for effective switching. Furthermore, considering the length of the tether between the bead surface and the spiropyran unit, the PS(15)SP sample (where 15 atoms separate the spiropyran and the polystyrene surface) was almost twice as efficient at switching compared to the PS(11)SP (where 11 atoms separate the spiropyran and the polystyrene surface).

In view of these results, PS(15)SP bead sample was used in all subsequent experiments to compare the ring closing relaxation kinetics in several solvents.

This involved inducing the formation of the MC state by exposure to the UV-LED for 1 minute, and recording reflectance spectra at fixed time intervals as equilibrium is re-established between the SP and MC forms. It is known from solution studies that this process follows first order kinetics⁶, with the thermodynamics and kinetics strongly influenced by the solvent. The use of SP-functionalised microbeads enables the switching behaviour to be examined in a wider range of solvents, including water, in which spiropyran is not soluble. During these measurements, the sample is kept in the dark to avoid the influence of the ambient light on the reversion to the SP form (**figure 3.8**).

The first order rate constants for the $SP \rightarrow MC$ conversion induced by UV-LED irradiation was estimated by fitting the normalised reflectance values at 560 nm using Microsoft Excel Solver^{28, 27} using **equation 3.2**.

Fitting the experimental data into the model described by the equation (**figure 3.8**), the rate constant for the ring closing in different solvents was determined as reported on **table 3.4** with all the experimental values not exceeding the 3% error from the estimated model (**figure 3.9**).

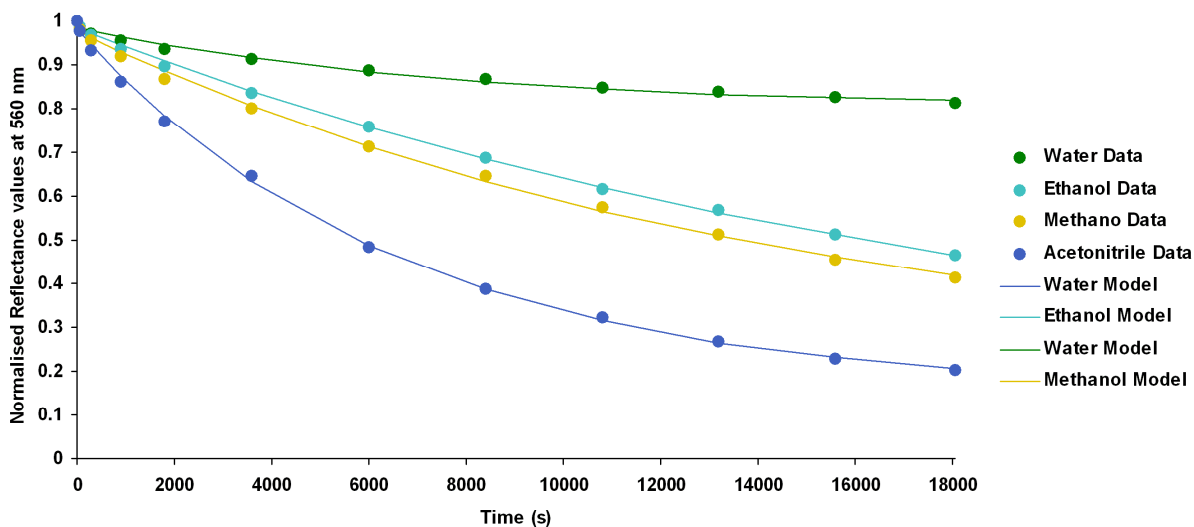


Figure 3.8: Normalised reflectance values at 560 nm of a PS(15)SP bead sample (0.01g in 1.3 ml of solvent) in different solvents. The decrease in reflectance intensity indicates MC form reverting to SP form in the dark after irradiation with a UV-LED. The residual error calculated between the data and the model in between does not exceed 3% at any point in the fitted curve (**figure 3.9**).

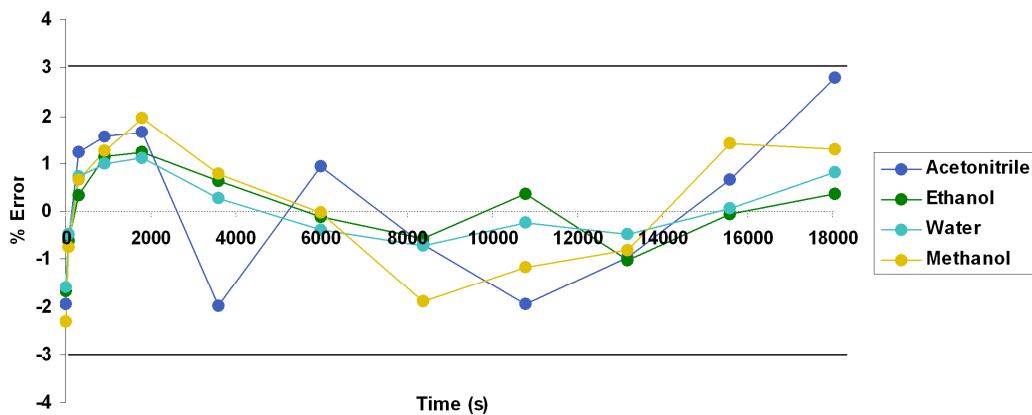


Figure 3.9: The residual error calculated between the data and the model does not exceed 3% at any point in the fitted curve.

Solvent	k_R (s⁻¹)	Ratio to Ethanol
Water	1.3×10^{-4}	2.6
Methanol	6.8×10^{-5}	1.3
Ethanol	5.0×10^{-5}	1
Acetonitrile	1.5×10^{-4}	3.0

Table 3.4: Rate constants for the reversion of MC to SP obtained from the best-fit curves in figure 8. On the right, the ratios to the ethanol rate constant are reported.

These results show that the equilibrium between the two forms strongly depends on the solvent type, which suggests that the surface immobilised dye is actively interacting with the solvent molecules. For example, in water the conversion of the MC to the SP form is strongly inhibited, and after 300 minutes MC is still the predominant form. This behaviour is not surprising, as the zwitterionic MC form is stabilised in highly polar environments compared to the more hydrophobic SP form.

Methanol and ethanol exhibit intermediate behaviour between water and acetonitrile. For example, after 5 hours the MC form is still present at around 50% of its initial concentration. In acetonitrile after 300 minutes, the MC has been almost fully converted to the SP form. Considering the kinetic values, methanol ($6.8 \times 10^{-5} \text{ s}^{-1}$) and ethanol ($5.0 \times 10^{-5} \text{ s}^{-1}$) are pretty close, even though, the rate constant obtained in methanol is slightly larger. Interestingly the value obtained for water ($1.3 \times 10^{-4} \text{ s}^{-1}$) is similar to that of acetonitrile ($1.5 \times 10^{-4} \text{ s}^{-1}$), despite the fact that the steady-state greatly favours MC in water, and SP in acetonitrile.

In general, the obtained values are lower when compared to relaxation times obtained for SP-1 in solution with the same solvents (**Chapter 1**), where the rate of the spiropyran closing is on the time scale of $10^{-2}/10^{-3} \text{ s}^{-1}$. Similar values are obtained for polystyrene doped film in dry state²⁷, where the reported closing kinetic is around 10^{-2} s^{-1} and in which spiropyran is simply incorporated within the polymeric matrix without any covalent immobilisation. This time scale are considerably faster when compared to closing kinetics recorded for the spiropyran immobilised on the polystyrene bead surface, which are on the $10^{-4}/10^{-5} \text{ s}^{-1}$ scale, around two orders of magnitude slower.

The fact that free spiropyran either in solution or entrapped within a polymer is showing faster relaxation kinetic is probably an effect of the higher degree of freedom of the molecule, when compared to a surface immobilised spiropyran on microbead shaped polymer.

3.5.4 Photostability

Another issue to be considered when dealing with spiropyran photochromic dyes is their photostability over time, due to a well documented photobleaching process^{3,29-32} that occurs when the molecule is exposed to UV-vis radiation for extended time periods. It is generally agreed that photodegradation is enhanced by the presence of free radical or singlet oxygen, by the formation of MC aggregates and by the light source used (especially in the UV region). It has been demonstrated that the introduction of antioxidant groups as free radical scavengers or the reduction of MC aggregation remarkably reduces the photodegradation^{27,30}. In the same way, moving to low-power light sources such as LEDs (less photon density) and the immobilisation of the spiropyran on the bead surface should reduce the extent of photodegradation, as was demonstrated previously with SP covalently immobilised on a PMMA (polymethylmetacrylate) film¹⁰. In this work, the switching efficiency in ethanol was evaluated by normalising the difference in the reflectance value at 560 nm to the initial values:

$$\%E = \frac{(R_{SPi} - R_{MCi})}{(R_{SP} - R_{MC})} \times 100 \quad [3.3]$$

where %E is the percent efficiency, R_{SPi} and R_{MCi} are the initial values of reflectance of the MC and the SP forms when the initial switching was performed and R_{SP} and R_{MC} are the reflectance values obtained in subsequent switching cycles.

According to this model, 100% is the maximum efficiency, when no photodegradation occurs, while 0% is when the photochromic dye is completely photobleached.

After 50 switching cycles (one minute irradiation with UV LED followed by one minute exposure to white LED), the efficiency was found to decrease by around 40% with respect to the initial switching values in two samples of freshly prepared PS(15)SP. For

both samples the final percent efficiency value is around 60% which directly corresponds to the proportion of surviving MC (**figure 3.10**).

This is an improvement compared to the solution studies reported by Li et al. in which the percentage of surviving MC in methanol after just 13 switching cycles (with a 30 s UV irradiation for each cycle, using high pressure mercury lamp) is around 56.4%³. However, it is not as efficient as other polymeric immobilisation strategies using a film matrix, where after more than 380 cycles using LEDs the decrease in photostability is around 14% (86% of surviving MC)¹⁰. Although the photostability of the spiropyran immobilised on the bead surface is improved when compared to the spiropyran in solution, due to the covalent immobilisation of the dye and to the use of low power light-sources such as LEDs, the fact that the microbeads are free to move and interact between each other, allowing eventual MC aggregation, make them less photostable when compared to film immobilisation strategy.

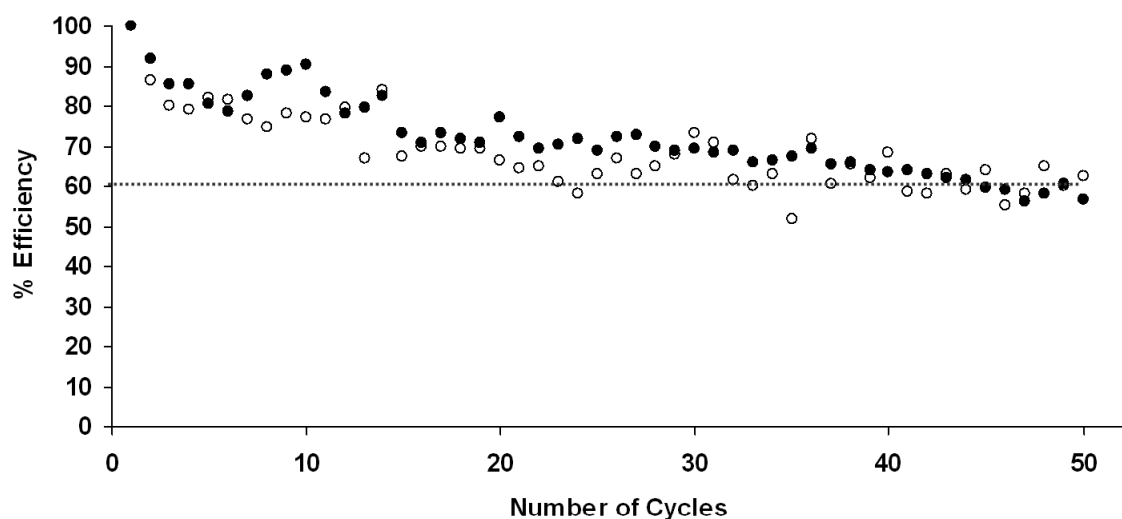


Figure 3.10: Decrease in switching efficiency of two samples (dotted and full circles) of PS(15)SP (0.01 g suspended in 1.3 ml of ethanol) after 100 switching events. The efficiency was evaluated monitoring the reflectance value at 560 nm, according to the reported formula and shows a decrease of ca. 40% after 50 cycles.

3.5.5 Ion-binding behaviour of spiropyran coated microbeads

Spiropyran functionalised microbeads offer the interesting possibility of control metal ion uptake and release using light, as only the MC form binds with metal ions. It should, therefore, be possible to determine when and where ion binding occurs (e.g. by illuminating with a UV-LED), and as the beads are mobile, the bound ions can be transported to another location, at which the ions can be released by illumination with a white LED.

Once the beads are reconverted again to the MC form, the surface is ready for re-use. Furthermore, the system is inherently self-indicating, and by monitoring the colour, it can be seen which form is present (SP or MC) and whether ions are bound (colour/UV-vis spectrum changes again) (**figure 3.11**).

Based on previous solution studies (**Chapter 1**), Ca^{2+} , Cu^{2+} , Co^{2+} , Cd^{2+} , Zn^{2+} , Hg^{2+} ions were chosen in order to investigate the ion binding behaviour of the MC form on the polystyrene microbeads surface. When the purple MC-activated beads are placed in contact with a copper (II) nitrate solution they undergo a further colour change from pink to orange. The change is reversible, upon irradiation with white light and replacement of the supernatant with fresh solvent, the SP form is restored, the metal is expelled, and the beads can be converted again to the MC form ready for another ion binding cycle.

These colour changes can be monitored by recording the UV-vis reflectance spectra. In the presence of Cu^{2+} ions the 560 nm band decreases and is shifted towards a lower wavelength (around 520 nm) and another band appears around 445 nm (**figure 3.12**).

When the same experiment is repeated using instead Ca^{2+} , Cd^{2+} , Hg^{2+} ions at the same concentration, in the same solvent no colour change is detected (**figure 3.12** and **figure 3.13**).

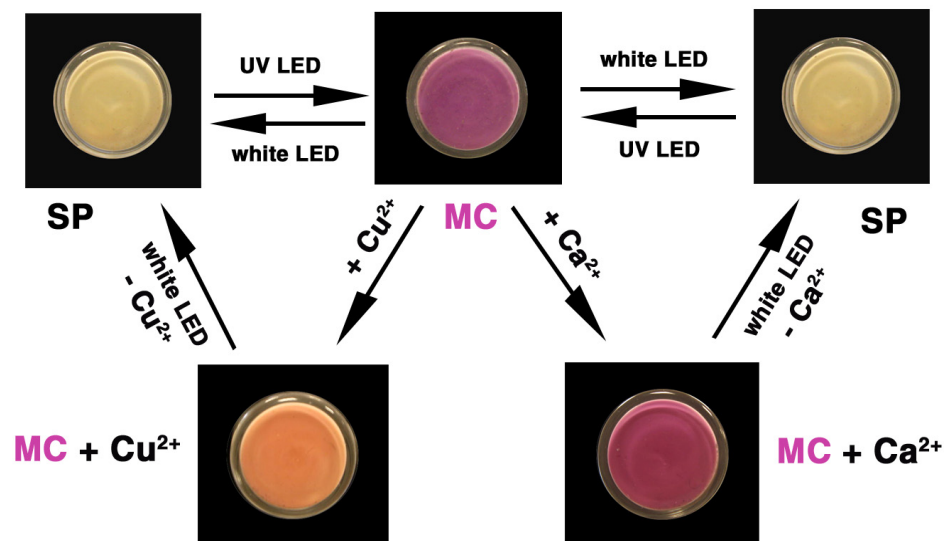


Figure 3.11: Microbead colour changes (PS(15)SP), 0.01g in 1.3 ml of ethanol) observed during switching between the SP and MC forms, and in the presence of Cu²⁺ and Ca²⁺ ions (final concentration 7.1×10^{-4} M in ethanol).

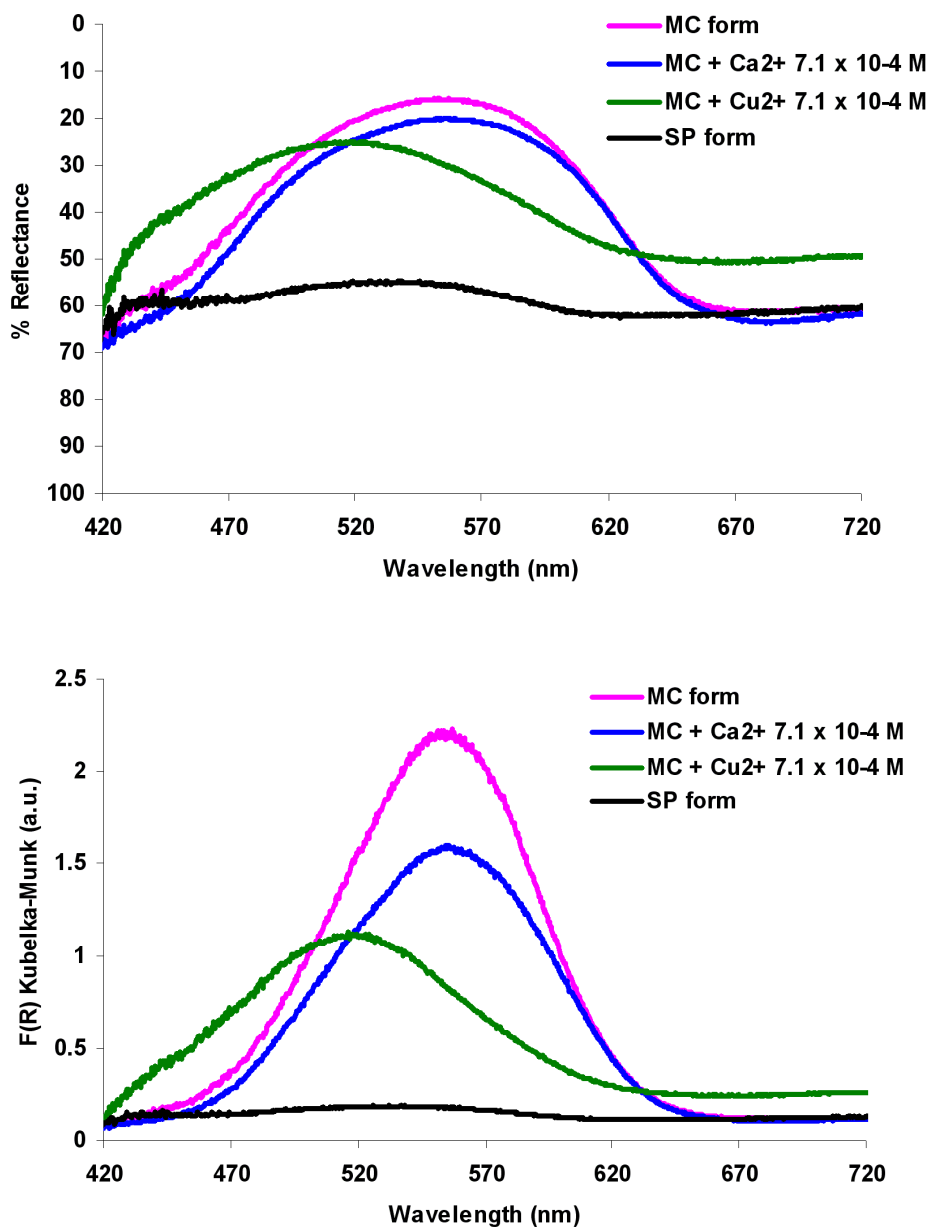


Figure 3.12: (Above) Reflectance spectra of the colour changes occurring on a sample of PS(15)SP (0.01g in 1.3 ml of ethanol): in the presence of Cu²⁺ the 560nm peak shift around 520 nm with an increase around 445nm, in the presence of Ca²⁺ no detectable spectra change is recorded. (Below) Graph showing the same reflectance spectra after mathematical conversion of the data using the Kubelka-Munk equation.

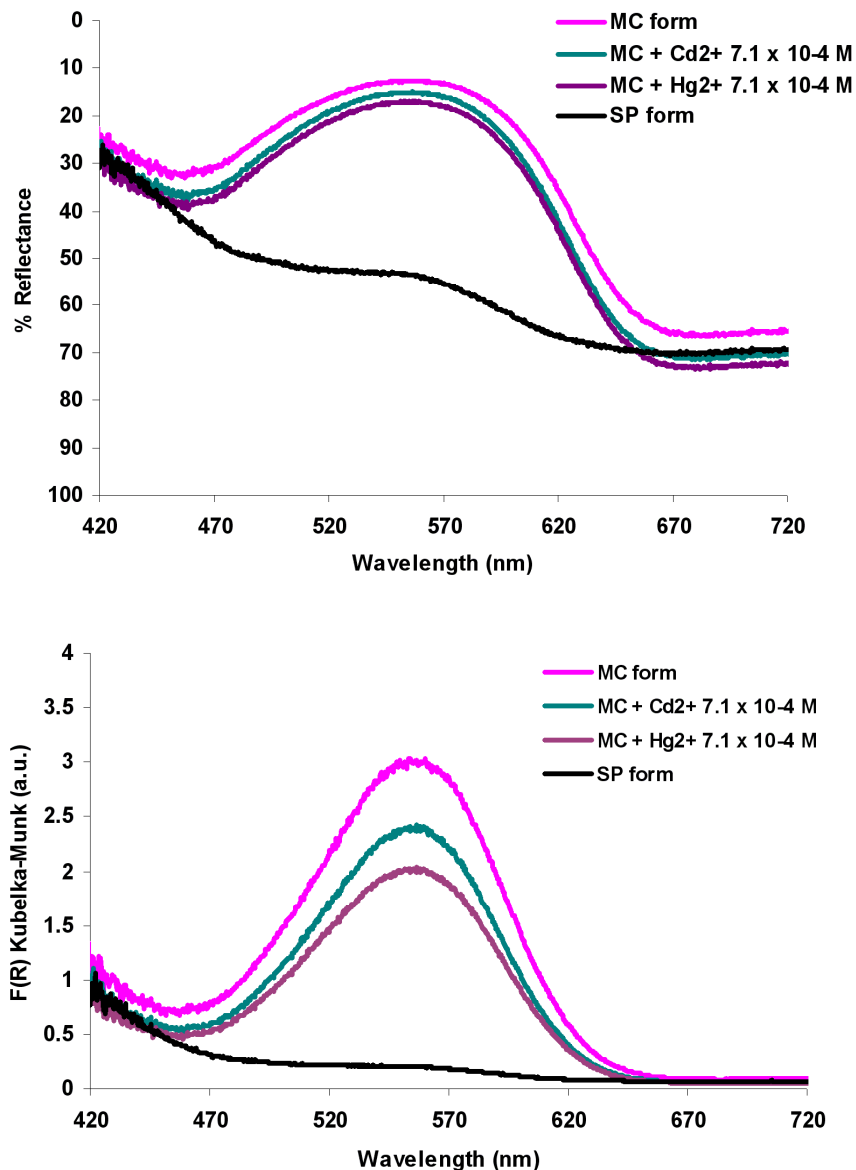


Figure 3.13: (Above) Reflectance spectra of the MC form of a sample of PS(15)SP (0.01g in 1.3 ml of ethanol): in the presence of Cd²⁺ and Hg²⁺: no detectable spectra change is recorded. (Below) Graph showing the same reflectance spectra after mathematical conversion of the data using the Kubelka-Munk equation.

In the presence of Co²⁺ and Zn²⁺, small shifts are observed in the MC spectra, from 560 nm to 540 nm (**Figure 3.14**), but no visual colour change could be detected.

The spectra of the MC in the presence of Co²⁺ and Zn²⁺ is affected in a similar way at the same concentration probably due partial complex formation.

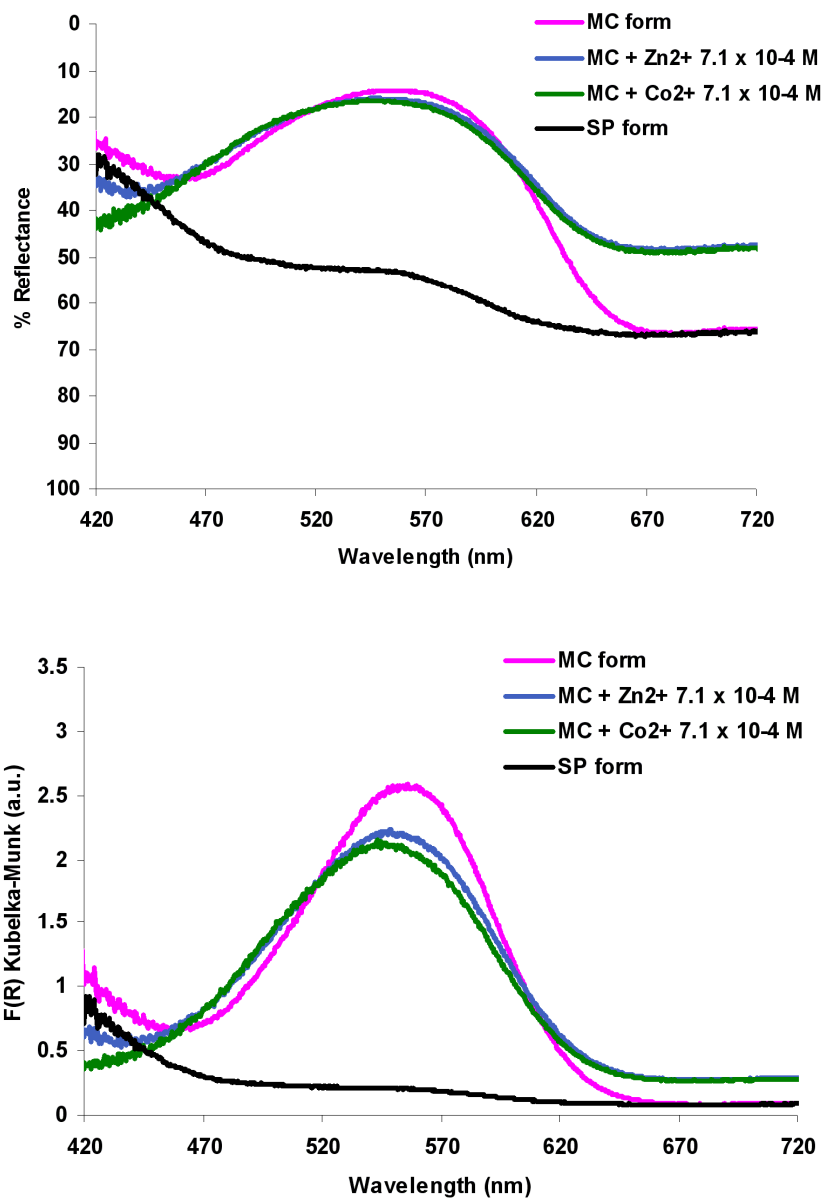


Figure 3.14: (Above) Reflectance graph showing the changes of the reflectance spectra of the MC form of a sample of PS(15)SP in the presence of Co²⁺ and Zn²⁺ ions (final concentration 7.1 x 10⁻⁴ M in ethanol) which produce a smaller shifts in the absorption band from 560 nm to 540 nm. (Below) Graph showing the same reflectance spectra after mathematical conversion of the data using the Kubelka-Munk equation.

The most striking colour and spectral change is observed in the presence of Cu²⁺ ions, where the 560 nm MC band decreases and is shifted towards a lower wavelength with the appearance of a new band around 445 nm.

Adding increasing Cu^{2+} to the beads converted in the MC form (7.1×10^{-6} M, 7.1×10^{-5} M and 7.1×10^{-4} M in ethanol) a gradual spectral change can be observed (**figure 3.15**) (after each measurement the beads are converted back to the SP form and washed 6 times with fresh ethanol before being converted again to the MC form and exposed to a new Cu^{2+} concentration).

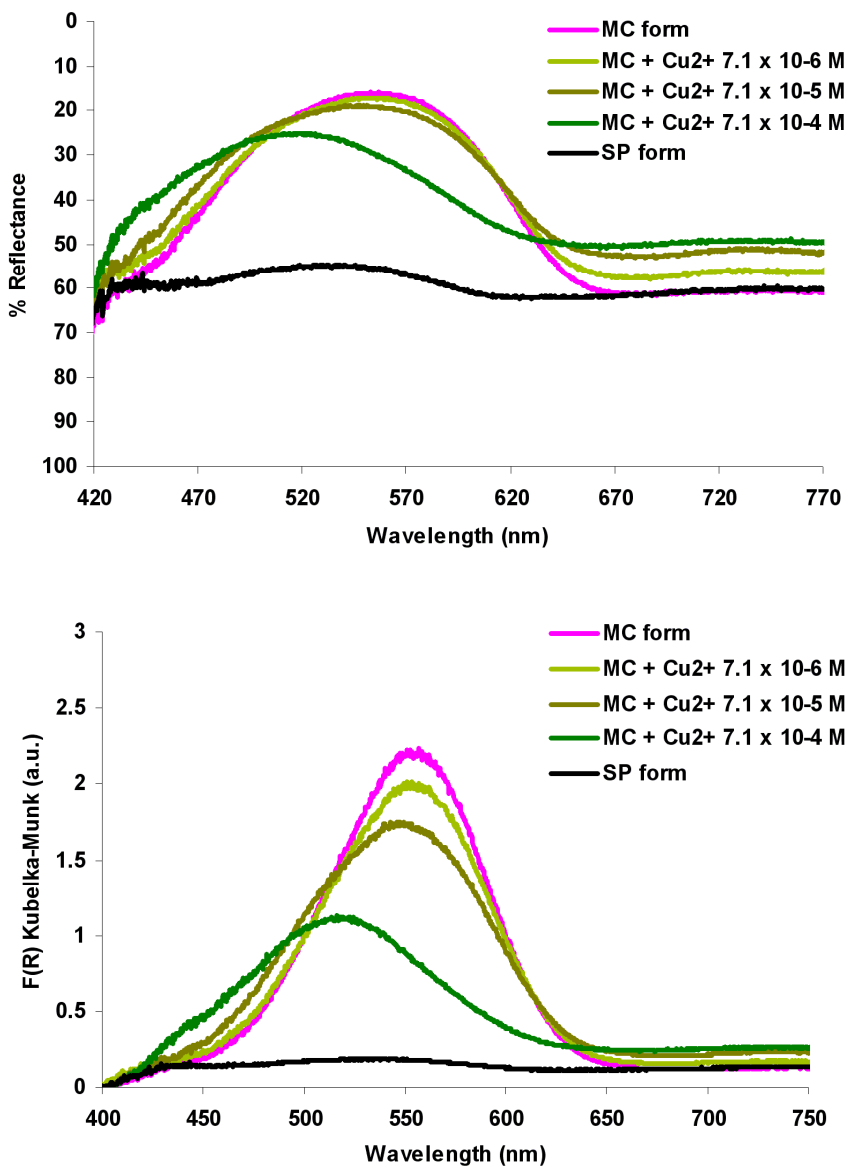


Figure 3.15: (Above) Spectral changes of a sample of PS(15)SP accompanying MC→MC-Cu²⁺ complex formation as the Cu²⁺ concentration is increased in the sample from 7.1×10^{-6} M to 7.1×10^{-4} M in ethanol. (Below) Graph showing the same reflectance spectra after mathematical conversion of the data using the Kubelka-Munk equation.

The spectral changes related to $MC \rightarrow MC-Cu^{2+}$ complex formation with the most striking absorbance shifts at 7.1×10^{-4} M where a new band appears at 445 nm and a visual colour change can be observed in the beads. The procedure adopted does not allow a kinetic evaluation of the process as the complex formation is essentially complete when the spectrum is taken.

The complex formation is fully reversible, as shown in (**Figure 3.16**), which shows 6 repeat cycles through SP, MC, $MC-Cu^{2+}$ complex, and back to SP. The spectra show that at 560 nm the MC has the highest absorbance while the $MC-Cu^{2+}$ complex has much lower value (the 560 nm band decreases in the presence of the metal ion), while the SP form has the lowest of all, as expected as this form has no absorbance in this region of the UV-vis spectrum. In contrast, at 445 nm, the $MC-Cu^{2+}$ has the highest absorbance whereas the MC and SP form values are lower.

In comparison, the presence of Ca^{2+} causes no change in the 560 nm MC band (**figure 3.12**), and therefore the spiropyran microbeads system can definitely differentiate between Ca^{2+} and Cu^{2+} ions.

We have found that Cu^{2+} produces the most striking blue-shift upon binding with MC, though other ions such as Co^{2+} do cause a smaller shift in the MC spectra upon binding⁴.

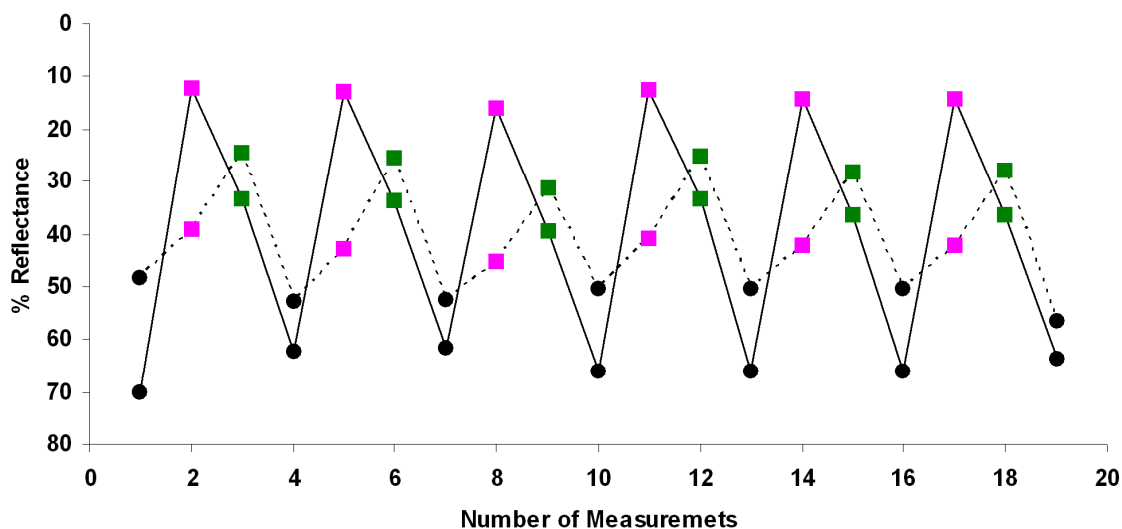


Figure 3.16: Switching cycles of PS(15)SP sample (0.01g in 1.3 ml of ethanol) between the SP (black circle), MC (pink square) form and $MC-Cu^{2+}$ complex (green square). The percentage reflectance values have been evaluated at 560 nm (continuous line) and at 445 nm (dotted line).

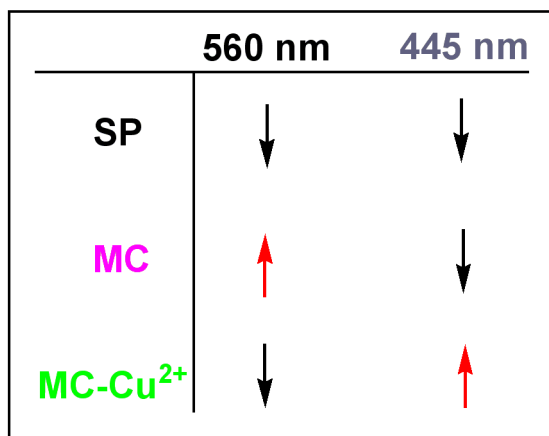


Figure 3.17: Schematic representation of the absorbance changes at 560 nm and 445 nm which are happening on the surface of PS(15)SP microbeads in the presence of the SP, MC and MC-Cu²⁺ complex.

Monitoring the absorbance at 445 nm and 560 nm it is possible to identify the state of the photochromic molecule and to know whether a binding event is happening on the bead surface (**figure 3.17**).

The SP form presents a low absorbance value both at 560 nm and 445 nm. When the MC form appears on the bead surface as a consequence of UV exposure, the 560 nm absorbance increases, while the 445 nm absorbance value remains the same. In the presence of Cu²⁺ both 560 nm and 445 nm absorbance values increase as a consequence of the complexation operated by the MC form. Then upon irradiation of the system with white light, both the 560 nm and 445 nm absorbances decrease and Cu²⁺ is released.

3.6 Conclusions

Polystyrene microbeads have been successfully functionalised with spiropyran and they have been characterised using SEM, contact angle and reflectance spectroscopy.

The most effective functionalisation occurred for the PS(15)SP sample, where 15 atoms divide the spiropyran unit and the polystyrene bead surface.

The spiropyran functionalised beads retain their photochromic behaviour and can be switched using light between the SP and MC forms. The thermodynamic ring closing process of the MC form is affected by the solvent type in terms of thermal conversion in the dark to the SP form, as it was previously recorded for SP-1 in solution (**Chapter 1**)

even though the kinetic values recorded for the spiropyran immobilised on the beads surface are sixty times slower than for the spiropyran in solution.

Different metal ions have been placed in contact with the MC form and we can conclude that the functionalised microbeads exhibit ion-binding behaviour and they can be photo-reversibly switched between an active (binding) and an inactive (non-binding) form. The active form selectively complexes Cu^{2+} and presents small affinities towards Zn^{2+} and Co^{2+} but appears to be unaffected in the presence of Ca^{2+} , Cd^{2+} , Hg^{2+} whereas the inactive form (SP) does not bind ions. These results show that spiropyran modified beads can be used for the photo-controlled selective accumulation and release of ions. Furthermore, the system is inherently self-indicating in the case of Cu^{2+} , as each form (SP, MC, $\text{MC}_2\text{-Cu}^{2+}$) has a different colour and UV-vis absorbance spectrum.

On the basis of this behaviour, the foundation for a photocontrolled system for retention and elution of metal ions can be laid: irradiation of the stationary phase with UV-LEDs causes retention of guest species due to the presence of the MC form, while subsequent exposure to white LEDs causes release of guest species into the mobile phase, providing a potential route to photodynamic liquid chromatography. Beads can be easily packed into capillary column that could be used for photo-controlled separations. This concept could also be usefully applied generally to photo-accumulation of ions, their transport to other locations and subsequent photo-release. The incorporation of spiropyran functionalised beads to create new photoswitchable stationary phases will be further discuss on **Chapter 5**.

3.7 References

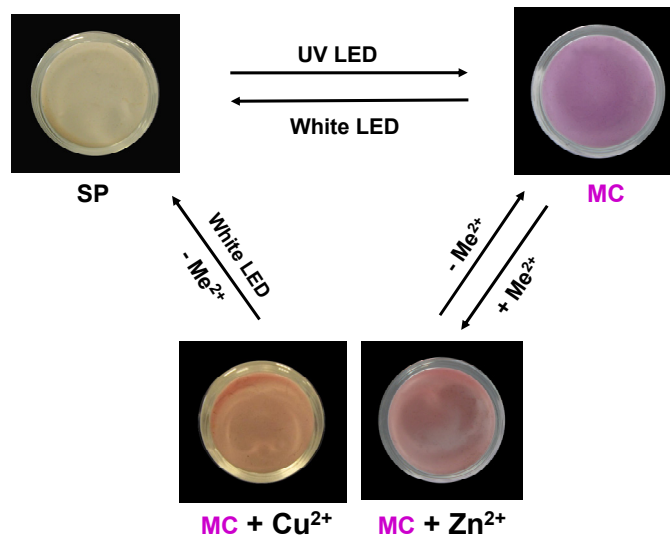
- (1) Minkin, V. I. *Chemical Reviews* **2004**, *104*, 2751-2776.
- (2) Dürr, H.; Bouas, L. H. *Photochromism - molecules and systems*; Elsevier: Amsterdam, Boston, 2003.

- (3) Li, X.; Li, J.; Wang, Y.; Matsuura, T.; Meng, J. *Journal of Photochemistry and Photobiology A: Chemistry* **2004**, *161*, 201-213.
- (4) Byrne, R. J.; Stitzel, S. E.; Diamond, D. *Journal of Materials Chemistry* **2006**, *16*, 1332-1337.
- (5) Görner, H.; Chibisov, A. K. *Journal of the Chemical Society, Faraday Transactions* **1998**, *94*, 2557-2564.
- (6) Görner, H. *Physical Chemistry Chemical Physics* **2001**, *3*, 416-423.
- (7) Zhou, J.-W.; Li, Y.-T.; Song, X.-Q. *Journal of Photochemistry and Photobiology A: Chemistry* **1995**, *87*, 37-42.
- (8) Suzuki, T.; Kato, T.; Shinozaki, H. *Chemical Communication* **2004**, 2036-2037.
- (9) Shao, N.; Zhang, Y.; Cheung, S.; Yang, R.; Chan, W.; Mo, T.; Li, K.; Liu, F. *Analytical Chemistry* **2005**, *77*, 7294-7303.
- (10) Radu, A.; Scarmagnani, S.; Byrne, R.; Slater, C.; Lau, K. T.; Diamond, D. *Journal of Physics D: Applied Physics* **2007**, 7238-7244.
- (11) Kim, M.-S.; Chung, W.-J.; Cho, S.-H.; Kim, B.-G.; Lee, Y.-S.; Kim, Y.-K. *Transducers* **2003**.
- (12) Ohshima, H.; Furusawa, K. *Electrical Phenomena at Interfaces: Fundamentals, Measurements, and Applications* Marcel Dekker, 1998.
- (13) Fujiwara, T.; Harada, J.; Ogawa, K. *Journal of Physical Chemistry B* **2004**, *108*, 4035-4038.
- (14) Paradkar, R. P.; Williams, R. R. *Applied Spectroscopy* **1996**, *50*, 753-758.
- (15) Paleologos, E. K.; Prodromidis, M. I.; Giokas, D. L.; Pappas, A. C.; Karayannis, M. I. *Analytica Chimica Acta* **2002**, *467*, 205-215.

- (16) Koji, S.; Toshihiko, N. *Journal of Photopolymer Science and Technology* **2001**, *14*, 233-238.
- (17) Hughes, V. K.; Ellis, P. S.; Burt, T.; Langlois, N. E. I. *Journal of Clinical Pathology* **2004**, *57*, 355–359.
- (18) Gade, J.; Palmqvist, D.; Plomgård, P.; Greisen, G. *Physics in Medicine and Biology* **2006**, *51*, 121-136.
- (19) Balkenius, A.; Kelber, A. *Journal of Experimental Biology* **2004**, *207*, 3307-3316.
- (20) Hoffmann, C. M.; Cronin, T. W.; Omland, K. E. *Evolution* **2006**, *60*, 1680-1691.
- (21) Yoshioka, S.; Kinoshita, S. *Journal of the Optical Society of America A* **2006**, *23*, 134-141.
- (22) Rosario, R.; Gust, D.; Hayes, M.; Jahnke, F.; Springer, J.; Garcia, A. A. *Langmuir* **2002**, *18*, 8062-8069.
- (23) MacLaren, D. C.; White, M. A. *Journal of Materials Chemistry* **2003**, *13*, 1701-1704.
- (24) Pauw, A. *American Journal of Botany* **2006**, *93*, 917-926.
- (25) Mäthger, L. M.; Hanlon, R. T. *Biology Letters* **2006**, *2*, 494-496.
- (26) García, M. T.; Gracia, I.; Duque, G.; Lucas, A. d.; Rodríguez, J. F. *Waste Management* **2009**, *29*, 1814-1818.
- (27) Stitzel, S.; Byrne, R.; Diamond, D. *Journal of Materials Science* **2006**, *41*, 5841-5844.
- (28) Diamond, D.; Hanratty, V. C. A. *Spreadsheet Applications in Chemistry using Microsoft Excel*; Wiley: New York, 1997.

- (29) Baillet, G.; Giusti, G.; Guglielmetti, R. *Journal of Photochemistry and Photobiology A: Chemistry* **1993**, *70*, 157-161.
- (30) Baillet, G.; Campredon, M.; Guglielmetti, R.; Giusti, G.; Aubert, C. *Journal of Photochemistry and Photobiology A: Chemistry* **1994**, *83*, 147-151.
- (31) Matsushima, R.; Nishiyama, M.; Doi, M. *Journal of Photochemistry and Photobiology A: Chemistry* **2001**, *139*, 63-69.
- (32) Demadrille, R.; Rabourdin, A.; Campredon, M.; Giusti, G. *Journal of Photochemistry and Photobiology A: Chemistry* **2004**, *168*, 143-152.

Photoreversible Ion-Binding using Spiropyran Modified Silica Microbeads



4.1 Introduction

Chapter 3 focused on the photoswitchable behaviour of spiropyran modified polystyrene beads. The conclusion was that polystyrene beads can be reversibly switched using LEDs between a white SP form and a pink MC form, which in the presence of copper ions undergoes another reversible self-indicating colour change¹. Irradiation with a UV LED (375 nm) for one minute switches the spiropyran functionalised beads to the MC form, while one minute irradiation with a white LED (430-760 nm) converts the MC back to the SP form. In the presence of Cu²⁺ ions the MC absorbance at 560 nm decreases and a new peak appears around 445 nm which is associated with the formation of the MC-Cu²⁺ complex. Subsequently, the metal ion can be easily expelled using a white LED, converting the MC back to the SP form.

Polystyrene beads present high light scattering in all of the four compatible solvents studied and this is due to non-matching of the refractive index of the beads and solvents (**Chapter 1**).

For this reason, absorbance spectroscopy cannot be used and the characterisation of their photoswitchable behaviour has been carried out by reflectance measurements using an *ad-hoc* designed set-up.

In the context of comparing the effect of different bead substrates, the immobilisation of spiropyran on silica beads has also been evaluated.

Silica beads are for their nature compatible with a wider range of solvents than polystyrene beads, and their refractive index is 1.37, which is very close to solvents such as ethanol (1.36), acetone (1.35), hexane (1.37), acetonitrile (1.34) and water (1.33).

Therefore, they can be analysed using absorbance spectroscopy which is an obvious advantage. The compatibility with a broader range of solvents with different physical properties also provides greater flexibility in controlling the switching equilibrium. The chemistry of the immobilisation process, similar to the one previously reported in the literature for the functionalisation of glass slides with spiropyran², involves firstly the modification of the silica surface with amino and carboxyl functional groups and afterwards the covalent immobilisation of a modified spiropyran moiety.

The chapter is therefore focused on the photoswitchable behaviour and light-modulated ion-binding properties of these spiropyran modified silica microbeads.

LEDs were chosen as light sources for controlling the photochromic equilibrium on the surface of the microbeads. We have previously demonstrated that using LEDs instead of more powerful light sources substantially reduces the well-known photodegradation processes³ that occur when the switching equilibrium between the SP and the MC form is performed repeatedly over time⁴⁻⁸. Despite the fact that the power of LEDs is much lower than the more commonly employed arc lamp light sources (1 mW/cm² compared to 50-100 W), the switching efficiency is relatively unaffected and repeated switching can be successfully performed^{3,9,10}.

4.2 Experimental: Materials and instruments

Silica microbeads 5 ± 0.35 μm diameter (5 % solid contents), N-(3-dimethylaminopropyl)-N'-ethylcarbodiimide hydrochloride (EDC hydrochloride), (3-Aminopropyl)triethoxysilane (APTES), 4-(triethoxysilyl)butyronitrile (TESBN), 1,8-diaminooctane, 1,4-diaminobutane, 4-(triethoxysilyl)butyronitrile, N,N'-Dicyclohexylcarbodiimide (DCC), 4-(dimethylamino)pyridine (DMAP), sulphuric acid 95-98%, hydrogen peroxide 30% w/w solution, calcium nitrate hydrate, copper(II) nitrate trihydrate, calcium chloride hexahydrate, mercury(II) chloride, zinc chloride, cadmium nitrate tetrahydrate, cobalt(II) nitrate hexahydrate were purchased from Sigma Aldrich (Ireland). Hydrochloric acid 32%, density 1.16 g/cm³ was purchased from Fisher Scientific.

Atomically smooth muscovite mica discs (diameter 9.5 mm) and circular glass coverslips (diameter 30 mm) were purchased from ProSci Tech, Australia.

Ammonia solution 25% was purchased from Sharlau Chemie (Spain) and 1'-(3-carboxypropyl)-3',3'-dimethyl-6-nitrospiro(2H-1)benzopyran-2, 2'-(2H)-indole (SPCOOH) was synthesised as described elsewhere² (**Chapter 1, Figure 1.21**).

Elemental analysis was carried out in the Microanalysis Department in University College Dublin using an Exeter Analytical C-440 Elemental Analyser.

Contact angle measurements were conducted on "DataPhysics OCA20 Goniometer" (Germany) which utilises "SCA 21 Software".

The UV light source used for contact angle evaluations was a BONDwand UV-365nm obtained from Electrolyte Corporation, USA while a Lloytron 60W desk lamp was used as a white light source. SEM images were taken using an S-3000N VP SEM, Hitachi, Japan.

UV (375 nm) and white (430-760 nm) LEDs were purchased from Roithner Laser Technik, Austria. Absorbance spectra were recorded using an Absorbance Plate Reader (BioTek Instruments, Inc., USA) and a Perkin Elmer UV-vis Spectrometer Lambda 900. Glass coated microplate 96 wells (370 μ l each) coated with a 200 nm layer of silicon dioxide was purchased from Antech (Ireland) in order to carry out measurements of the beads in different solvents.

Sample spinning was carried out using a ROTOFIX 32 centrifuge (Global Medical Instrumentation, Inc., USA.). Homogeneous suspensions of microbeads were generated using a Branson Ultrasonic Cleaner 5510 from Branson Ultrasonics Corporation, USA. The AFM microscope used was a JPK Biowizard II (JPK Instruments AG, Berlin, Germany) and the data were processed using JPK AFM software.

Cantilevers were PNP-DB Pyrex-Nitride Cantilevers with a 65 nm chromium/gold coating for high laser reflectivity (Nanoworld AG, Switzerland). They present a pyramidal tip with a length of 100 μ m, 40 μ m width and 3.5 μ m height.

For the bead attachment to the cantilever tip a DC-3K micromanipulator from Märzhäuser Wetzlar (Germany) and a 2 part epoxy-glu were used (Farnell, Ireland).

4.3 Synthesis and characterisation of spiropyran functionalised silica microbeads

4.3.1 Amino functionalisation of the silica microbead surface

A sample of a suspension of silica microbeads (0.1 g in 2 ml of water) was diluted with 22.5 ml ethanol. 2.5 ml of 25% ammonia solution and 2 ml of APTES were added and the mixture stirred under reflux for 48 hours. The microbead suspension was then cooled, separated from the reaction mixture by centrifugation, suspended in 4 ml of ethanol and washed 6 times with fresh ethanol. The resulting microbeads were then stored in 3 ml of ethanol at 4 °C in the dark.

The washing procedure consists of a four step process:

- Centrifugation of the suspension for 3 minutes at 4000 rpm.
- Removal of the supernatant, addition of 4 ml of fresh solvent.
- Sonication of the suspension for 5 minutes.
- Subsequent further centrifugation.

4.3.2 Carboxyl functionalisation of the silica microbead surface

A sample of a suspension of silica microbeads (0.1 g in 0.5 ml of water) was diluted with 3 ml of concentrated hydrochloric acid and refluxed for 30 minutes. The microbead suspension was then cooled and washed five times with water. The sample was then dried in the dark and resuspended in 3 ml of toluene. 1 ml of 4-(triethoxysilyl)-butyronitrile (TESBN) was added and the mixture refluxed for 24 hours.

The resulting nitrile functionalised beads were then washed five times with toluene and dried overnight in the dark. They were then resuspended in a 5 ml solution of 50% sulphuric acid, refluxed for 3 hours, and finally washed 5 times with water and 5 times with ethanol. The resulting carboxylated silica microbeads were stored in 3 ml of ethanol at 4 °C in the dark.

4.3.3 Covalent immobilization of spiropyran on amino functionalised silica microbeads

3 ml of a 15 mg ml⁻¹ solution of SPCOOH in ethanol was added to 2 ml of an 11 mg ml⁻¹ solution of EDC in ethanol. The reaction mixture was stirred for half an hour at room temperature in the dark. A 1 ml suspension of 0.1 g of the amino functionalised microbeads in ethanol was added to the spiropyran/EDC solution and the reaction mixture stirred for 72 hours at room temperature in the dark (**Figure 4.1**). Finally, the spiropyran functionalised microbeads (Si(10)SP) were washed 10 times with ethanol following the above procedure and stored at 4 °C in the dark.

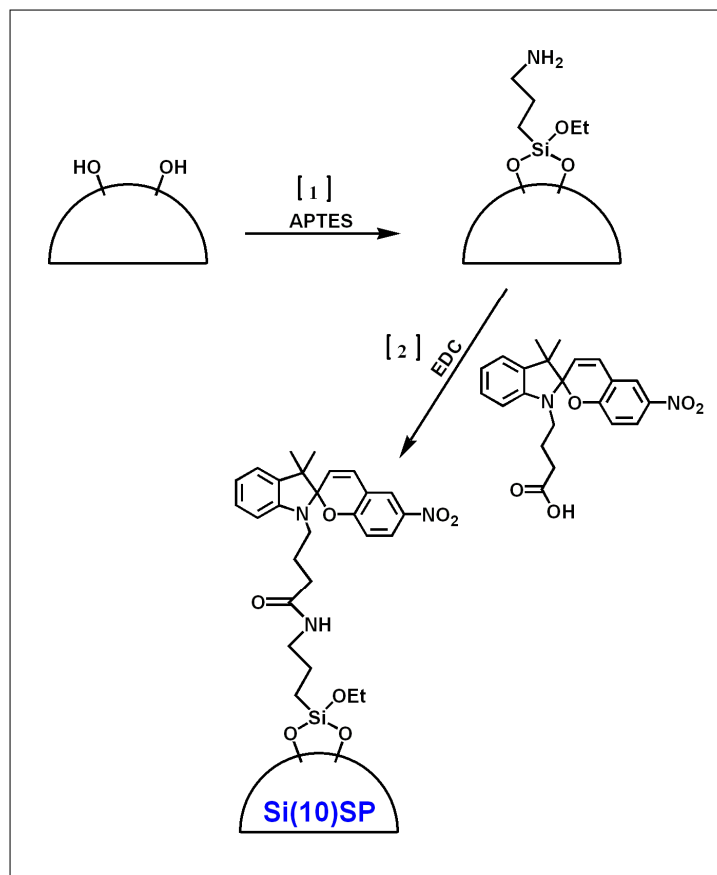


Figure 4.1: Reaction scheme on the silica microbead surface. The first step (1) involves the amination coating of the silica surface and followed by (2) the formation of an amide group using EDC catalysis between the amine group on the bead surface and the carboxylic group on the SPCOOH derivative.

4.3.4 Covalent immobilization of spirocyan on carboxyl functionalised silica microbeads using 4 and 8 carbons diamino linkers

A 3 ml suspension of 0.1 g of the carboxyl functionalised microbeads in ethanol was added to 60 mg of EDC and stirred at room temperature for 30 minutes. Then 50 mg of 1-8 diaminooctane (8 carbons linker) or 30 mg of 1,4 diaminobutane (4 carbons linker) was added and the suspension stirred at room temperature for 24 hours. The microbeads were then washed five times with fresh ethanol.

In parallel 3 ml of a 15 mg ml⁻¹ solution of SPCOOH in ethanol was added to 2 ml of an 11 mg ml⁻¹ solution of EDC in ethanol. The reaction mixture was stirred for half an hour at room temperature in the dark.

Then a 1 ml suspension of 0.1 g of the 8 or 4 carbons amino linker functionalised microbeads in ethanol was added to the spiropyran/EDC solution and the reaction mixture stirred for 72 hours at room temperature in the dark (**Figure 4.2**)

Finally, the spiropyran functionalised microbeads Si(16)SP and Si(20)SP) were profusely washed 10 times with ethanol following the above procedure and stored at 4 °C in the dark.

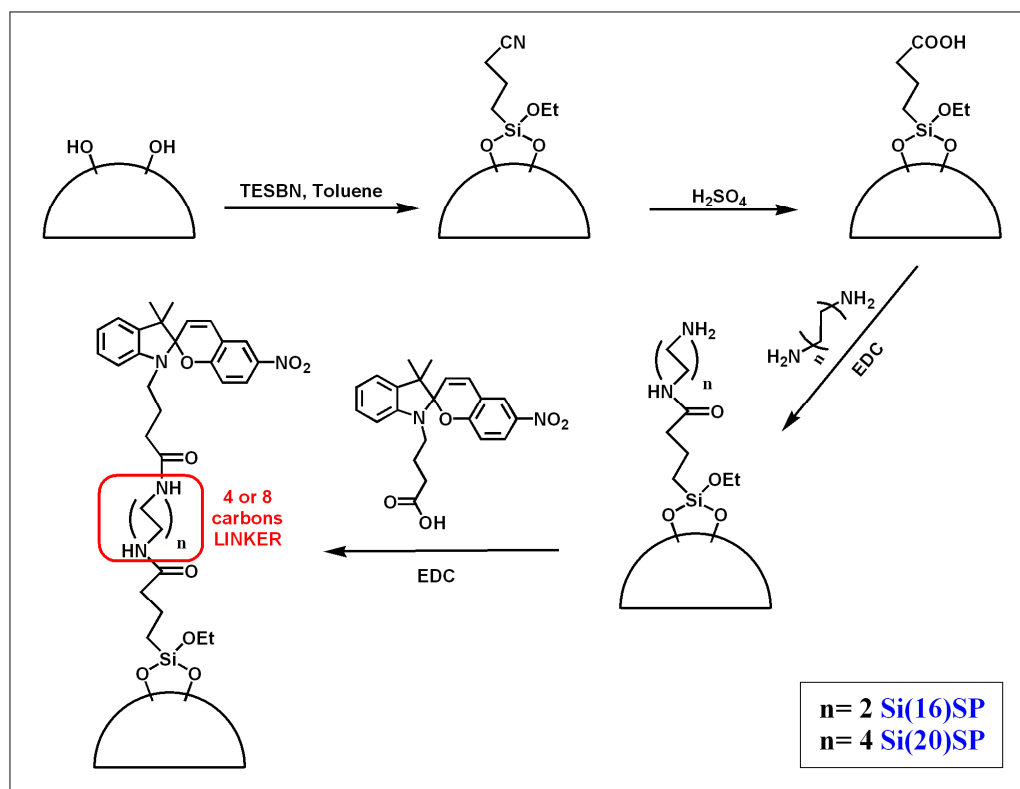


Figure 4.2: Reaction scheme on the silica microbead surface. The first step involves nitrile functionalisation of the silica surface and followed by conversion of the nitrile groups to carboxyl groups. Then the carboxyl groups are coupled with 1,4 diaminoctane or 1,8 diaminobutane using EDC to obtain an amino functionalised surface which is finally coupled again using EDC with the carboxylic groups on the SPCOOH derivative to obtain spiropyran functionalised beads where 16 or 20 atoms respectively, are separating the bead surface and the spiropyran moiety (Si(16)SP and Si(20)SP).

4.3.5 Physisorption of spiropyran on silica microbeads

In order to compare the characteristics of covalently functionalised beads, a sample of silica beads with physisorbed SPCOOH was prepared (Si(PA)SP).

An aliquot of a suspension of the previously amino functionalised silica microbeads (0.025 g in 3 ml of ethanol) was added to 1 ml of a 15 mg ml⁻¹ ethanolic solution of SPCOOH and the mixture stirred for 72 hours in the dark at room temperature. The beads were then washed 10 times with fresh ethanol using the above reported procedure and stored at 4 °C in the dark.

4.3.6 Elemental analysis

Elemental Analysis was carried out on five samples of silica microbeads: silica microbeads functionalised with carboxyl and amino groups, carboxylated silica microbeads further functionalised with 8 carbons amino linker and spiropyran functionalised silica microbeads of Si(10)SP and Si(20)SP types, in order to evaluate the relative percentage of carbon which appears as a consequence of the surface functionalisation. The detected percentage values for nitrogen were not considered, as they were as low as the instrument detection limit.

The bead samples were dried of ethanol, weighed and analysed for the elements whose relative percentages were compared to investigate the efficiency of the functionalisation.

4.3.7 Contact angle measurements

Contact angle measurements were carried out on Si(10)SP sample. The sample preparation was carried out by placing 1 ml of a 1mg/ml solution of microbeads in ethanol on circular glass coverslips (30 mm diameter) which were then dried overnight in the dark.

The samples were then alternatively irradiated with UV and white light for 5 minutes and the contact angle measurement was taken soon after each irradiation.

4.3.8 Atomic force microscopy (AFM)

Atomic force microscopy was used to investigate the spiropyran functionalisation of microbeads by comparing the force curves that originate when a single spiropyran functionalised (Si(10)SP) and non-functionalised silica microbead attached to the cantilever is brought into contact with spiropyran modified and non-modified glass surfaces. For this purpose a functionalised Si(10)SP and a plain silica microbead were

immobilised on a gold AFM tip, and glass slides were functionalised with spiropyran through an esterification procedure using DCC/DMAP as catalyst.

Bead attachment on the cantilever tip was accomplished according to the following procedure (**Figure 4.3**):

A) Epoxy-glue uptake: epoxy-glue is deposited on a glass slide and, using a microscope combined with a micromanipulator, a small amount of glue is taken up onto the micromanipulator tip.

B) Deposition of Epoxy-glue on the side of the cantilever tip: the micromanipulator tip carrying the glue is placed in contact with the side of the cantilever tip in order to deposit some of the glue on the cantilever tip.

C) The glue coated cantilever is then attached to the AFM for bead capturing. The cantilever tip is pushed in contact with one bead deposited on an atomically smooth mica surface. During the procedure, below the AFM head, a microscope is present and the whole process of bead approaching is monitored using video microscopy.

D) When the cantilever is removed from the surface, bead attachment to the side of the cantilever tip can be verified using the microscope. Then the epoxy-glue which holds the bead on the cantilever tip is left curing overnight to ensure strong bonding to the side of the tip (**Figure 4.4**)

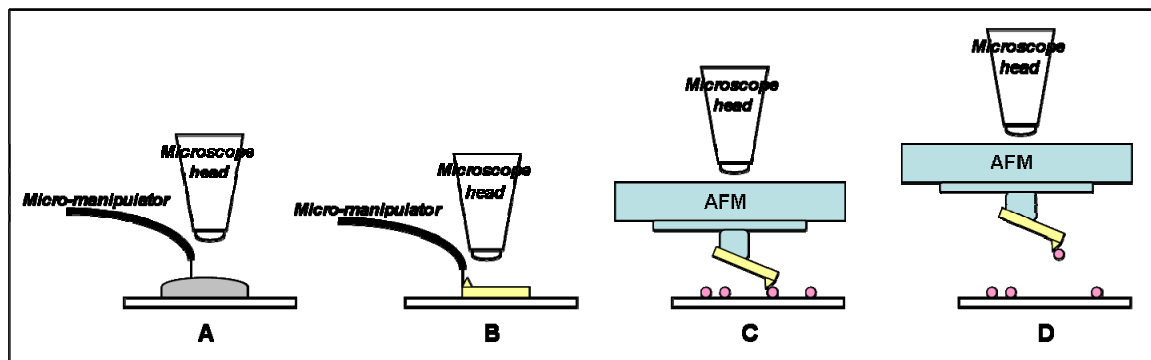


Figure 4.3: Procedure for bead immobilisation on cantilever tip.

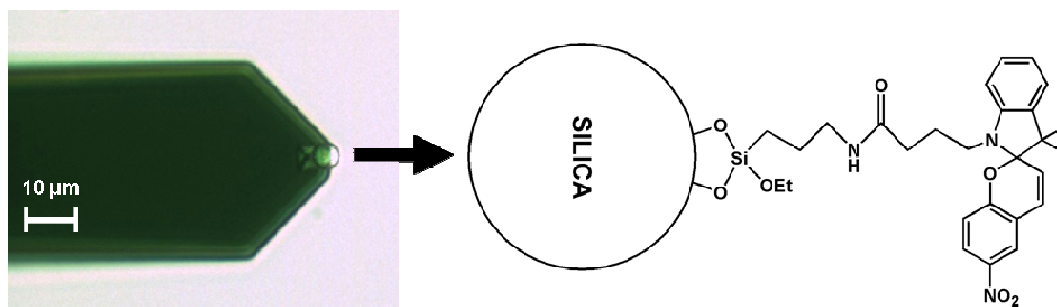


Figure 4.4: Top view microscope image of the cantilever with a 5 µm spiropyran modified silica bead (Si(10)SP) attached to the side of the tip.

4.3.9 Spiropyran glass slide functionalisation

In order to carry out AFM force measurements using cantilevers a glass slide was functionalised with spiropyran according to the following procedure (**figure 4.5**).

Piraña activation of the glass slide:

The glass slide was immersed in piraña solution (3:1 H₂SO₄:H₂O₂ (30% solution)) for 30 minutes at 50 °C.

Then the slide was profusely washed with deionised water and subsequently with fresh acetonitrile and finally dried under nitrogen.

Spiropyran attachment:

A solution containing 2.5 mg of SPCOOH, 1.3 mg of N, N'-Dicyclohexylcarbodiimide (DCC) and 0.07 mg of 4-Dimethylaminopyridine (DMAP) in acetonitrile was prepared. As soon as possible after the piraña treatment, the glass slide was immersed in this solution and the reaction was left stirring overnight at room temperature in the dark.

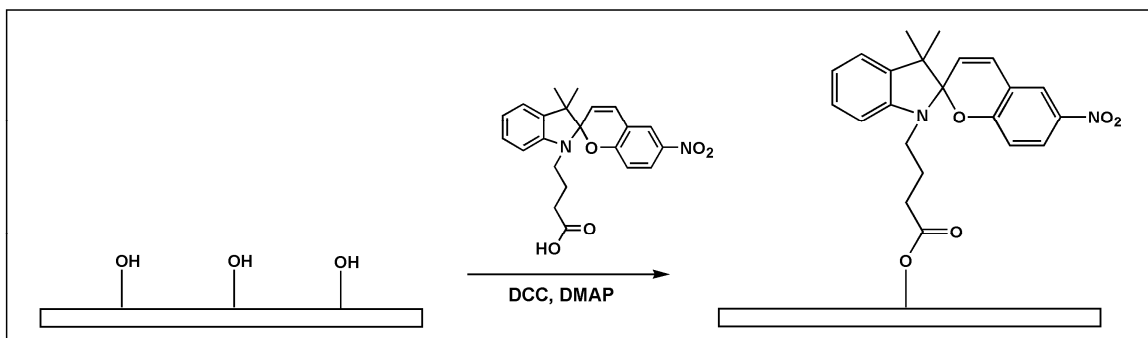


Figure 4.5: Reaction scheme for the functionalisation of a glass slide with spiropyran. The piranha activated silicon surface is refluxed with a SPCOOH solution pre-treated with DCC and catalytic amount of DMAP to achieve esterification between spiropyran and the glass surface.

4.4 Optical properties of the spiropyran functionalised polystyrene microbeads

4.4.1 Sample preparation for UV-vis spectroscopic analysis

The optical properties of the spiropyran functionalised microbeads were evaluated using a Plate Well Spectrometer. 1.2 ml of a 0.0125 g suspension of microbeads in ethanol was placed in each plate well and left for 1 hour in the dark to enable complete settlement of the microbeads and avoid interferences in the spectra due to settlement processes happening in the suspension. After this period, the microbeads formed a compact homogeneous layer which was suitable for obtaining UV-vis absorption spectra because of the semi-transparent nature of the silica microspheres.

4.4.2 Switching properties of the spiropyran functionalised silica microbeads

The optical properties of the functionalised silica microbeads were evaluated for the three different immobilisation strategies (Si(10)SP, Si(16)SP and Si(20)SP) using the following procedure:

- The microbeads were irradiated for 10 minutes with a white LED to make sure that the spiropyran was predominantly in the SP form.

- The microbeads were irradiated with the UV LED for 5 minutes, with spectra obtained after each minute (i.e.: after 1,2,3,4 and 5 minutes irradiation). At this stage, the beads were predominantly in the MC form.
- The microbeads were then irradiated with the white LED for 5 minutes, with spectra obtained after each minute (i.e.: after 1,2,3,4 and 5 minutes irradiation). This caused the MC to switch back to the SP form.

4.4.3 Evaluation of the spiropyran immobilisation strategies

The influence of immobilisation strategy on switching efficiency was evaluated for the three different spiropyran functionalised microbead samples (covalently immobilised spiropyran, Si(10)SP and Si(20)SP and physically adsorbed Si(PA)SP). 1.2 ml containing 0.0125 g of each microbead-type in ethanol were cycled between the SP and MC forms using UV and white LEDs using the following procedure:

- The microbeads were irradiated for 4 min with a white (430-760 nm) LED.
- The absorbance was recorded at 558 nm.
- The microbeads were then irradiated with a UV (375 nm) LED for 2 min.
- The absorbance was recorded at 558 nm.

This process was then repeated for 5 times and the absorbance values at 558 nm plotted against the number of measurements.

4.4.4 Influence of solvent on MC→SP photo-induced kinetics

The kinetics of photo-induced ring closing (i.e. MC→SP conversion) of Si(10)SP samples was investigated in seven different solvents: acetone, DMF, chloroform, toluene, acetonitrile, ethanol and water using the following procedure.

Sample preparation was carried out by placing 0.3 ml of a 3 mg suspension of spiropyran functionalised microbeads in each plate well. The suspensions were left for 1 hour in the dark to enable complete settlement of the microbeads and avoid artefacts in the spectra arising from settlement processes happening in the suspension.

Once the microbeads had settled the plate wells was left air drying for four days in order to assure that all the ethanol was evaporated.

Then on each of the seven wells 0.3 ml of the corresponding solvent was placed and the microbeads were exposed to white LED illumination for 4 minutes and then to UV LED illumination for 2 minutes, while the corresponding spectra of the SP and the MC forms were recorded in each solvent. After irradiation with the UV LED, absorbance values were automatically recorded at 550 nm in each well for 90 minutes every 1 minute (90 minutes is a time limitation due to the fact that after this time limit some of the solvents undergo complete evaporation). During the experiment, the plate wells were kept in the dark inside the plate well reader.

4.4.5 Photostability evaluation of the surface immobilised spiropyran

The photostability of the surface immobilised spiropyran was evaluated by repeatedly cycling a sample of Si(10)SP beads between the SP and the MC form. A sample of a 0.0125 g of microbeads in 1.2 ml of ethanol was cycled 20 times between the SP and MC forms using UV and white LEDs. Cycles were performed by irradiating the sample with a white LED for 4 minutes followed by UV irradiation for 2 minutes. Each cycle was repeated 20 times while monitoring the reflectance values at 558 nm.

4.4.6 Evaluation of metal ion interactions with spiropyran functionalised microbeads

Spiropyran functionalised microbeads (Si(10)SP) suspended in ethanol were exposed to different metal ion ethanolic solutions in order to evaluate the extent of complex formation at the bead surface. The metal ions used were: Ca^{2+} (from $\text{Ca}(\text{NO}_3)_2$ and CaCl_2 to test any possible effects deriving from the anion, Cu^{2+} (from $\text{Cu}(\text{NO}_3)_2$), Hg^{2+} (from $\text{Hg}(\text{NO}_3)_2$), Cd^{2+} (from $\text{Cd}(\text{NO}_3)_2$), Co^{2+} (from $\text{Co}(\text{NO}_3)_2$) and Zn^{2+} (from ZnCl_2). Each experiment was carried out using the following procedure:

- In each well a sample of 0.0125g of microbeads in 1.2 ml of ethanol was exposed to a white LED (430-760 nm) for 4 min to ensure the SP form was predominant.
- The spectrum of the colourless SP form was obtained.

- The microbeads were exposed to a UV (375 nm) LED for 2 min to promote SP conversion to the MC form.
- The spectrum of the coloured MC form was obtained.
- 0.1 ml of 10^{-2} M of metal ion ethanolic solution (final concentration 7.7×10^{-4} M) was added.
- The resulting spectrum was taken immediately after.

4.5 Results and discussion

4.5.1 Elemental Analysis

Elemental Analysis was carried out on five types of functionalised silica microbeads in order to evaluate the relative percentage of carbon which is present on the covalently attached functional groups, but not in the silica microbeads. These are: silica microbeads functionalised with carboxyl and amino groups, carboxylated silica microbeads further functionalised with 8 carbons amino linker and spiropyran functionalised silica microbeads of Si(10)SP and Si(20)SP types). The results are presented on **table 4.1**.

For an evaluation of the different covalent immobilisation strategies carbon element percentages are more reliable than proton percentages as protons could be present on the silica surface in form of free hydroxyl groups.

SAMPLE	%C
1) Silica microbeads functionalized with carboxyl groups	0.44
2) Carboxylated silica microbeads further functionalised with 8 carbons amino linker	0.85
3) Spiropyran functionalised silica microbeads (Si(20)SP)	1.58
4) Silica microbeads functionalized with aminogroups	2.75
5) Spiropyran functionalised silica microbeads (Si(10)SP)	3.36

Table 4.1: Values of the carbon percentages obtained by experimental analysis for 5 different types of functionalised silica microbeads. The carbon percentages are expressed as % of the total mass of the sample and their accuracy is $\pm 0.15\%$.

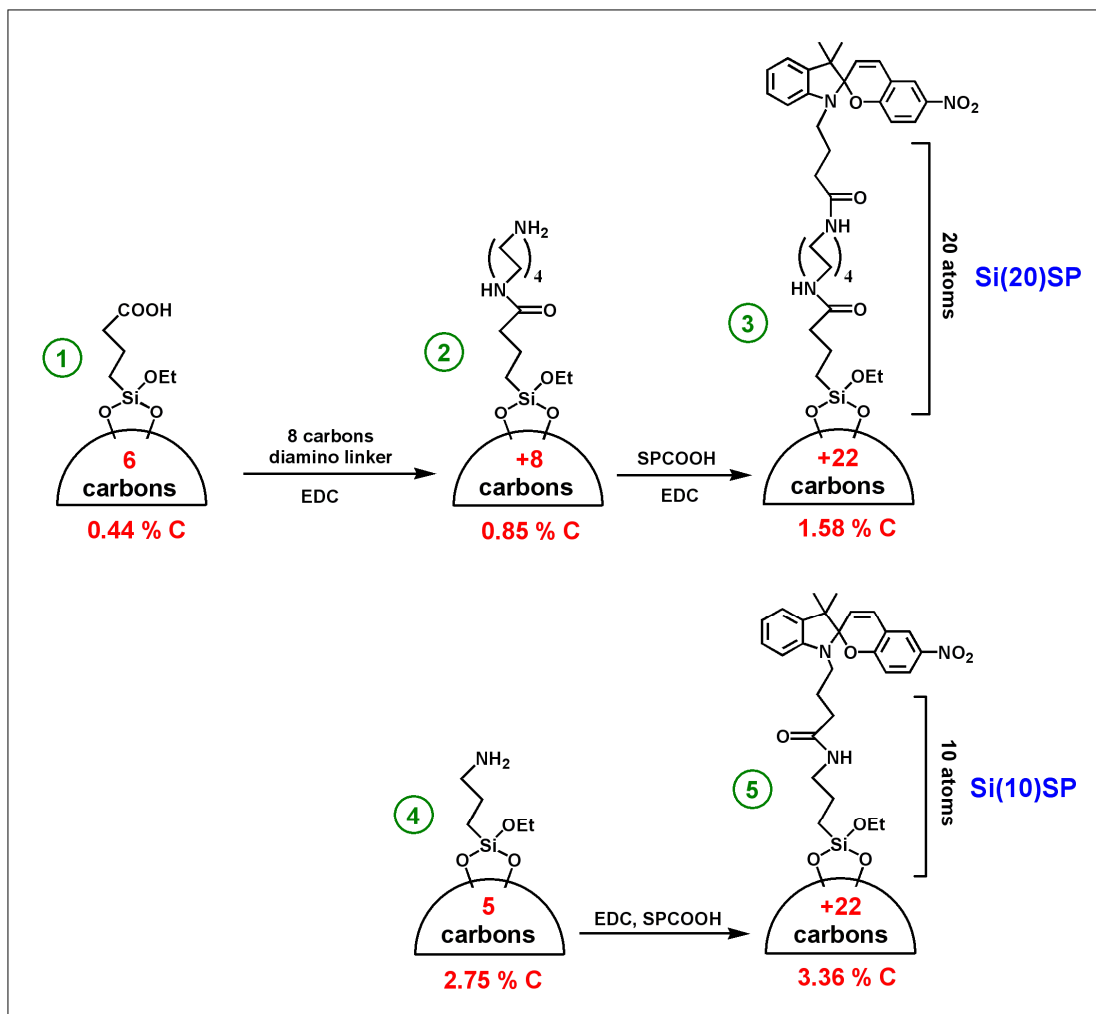


Figure 4.6: Scheme representing the two different silica beads functionalisation strategies with spiropyran (Si(10)SP and Si(20)SP). For each step, the increasing number of carbons and the carbon percentages determined by elemental analysis are reported.

Functionalisation of the bead with aminogroups produces a carbon percentage increase of 2.75% ((4), **figure 4.6**), deriving from the 5 carbons present on each of the APTES. Carboxyl functionalisation with TESBN followed by treatment with H_2SO_4 is less efficient, generating only a 0.44% increase in carbon derived from 6 carbons present on each TESBN group. The carboxyl functionalised silica surface was then further modified via amide bond formation with an 8-carbons diamino linker. This process leads to a carbon percentage increase of 0.41% which brings the overall carbon percentage increase to 0.85% due to the two-steps pre-spiropyran attachment surface functionalisation procedure((1 and 2), **figure 4.6**). This percentage is still significantly

lower when compared to the increase when the surface is modified using amino groups. Functionalisation with carboxyl groups followed by further functionalisation with an 8 carbons amino linker produced a carbon increase of 0.85% which corresponds to 14 carbons. The aminogroups functionalisation produces an increase of 2.75% corresponding to 5 carbons. If the silica surface coverage was the same for the two functionalisation strategies the carbon percentage increase for the carboxyl group functionalisation strategy followed by further functionalised with 8 carbons amino linker should be 7.7%.

This implies that for every 9 aminogroups attached on the plain silica surface only one carboxyl group with an 8 carbons amino linker is present on the other silica sample.

In contrast the spiropyran attachment step (each spiropyran molecule contributing 22 carbons), produces increase in carbon percentage which is similar for both the Si(10)SP sample (+0.61%) and the Si(20)SP sample (+0.73%).

In the Si(10)SP microbead sample the spiropyran attachment is definitely the limiting factor, as the amino functionalisation step contributes a 2.75% increase in carbon (5 carbons for each attached molecule) while the spiropyran attachment step contributes only a further 0.61% although there are 22 carbons for each spiropyran molecule attached. If all the amino group sites were occupied by spiropyran, the total carbon increase should be around 12%. From the experimental data the increase is only 0.61%, which means that there is approximately 1 spiropyran molecule every 20 aminogroups. Considering that every spiropyran molecule is carrying 22 carbons, the elemental analysis data suggests that the reason for the spiropyran step being a limiting factor in the functionalisation procedure is the need for a spatial distance between the spiropyran units.

In the Si(20)SP bead sample, the silica functionalisation with spiropyran is carried out in 3 steps. Functionalisation with carboxyl group ((1) 6 carbons, **figure 4.6**) leads to a carbon increase of 0.44%. Further functionalisation with amino linker ((2) 8 carbons, **figure 4.6**) produces a further carbon increase of 0.41%. This means that roughly (taking into account the $\pm 0.15\%$ accuracy) each carboxyl group is occupied by a diamino linker. Therefore 0.85% carbon percentage after the first two steps corresponds to a 14 carbons linker chain.

The final spiropyran attachment step ((3) 22 carbons, **figure 4.6**) causes an increase of 0.73%. Consequently there is approximately 1 spiropyran molecule every 2 binding sites. Considering that this functionalisation strategy in the pre-spiropyran attachment step produces 9 binding sites less for each aminogroups attached in the other strategy, the relative spiropyran ratio is 1 to 18.

Although the spiropyran coverage is similar for the two different immobilisation strategies, in the following sections it will be demonstrated that the spiropyran switching is more efficient in the Si(10)SP sample compared to the Si(20)SP or Si(16)SP samples, as the MC absorption band is significantly less intense for these when compared to that of the Si(10)SP. The appearance of the MC form on the Si(10)SP bead surface generates a much more dramatic spectral change than for the equivalent Si(16)SP and Si(20)SP samples. For this reason the Si(10)SP sample was used for the subsequent characterisation of the optical properties of the spiropyran functionalised beads.

4.5.2 Contact angle measurements

1 mg in 1 ml of silica functionalised microbeads (Si(10)SP) in ethanol were deposited on a glass slide and dried overnight.

Contact angle measurements were carried out on the bead layer using a water droplet to investigate the effect of the photoswitching between the SP and the MC forms (**Figure 4.7**). When irradiated with white light the bead layer has a pale yellow colour and the spiropyran is present in the non-polar SP form. The contact angle of a water droplet on the surface has an average value of $122^\circ (\pm 1.3)$ just after deposition (calculated from three measurements in three different spots of the sample, **table 4.2**). After 3 seconds the contact angle drops down to $98^\circ (\pm 1.6)$ and then the droplet slowly disappears over a period of ca. 5 minutes. Upon UV light irradiation the bead layer turns deep purple and the contact angle of a water droplet on the surface is $112^\circ (\pm 1.1)$ just after deposition, 10° difference when compared to the white light irradiation. After 3 seconds the contact angle drops to $49^\circ (\pm 0.6)$ and then the droplet quickly disappears in ca. 10 seconds due to the higher polarity of the MC form, which predominates after UV exposure.

Furthermore the greater polarity of the silica matrix compared to polystyrene, enhances the formation of the MC form even in dry state (as it can be seen from the much stronger

colour intensity of the MC form on the silica beads in comparison to the polystyrene beads (**Chapter 3**), and this contributes to the larger difference in the contact angles between the two forms.

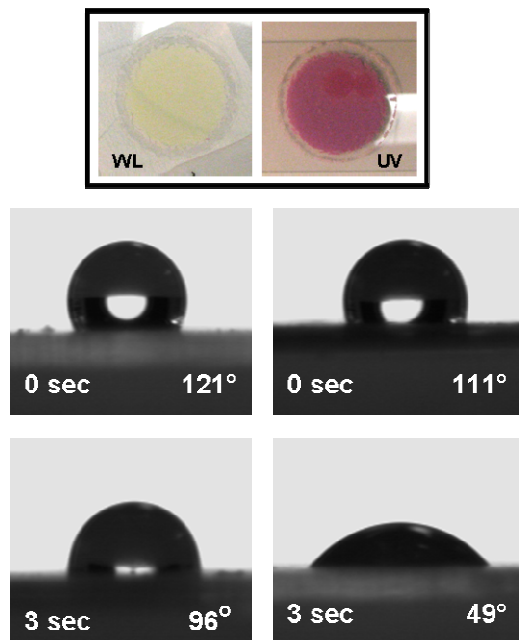


Figure 4.7: (Above) Images of the silica microbead sample deposited on the surface of a glass disc. On the left the sample has been irradiated with white light (pale yellow disc), on the right with UV light (purple disc).

(Below) Contact angle differences between the water droplet deposited on the spiropyran functionalised microbeads in the SP form (*left*, drop n. 1 after 0 and 3 seconds, see **table 4.2**) and the droplet deposited on the MC activated microbeads (*right*, drop n. 4 after 0 and 3 seconds, see **table 4.2**).

SPIROPYRAN FUNCTIONALISED SILICA BEADS (Si(10)SP) deposited on glass slide	LEFT angle	RIGHT angle
Drop n. 1 white light irradiation (5 min) (contact angle measured after 0 sec)	121.6	121.7
Drop n. 1 white light irradiation (5 min) (contact angle measured after 3 sec)	95.9	96.2
Drop n. 2 white light irradiation (5 min) (contact angle measured after 0 sec)	123.0	123.4
Drop n. 2 white light irradiation (5 min) (contact angle measured after 3 sec)	98.2	98.9
Drop n. 3 white light irradiation (5 min) (contact angle measured after 0 sec)	120.5	120.5
Drop n. 3 white light irradiation (5 min) (contact angle measured after 3 sec)	99.5	98.7
Drop n. 4 UV light irradiation (5 min) (contact angle measured after 0 sec)	111.4	110.6
Drop n. 4 UV light irradiation (5 min) (contact angle measured after 3 sec)	48.7	50.1
Drop n. 5 UV light irradiation (5 min) (contact angle measured after 0 sec)	112.2	111.8
Drop n. 5 UV light irradiation (5 min) (contact angle measured after 3 sec)	49.4	50.8
Drop n. 6 UV light irradiation (5 min) (contact angle measured after 0 sec)	113.7	112.9
Drop n. 6 UV light irradiation (5 min) (contact angle measured after 3 sec)	48.3	49.4

Table 4.2: Contact angle values acquired when a water droplet is placed on a layer of spiropyran functionalised silica microbeads deposited on a glass disc and photoswitched between the SP and the MC form.

4.5.3 AFM force curve measurements

Using an atomic force microscope it is not only possible to map a surface and in so doing obtain information about its morphology, but it is also possible to obtain information about the interactions that are occurring between the tip and a surface when the tip attached to the cantilever is moved towards the surface in one direction. The vertical position of the tip and the deflection of the cantilever are recorded and converted to force versus distance curves which are called force curves.

AFM force curve measurements have been carried out in order to obtain more information about the Van der Waals and adhesion or repulsion forces that take place when the cantilever tip is in very close contact with a surface.

The force vs. distance curve obtained with this methodology is a plot of the deflection of the cantilever vs. the extension of the piezoelectric scanner.

As the piezoelectric scanner extends towards the sample surface, the cantilever remains undeflected until it comes close enough to the surface for the tip to experience attractive Van der Waals forces. When this happens the cantilever bends towards the surface and as the scanner continues to extend, the cantilever deflects linearly (**figure 4.8**).

After full extension, as the scanner pulls the tip away from the surface, the cantilever begins to retract and the cantilever retraces a similar curve, but typically a greater force is necessary to overcome the adhesion forces and move the tip away from the surface.

The possibility of measuring these tip-surface interactions has found a wide variety of applications in colloid and surface science in the past decade, where this technique has been used to investigate:

- pull off forces between the cantilever tip and a structured or modified silicon disc¹¹
- adhesion forces between a polysaccharide and a protein modified glass surface
- a colloid probe prepared by attaching modified latex microspheres to a tipless cantilever¹²
- the morphology and surface roughness of several commercially available microspheres¹³.

In our case AFM force curve measurements were carried out primarily to evaluate the surface interactions of the spiropyran functionalised silica microbeads.

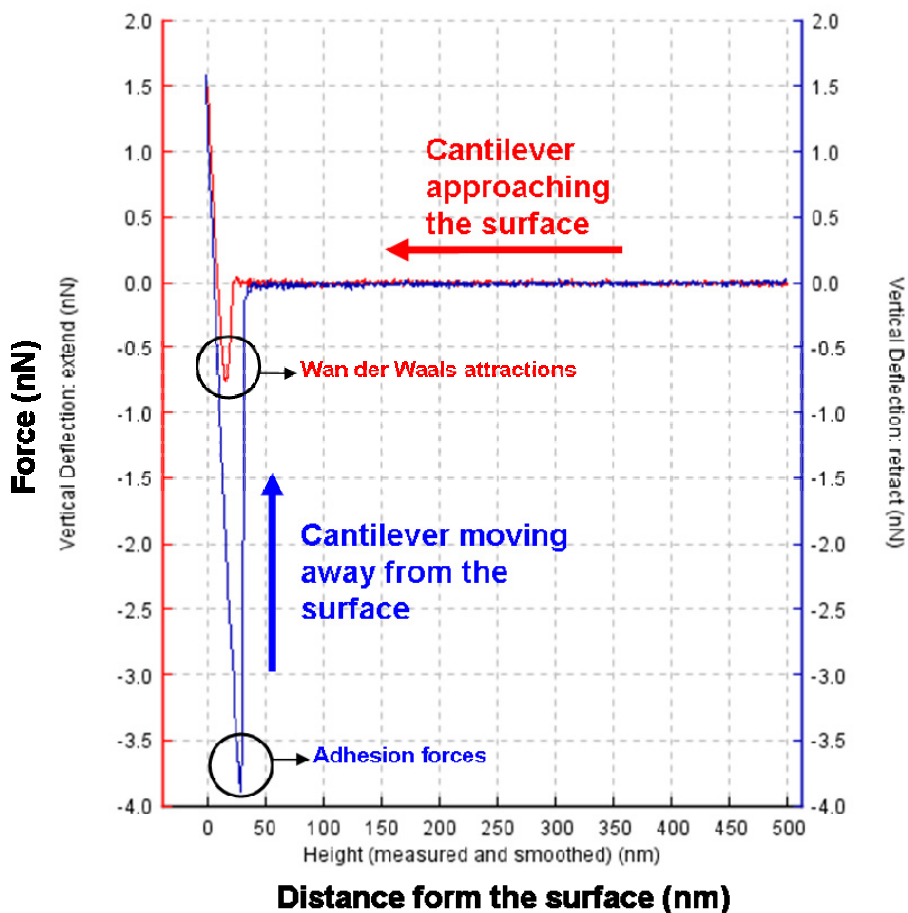


Figure 4.8: Red lines represent the “extend curves”, i.e. when the cantilever is moved towards the surface. The blue lines represent “retract curves”, i.e. when the cantilever is retracted from the surface. In this case, when the cantilever approaches the surface, Van der Waals forces appear (producing a negative peak when the tip is very close to the surface, in this case 25 nm as reported in the graph). When the cantilever is moved away from the surface, an adhesion peak is appears, which is bigger than the Van der Waals peak, as it has to overcome this force to detach itself from the surface.

This force curve was obtained using a cantilever presenting a Si(10)SP bead attached to the tip approached towards a spiropyran functionalised glass surface while the whole system was kept under 10^{-3} M HCl in ethanol.

In order to perform AFM force measurements it is necessary to create a suitable surface that can interact with the spiropyran functionalised silica microbead attached to the cantilever tip.

To increase the forces generated in the presence of the SP and the MC forms it was decided to use a glass surface which was itself functionalised with spiropyran as this might amplify the resulting interactions between the spiropyran isomers present on both the surfaces.

The modification of the glass slide with spiropyran was carried out by esterification catalysed by DCC/DMAP between the carboxyl group on the SPCOOH and hydroxyl groups generated on the glass surface by piranha treatment (**figure 4.5**).

Absorbance UV-vis measurements on the modified glass slide were carried out by alternatively exposing the glass slide to UV and white light irradiation. Under UV light exposure a weak absorbance is observed around 610 nm (**figure 4.8**). The MC band is shifted towards longer wavelength due to the fact that the absorbance measurement was taken in air which is a non-polar environment.

This peak disappears under white light irradiation, proving the presence of the spiropyran, probably as a thin monolayer, as the absorbance peak is extremely weak and the MC cannot be detected by eye.

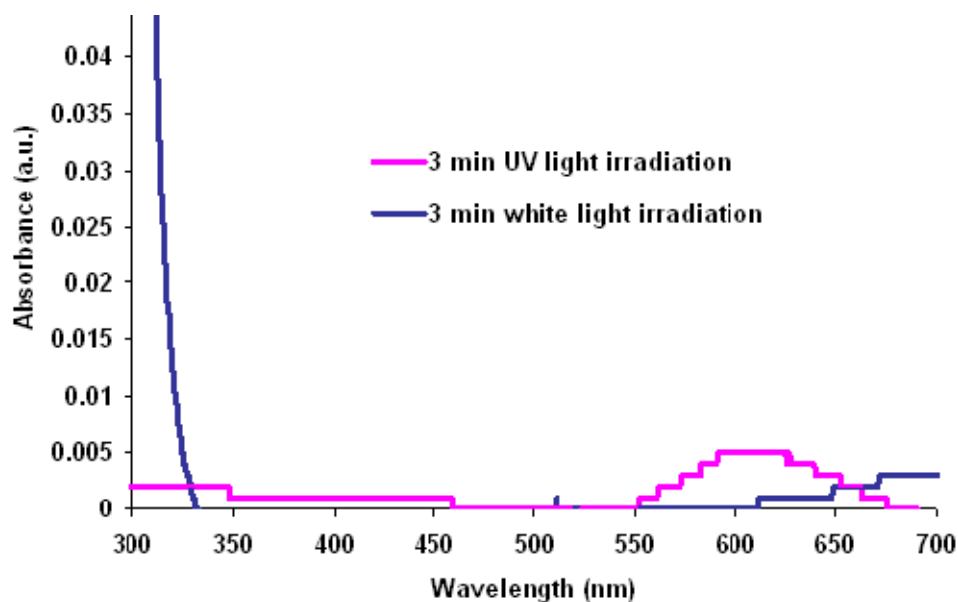


Figure 4.9: UV-irradiation of the glass slide in ethanol leads to the appearance of a peak around 610 nm which disappears after irradiation with white light. This is evidence of photoswitching between the SP \leftrightarrow MC isomers on the glass surface.

Contact angle measurements were also performed on the glass slide surface to further investigate the SP ↔ MC photoswitching.

For this purpose a spiropyran functionalised glass slide was switched using white and UV light irradiation between the SP and the MC forms.

In the SP form, under white light irradiation, the contact angle measured is $60^\circ (\pm 5.2^\circ)$. After UV irradiation (365 nm) a decrease in the contact angle of 10° is recorded due to the increased polarity of the MC form (**figure 4.10**).

These UV-vis and contact angle measurements confirm the switching between the SP and the MC form on the glass surface. This slide was further employed for the AFM force curve measurements.

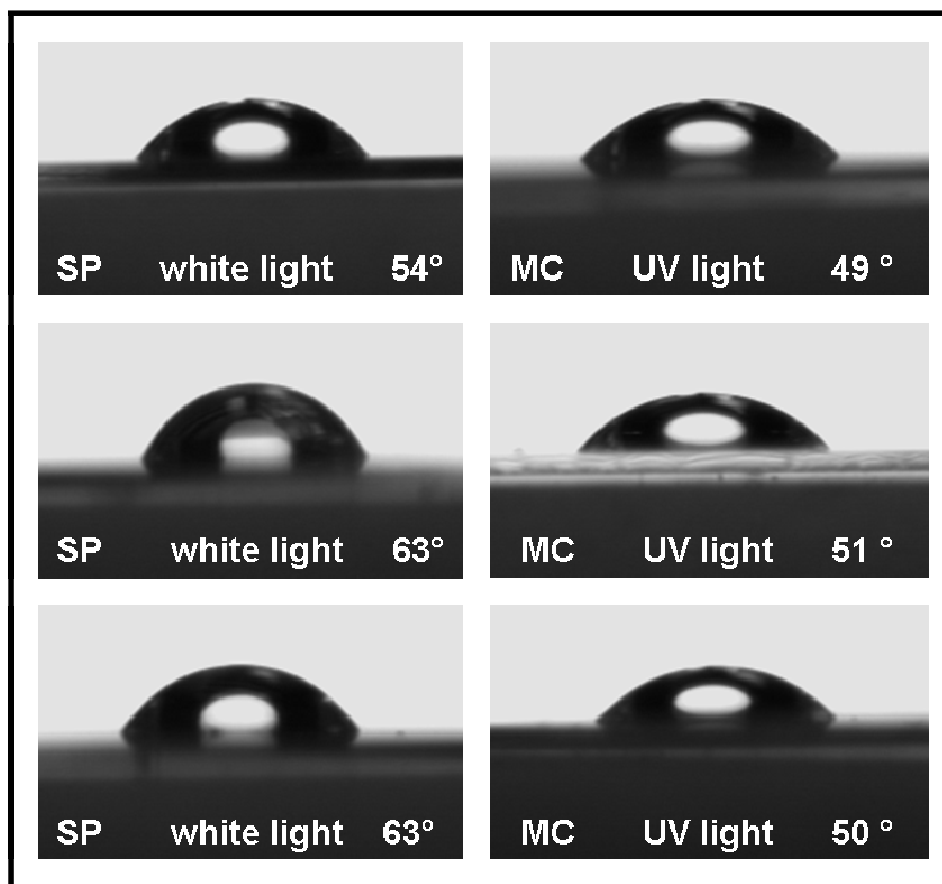


Figure 4.10: Scheme of the contact angle measurements taken on the spiropyran functionalised glass slide. The presence of the MC form causes a decrease of 10° in the contact angle when compared to the contact angle of the water droplet when the glass slide is in the SP form .

Our first intent was to try to distinguish between the SP and the MC force in terms of force curves using a spiropyran modified silica microbead attached to a cantilever tip which was brought into contact with a spiropyran modified glass surface (in order to double the effect of the switching) while white and UV LEDs were alternatively irradiating the whole system (**figure 4.11**).

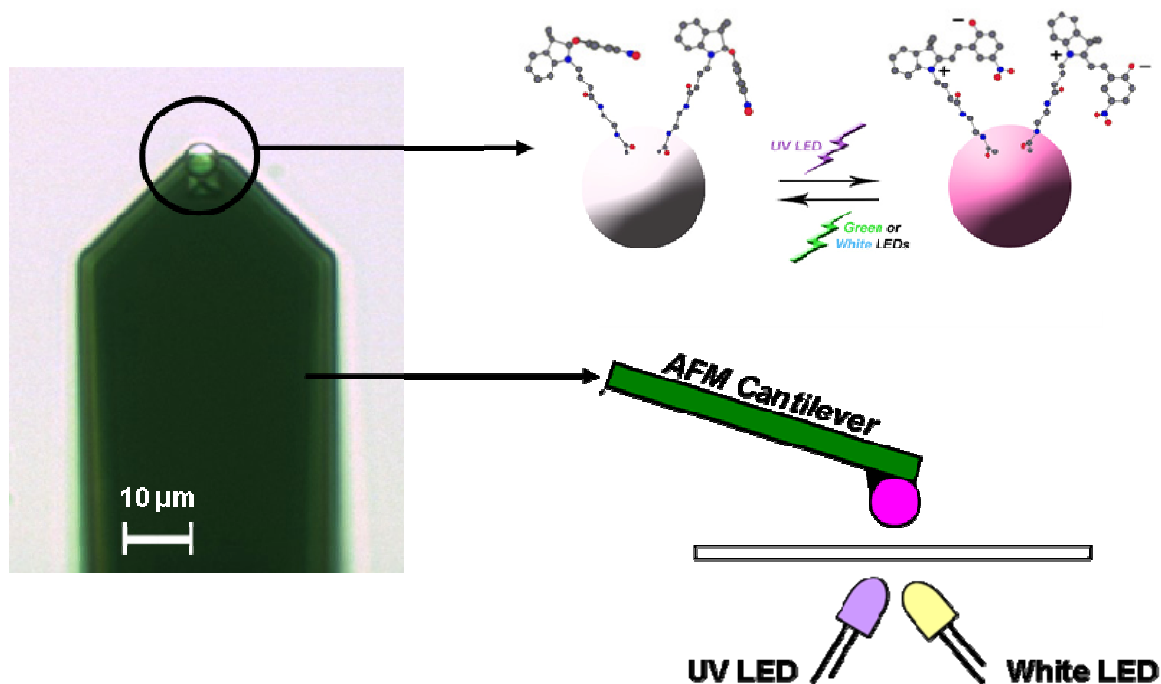


Figure 4.11: Experimental set-up for force curve measurements performed when a cantilever carrying a spiropyran modified silica beads is placed in contact with a spiropyran modified glass slide while the whole system is alternatively irradiated with white and UV LEDs

It was expected to record an increase of the adhesion forces when in the presence of the MC forms in both the silica bead and the glass slide, the positive and negative charge present in the two MC forms would attract each other in a complementary way.

These adhesions would then decrease when the MC forms were converted back to the SP form.

When the experiment was carried out, contrary to expectations, the differences between the force curves that were recorded when the two systems (Si(10)SP bead and spiropyran modified glass surface) were in the SP and subsequently in the MC form

were not significant enough (on an average of 25 force curves recorded for each form) to be able to distinguish between the two isomers.

This is probably due to the fact that we cannot predict the amount and the homogeneity of the spiropyran coating in the silica microbead for the particular area exposed to the glass slide and we cannot control the molecular orientation of the SP/MC isomers on the two surfaces when they are close together.

Interestingly it was possible to clearly distinguish between a non-functionalised and a spiropyran functionalised surface and AFM force curves were recorded using different combinations of functionalised and non-functionalised silica microbeads and glass surfaces.

Force curves were initially measured using a plain silica bead attached to the cantilever tip against a plain glass surface consistent repulsions were present, as a consequence of the negatively charged silica surface both on the bead attached to the cantilever and on the glass slide (**figure 4.12**).

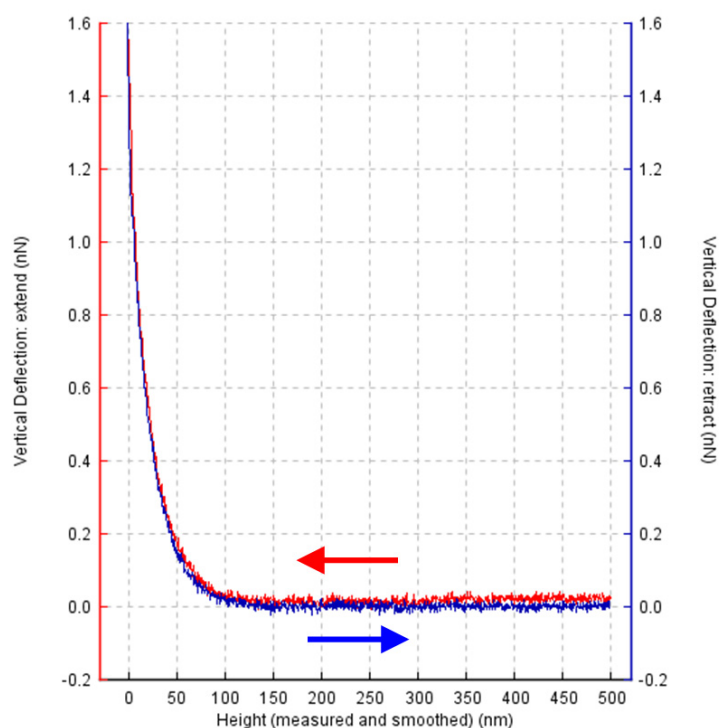


Figure 4.12: Force curve which generate when plain silica bead is moved towards a plain glass slide: strong repulsion forces are evident.

Red lines represent the “extend curves”, i.e. when the cantilever is moved towards the surface. The blue lines represent “retract curves”, i.e. when the cantilever is retracted from the surface.

Then a spiropyran functionalised silica bead (Si(10)SP) was analysed against a plain glass surface. In this case small Van der Waals and adhesion forces appear with a vertical deflection between 0.1 and 0.2 nN (**figure 4.13**). This indicates that the presence of spiropyran on the bead surface increases the interactions between the two surfaces.

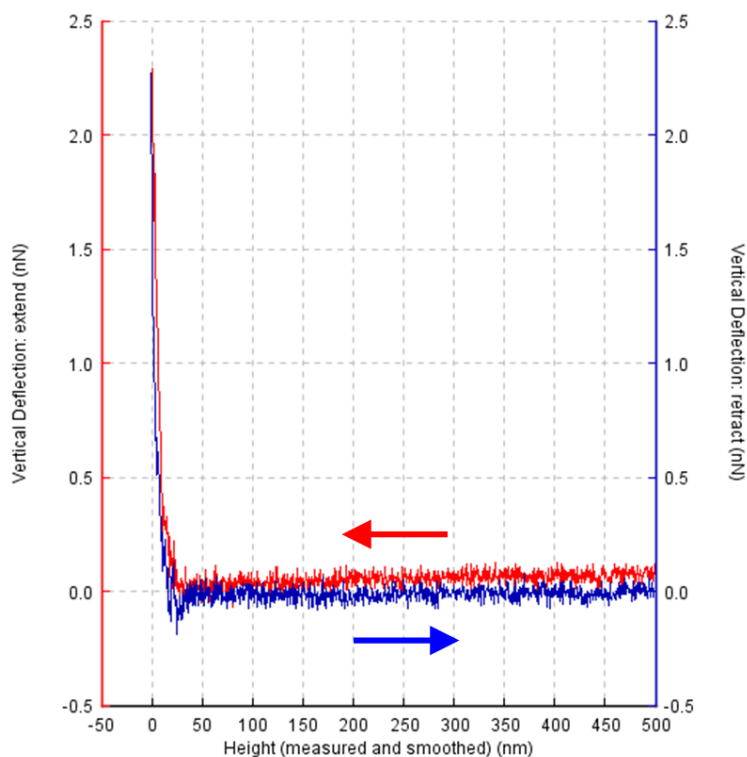


Figure 4.13: Force curve which generate when a spiropyran functionalised bead is moved towards a plain glass slide: Van der Waals and adhesion forces were recorded due to the presence of spiropyran on the bead surface.

Red lines represent the “extend curves”, i.e. when the cantilever is moved towards the surface. The blue lines represent “retract curves”, i.e. when the cantilever is retracted from the surface.

Finally, when the experiment was carried out by moving a Si(10)SP bead towards a spiropyran functionalised glass surface strong Van der Waals and adhesions forces are detected with a vertical deflection of 0.5 nN, and the force curves are consistent along the sample (**figure 4.14**) for movement towards and away from the surface.

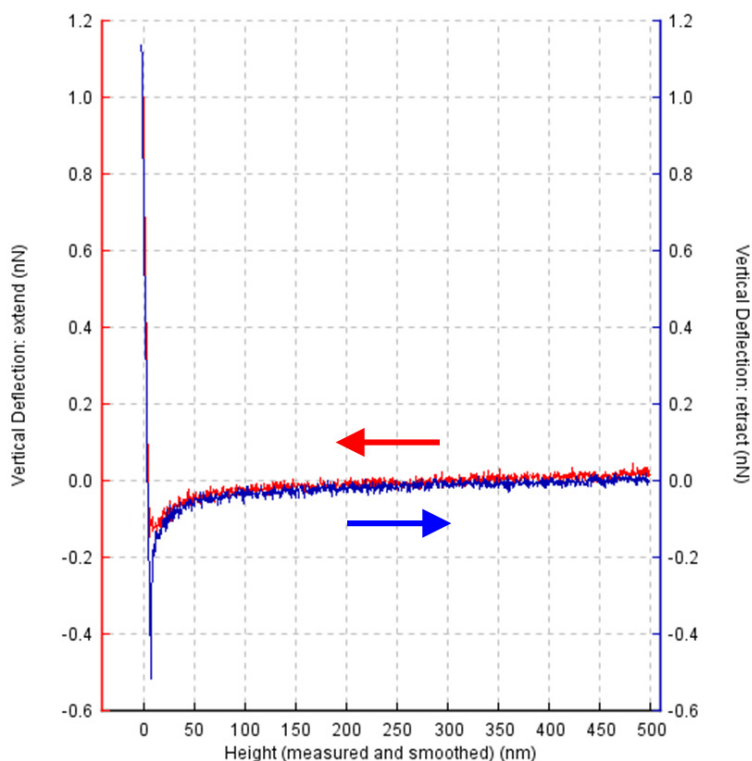


Figure 4.14: Force curve which generate when a spiropyran functionalised bead is moved towards a spiropyran functionalised glass slide: strong Van der Waals and adhesion forces are present.

Red lines represent the “extend curves”, i.e. when the cantilever is moved towards the surface. The blue lines represent “retract curves”, i.e. when the cantilever is retracted from the surface.

The dramatic change in the shape of the force curve indicates that completely different interactions between the two surfaces are occurring whether or not the spiropyran is present and it is a good indication of the consistent surface changes which are occurring as a consequence of the functionalisation process.

4.5.4 Optical properties of spiropyran coated microbeads

It was previously demonstrated that covalently spiropyran functionalised polystyrene microbeads could be successfully switched between the pink MC form and the colourless SP form, using a UV LED 375 nm (for the SP \rightarrow MC conversion), and a white LED 430-760nm (for the MC \rightarrow SP conversion)¹.

Similarly, spiropyran modified silica microbeads can be efficiently switched with UV and white LEDs between a pink MC and a colourless SP form (**figure 4.15**).

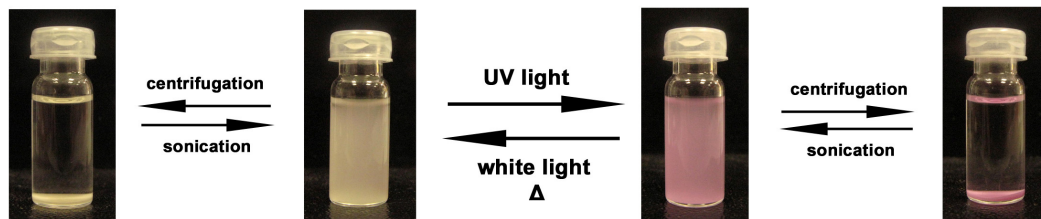


Figure 4.15: Si(10)SP microbead sample (0.025 g in 1.3 ml ethanol) in a glass vial is switched between the colourless SP form and the purple MC form. The centrifugation process demonstrates that the colour change is happening on the microbead surface and not in the solution medium, as when the beads are settled at the bottom of the vial, the resulting supernatant solution is clear.

In order to evaluate the switching efficiency of spiropyran modified microbead samples, UV and white LEDs were used as light sources for the irradiation of the different silica bead samples (deriving from the different immobilisation strategies) that were exposed to increasing irradiation to estimate the optimum exposure time for efficient switching. The results show that in a sample of Si(10)SP the conversion from the SP to the MC form is essentially complete after 2 minutes irradiation, as further irradiation does not cause any appreciable increase in the absorbance value at 558 nm. For the reverse MC→SP switching, complete conversion was achieved after 4 minutes irradiation with the white LED, by which time the characteristic 558 nm MC peak had disappeared (**figure 4.16**).

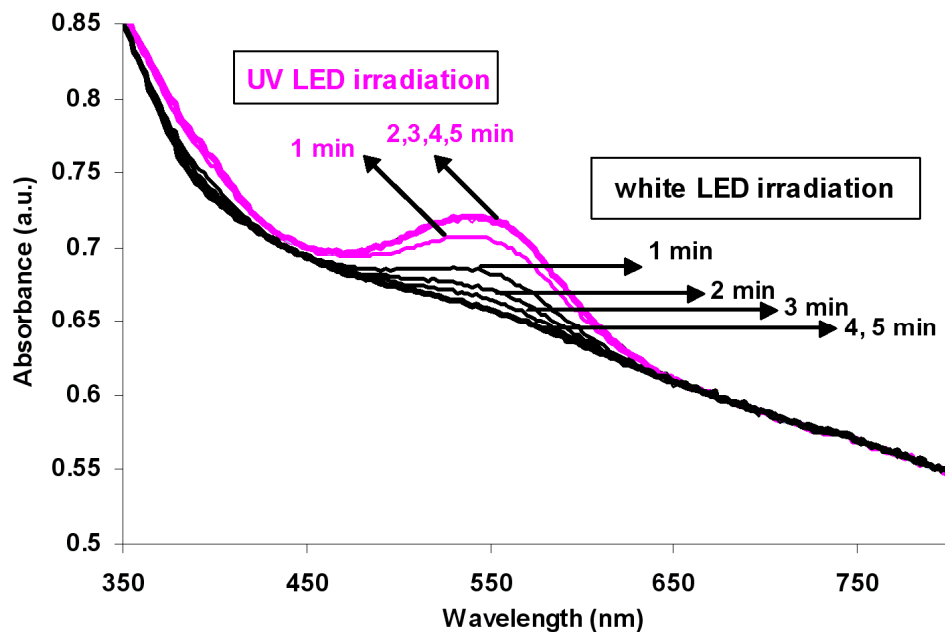


Figure 4.16: UV-vis spectra of a Si(10)SP microbead sample, irradiated first with UV LED for 5 minutes (blue lines), with spectra obtained after each minute (i.e.: after 1,2,3,4 and 5 minutes irradiation) and then with white LED for 5 minutes (black lines) with spectra obtained after each minute (i.e.: after 1,2,3,4 and 5 minutes irradiation). Two minutes UV LED irradiation is enough to reach the maximum absorbance value for the MC form at 558nm, while 4 minutes white LED exposure is required to convert the MC back to the SP form.

The same experiment was carried out on Si(16)SP and Si(20)SP samples. In these cases the conversion from the SP to the MC form using UV LED and the reconversion back from the MC to the SP form using white LED were both completed in 2 minutes (**figure 4.17**). It was noticed that the MC absorbance was extremely weak in both Si(16)SP and Si(20)SP samples compared to Si(10)SP.

The magnitude of the absorbance of the Si(10)SP sample, evaluated by subtracting the absorbance values of the SP and MC spectra at 558 nm ($MC Ab_{558nm} - SP Ab_{558nm}$), was 0.06 units. In comparison the differential value obtained for Si(16)SP and Si(20)SP samples at the same concentration in ethanol is 0.02 units. The resulting visual effect is a very weak coloration of the MC in the Si(16)SP and Si(20)SP samples compared to a more intense colour change in the Si(10)SP sample.

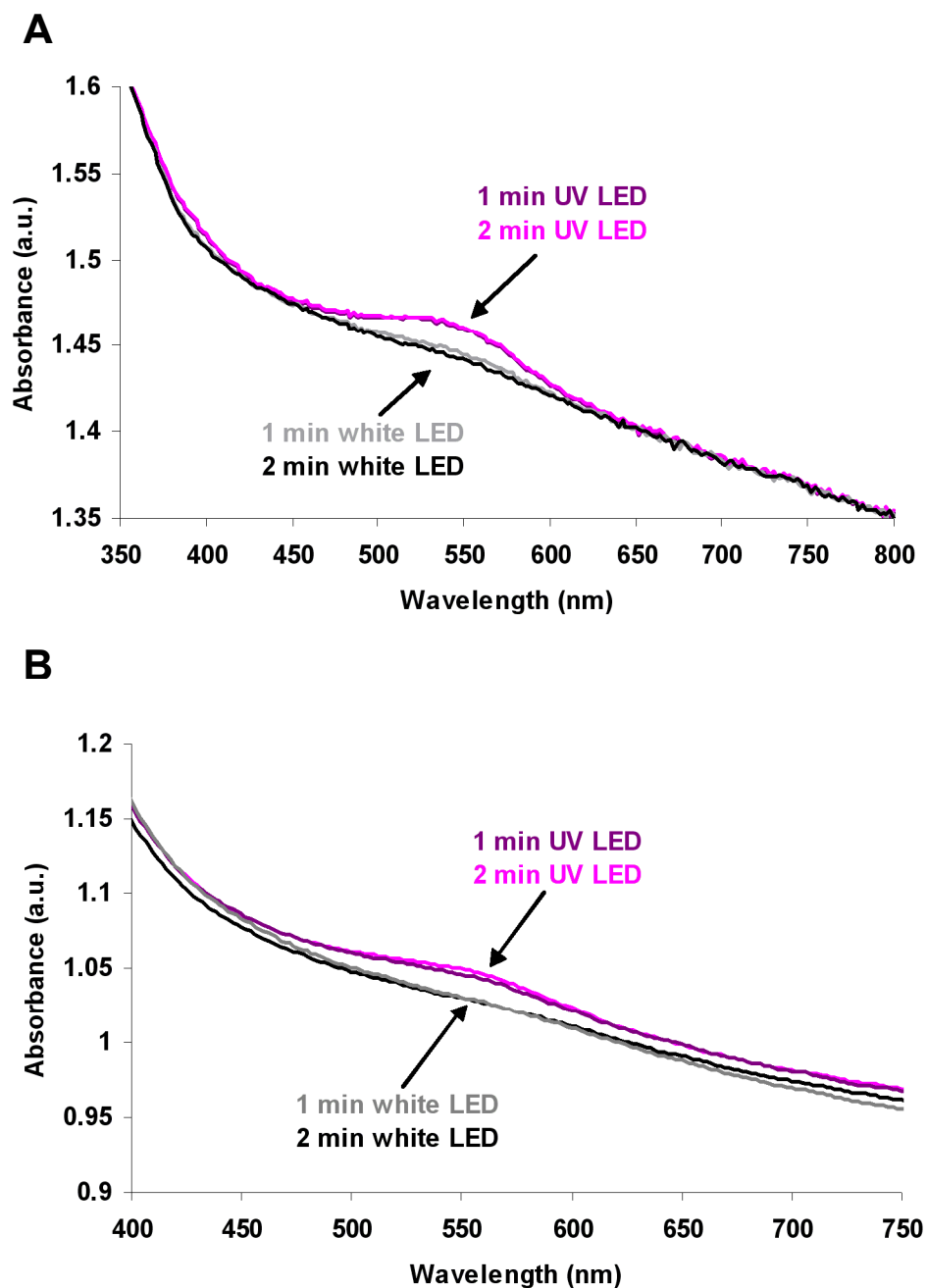


Figure 4.17: UV-vis spectra of (A) Si(16)SP sample and (B) Si(20)SP sample. The samples were irradiated firstly with UV LED for 2 minutes, enough to reach the maximum absorbance value for the MC form at 558nm, and then with white LED for 2 minutes, which are required to convert the MC back to the SP form.

Considering the atoms which are present between the surface and the spiropyran unit, in the case of the Si(10)SP sample 10 spacer atoms can be counted. This number increases to 16 and 20 in the case of Si(16)SP and Si(20)SP samples respectively.

In the previous chapter the distance between the polystyrene surface and the spiropyran unit was of 11 atoms in the case of PS(11)SP and 15 atoms for PS(15)SP (**figure 4.18**). The amount of spacers in the case of the spiropyran polystyrene beads treated in the previous chapter are lower when compared to the number of atom spacers in the Si(16)SP and Si(20)SP samples, while it is higher compared to the number of atom spacer in the Si(10)SP sample.

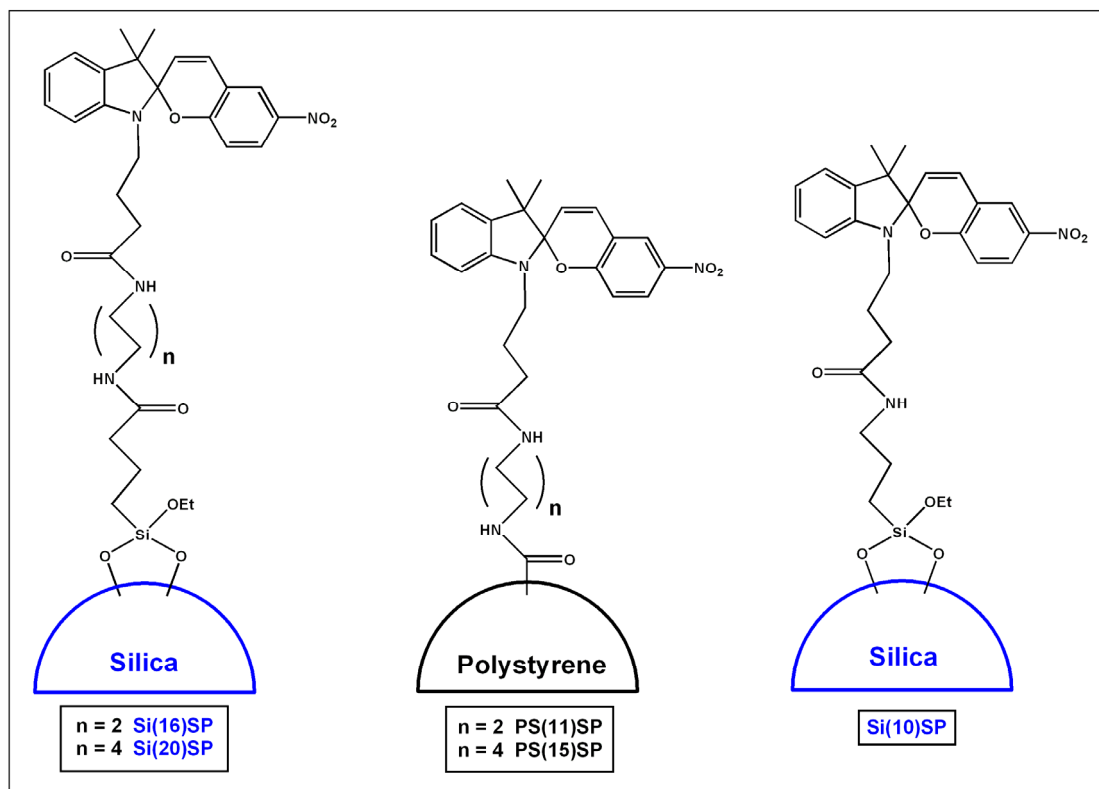


Figure 4.18: Schematic representation of the 6 immobilisation strategies adopted for the spiropyran attachment to the polystyrene and silica microbead surfaces.

When close SEM imaging of the surface of 5 μm silica and polystyrene microbeads were taken (**figure 4.19**) a roughness of the polystyrene polymeric surface compared to the smoother, uniform and non-porous silica surface could be noticed.

Small artefacts on the surface of the polystyrene polymeric beads could indicate the presence of small porous which probably makes the need for spacer atoms between the spiropyran unit and the bead surface stronger in order to have the spiropyran unit exposed enough to undergoes photo-isomerisation and complex formation.

On a smoother surface a larger number of atom spacers may cause molecular wrapping and perhaps this could explain the substantially higher photoswitching ability of the Si(10)SP sample compared to the Si(16)SP and Si(20)SP samples.

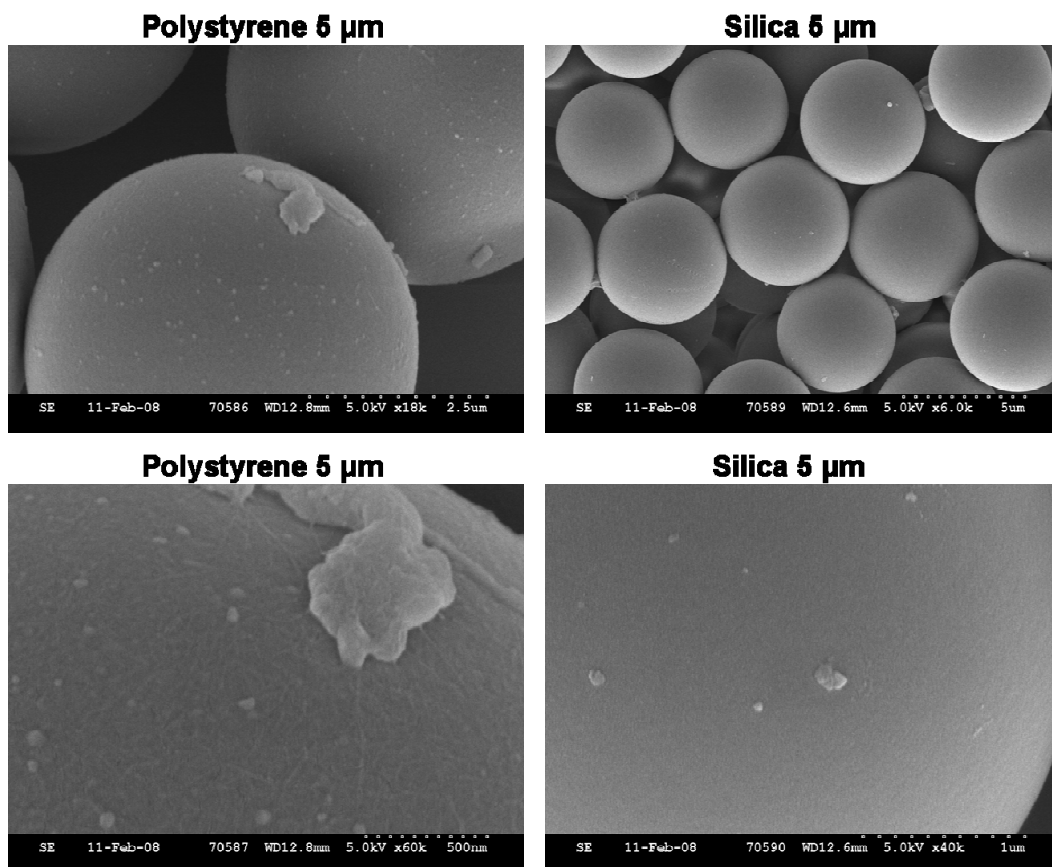


Figure 4.19: SEM images of 5 μm plain silica (right) and plain polystyrene (left) microbeads.

The switching efficiencies of the different microbead samples (Si(10)SP, Si(20)SP and Si(PA)SP) were then further evaluated by repeatedly cycling the three samples from the SP to the MC form. The switching cycle SP \leftrightarrow MC (performed by irradiating the samples alternatively for 2 min with UV LED, followed by 4 min with a white LED) on all the three samples was repeated 5 times and the differences in absorbance values at 558nm ($MC Ab_{558nm} - SP Ab_{558nm}$) plotted (**figure 4.20** and **figure 4.21**).

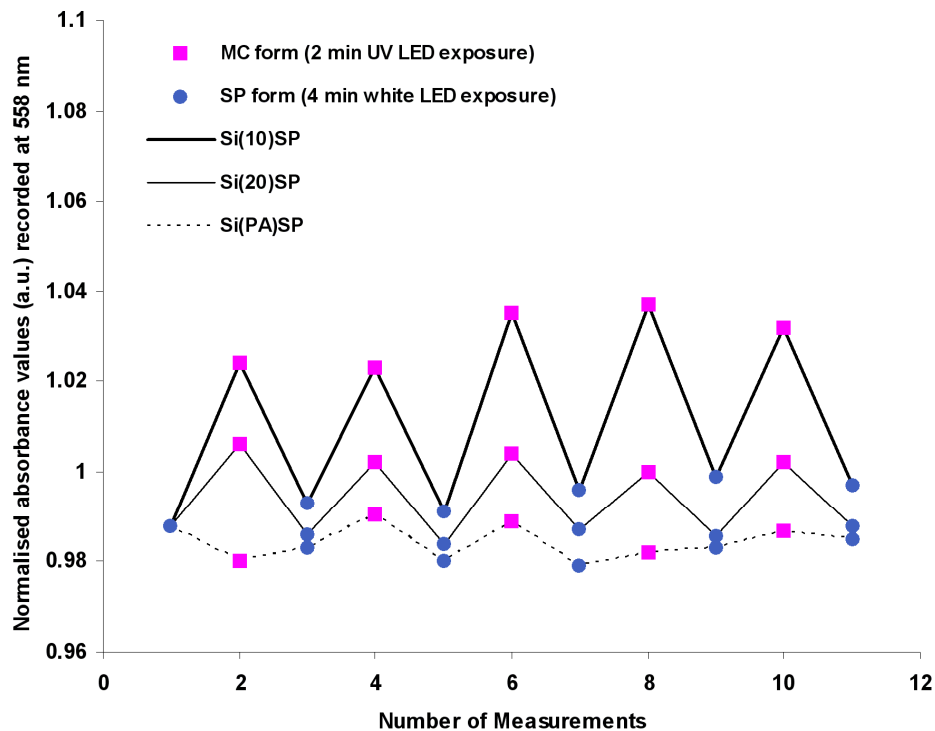


Figure 4.20: Graph showing five switching cycles performed on Si(PA)SP, Si(10)SP and Si(20)SP samples. Each cycle was carried out by alternatively irradiating the samples (0.0125 g of microbeads in 1.2 ml ethanol suspension) for 2 min UV LED (to induce the formation of the MC form) and 4 min with white LED (to induce the formation of the SP form). The absorbance values at 558 nm were recorded and normalised for the three samples. A much larger absorbance difference at 558 nm between the SP and the MC form is evident in the case of the Si(10)SP sample when compared to the Si(PA)SP and Si(20)SP samples.

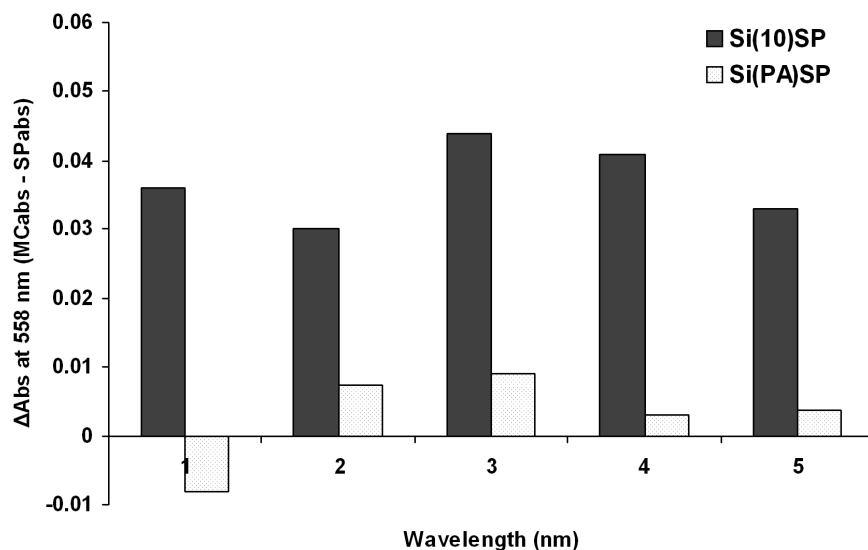


Figure 4.21: Differences in absorbance values at 558nm (MC Abs_{558nm} - SP Abs_{558nm}) extracted from five switching cycles (2 min UV LED and 4 min white LED) on a Si(10)SP microbead sample compared to Si(PA)SP microbeads sample. Both samples contain 0.0125 g microbeads in 1.2 ml ethanol suspension. A much larger absorbance difference is evident in the case of the microbeads with covalently bound SP indicating that the SP molecules have enough conformational freedom to switch between the SP and MC forms efficiently.

The graph clearly shows the effectiveness of the covalent immobilization over the physical absorption and of the more efficient spiropyran switching on the Si(10)SP sample compared to the Si(20)SP sample. There is almost no significant difference between the absorbance value at 558 nm for the SP-PA sample, while there is obvious switching between the SP and MC forms in the case of the Si(10)SP sample, demonstrating that the covalent immobilisation allows effective switching. As previously reported, the presence of a tether spacer groups increases the degree of conformational flexibility allowing an efficient spiropyran switching¹⁰. In the case of the Si(10)SP sample, the tether is obviously sufficiently long enough to allow the molecular re-arrangement accompanying SP↔MC switching to happen in a free manner. The low switching efficiency of the Si(20)SP sample is probably due to an excessively long spacer which hinders the molecular isomerisation. Therefore the silica Si(10)SP microbead samples were used for further investigation of its photo reversible properties.

4.5.5 Influence of solvent on MC→SP kinetics

In comparison to polystyrene, silica microbeads are more stable towards a wider range of solvents and the spiropyran switching behaviour on their surface can therefore be analysed using a larger number of solvents with different polarities. The influence of different solvents was analysed by adding eight different solvents to 3 mg layers of dry spiropyran functionalised microbeads deposited at the bottom of eight different wells. The solvents used were: DMF, acetone, acetonitrile, chloroform, ethanol, water, toluene and hexane. Once the microbeads were immersed in the corresponding solvent the formation of the MC form on the microbead surface was induced by exposing each layer to UV light for 2 minutes and the corresponding spectra were recorded (**figure 4.22**).

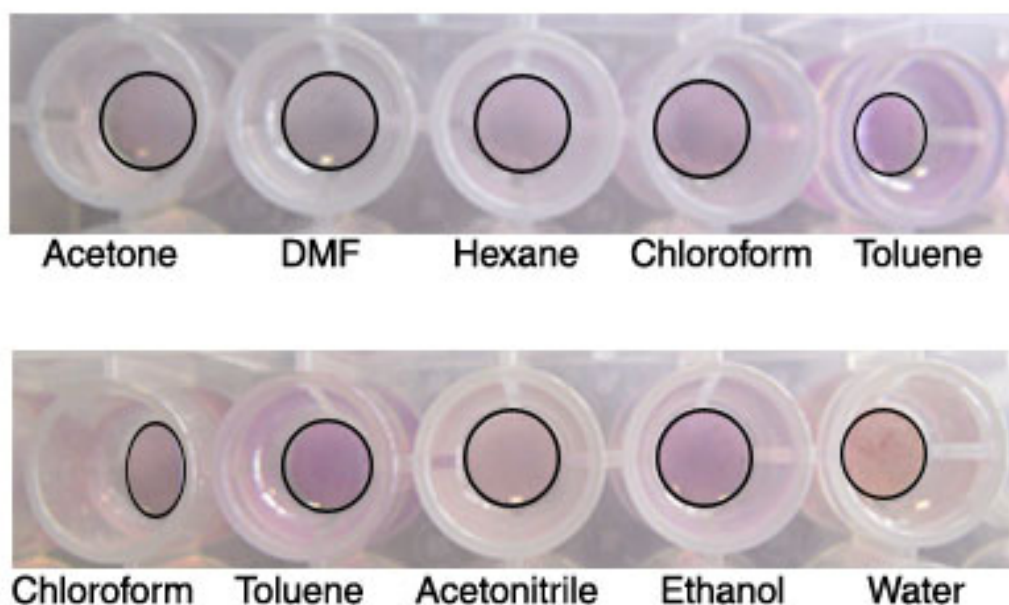


Figure 4.22: Picture showing the MC form coloration on silica microbead layers (Si(10)SP) in eight different solvents after 2 minutes UV light irradiation. On each well 3 mg of Si(10)SP beads sample are present suspended in 0.3 ml of the corresponding solvent.

The recorded spectra obtained from the MC in the different solvents show that the MC absorbance max is slightly shifting according to the solvent type.

The lowest values are recorded for acetone and water where the MC absorbance max are around 535 and 540 nm respectively.

Acetonitrile shows an absorbance around 550 nm, toluene, chloroform and hexane around 560 nm, DMF at 565 nm (even though the signal is extremely low) and ethanol at 558 (figure 4.23 and figure 4.24).

The results show a trend which is quite different from the more dramatic batho and hypsochromic shifts which are happening for the MC in solution in solvents with different polarities as the variation range of the MC absorbance max is significantly smaller.

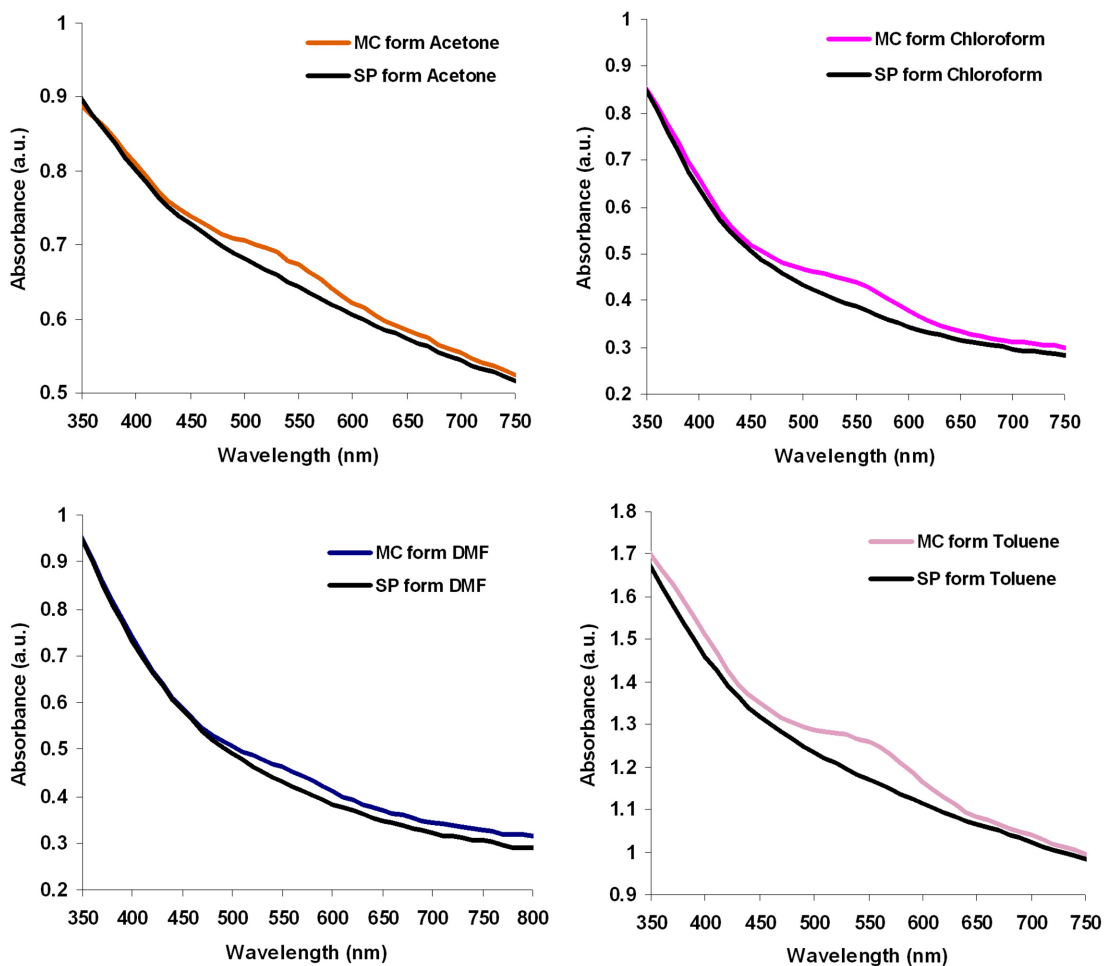


Figure 4.23: Graphs showing the spectra of the SP and MC form in DMF, chloroform, acetone and toluene.

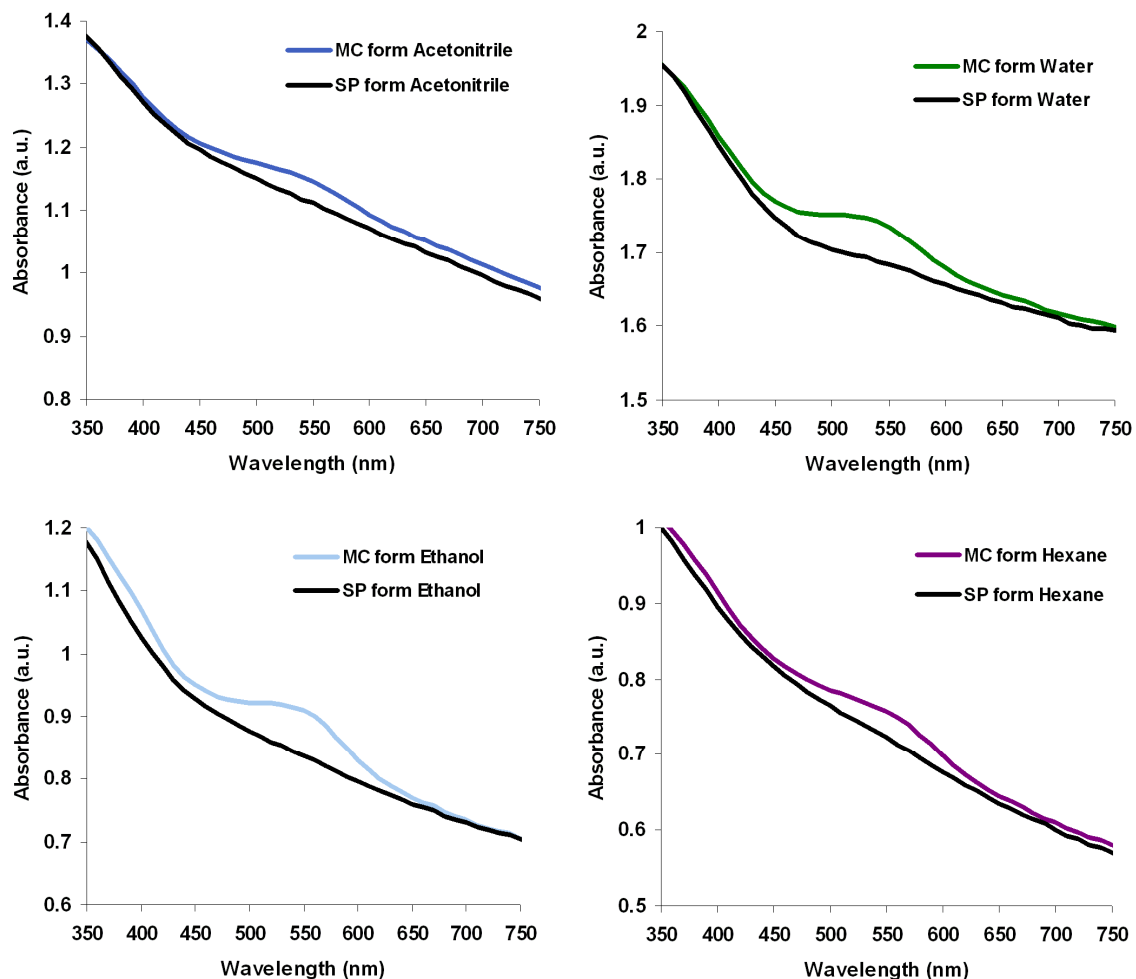


Figure 4.24: Graphs showing the spectra of the SP and MC form in acetonitrile, water, ethanol and hexane.

The MC form in toluene solution shows an absorbance max of 602 nm, significantly higher compared to 560 nm recorded for the spiropyran silica beads in the same solvent. Similarly in acetone solution, the MC form exhibit an absorbance max of 560 nm which drops to 535 nm when the MC is immobilised on the silica bead surface.

The MC form in ethanol solution shows an absorbance max of 540 nm, while in the silica beads in ethanol the absorbance is recorded at 558 nm.

This is probably due to a sort of masking effect of the polar silica matrix which surrounds the spiropyran molecules. Probably the presence the silica environment close to the photochromic dye is bringing an attenuation of the polar and non-polar

environment of the different solvents in which the beads are suspended and smaller range of absorbance max values in the different solvents is observed.

Smaller shifts in both directions are still observed for more polar or more non-polar solvents, but the extent of this range is significantly less pronounced when compared to the behaviour of the MC form in solution, where the variation range goes from 540 nm (ethanol) to 602 nm (toluene).

Taking ethanol as a reference, small hypsochromic shift is observed when the beads are exposed to water, acetonitrile and acetone while in acetone, toluene, chloroform, hexane and DMF small bathochromic shifts towards higher wavelength are recorded (**figure 5.25**). Conversely of what is happening for the MC form in solution, in the silica beads the MC absorbance max in acetone and acetonitrile is lower when compared to the one in ethanol, following in this way the SPP polarity scale, according to which acetone and acetonitrile are more polar than ethanol so that the MC absorbance max should be consequently lower.

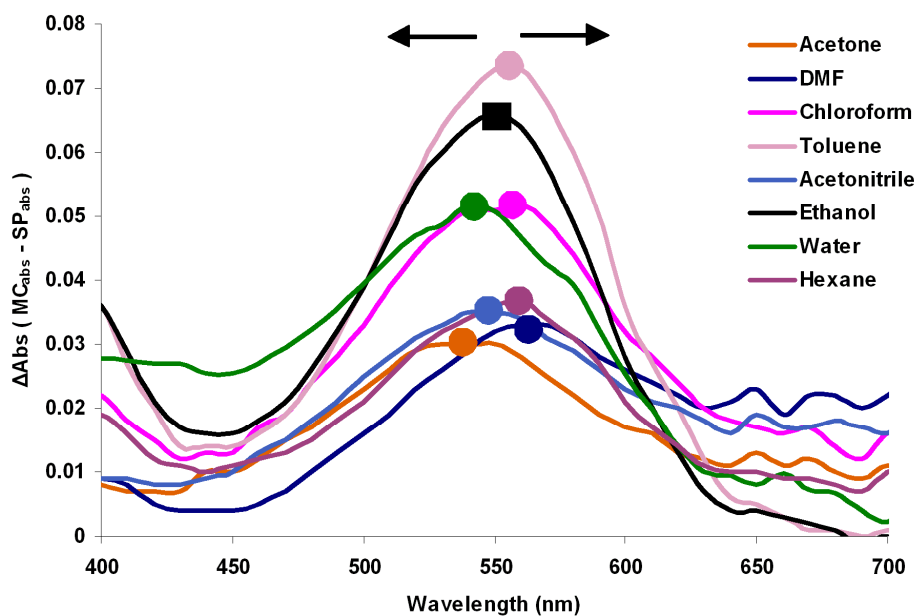


Figure 4.25: Graph showing the differential absorbance spectra (MC Abs - SP Abs) for samples of Si(10)SP (3 mg in 0.3 ml of the corresponding solvent) suspended in acetone, DMF, chloroform, toluene, acetonitrile, ethanol, water, hexane.

In general when the spiropyran modified silica beads are placed in solvents with different polarity, the MC absorbance maximum is considerably shifting according to the solvent polarity, but the wavelengths range is much smaller (from 535 nm to 565 nm) when compared to the free MC in solution (from 540 to 602). This effect, which appears after incorporation of the photochromic unit on the microbeads, is possibly caused by the influence of the matrix on the immediate surrounding environment of the MC, decreasing the stronger direct effect of the solvent polarity which is verified when the MC is free in solution.

The thermodynamic ring closing equilibrium of the MC form towards the SP form is also affected by the solvent type. It is known from solution studies that this process follows first order kinetics¹⁴, with the thermodynamics and kinetics strongly influenced by the solvent polarity.

The use of silica spiropyran functionalised microbeads enables the switching behaviour to be examined in a wider range of solvents compared to polystyrene microbeads, which are dissolved by chloroform, acetone and aromatic solvents such as toluene.

Therefore after the MC was formed on the surface of the silica microbeads placed in the eight different solvents, the absorbance values were recorded at 550 nm and 560 nm every minute for 90 minutes and the normalised absorbance values were plotted against time (**figure 4.26** and **figure 4.27**).

The wavelengths chosen to record the kinetic curves were limited by the instrument, which allows the recording of one wavelength value for all the samples and limits the wavelength type to 550 nm or 560 nm. For this reason two experiment kinds were carried out collecting the absorbance data either at 550 nm or 560 nm. Both experiments confirmed the calculated values for the rate constant values (k_R).

For this discussion the figures are showing the results obtained using the absorbance values recorded at 550 nm, even though the rate constant values are calculated as an average between both the absorbance values obtained at 550 nm and 560 nm.

The choice of the time scale was also a limitation due to the fact that after 90 minutes some of the solvents undergo evaporation.

During the kinetic measurements, the sample is kept in the dark inside the plate well reader to avoid the influence of the ambient light and the recording of absorbance values is automated.

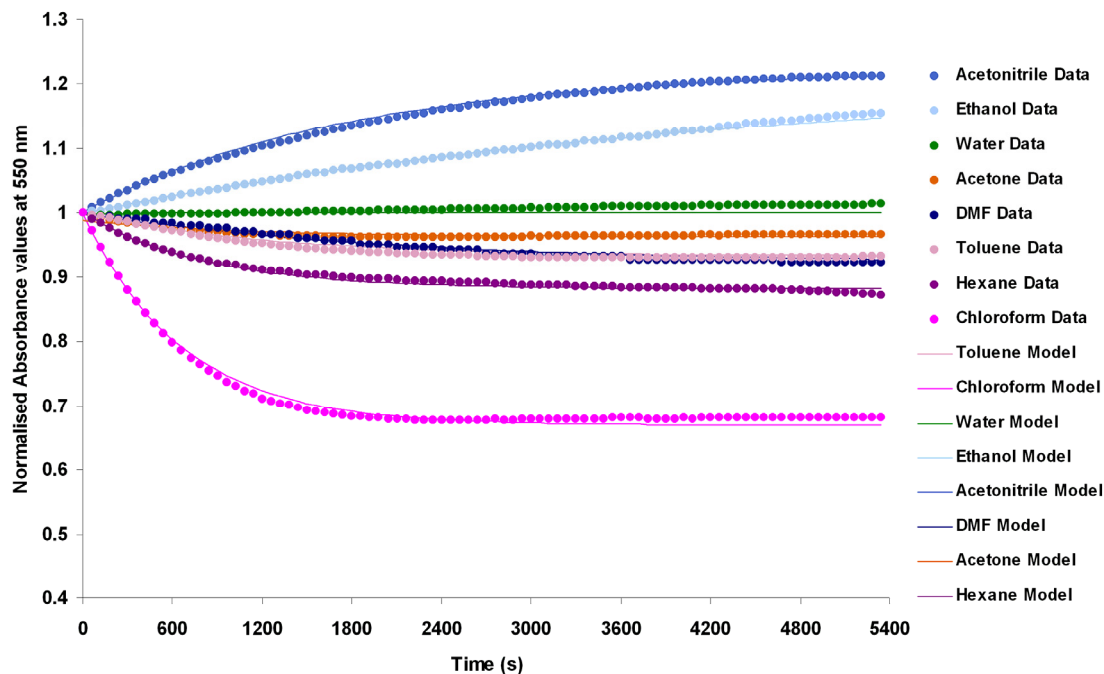


Figure 4.26: First order kinetic curves obtained plotting time against the normalised absorbance values at 550 nm of the spiropyran immobilised on a Si(10)SP microbead sample in different solvents. The residual error calculated between the data and the model in between does not exceed 3% at any point in the fitted curve (**figure 4.26**).

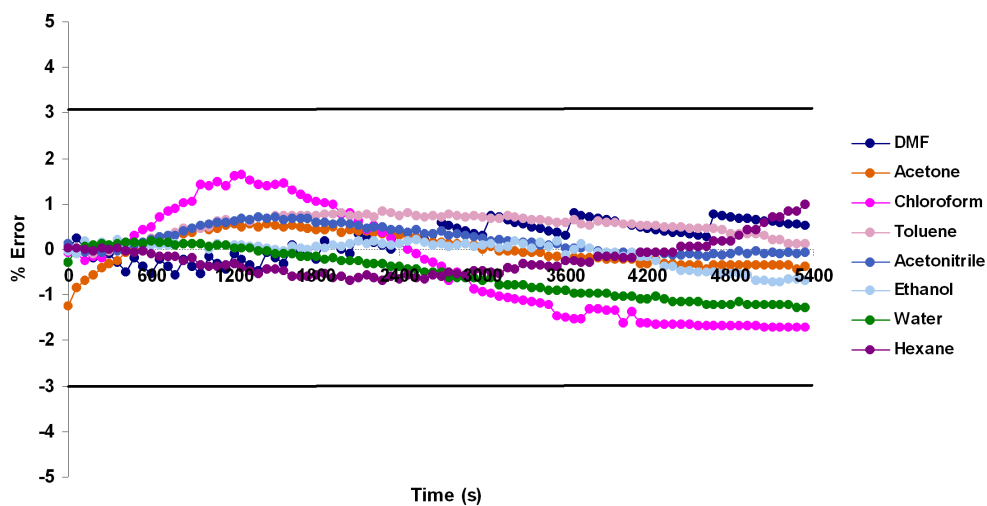


Figure 4.27: The residual error calculated between the data and the model in between does not exceed 3% at any point in the fitted curve.

The first order rate constants were estimated by fitting the normalised absorbance values at 550 nm and 560 nm using Microsoft Excel Solver^{15,9}, using the following equation (**Table 4.3**):

$$y = ae^{k_R t} + b \quad [4.1]$$

where y is the normalised absorbance at 550 nm or 560 nm, a is the pre-exponential factor, k_R is the rate constant and b is the asymptotic value.

Our results show that the equilibrium between the two forms strongly depends on the solvent type, which suggests that the surface immobilised dye is actively interacting with the solvent molecules. In two of the polar solvents used (ethanol and acetonitrile) the kinetic curves show an increase of the absorbance value at 550 nm and 560 nm. This means that MC concentration in these solvents in the dark is increasing, probably due to the increasing polar environment as a consequence of the polar solvent evaporation over time. In water the conversion of the MC to the SP form is strongly inhibited, and after 90 minutes MC is still the predominant form. This behaviour is not surprising, as the zwitterionic MC form is stabilised in highly polar environments compared to the more hydrophobic SP form. In addition the equilibrium position is reached relatively quickly compared to the other solvents, with a $k_{R(\text{water})} = 2.9 \times 10^{-3} \text{ s}^{-1}$, the highest among all the studied solvents by an order of magnitude.

Solvent	k_R 550nm (s^{-1})	k_R 560nm (s^{-1})	Ratio to Ethanol
DMF	4.8×10^{-4}	5.2×10^{-4}	2.2
Acetone	8.6×10^{-4}	8.4×10^{-4}	3.7
Chloroform	1.5×10^{-3}	1.5×10^{-3}	6.6
Toluene	8.2×10^{-4}	8.3×10^{-4}	3.6
Acetonitrile	5.5×10^{-4}	5.3×10^{-4}	2.3
Ethanol	2.1×10^{-4}	2.4×10^{-4}	1
Water	2.2×10^{-3}	2.9×10^{-3}	11.2
Hexane	1.2×10^{-3}	1.3×10^{-3}	5.4

Table 4.3: Rate constants for the ring closing and ring opening equilibrium obtained from the best-fit curves of the normalised absorbance values in **figure 4.25** (recorded at 550 nm) and the values recorded at 560 nm. On the right column the ratio to the ethanol rate constant is reported.

Relatively high rate constant are observed for non-polar solvents such as chloroform and hexane, where the equilibrium position is reached 6.6 and 5.4 times quicker than in ethanol, with k_R ($MC \rightarrow SP$) values of $1.5 \times 10^{-3} \text{ s}^{-1}$ and $1.2 \times 10^{-3} \text{ s}^{-1}$ respectively. In acetone, toluene, acetonitrile and DMF the k_R ($MC \rightarrow SP$) values are smaller ranging from $8.6 \times 10^{-4} \text{ s}^{-1}$ (acetone) to $5.2 \times 10^{-4} \text{ s}^{-1}$ (DMF).

In general, the obtained values are higher by an order of magnitude when compared to relaxation times obtained for spiropyran functionalised polystyrene microbeads where the rate constants are around $10^{-4}/10^{-5} \text{ s}^{-1}$, showing that the ring closing is happening faster within the silica beads matrix.

On the other hand, the relaxation times recorded for the covalently bond spiropyran on the silica beads are much lower when compared to spiropyran doped polystyrene films⁹ previously described in the literature, where the rate of the spiropyran closing is around 10^{-2} s^{-1} . However, in those studies the SP was entrapped within a polymer layer, whereas in this case, the SP is covalently immobilised on the microbead surface.

4.5.6 Photostability evaluation of the surface immobilised spiropyran

The photostability of the spiropyran immobilised on the bead surface in ethanol was evaluated by normalising the difference in the absorbance value at 558 nm to the initial absorbance values according to the formula:

$$\%E = \frac{(A_{SPi} - A_{MCi})}{(A_{SP} - A_{MC})} \times 100 \quad [4.2]$$

where E is the percent efficiency, A_{SPi} and A_{MCi} are the initial values of absorbance of the MC and the SP forms when the initial switching was performed and A_{SP} and A_{MC} are the absorbance values obtained in subsequent switching cycles.

According to this model, 100% is the maximum efficiency, when no photodegradation occurs, while 0% is when the photochromic dye is completely photobleached.

After 20 switching cycles (two minutes irradiation with UV LED followed by four minutes exposure to white LED), the efficiency was found to decrease by around 17%

with respect to the initial switching values of the freshly prepared sample of Si(10)SP (**figure 4.28**).

This decrease in switching efficiency is similar but slightly lower than the one obtained in the previous chapter with the spiropyran functionalised polystyrene microbead (PS(15)SP), where the decrease was 22% after 20 cycles (**figure 4.28**).

These are improvements compared to the solution studies reported by Li et al. in which the percentage of surviving MC in methanol after just 13 switching cycles (with a 30 second UV irradiation for each cycle, using high pressure mercury lamp) is around 56.4%⁷. However, it is not as efficient as other polymeric immobilisation strategies using a film matrix, where after more than 370 cycles using LEDs the decrease in photostability is around 14% (which translates in 86% of surviving MC)³. As in the case of the spiropyran modified polystyrene beads, this is probably due to the fact that the microbeads are free to move and interact between each other, allowing eventual MC aggregation.

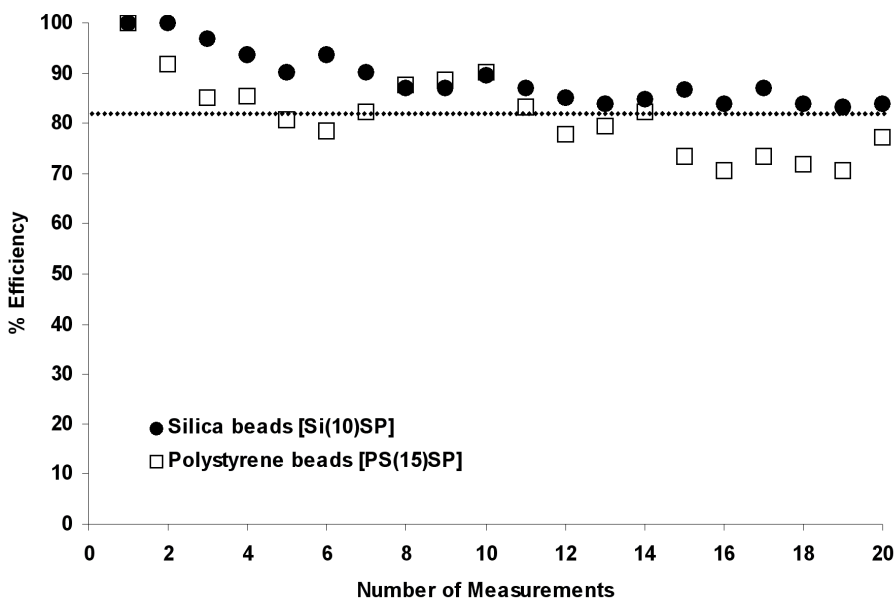


Figure 4.28: Decrease in switching after 40 switching events of a spiropyran functionalised silica microbead sample Si(10)SP (0.0125 g in 1.2 ml ethanol suspension) compared to a spiropyran functionalised polystyrene microbead sample PS(15)SP (0.01 g in 1.3 ml of ethanol). The efficiency was evaluated monitoring the reflectance value at 558 nm, according to the reported formula, showing a decrease after 20 cycles of 17% for Si(10)SP and 22% for PS(20)SP.

4.5.7 Photoreversible ion-binding properties

The reversible binding properties of MC towards a range of different metal ions have been widely reported in the literature¹⁶⁻¹⁸ and even though the phenolate of the MC form is not a particularly selective, the nitro spiropyran derivative used in these studies is particularly sensitive to certain transition metals such as Co^{2+} , where the Job's plot has shown a 1 (Co^{2+}) : 2 (MC ligand) stoichiometry¹⁰, Cu^{2+} , whose chelating properties towards the MC form has been demonstrated both in solution¹⁹ and on a polymeric surface³, and Zn^{2+} where again a 2:1 ligand:metal molar ratio has been shown in solution studies²⁰ and complex formation was demonstrated with surface immobilised MC²¹.

In contrast, alkaline earth ions such as Ca^{2+} and Mg^{2+} do not bind effectively with simple spiropyran derivatives and only exhibit binding behaviour with MC when the two merocyanines are pre-arranged in a bis-benzospiropyranindoline bidentate ligand²².

On the basis of literature investigations and previous solution studies, Cu^{2+} , Hg^{2+} , Cd^{2+} , Co^{2+} , Zn^{2+} and Ca^{2+} ions were tested in order to investigate the ion complexation properties of the Si(10)SP microbeads. To test for anion effects, both the chloride and nitrate salts of Ca^{2+} , (a metal ion that does not cause any appreciable change in the MC spectrum) were prepared in ethanol (final concentration 7.7×10^{-4} M) and placed in contact with microbeads in the MC form. In both cases, no significant spectral changes were observed and the 558 nm peak of the MC remained unaffected in the presence of Ca^{2+} (**figure 4.29**). This demonstrates that Ca^{2+} ions have no interaction with the silica-SP(C-0) microbeads and that the anion has no independent effect.

Subsequently the effect of ethanolic solutions of Cu^{2+} , Hg^{2+} , Cd^{2+} , Co^{2+} , Zn^{2+} at the same concentration in ethanol were tested. As with Ca^{2+} , no spectral changes were observed with Hg^{2+} ions (**figure 4.29**), whereas blue shifts at the MC maximum absorbance wavelength occurred in the presence of Cd^{2+} and Co^{2+} ions, from 558 nm to 540 nm, and to 550 nm respectively (**figure 4.30**).

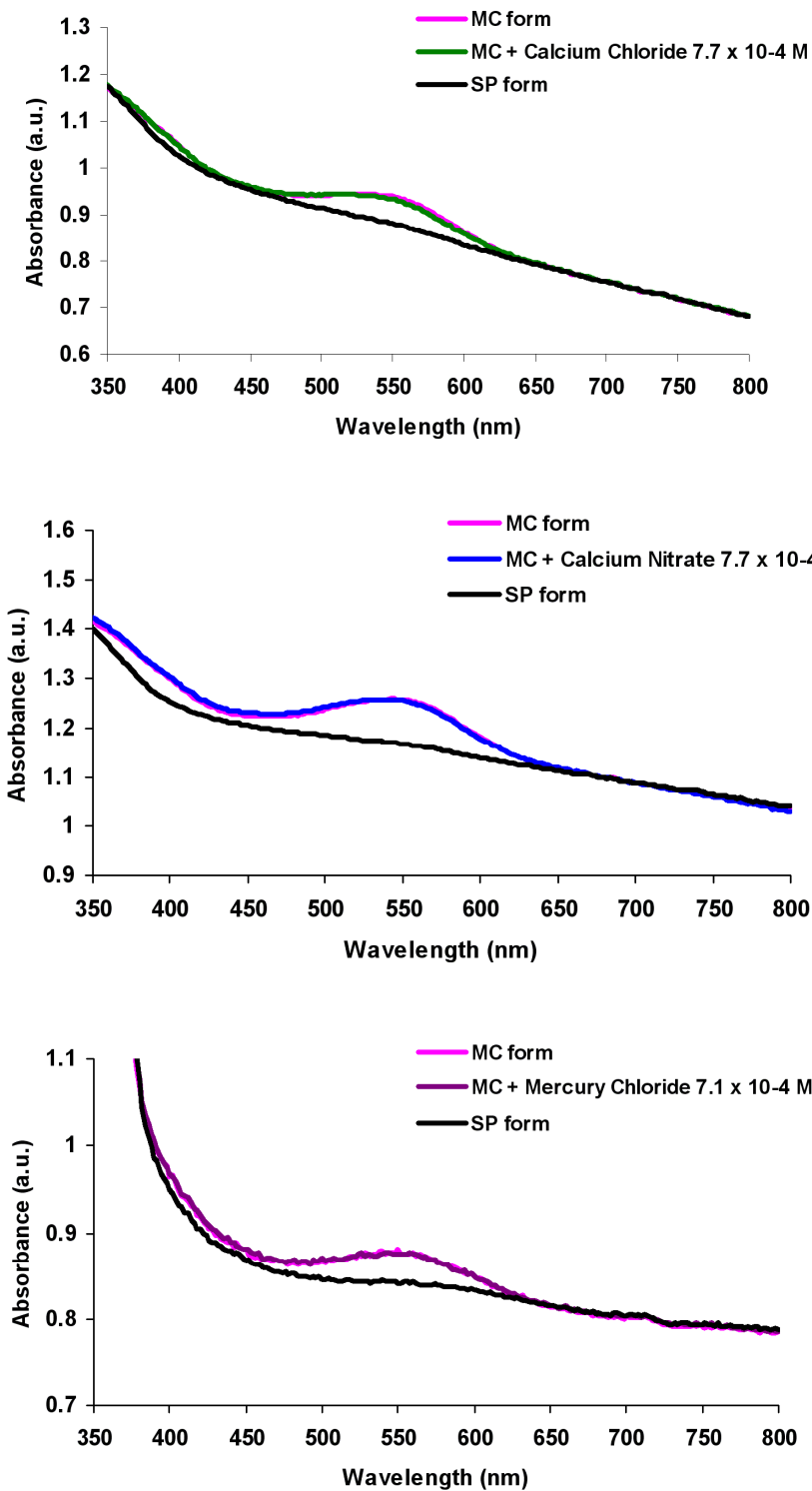


Figure 4.29: Absorbance spectra of silica Si(10)SP microbeads (0.0125 g in 1.2 ml ethanol suspension) switched from the SP to the MC form. No spectral changes are observed upon addition of Hg^{2+} and Ca^{2+} (final concentration 7.7×10^{-4} M in ethanol).

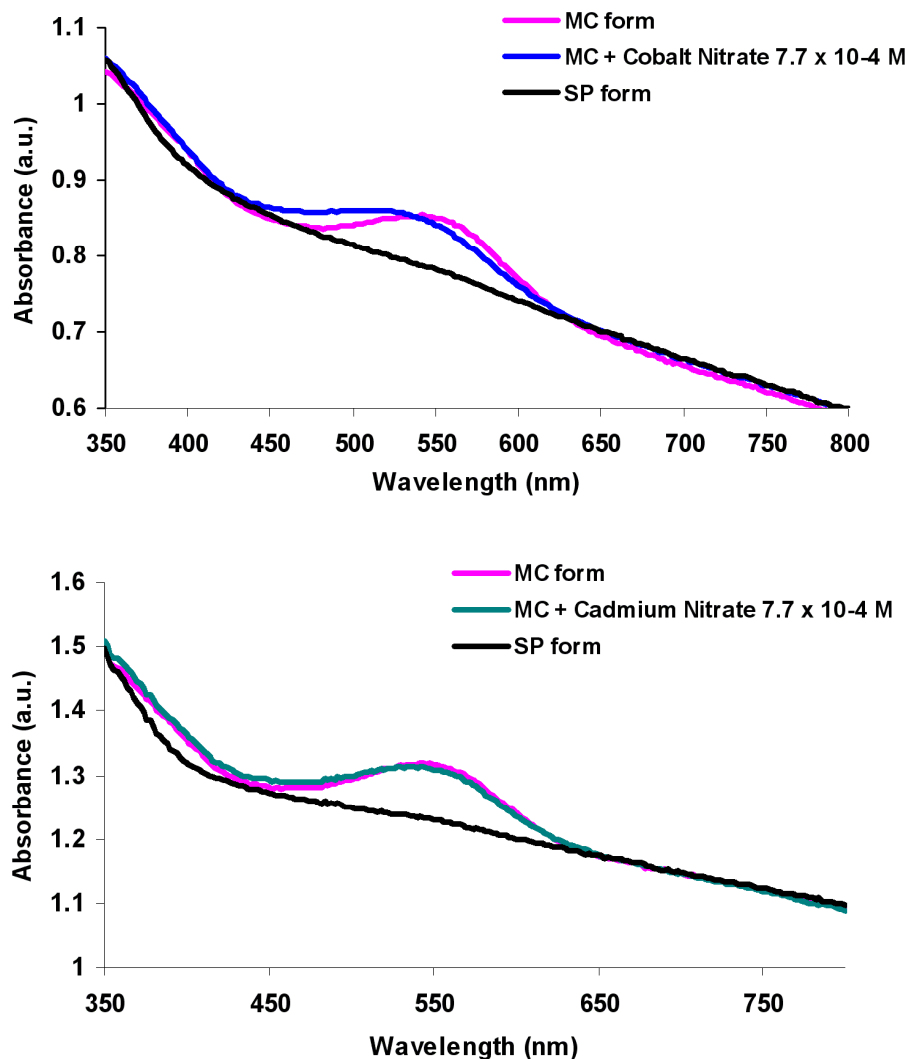


Figure 4.30: Absorbance spectra of Si(10)SP microbeads (0.0125 g in 1.2 ml ethanol suspension) switched from the SP to the MC form and after the addition of Co^{2+} and Cd^{2+} : small blue spectral shifts of the 558nm MC peak were recorded, to 550nm (Cd^{2+}) and to 540nm (Co^{2+}).

However, much larger effects were observed in the case Zn^{2+} and Cu^{2+} ions. In the presence of Zn^{2+} , a clear visual colour change from purple (MC) to light pink (MC-Zn^{2+}) can be observed (**figure 4.31**). This is caused by a decrease in the MC absorbance band at 558 nm and the emergence of a new absorbance band centred around 525 nm arising from the MC-metal ion complex (**figure 4.32**).

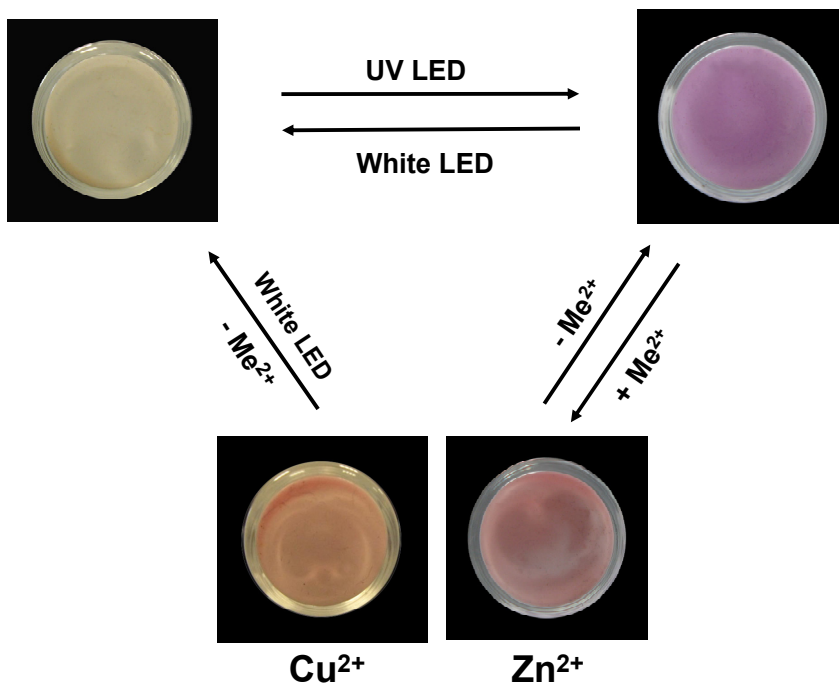


Figure 4.31: Visual colour changes observed with Si(10)SP microbeads (0.025 g in 1.3 ml ethanol) at the bottom of a sample vial that accompany switching from the colourless SP form to the pink MC form, and after addition of Cu²⁺ and Zn²⁺ to the MC form.

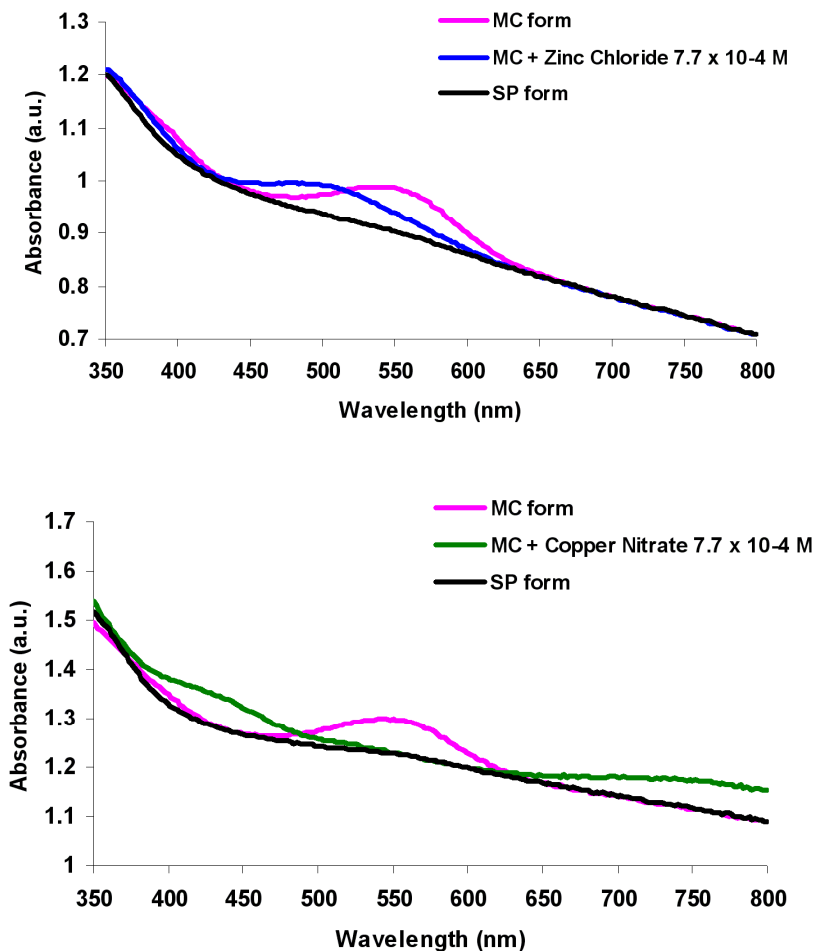


Figure 4.32: Absorbance spectra of Si(10)SP microbeads (0.0125 g in 1.2 ml ethanol suspension) underlying these colour changes. Upon addition of Cu^{2+} ions, the 558nm MC peak disappears, and new peak maxima appear at 440nm and 750nm; addition of Zn^{2+} leads to reduction in the MC 558nm absorbance and appearance of a new band around 525nm.

Similarly, addition of Cu^{2+} ions at the same concentration to microbead sample converted to the MC form resulted in a colour shift from purple to orange (MC- Cu^{2+} complex) occurred, which arose from the disappearance of the 558 nm MC peak and the simultaneous appearance of two new absorbance bands at 440 nm and 750 nm (**figure 4.31 and 4.32**).

In both cases, after the formation of the MC-metal ion complex, replacement of the metal ion solution with clean ethanol, followed by irradiation of the microbeads for 4 minutes with a white LED leads to expulsion of the bound Cu^{2+} ions and complete reformation of the SP form on the beads. Following this, irradiation of the microbeads

for 2 minutes with the UV-LED converted the SP back to the MC form, ready for another metal ion uptake and release cycle.

The binding and releasing cycles between the SP \leftrightarrow MC \leftrightarrow MC-metal complex have been successfully repeated five times using the same microbead sample for both Cu^{2+} and Zn^{2+} ions, demonstrating that the spiropyran coated silica microbeads represent a reversible ion binding and detecting system, whose properties can be externally modulated by light (**figure 4.33** and **figure 4.34**).

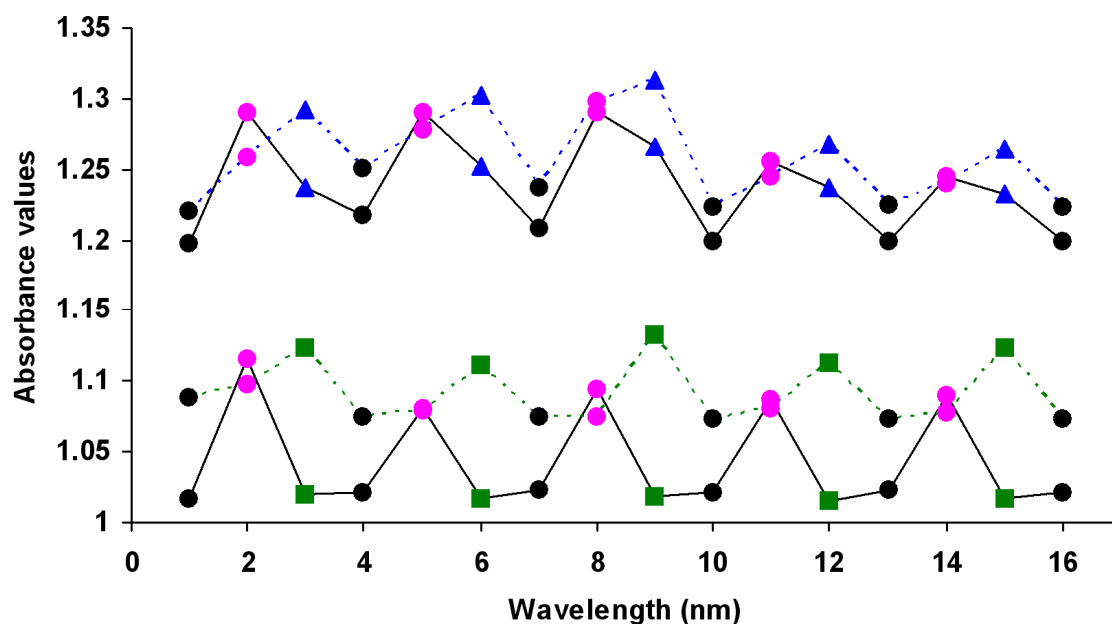


Figure 4.33: Absorbance values of silica-SP(C-0) microbeads (0.0125 g of microbeads in 1.2 ml ethanol suspension) plotted after performing of five switching cycles from the SP form (empty circle), MC form (full circle) and from here to the MC- Cu^{2+} complex (green square) and MC- Zn^{2+} complex (blue triangle). The absorbance values have been monitored at 558nm (continuous line) 525nm (blue dotted line) and at 440nm (green dotted line), where the maximum spectral differences between the MC and the MC-ion complex forms appear.

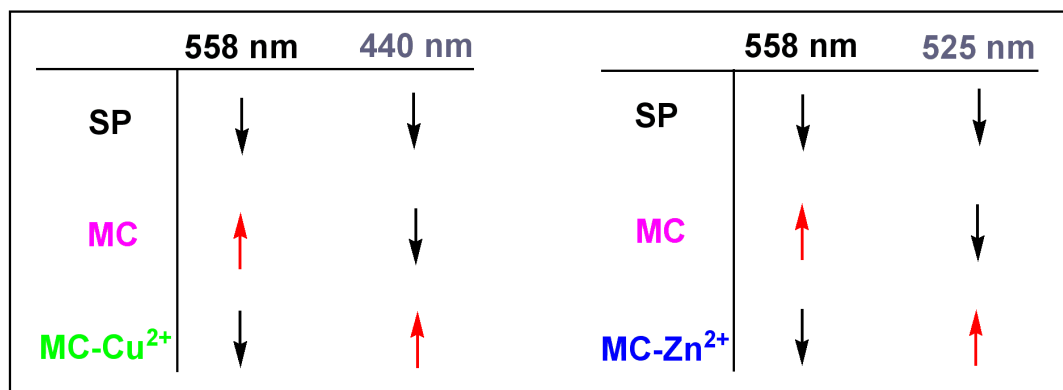


Figure 4.34: Schematic representation of the absorbance changes at 558 nm, 440 nm and 525 nm which are happening on the surface of Si(10)SP microbeads in the presence of the SP, MC and MC-Cu²⁺ and MC-Zn²⁺ complex.

This behaviour has important implications for light-controlled ion uptake and release. For example, pre-concentration of metal ions from solution can be affected on beads within chromatography, flow-injection analysis or lab-on-a-chip platform, using light to control where and when binding/release occurs. For example, beads can be used to pick up ions at one location within a flow system, transport the ‘cargo’ to a second location, where they are released, again using light to control where and when these events occur.

4.6 Conclusions

Silica microbeads have been successfully functionalised with spiropyran using different immobilisation strategies. The different covalent immobilisation path has been evaluated and the functionalisation type Si(10)SP has been demonstrated to be the more efficient.

The spiropyran ring closure equilibrium from the MC to the SP form on the silica bead surface is influenced by the solvent type even though the range of MC absorbance shifts due to the solvent type is not as broad as for the MC in solution, probably because of the influence of the silica environment which surrounds the microbeads.

Investigations on the ion-binding properties shows that the spiropyran functionalised silica microbeads are inherently self-indicating entities capable of switching between non ion-binding (inactive) and ion-binding (active) forms, with switching between these states, and indeed the uptake and release of the bound ions controlled entirely using light of an appropriate wavelength. The microbeads surface can be modulated between a

colourless inactive SP form and an active binding MC form which is highly coloured and undergoes further reversible colour changes in the presence of Cu^{2+} and Zn^{2+} ions, with smaller spectral changes occurring in the presence of Cd^{2+} and Co^{2+} , while it is insensitive to Ca^{2+} and Hg^{2+} .

Therefore, these self-indicating beads could form the basis of a system capable of selectively binding certain metal ions from mixtures, but only when switched to the 'active' state using UV-light. The acquired ions can subsequently be released when the beads are illuminated using white (or green) light. Clearly, this behaviour could have many interesting applications in selective pre-concentration on certain ions, transport of bound ions to remote locations, and controlled release of bound ions, using light as the external controlling stimulus. The same underlying mechanisms may also be applicable to selective uptake and release of other species, such as amino acids or more complex guests²³.

The spiropyran functionalisation of polystyrene and silica microbeads has shown in both cases the possibility of having bead-based systems that can be reversibly switched using light between a SP and a MC form with similar photo-fatigue resistance over a number of switching events.

In both surface types the MC form in the presence of certain metal ions undergoes further colour and spectral changes which are indications of the complex formation. Then upon white light exposure the metal can be released, the SP form restored and this behaviour can be cycled several times.

However there are differences between the two bead types that need to be considered.

The MC form on the silica bead surface is particularly sensitive both to Cu^{2+} and Zn^{2+} ions; silica beads present a smoother surface and a better stability towards a wider variety of solvents. They can be analysed using both absorbance and reflectance spectroscopy and the polarity of their surface enhances the stability of the MC form.

On the contrary polystyrene beads are stable within a very limited number of solvents, their surface is porous and longer tethers are needed between the spiropyran and the bead surface for an effective $\text{SP} \leftrightarrow \text{MC}$ switching. Their spectral properties can only be analysed using reflectance spectroscopy due to their high refractive index and their MC undergoes strong colour and spectral changes only in the presence of Cu^{2+} .

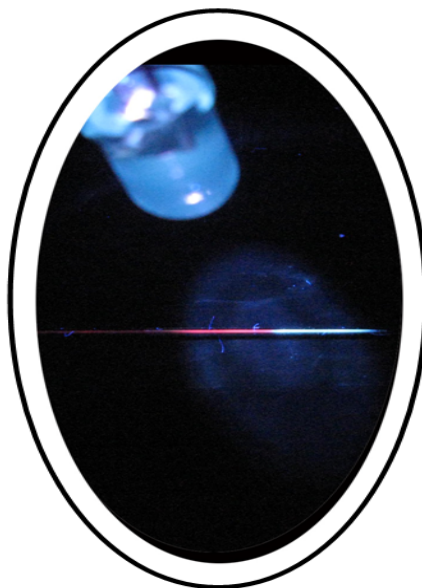
For their versatility and higher stability spiropyran functionalised silica microbeads have been chosen for capillary packing in order to create a new photo-switchable stationary phase for metal binding and release which is object of discussion in **Chapter 5**.

4.7 References

- (1) Scarmagnani, S.; Walsh, Z.; Alhashimy, N.; Radu, A.; Paull, B.; Macka, M.; Diamond, D. *Conf Proc IEEE Eng Med Biol Soc.* **2007**, 4096-4097.
- (2) Rosario, R.; Gust, D.; Hayes, M.; Jahnke, F.; Springer, J.; Garcia, A. A. *Langmuir* **2002**, *18*, 8062-8069.
- (3) Radu, A.; Scarmagnani, S.; Byrne, R.; Slater, C.; Lau, K. T.; Diamond, D. *Journal of Physics D: Applied Physics* **2007**, 7238-7244.
- (4) Baillet, G.; Giusti, G.; Guglielmetti, R. *Journal of Photochemistry and Photobiology A: Chemistry* **1993**, *70*, 157-161.
- (5) Baillet, G.; Campredon, M.; Guglielmetti, R.; Giusti, G.; Aubert, C. *Journal of Photochemistry and Photobiology A: Chemistry* **1994**, *83*, 147-151.
- (6) Matsushima, R.; Nishiyama, M.; Doi, M. *Journal of Photochemistry and Photobiology A: Chemistry* **2001**, *139*, 63-69.
- (7) Li, X.; Li, J.; Wang, Y.; Matsuura, T.; Meng, J. *Journal of Photochemistry and Photobiology A: Chemistry* **2004**, *161*, 201-213.
- (8) Demadrille, R.; Rabourdin, A.; Campredon, M.; Giusti, G. *Journal of Photochemistry and Photobiology A: Chemistry* **2004**, *168*, 143-152.
- (9) Stitzel, S.; Byrne, R.; Diamond, D. *Journal of Materials Science* **2006**, *41*, 5841-5844.

- (10) Byrne, R. J.; Stitzel, S. E.; Diamond, D. *Journal of Materials Chemistry* **2006**, *16*, 1332-1337.
- (11) Bachmann, D.; Hierold, C. *Journal of Micromechanics and Microengineering* **2007**, 1326.
- (12) Xu, L.-C.; Logan, B. E. *Langmuir* **2006**, *22*, 4720-4727.
- (13) Van Zwol, P. J.; Palasantzas, G.; Van de Schootbrugge, M.; Hosson, J. T. M.; Craig, V. S. J. *Langmuir* **2008**, *24*, 7528-7531.
- (14) Görner, H. *Physical Chemistry Chemical Physics* **2001**, *3*, 416-423.
- (15) Diamond, D.; Hanratty, V. C. A. *Spreadsheet Applications in Chemistry using Microsoft Excel*; Wiley: New York, 1997.
- (16) Görner, H.; Chibisov, A. K. *Journal of the Chemical Society, Faraday Transactions* **1998**, *94*, 2557-2564.
- (17) Chibisov, A. K.; Gorner, H. *Chemical Physics* **1998**, *237*, 425-442.
- (18) Wojtyk, J. T. C.; Kazmaier, P. M.; Buncel, E. *Chemistry of Materials* **2001**, *13*, 2547-2551.
- (19) Zhou, J.-W.; Li, Y.-T.; Song, X.-Q. *Journal of Photochemistry and Photobiology A: Chemistry* **1995**, *87*, 37-42.
- (20) Collins, G. E.; Choi, L.-S.; Ewing, K. J.; Michelet, V.; Bowen, C. M.; Winkler, J. D. *Chemical Communication* **1999**, 321-322.
- (21) Wen, G.; Yan, J.; Zhou, Y.; Zhang, D.; Mao, L.; Zhu, D. *Chemical Communications* **2006**, 3016-3018.
- (22) Filley, J.; Ibrahim, M. A.; Nimlos, M. R.; Watt, A. S.; Blake, D. M. *Journal of Photochemistry and Photobiology A: Chemistry* **1998**, *117*, 193-198.
- (23) Byrne, R.; Diamond, D. *Nature Materials* **2006**, *5*, 421-424.

**INCORPORATION OF
PHOTOCHROMIC SPIROPYRAN
BEADS AND MONOLITHS
INTO FLOW MICRO-SYSTEMS**



5.1. Introduction

The covalent attachment of SPCOOH to the surface of polystyrene and silica microbeads was discussed previously (**Chapter 3 and 4**).

The resulting SP-functionalised microbeads can be switched back and forth between the SP and MC forms using a 375 nm UV-LED (SP → MC switching) and a 430-760nm white LED (MC → SP switching)^{1,2}. Furthermore, when the ‘activated’ beads (i.e., in the MC form) come in contact with Cu²⁺ or Zn²⁺ solutions, the microbeads undergo further spectral and visible colour changes, due to the formation of MC-M²⁺ complexes (where M²⁺ = Cu²⁺, Zn²⁺). Subsequently exposure of the beads to illumination with a white LED causes the metal-ion guest to be expelled and the ‘inactive’ SP form is restored, ready for another ion-binding event. In contrast, similar experiments involving other metal ions like Ca²⁺ show no appreciable colour and spectral changes.

This light-modulated ion retention and release behaviour, coupled with inherent self-indication of the bead state based on colour/spectral changes, opens the possibility of developing photocontrolled stationary phases that can be activated and deactivated using light, allowing flexible and intelligent use of the column. For example, a column could be held in an inactive (SP) form until ion-retention is required, and then activated using UV light, either wholly or partially. Subsequently, the column could be deactivated, and the retained ions released into the mobile phase using white light. The column could then be re-activated for further use using the same procedure. In addition, simple observation or reflectance colour measurements would indicate the status of the column – whether it is active or inactive, and to what degree it is populated with metal ions. In this chapter we demonstrate this principle by comparing the behaviour of SP-functionalised silica microbeads in a packed microcapillary column when exposed to Zn²⁺ and Ca²⁺ ions. The SP-functionalised beads were packed in-situ using a novel approach which is described below.

In parallel, on the basis of a collaboration paper submitted by Walsh and al.³, a new stationary phase based on a polymeric monolith which incorporates an acrylated spiropyran monomer has been developed and its possible use as a photochromic electro-osmotic pump evaluated. It was demonstrated that spiropyran monoliths in an acidic environment (10⁻³ M HCl) can generate an electro-osmotic flow in the

presence of an applied voltage and that the flow generated can be modulated to some degree by the means of light irradiation.

The new proposed monolith is based on an acrylated spiropyran monomer (see **Chapter 1**) whose photochromism differs from the discussed styrene spiropyran monomer which contains a nitro-group in the ortho position of the benzopyran ring.

The acrylated spiropyran monomer, without this nitro group is particularly sensitive to protonation, and in an acidic environment the MC-H⁺ form is the stable form which produces a highly positively charged surface⁴ that can be re-converted to the SP form by white light exposure. Thus this highly charged surface should produce a relatively high flow rate under electro-osmotic conditions due to the more effective formation of the double layer.

In this chapter, the creation of these new stationary phases and their light-modulated behaviour will be discussed in terms of light-induced reversible ion-binding capability (functionalised microbead packed column) and light-modulated electro-osmotic flow (spiropyran functionalised acrylate monolith).

5.2 INCORPORATION OF SPIROPYRAN FUNCTIONALISED SILICA BEADS IN A FLOW SYSTEM FOR Zn²⁺ DETECTION

5.2.1 Experimental: Materials and instruments

(1'-(3-carboxypropyl)-3',3'-dimethyl-6-nitrospiro(2H-1)benzopyran-2, 2'-(2H)-indole) (SPCOOH, Fig. 1) was synthesized as reported elsewhere⁵.

Plain silica microbeads (5 ± 0.35 µm diameter, 5 % solid contents), butyl methacrylate (BuMA), ethylene dimethacrylate (EDMA), decanol, 2,2-dimethyl-2-phenylacetophenone (DAP), UV photoinitiator, λ_{max} = 255 nm), calcium nitrate hydrate and zinc chloride were purchased from Sigma Aldrich (Ireland). Si(10)SP microbeads were prepared according to a previously reported procedure¹ (**Chapter 4**).

255 nm UV-LEDs were purchased from Sensor Electronic Technologies, Ltd., USA. Polymicro transparent polytetrafluoro ethylene (PTFE) coated fused silica capillaries (100 µm internal diameter, 375 µm external diameter) were purchased from Composite Metal Services Ltd (United Kingdom).

Sample spinning was carried out using a ROTOFIX 32 centrifuge (Global Medical Instrumentation, Inc., USA.). Capillary flushing after the monolith synthesis was performed using an HPLC pump (Shimadzu, Japan). Sample additions into the packed capillary were performed using an RS485 peristaltic pump from Lambda Laboratory Instruments (Switzerland, Europe).

The purposely designed capillary holder for reflectance measurement was fabricated in black ABS with a Stratasys 3D printer. The two parts of the holder (the probe and the capillary case) were designed using a standard CAD/CAM software package (ProEngineer). In order to evaluate the colour changes happening on the SP-functionalised beads packed into the microcolumn, reflectance UV-vis spectra were recorded using an Ocean Optics spectrometer (S2000) combined with a reflection probe which was connected to deuterium (215-400 nm) and halogen (400-1700 nm) light sources (current 85V/0.3A, Ocean Optics Inc., Eerbeek, Netherlands) (**Chapter 2**). A white reflectance standard WS-1-SL was used to standardise the measurements at 100% reflectance (Ocean Optics Inc., Eerbeek, Netherlands).

5.2.2 Synthesis of monolithic frits and packing of microcolumn with Si(10)SP microbeads

The capillary packing of the spiropyran functionalized silica microbeads was carried out synthesising a short plug of monolithic polymer, which functioned as a retaining frit⁶. Before polymerisation of the monolithic frit the walls of the polytetrafluoroethylene (PTFE) coated fused silica capillaries were pre-treated with a silanising agent to ensure that the monolithic frit would be well anchored to the walls⁷.

After this pre-treatment procedure was completed, the monolithic frits were synthesised within the capillary mold using UV light initiated in-situ polymerisation, following a similar procedure similar to that described by Abele et al⁸. Butyl methacrylate (BuMA) and ethylene glycoldimethacrylate (EDMA) were chosen as the monomer and cross-linker, respectively, as they do not exhibit any ion-exchange properties and so will not interact with the sample metal ions. Therefore, any metal-ion binding behaviour will be due to the SP-functionalised beads and not the monolithic retaining frit.

For the frit synthesis, a solution of total volume of 200 μL was made up, consisting of 48 μL BuMA, 32 μL EDMA and 120 μL of decanol as the porogenic solvent*. Approximately 0.77 mg of DAP was added to initiate the polymerisation. The mixture was sonicated to dissolve the initiator, purged to remove dissolved oxygen and finally filled into pre-treated PTFE coated capillaries by capillary action. Using rubber septa as a photo-mask a length of capillary 3-5 mm long was exposed to UV light from a 255 nm LED (forward current = 20 mA) to initiate the in-situ polymerisation. The LED was placed perpendicular to the capillary at a distance of 1 mm and the polymerisation allowed to proceed for 1 h. After this time, the light source was turned off and the capillary flushed with methanol using a LC-10 AD HPLC pump, in order to remove any non-reacted components of the polymerisation mixture. The resulting polymeric monolith typically has a pore size of around 1-2 μm , which efficiently retains the 5 μm diameter Si(10)SP beads during the packing process, while still presenting a relatively low back pressure.

For the packing stage, a slurry of the packing beads was made up using a small amount of ethanol. A length of polytetrafluoroethylene tubing was filled with the slurry and connected between the outlet to the HPLC pump and the capillary containing the monolithic frit. The pump was turned on to allow the eluent to flow at $10\mu\text{l min}^{-1}$ (this was reduced if the back pressure exceeded around 10 MPa). In short the eluent simply pushes the beads from the tubing into the capillary column to produce the packed capillary column. When ca. 1 cm of the capillary length was packed with beads, the loop was removed and the capillary column reattached directly to the pump. Methanol was then flushed through for 30 minutes, as this gives a tighter packing of the beads and therefore reduces the likelihood of voids forming.

*Porogen = solvent which allows the formation of a polymeric monolith with a porous structure.

5.2.3 Experimental set-up for continuous flow reflectance measurements on Si(10)SP beads packed capillary

The previously described capillary holder for reflectance measurement (**Chapter 2**) consists of a probe case in which the reflectance fiber can be inserted. The optical fibre is held effectively in place by its tight fit to the specially designed upper part of the holder. The lower part has a narrow hole of 0.5 mm diameter in the middle and extrusions at each side of the hole for securing the attachment to the probe case. When the two parts are attached together the capillary can simply be inserted by threading it in the orifice of the capillary case, while the optical fiber is positioned perpendicularly to the capillary at a fixed distance. The reflectance optic fiber has two components: one is connected to the detector system and the other is responsible for light irradiation of the capillary.

When the capillary is connected to a peristaltic pump, continuous flow reflectance measurement can be performed, with a real time reflectance monitoring at the capillary surface while different solutions are pumped (**figure 5.1**).

When spiropyran functionalised microbeads Si(10)SP are packed inside the capillary using a monolithic frit, the state of the photochromic compounds immobilised on the surface can be monitored by real time reflectance measurements and the switching between the SP and MC forms can be monitored by alternatively irradiating the capillary with the UV and visible light sources connected to the fiber.

Simultaneously different solutions can be flushed inside the capillary, and in the presence of metal ions, complex formation can be detected when the beads are in the Si(10)SP form.

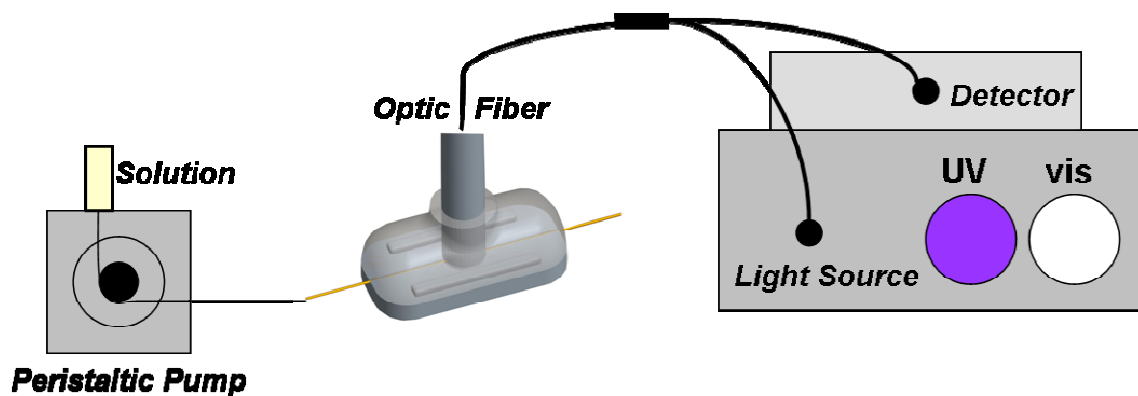


Figure 5.1: Scheme of the experimental set up. From the left: peristaltic pump with a solution reservoir, connected to the capillary positioned inside the holder (middle), in which is inserted, perpendicularly to the capillary, the fiber optic. The optic probe presents two exits, one to the detector, the other to the light two sources, a deuterium lamp emitting in the UV region, and an halogen lamp emitting in the visible region, that can be separately controlled.

The binding and release of metal ions by the packed capillary was evaluated according to the following procedure:

- Flush the capillary with the desired solution for 30 min at a flow rate of 0.5 ml/hour.
- Irradiate with the halogen lamp (visible light) for 3 min to promote MC→SP switching (ensures the beads are predominantly in the inactive SP form).
- Turn the halogen lamp off.
- Record the visible spectrum by turning on the halogen lamp for 1 s.
- Irradiate with the deuterium lamp (UV-light) for 3 min to promote SP→MC switching (ensures the beads are predominantly in the active MC form which can bind metal ions).
- Turn the deuterium lamp off.
- Record the visible spectrum by turning on the halogen lamp for 1 s.

This procedure was repeated in the presence of five different solutions, pure ethanol, 10^{-3}M , $5 \times 10^{-4}\text{M}$, 10^{-4}M Zn^{2+} and 10^{-3}M Ca^{2+} , all as ethanolic solutions, washing the capillary for 30 minutes with pure ethanol between each ion sample solution to ensure there is no carryover.

5.3 Results and discussion

5.3.1 Reflectance measurements on Si(10)SP beads packed capillary

The use of the photo-initiated polymeric frit to form the packed capillary is much more convenient than the conventional approach, which typically involves using pre-formed silica frits which are held in position with large stainless steel ferrules. In contrast, using the in-situ photopolymerised frits⁶ means that these ferrules are not needed, which facilitates the positioning of external detectors such as non-contact conductivity, or (as in this case) reflectance spectroscopy, as the capillary can be simply inserted through the purposely designed holder and the reflectance spectra from the packed capillary column recorded.

Despite the fact that the area under illumination is small (ca. 100 μm , the main spectral features and associated colour changes can be clearly distinguished, although the quality of the spectral data decreases sharply below about 450 nm as reported from supplier (figure 5.2).

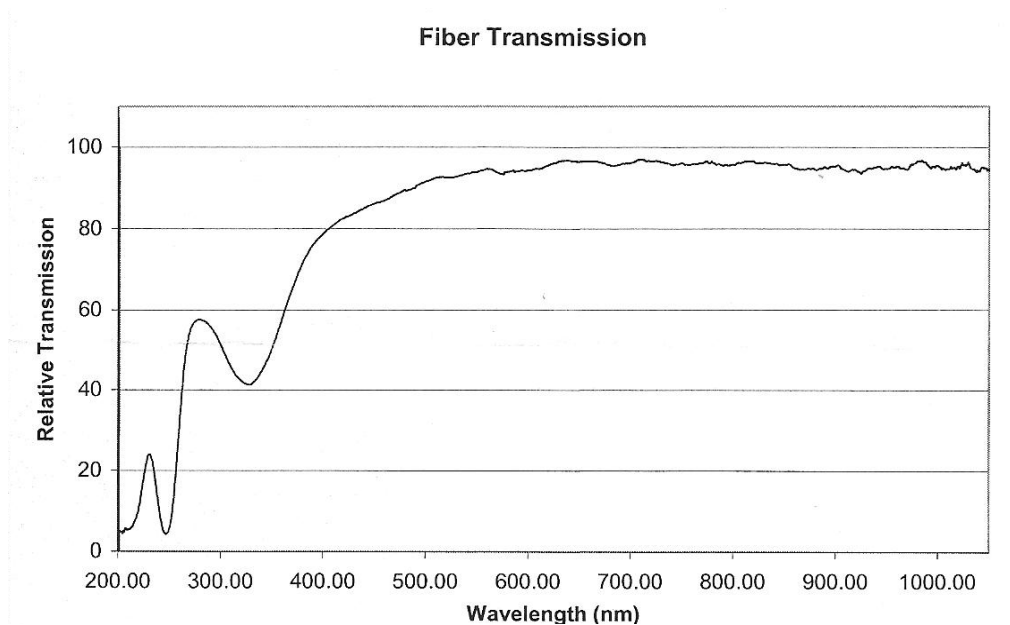


Figure 5.2: Graph showing the inherent optic fiber transmission (from Ocean Optic Inc.). The light transmission signal is maximum from 500 nm and 1000 nm and start to significantly decreasing below 450 nm, reaching its minimum values below 250 nm.

When the reflectance measurements are carried out on the capillary the signal generated by the MC on the Si(10)SP beads has a relative reflectance intensity of 2% (**figure 5.4**) at 560 nm. The signal is pretty low when compared to the peak generated by the PS(15)SP beads on the vial (**Chapter 3**) which is around 50%.

The generation of a considerably lower signal means that when measuring reflectance of the MC-Cu²⁺ complex ($\lambda_{\text{max}} = 440 \text{ nm}$) on the silica bead surface, the instrumental error becomes significant and the signal cannot be distinguished from the noise, as the instrumental detection limit significantly decreases below 450 nm. For this reason the formation of the MC-Cu²⁺ cannot be efficiently detected, but it possible to record the formation of the MC-Zn²⁺ complex, whose signal is centred at 525 nm.

5.3.2 Optical properties of the on Si(10)SP beads packed capillary

Exposure of the Si(10)SP to the deuterium lamp for 3 minutes in the presence of ethanol mobile phase leads to a clear change in colour, indicating that effective SP \rightarrow MC switching has occurred (**figure 5.3**). The recorded reflectance spectra (**Figure 5.4 A**) confirms that the colour change is due to an increase in absorbance centred around 560 nm, which is characteristic for the presence of the active MC form¹. Subsequent exposure of the packed capillary to the halogen lamp for 3 minutes reverses this process and the beads revert to the inactive SP form.

The obtained reflectance spectra were converted using the Kubelka-Munk equation, but the resulting graph (**figure 5.4 B**) doesn't show any significant improvement in terms of base line and peak shape, so that in order to highlight the spectral differences between the different forms, the relative reflectance data were obtained by subtraction of the SP reflectance spectra to the MC one (**figure 5.4 below**) so that the absorbance increase around 560 nm, associated with the MC form, is more clearly visible.:

$$R_{\text{REL}} = \% R_{\text{SP}} - \% R_{\text{MC}} \quad [5.1]$$

where R_{REL} is the relative reflectance, $\%R_{\text{SP}}$ is the percentage reflectance of the SP form and $\%R_{\text{MC}}$ is the is the percentage reflectance of the MC form.

The same equation can be applied to any recorded reflectance spectra obtaining a relative reflectance spectra to the SP form:

$$R_{\text{REL}} = \% R_{\text{SP}} - \% R \quad [5.2]$$

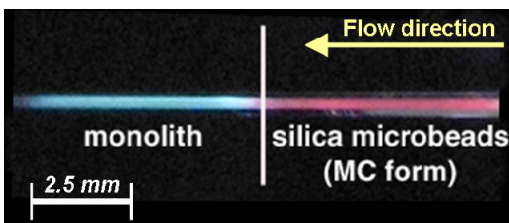


Figure 5.3: Picture of the packed capillary under UV light irradiation: the microbeads side (Si(10)SP) can be clearly distinguished by the characteristic purple MC from the polymeric monolith, which acts as a retaining frit to facilitate bead packing and flushing without any leakage and beads loss.

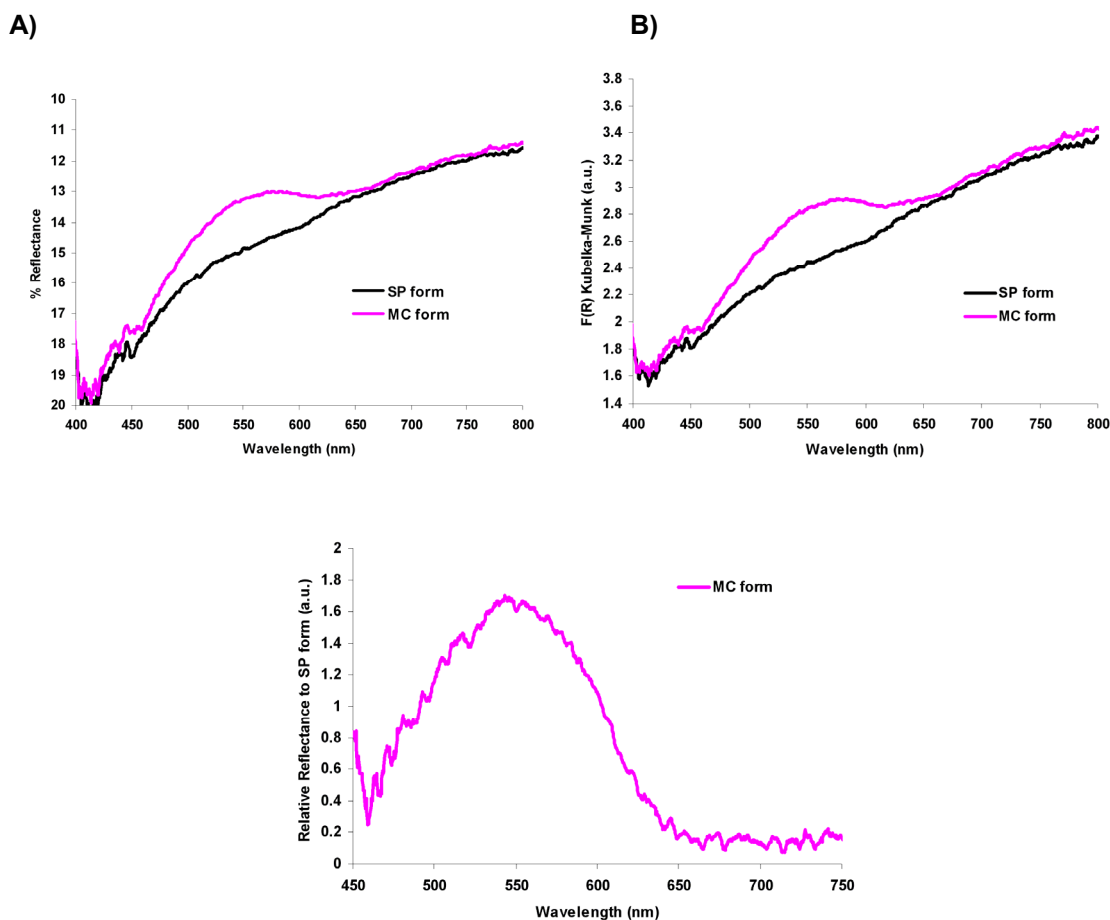


Figure 5.4: (Above, **A**) Reflectance spectra changes accompanying exposure of the packed capillary to a deuterium source for 3 minutes. (Above, **B**) Graph showing the conversion of the same reflectance spectra using the Kubelka-Munk equation. The characteristic increase in absorbance associated with the MC form is centred around 560 nm confirming that the colour change is due to SP→MC switching. (Below) MC reflectance graph obtained by subtraction

from the SP spectra. The absorbance increase around 560 nm, associated with the MC form, is more clearly visible.

In order to evaluate the effect of metal ions on the beads, 10^{-3} M ethanol solutions containing Zn^{2+} and Ca^{2+} , respectively, were sequentially pumped into the capillary for 30 min using the procedure described above. In the presence of the SP form, under white light irradiation (using tungsten lamp), no spectral change of the SP form is observed (**figure 5.5**). Following that, the beads were activated ($\text{SP} \rightarrow \text{MC}$) by illumination with the deuterium lamp for 3 minutes and the reflectance spectra obtained. The results show that in the presence of Zn^{2+} 10^{-3} M, the MC spectrum changes dramatically, with a large decrease of the 560 nm band being clearly evident, along with the appearance of a new band centred around 520 nm (**figure 5.6**), which is consistent with the formation of the MC- Zn^{2+} complex. In contrast, in the presence of 10^{-3} M Ca^{2+} , no spectral changes are evident (**figure 5.7**). When the capillary is subsequently exposed for 3 minutes to white light using the tungsten lamp, the beads return to the colourless SP form, and the Zn^{2+} guest is expelled into the mobile phase.

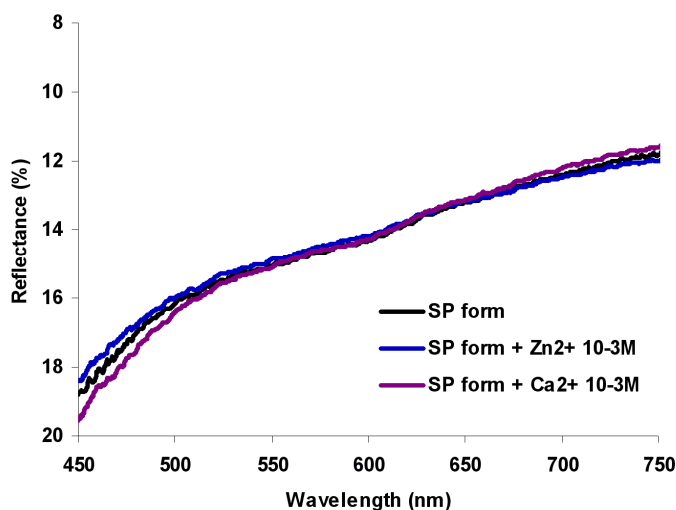


Figure 5.5: (Above) Effect of 10^{-3} M Zn^{2+} and Ca^{2+} ions on the reflectance spectrum of the SP forms. No spectral change of the SP form is observed when 10^{-3} M Zn^{2+} or Ca^{2+} is flushed into the column.

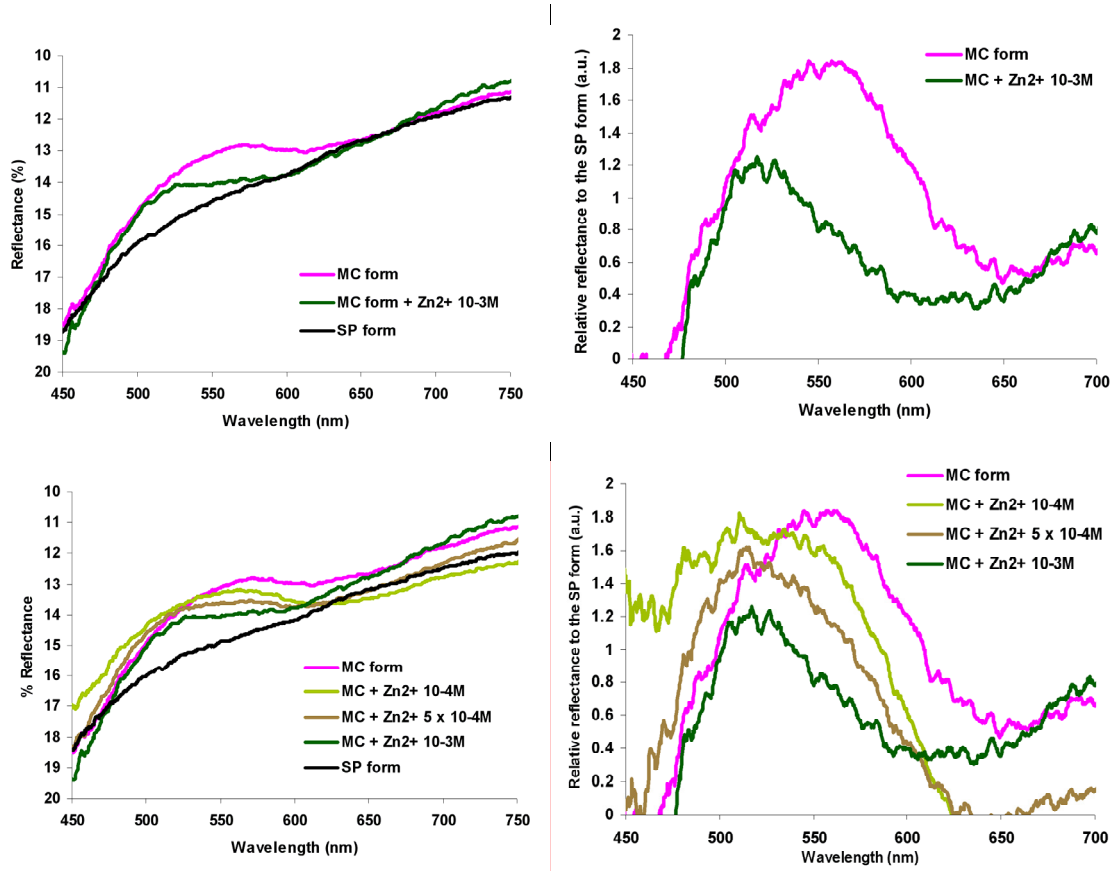


Figure 5.6: (Above) Effect of 10^{-3} M Zn^{2+} ions on the reflectance spectrum of the MC and SP forms. While a significant decrease in the 560 nm band and a new band around 520 nm is associated with the MC- Zn^{2+} complex, no spectral change of the SP form is observed when 10^{-3} M Zn^{2+} is flushed into the column.

(Below) Effects of different Zn^{2+} ion concentrations in the capillary in the presence of the MC form. From the initial MC reflectance spectrum (reflectance graphs obtained by subtraction from the SP spectra) a significant decrease in the 560 nm band of the MC form is evident and a new band associated with the MC- Zn^{2+} complex gradually appears, as the concentration increases, centred around 520 nm.

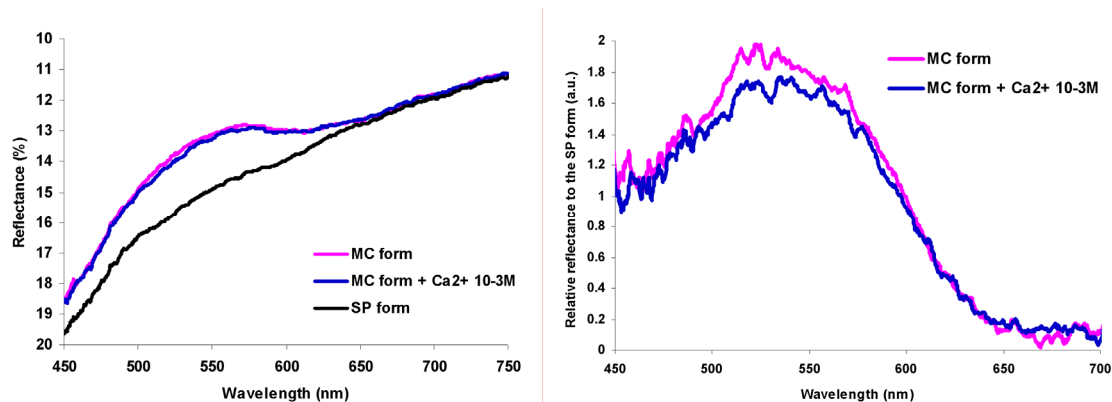


Figure 5.7: Effect of 10^{-3}M Ca^{2+} ions in the capillary on the reflectance spectrum compared to the initial MC reflectance spectrum (reflectance graphs obtained by subtraction from the SP spectra). In contrast to Fig. 5, no significant effect is observed.

Experiments carried out using different Zn^{2+} concentrations show how the decrease of the 560nm band of the MC form and the increase of the new band associated with the MC- Zn^{2+} complex around 520 nm complex are dependent on the ion concentration (**figure 5.6**). Increasing Zn^{2+} concentration (from 10^{-4}M to 10^{-3}M) cause a gradual decrease of the 560 nm MC band and the formation of the new MC- Zn^{2+} band around 520 nm.

These results suggest that the capillary column packed with SP-labelled microbeads can selectively retain certain ions under photonic control. When the beads are in the SP-form, there is no retention behaviour and metal ions pass through the column. However, upon exposure to UV light, the beads switch to the active MC-form, which is indicated by the development of the purple colour, and characteristic absorbance band at 560 nm. In this activated form, the beads will retain certain metal ions such as Zn^{2+} , further spectral and colour changes occurring that are associated with the formation of MC- M^{2+} complexes – in the case of Zn^{2+} , the 560 nm band decreases in intensity and a new band appears at 520 nm. In contrast, Ca^{2+} ions produce no discernable colour change, and the absorbance spectrum is essentially unaffected.

INPUTS		$\frac{R_{REL} \text{ 560 nm}}{R_{REL} \text{ 520 nm}}$
SP + Me ²⁺ (Ca ²⁺ or Zn ²⁺) =	SP	→ ≈ 1
SP + ⚡ (UV light) =	MC	→ > 1
SP + ⚡ (UV light) + Ca ²⁺ =	MC	→ > 1
SP + ⚡ (UV light) + Zn ²⁺ =	MC-Zn ²⁺ complex	→ < 1
$MC_2-Zn^{2+}(10^{-3}M) < MC_2-Zn^{2+}(5 \times 10^{-4}M) < MC_2-Zn^{2+}(10^{-4}M) < 1$		$\frac{R_{REL} \text{ 560 nm}}{R_{REL} \text{ 520 nm}}$
PHOTODEGRADATION: MC band decreases		→ ≈ 1

Table 5.1: Effects of different input variables (light exposure and different metal ions) on the packed beads capillary system. Under UV light irradiation, the SP converts to the MC form and the ratio between the relative reflectance values ($R_{REL} = \%R_{SP} - \%R$) at 560 nm and 520 nm is > 1. The same it's happening when no binding event is occurring, in the presence of Ca²⁺, where the MC spectrum remain unchanged and the ratio between the relative reflectance value at 560 nm and 520 nm is still > 1. On the contrary in the presence of Zn²⁺, due to the formation of the MC-Zn²⁺ complex, the ratio between the relative reflectance value at 560 nm and 520 nm inverts and becomes < 1, decreasing as the Zn²⁺ increases. Finally when photodegradation is occurring, the MC visible absorption band decreases, producing a decrease of the relative reflectance ratio which approaches ≈ 1 when the degradation is complete.

Analysing the relative reflectance spectra of the obtained data, the packed beads capillary behave as a sort of logic gates in which the inputs signal are UV light and metal ions and the output is the ratio between the relative reflectance values (**equation [5.2]**) at 560 nm (MC form) and the one at 520 nm (MC-Zn²⁺ complex) (**table 5.1**).

In the presence of SP form, when metal ion such as Zn²⁺ or Ca²⁺ are injected, no reflectance spectral change is observed (**figure 5.5**) and the ratio $R_{REL} 560 \text{ nm} / R_{REL} 520 \text{ nm}$ is ≈ 1 . If the SP form is exposed to UV light, the MC form appears and the ratio $R_{REL} 560 \text{ nm} / R_{REL} 520 \text{ nm}$ becomes >1 .

When the SP form is exposed to UV light and Ca²⁺ ions, the reflectance spectra of the MC form remain unchanged (**figure 5.7**) and so is the ratio $R_{REL} 560 \text{ nm} / R_{REL} 520 \text{ nm}$ which is still >1 .

On the contrary if the SP form is exposed to UV light and to Zn²⁺ ions, the reflectance spectra of the MC form shifts to lower wavelengths (**figure 5.6**), due to complex formation and the ratio $R_{REL} 560 \text{ nm} / R_{REL} 520 \text{ nm}$ reverts and becomes < 1 .

Adding to this, as the Zn²⁺ ions concentration increases, the ratio $R_{REL} 560 \text{ nm} / R_{REL} 520 \text{ nm}$ decreases, giving an indication of the concentration of the complex.

Furthmore, photobleaching can be easily distinguished from complexation, as when photodegradation is occurring, the MC spectra decreases in intensity and the $R_{REL} 560 \text{ nm} / R_{REL} 520 \text{ nm} \approx 1$.

The bead column can therefore be present in three different states which show characteristic colours and reflectance spectra, under the action of UV light and Zn²⁺ ions. These spectral changes laid the basis for a potential novel “monomolecular” logic gate based on multistate photochromic spiropyran within a flow-system.

5.4 INCORPORATION OF SPIROPYRAN MONOLITH ON MICROCHIP FOR PHOTO-CONTROLLED ELECTRO-OSMOTIC FLOW (EOF)

5.4.1 Experimental: Materials and instruments

Acryl ester of (1',3',3' trimethyl-6-hydroxyspiro(2H-1)benzopyran-2, 2'-indole) (Acrylated SP, **Figure 5.8**) was synthesised in our group by Dr. Robert Byrne according to the previously reported procedure⁴.

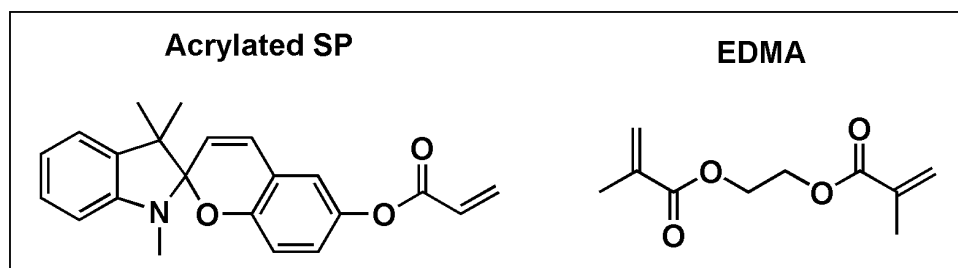


Figure 5.8: Structure of Acrylated SP monomer and EDMA cross linker used for the spiropyran acrylate based monolith synthesis.

Brilliant Green and Ethylene glycol dimethacrylate (EDMA), azobisisobutyronitrile (AIBN) were purchased from Sigma Aldrich (Ireland).

Hydrochloric acid 32%, density 1.16 g/cm³ was purchased from Fisher Scientific. Standard solutions of HCl 10⁻² M and 10⁻³ M were prepared by serial dilutions of 10⁻¹ M HCl stock solution.

Polymicro transparent polytetrafluoro ethylene (PTFE) coated fused silica capillaries (100 μm internal diameter, 375 μm external diameter) were purchased from Composite Metal Services Ltd (United Kingdom).

Capillary flushing after the monolith synthesis was performed using an HPLC pump (Shimadzu, Japan). Subsequent HCl flushing was performed using a capillary fitting syringe. For the purposely designed capillary holder for reflectance measurement see **Experimental** section 5.2.1.

Monolith pictures were taken using a A SVM-340 Synchronised Video Microscope (LabSmith, USA) while a S-3000N VP-SEM (Hitachi, Japan) was used for SEM imaging. In order to generate the different voltages and record the correspondent

current values, a 0-30 kV high voltage power supply from Unimicro Technologies (Pleasanton, CA, USA) was used.

Inert acrylic Pressure sensitive adhesive (PSA) polyester film was purchased from ARcare 8890, Adhesives Research Ltd., Limerick, Ireland).

Channels in the microfluidic chip were first designed using CAD 3D Excalibur software (Progressive Software Corporation, USA) and then fabricated by direct micro-milling (Datron 3D M6, Datron Technology Ltd., Milton Keynes, UK).

Poly ether ether ketone (PEEK) tubing was obtained from Upchurch Scientific (Oak Harbour, WA, USA). PMMA sheets were obtained from Goodfellow Cambridge Limited (UK). 5 min epoxy glue was purchased from Bondloc, Worcestershire, UK.

10 μ l glass syringe was purchased from SGE Australia Pty. Ltd. and filled with 10⁻³ M aqueous solution of brilliant green in order to optimise the meniscus visualisation.

White LEDs (430-760 nm) were purchased from Roithner Laser Technik, Austria.

5.4.2 Synthesis of spiropyran acrylate monolith

Prior to monolith polymerisation, the walls of the polytetrafluoroethylene (PTFE) coated fused silica capillaries were pre-treated with a silanising agent to ensure that the monolithic frit would be well anchored to the walls⁷.

Acrylated SP and EDMA were chosen as the monomer and cross-linker, respectively.

For the synthesis, a solution was made up consisting of 40 μ L EDMA, 6 mg of acrylated SP, 0.9 mg of AIBN and 60 μ L of butanol as the porogenic solvent. The mixture was sonicated to dissolve the monomer and the initiator, purged to remove dissolved oxygen and finally filled into pre-treated PTFE coated capillaries by capillary action. Using rubber septa to close both ends a length of capillary 10 cm long was placed on a water bath at 60° for 90 minutes to initiate the in-situ polymerisation.

Then the capillary was flushed with methanol using a LC-10 AD HPLC pump, in order to remove any non-reacted components of the polymerisation mixture.

The resulting polymer exhibits a macro-porous structure in which the globule size is around 1 μ m (**figure 5.9**).

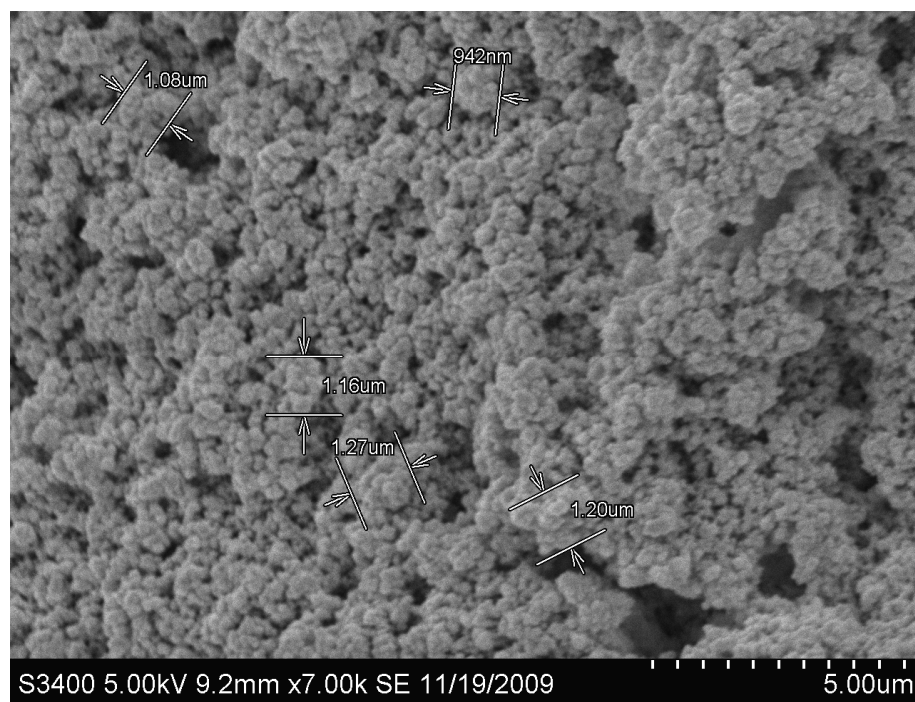
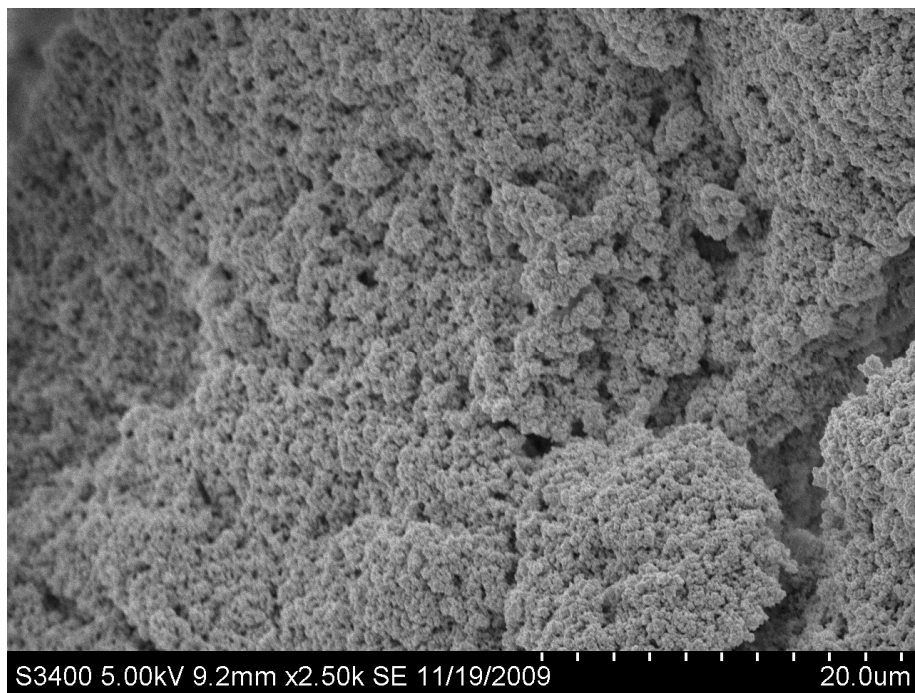


Figure 5.9: SEM images of a cross section of the polymeric porous structure of the SP acrylate monolith.

5.4.3 Investigation of the photochromic behaviour in the presence of HCl

The spiropyran monolith was flushed with HCl solutions at three different concentrations: 10^{-1} M, 10^{-2} M and 10^{-3} M. Reflectance spectra of the monolith in the presence of HCl were recorded using the capillary reflectance set-up (**figure 5.10**) described on **Chapter 2**. Then the effect of white light on protonation was evaluated by measuring the reflectance spectra every 20 s for 400 s while exposing the monolith flushed with HCl to white light irradiation.

The measurements were carried out by keeping the monolith inside the capillary holder and leaving the halogen light (irradiation range 400 nm – 1700 nm) of the optic fiber turned on while the reflectance recording probe of the fiber was automatically capturing the reflectance spectra processed by the ocean optic software at fixed time intervals (**figure 5.11**).

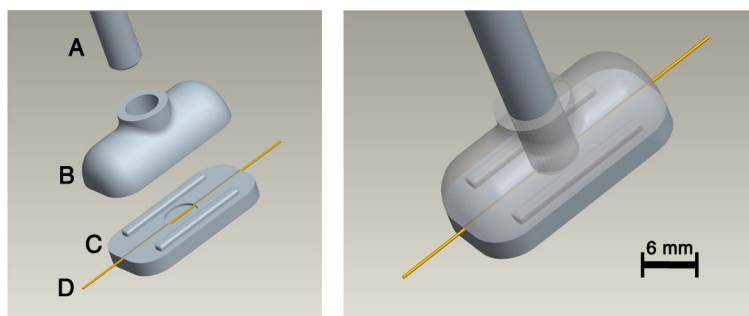


Figure 5.10: In-house designed set up for reflectance measurements on capillaries. (A) Reflectance optic fibre. (B) Lid presenting an aperture for the insertion of the optic fibre. (C) Base where a 500 μm deep open channel allows the insertion of the capillary for reflectance measurement. (D) Capillary (100 μm inner diameter) bearing the spiropyran monolith.

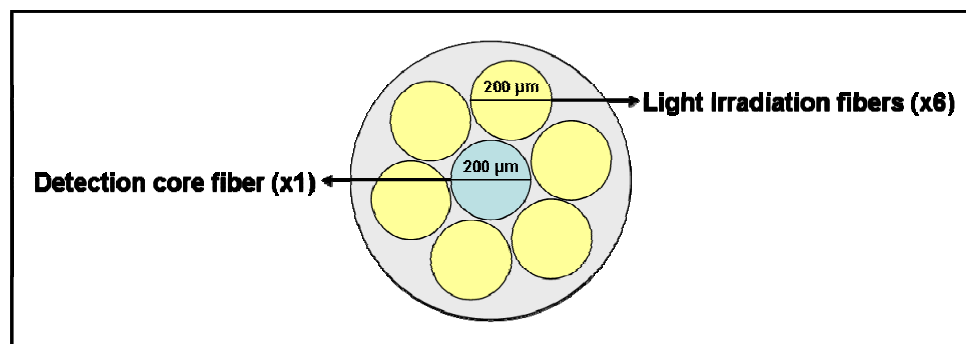


Figure 5.11: Reflectance fiber cross section: it includes 6 external illumination fibers of 200 μm diameter (which is turned on to emit halogen light from 400 nm to 1700 nm) and a central recording fiber of 200 μm diameter.

5.4.4 Microfluidic chip for electro-osmotic flow measurement

The spiropyran modified monolith was incorporated into a microfluidic chip for electro-osmotic flow measurement (EOF) measurement.

A microfluidic chip 16 mm x 19 mm x 5 mm with channels 8 mm x 0.4 mm x 0.4 mm was fabricated by direct micro-milling as described by Nie et al⁹ (**figure 5.12**). After milling, the PMMA sheets were washed thoroughly with ethanol to remove traces of dust and excess PMMA, then the 8 mm long spiropyran monoliths were encased in the channels. The capillaries were held in place in the channels using a drop of 5 min epoxy glu before the channels were covered with a layer of pressure sensitive adhesive, (PSA) and a second, unmilled sheet of PMMA 0.5 mm thick. The so-assembled microchip was then placed in a vice for several minutes to ensure sealing of all components. 1 cm lengths PEEK (poly ether ether ketone) tubing were used as inlet and outlet tubing and were connected to 1.5 ml plastic vials which served as solvent reservoirs.

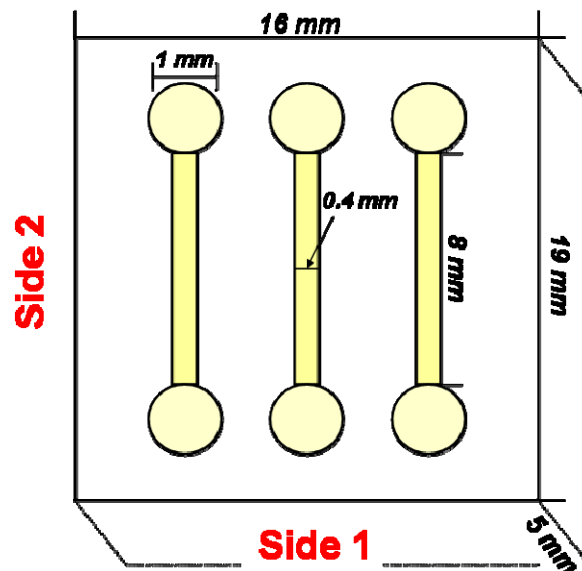


Figure 5.12: Schematic representation of the top view of the microfluidic chip which incorporates three 8 mm long monoliths for EOF measurement.

5.5 Results and discussion

5.5.1 Photochromic properties of spiropyran acrylate monolith

In the literature, the synthesis of a photoresponsive poly(N-isopropylacrylamide) hydrogel in which a N-isopropylacrylamide is polymerised together with acrylated SP monomer has been reported. This polymer can be switched in the presence of acid between a positively charged form, due to the presence of a protonated MC form (MC-H⁺) and a non-charged SP form by irradiation with white light. The formation of MC-H⁺ leads to gel expansion in an acidic environment and shrinkage when white light is applied due to proton release as a consequence of re-formation of the SP form, which leads to release of the protons from the gel surface⁴.

In the same way the spiropyran acrylate monolith can be switched in the presence of acid between a MC-H⁺ form and a non-charged SP form (**figure 5.13**).

It is known that the presence of a nitro-group in ortho or para position of the benzopyran ring results in decrease in the energy which is necessary for the charge transfer transition which accompanies MC formation¹⁰. In the case of the acrylated SP, the absence of the nitro group in the benzopyran ring doesn't allow stable conversion to the MC form under UV-light irradiation and the presence of MC form cannot be detected.

However, in an acidic environment, the protonation of the phenolate group is highly favoured, and the formation of the MC-H⁺ form is spontaneously induced.

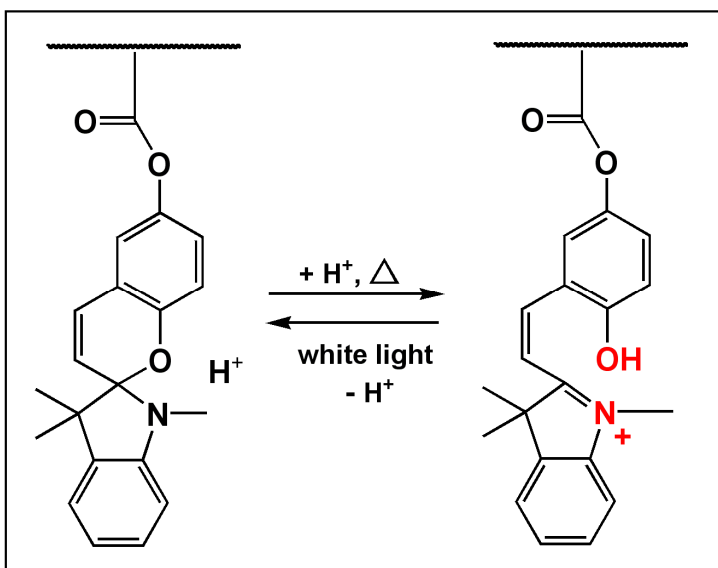


Figure 5.13: Acrylated SP switching in an acidic environment between the MC-H⁺ form (right) and the SP form (left) when irradiated with direct white light.

In the presence of acid, the spiropyran monolith converts to the MC-H⁺ form which has a characteristic yellow colour. Irradiation with white light caused protons to be released due to reversion to the SP form (**figure 5.14**).

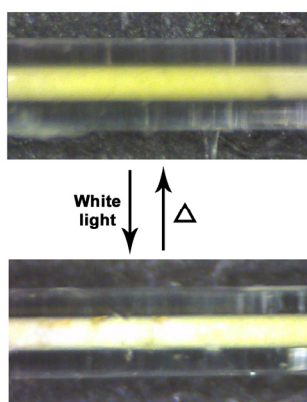


Figure 5.14: Picture of the spiropyran acrylate monolith flushed with HCl 10⁻² M switched between the MC-H⁺ form, in the absence of light exposure and the SP form when irradiated with direct white light.

In the presence of increasing concentration aqueous HCl, (from 10^{-1} M to 10^{-3} M), the monolith turned yellow as a consequence of the MC-H⁺ formation. Reflectance spectra were recorded using the the reflectance set-up for capillaries, and a band around 450 nm was clearly evident, as the acid concentration was raised (**figure 5.15**).

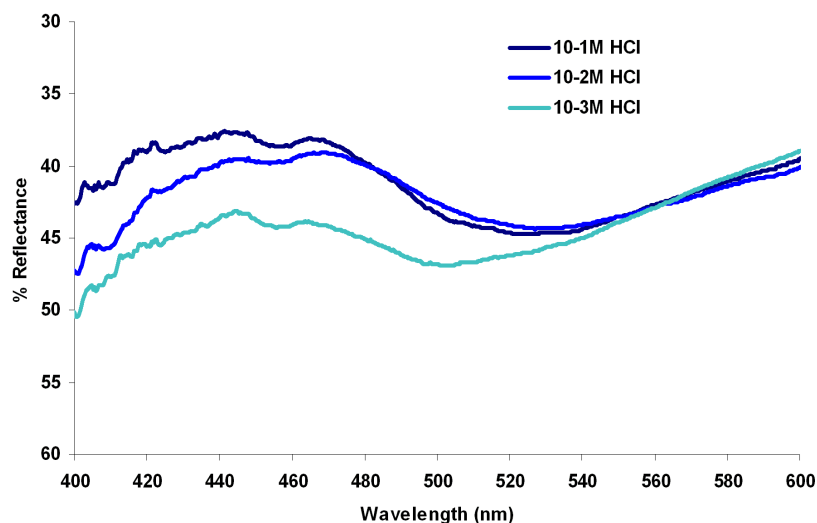


Figure 5.15: Reflectance spectra of the spiropyran acrylate monolith exposed to three different concentrations of HCl: 10^{-1} M, 10^{-2} M and 10^{-3} M. In the increasing acidic environment, a band can be recorded centred around 450 nm which corresponds to the yellow colouration of MC-H⁺.

The conversion of the MC-H⁺ form to the SP form was evaluated in terms of ring closing kinetics under white light irradiation. The spiropyran monolith, encased in the capillary holder for reflectance measurements (**figure 5.10**), was flushed with HCl in order to obtain the MC-H⁺ form and subsequently using the reflectance fiber probe, reflectance spectra were acquired at fixed 20 s time intervals, while the monolith was exposed to halogen light (400-1700 nm) (**figure 5.11**).

Under white light exposure, the 450 nm band associated with the MC-H⁺, decreases with exposure time due to the release of protons and regeneration of the SP form (**figure 5.16**).

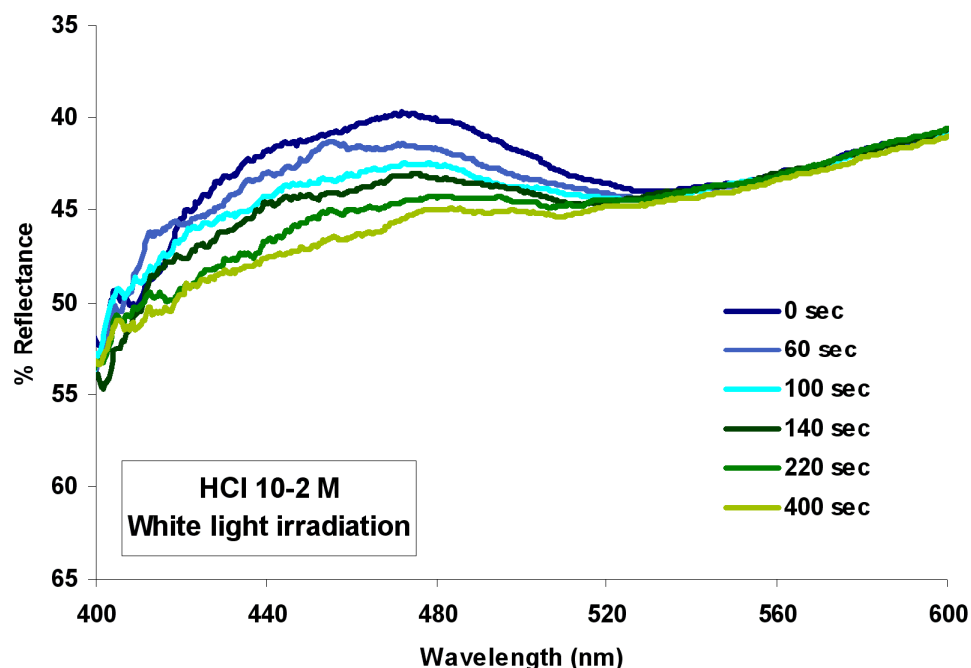


Figure 5.16: Reflectance spectra of the spiropyran acrylate monolith flushed with HCl 10^{-2} M exposed to white light. The 450 nm band decreases as a consequence of increasing light exposure.

Three spiropyran monoliths (3 cm length) were flushed with 3 different HCl solutions (10^{-1} M, 10^{-2} M, 10^{-3} M) and the ring closing kinetics evaluated as a function of the acid concentration while under exposure to white light.

The first order rate constants were estimated by fitting the normalised reflectance values at 450 nm (**figure 5.17**) using Microsoft Excel Solver^{11,12} using the following equation (**table 5.2**):

$$y = ae^{k_R t} + b \quad [5.3]$$

where y is the normalised absorbance value at the MC- H^+ absorbance λ_{max} , a is the pre-exponential factor, k_R is the rate constant and b is the asymptotic value.

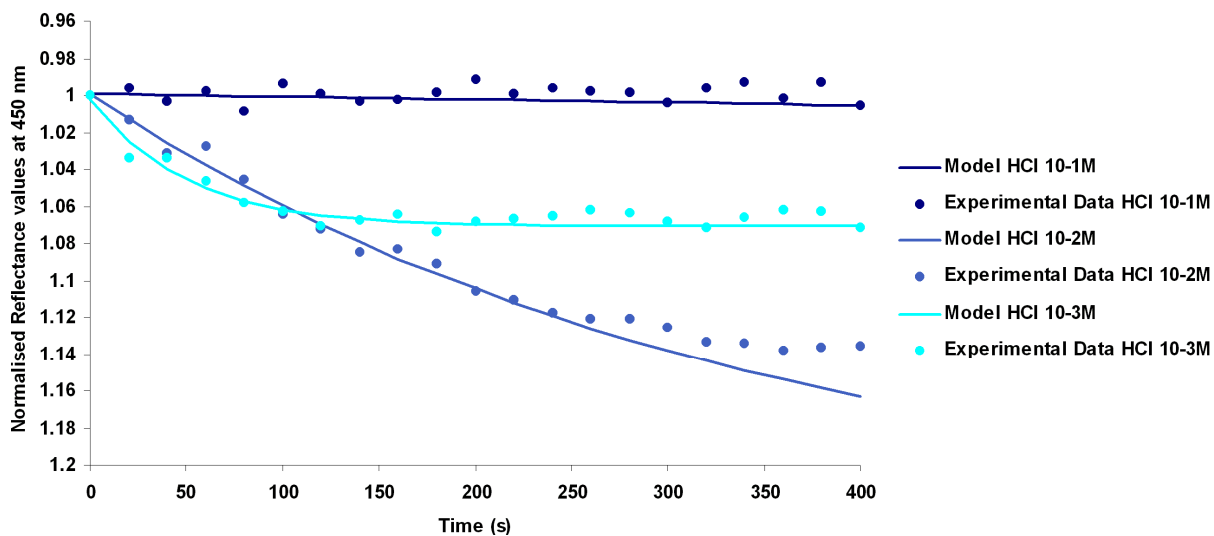


Figure 5.17: First order kinetic curves obtained plotting time against the normalised reflectance values at the MC-H^+ λ_{max} in each solvent (10^{-1} M, 10^{-2} M and 10^{-3} M).

For the kinetic curve of the monolith in HCl 10^{-2} M, the accuracy of the model sharply decreases in the final part and additional experimental points would be probably required for a more accurate determination of the rate constant. However, as our main focus is to determine in which solution is occurring the more rapid and complete switching between the MC-H^+ form and the SP form, this analysis of the trend of the experimental points is satisfactory.

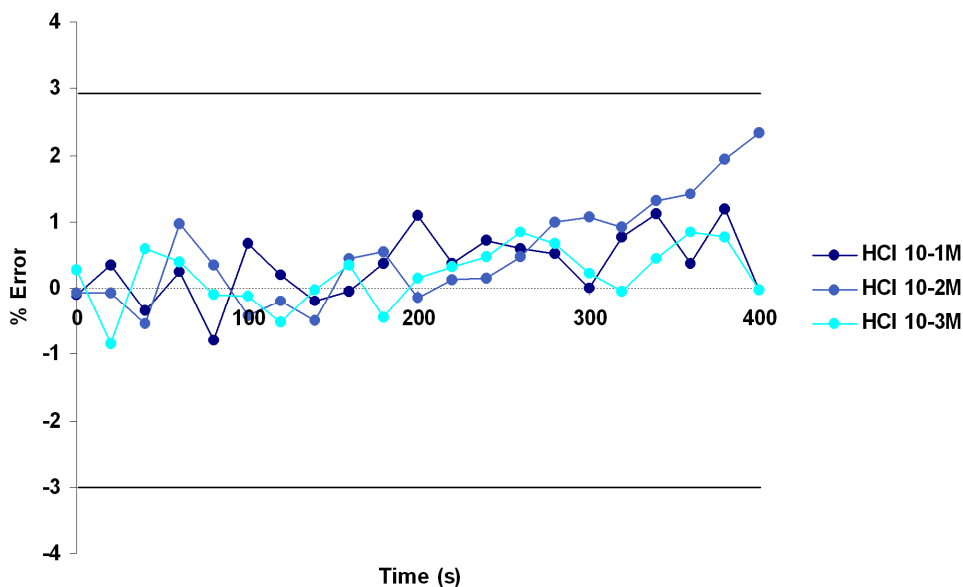


Figure 5.18: The residual error calculated between the data and the model does not exceed 3% at any point in the fitted curves shown in **figure 5.17**.

SOLVENT	$k_R(\text{s}^{-1})$	Ratio to HCl 10^{-1} M
HCl 10^{-1} M	0.25×10^{-3}	1
HCl 10^{-2} M	0.29×10^{-2}	11.6
HCl 10^{-3} M	0.20×10^{-1}	80

Table 5.2: Rate constants for the ring closing equilibrium obtained from the best-fit curves of the normalised reflectance values in **figure 5.17**, recorded at 450 nm in HCl concentration. The rate constants are compared in terms of ratio to ring closing kinetic in HCl 10^{-1} M.

The obtained values for the ring closing rate constant are clearly related to the acid concentration used to generate the MC-H⁺ form on the monolith.

The higher the HCl concentration, the longer the time required for the re-conversion to the SP form. The ring closing kinetic is almost 12 times faster for the monolith flushed with HCl 10^{-2} M when compared to the one where HCl 10^{-1} M was injected and 80 times faster in the presence of HCl 10^{-3} M.

Looking at the first order kinetic curves shown in **figure 5.17**, the steady state (which corresponds to the re-formation of the SP form) of the reflectance value at 450 nm in the presence of 10^{-3} M HCl is reached after only 100 s. In the case of HCl 10^{-2} M injection, the steady state is achieved after 300 s, while for the HCl 10^{-1} M flushing the SP form is not completely re-formed even after 400 s and the reflectance values at 450 nm only slightly changed from the initial value.

A rapid and complete switching between the MC-H⁺ form and the SP form will assure a more efficient detection of changes happening in the EOF as a consequence of the molecular isomerisation and for this reason HCl 10^{-3} M was chosen as the electrolyte in order to perform EOF measurements.

5.5.2 EOF evaluation

In order to evaluate the EOF when a voltage is applied between the two ends of the monolith, a PMMA microchip was built with three 8 mm long spiropyran functionalised monoliths (**figure 5.19**) incorporated into 8 mm x 0.4 mm x 0.4 mm channels. At the two ends of each channel two tubes were placed as inlet and outlet for the HCl solution. Each tube was connected to a 1.5 ml reservoir containing 10^{-3} M HCl. The working

electrodes were then placed inside the reservoirs (**figure 5.20** and **figure 5.21**).

The spiropyran acrylate monolith was irradiated using a 3x3 square array of 9 white LEDs (430-760 nm) placed on the bottom of the chip were the thickness of the PMMA is lower and the light irradiation is more efficient.

LEDs were chosen as they are relatively low-power light sources with insignificant heating effect when compared to conventional lamps. Typically LEDs present ca. 1 mW/cm² power compared to the power of arc lamp light sources reported in most papers, which are typically 50-100 W. Despite this much lower power, LEDs have shown to effectively switch the MC ↔ SP system with minimal photobleaching¹².

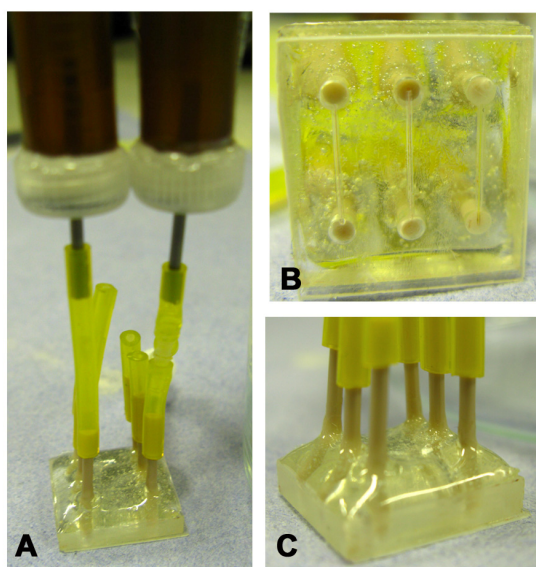


Figure 5.19: Picture showing the microchip incorporating the three spiropyran acrylate monoliths. A) Microchip connected to the reservoirs; B) bottom view of the microchip with the three spiropyran monoliths (8 mm length) are incorporated; C) side view of the microchip with the encased peek tubings.

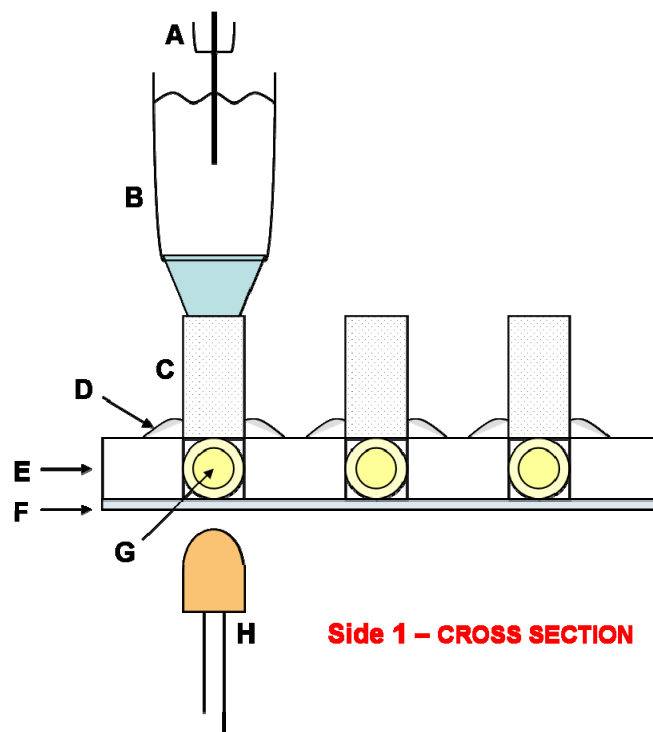


Figure 5.20: Schematic representation of the microchip side 1 cross section (see **figure 5.12**).
 A) Electrode; B) 1.5 ml 1mM HCl reservoir; C) Peek tubing; D) epoxy glue; E) PMMA sheet 5 mm thickness; F) second sheet of PMMA (0.5 mm thickness) which closes the channels and is attached to E with a layer of pressure sensitive adhesive (PSA); G) Spiropyran monolith 8 mm length; H) White LED (430-760 nm) part of a 3x3 square array of 9 LEDs.

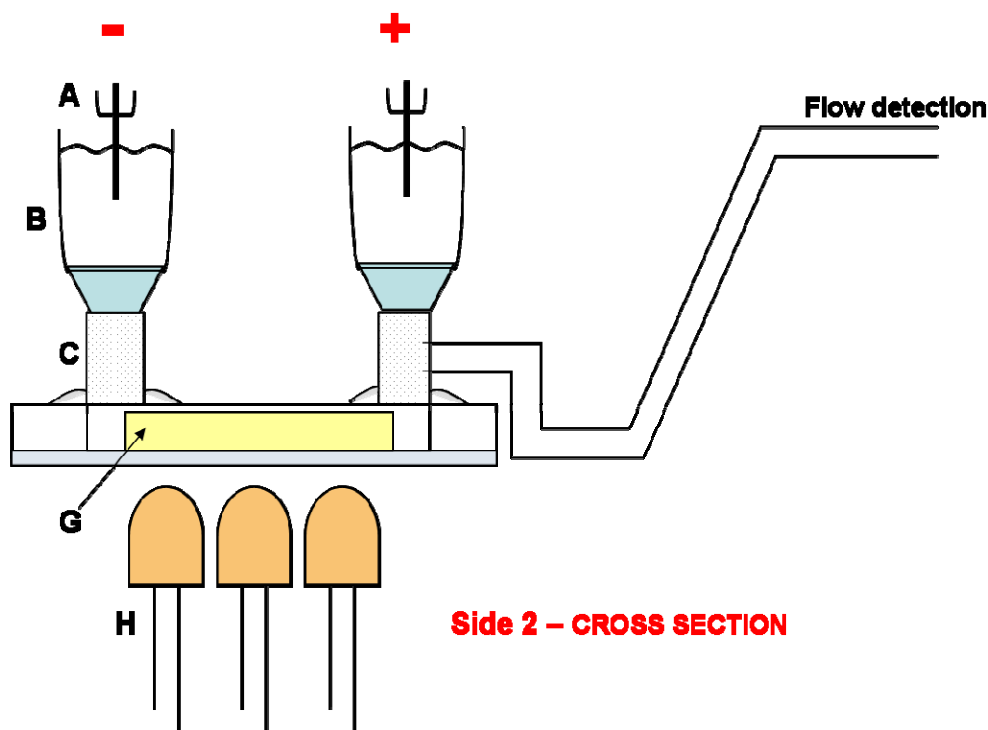


Figure 5.21: Schematic representation of the microchip side 2 cross section (see **figure 5.12**).
 A) Electrode; B) 1.5 ml 1 mM HCl reservoir; C) Peek tubing; G) Spiropyran monolith 8 mm length; H) White LEDs (430-760 nm) as part of a 3x3 square array of 9 LEDs.

The EOF effect was measured in the presence of the SP form, which was induced by irradiating the monoliths with white LEDs and in the presence of the MC-H⁺ form, generated spontaneously under acidic conditions (10⁻³ M HCl).

The EOF measurement was carried out according to the procedure reported by Fu-Qiang Nie and al.^{9,13}. The microchip was filled with 10⁻³ M HCl solution and connected through a capillary outlet to a 10µl glass syringe filled with an aqueous solution of 10⁻³ M brilliant green leaving an air gap between the HCl liquid front and the front of the brilliant green solution. The flow rate was calculated by tracing the working fluid/air meniscus and timing its movement. The choice of a coloured green solution greatly enhances the visualisation of the meniscus.

The absence of a downstream load pressure was ensured by the outlet being directly open to the atmosphere and being placed at the same level of the 10⁻³ M HCl reservoirs.

Once the microchip was filled with working liquid and connected to the syringe for flow measurements, the system was left equilibrating for one hour before measurements were made in order to ensure the system was at equilibrium before a voltage was applied.

EOF is generated as a consequence of the formation of electrical double layer at the liquid solid interface. When an electric field is applied, the mobile hydrated ions in solution move in response to the electric field dragging the bulk of the solution with them (see **Figure 1.2, Chapter 1**).

In an acid environment the surface of the spiropyran monolith is positively charged because of the presence of the MC-H⁺ form which appears yellow. As a consequence there is the formation of an electrical double layer and when a voltage is applied the mobile ions move in response of the electric field dragging the bulk solution and generating EOF. In this case, as the surface is positively charged, overall the EOF moves from the anode to the cathode. If the polarity of the voltage is inverted no EOF and no current is observed.

In the presence of 10⁻³ M HCl, the monolith surface is preferentially in the MC-H⁺ form (when no white light irradiation is applied). When the voltage is applied, EOF is generated which increases proportionally to the applied voltage (**figure 5.22**) from ca. 0.8 µl/min (at 0.1 kV) to 1.6 µl/min (at 1 kV).

When the same measurement is performed while exposing the microchip to white LEDs irradiation for one hour, the EOF decreases of an average 15%, which reaches its maximum at 1 kV where it decreases of 19% (**table 5.3**).

The experiments have been repeated in triplicate and statistics shows reproducibility and a consistent decreasing of the EOF when the microchip is exposed to white light irradiation.

We can therefore conclude that the EOF (and therefore the flow rate) increases when an external voltage is applied and that under white light exposure, the flow rate is always lower than the equivalent flow rate in the dark.

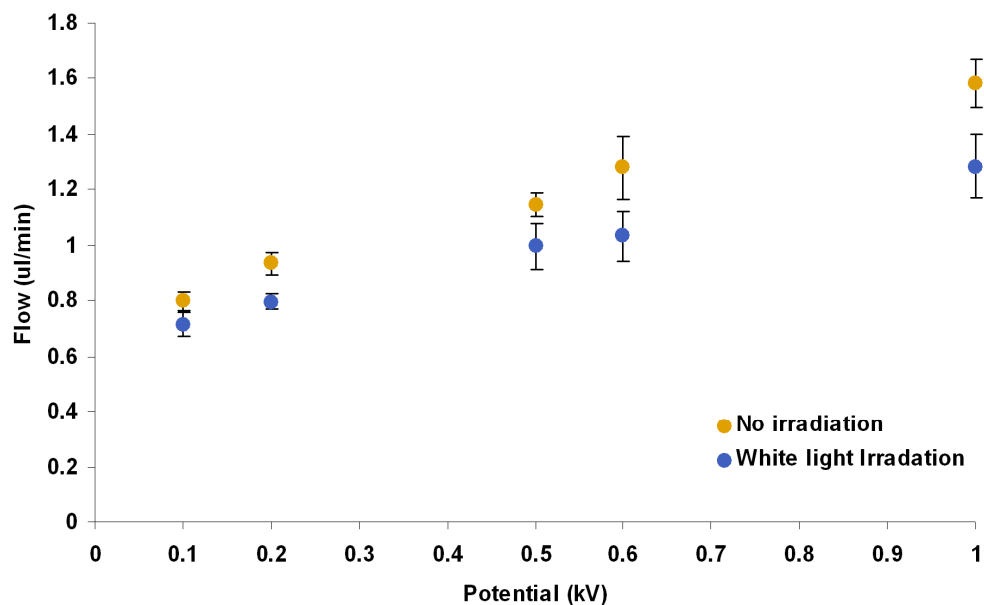


Figure 5.22: Graph showing the EOF increase as an effect of the application of an increasing potential both for the spiropyran acrylate monolith in the MC-H⁺ form (no irradiation) and for the monolith in the SP form (white light irradiation). Statistics shows that the EOF generated with or without white light irradiation is substantially different (n=3).

Applied Voltage (kV)	No Irradiation (mean flow rate value) (µl/min)	White light Irradiation (mean flow rate value) (µl/min)	EOF DECREASE (%)
0	0	0	0
0.1	0.80 (± 0.03)	0.72 (± 0.04)	10.4
0.2	0.94 (± 0.04)	0.80 (± 0.02)	14.8
0.5	1.15 (± 0.04)	0.99 (± 0.08)	13.1
0.6	1.28 (± 0.11)	1.03 (± 0.09)	19.3
1	1.60 (± 0.08)	1.28 (± 0.10)	19.0

Table 5.3: Table showing the mean flow rate values recorded when applying an increasing potential to the spiropyran functionalised monolith. The experiments were carried out exposing and not exposing the microchip to white light irradiation. On the left the % of EOF decrease when the microchip is irradiated with white light irradiation is reported.

The fact that the EOF cannot be completely suppressed is probably due to the fact that the white LEDs irradiation cannot reach homogeneously the entire thickness of the monolith, leaving the spiropran units close to the central core in the MC-H⁺ form. White light has the general effect of causing a partial re-conversion to the SP form, decreasing the amount of positive charges on the surface and so decreasing the EOF.

The current was monitored during these experiments. In the presence of both the SP form and the MC-H⁺ form the current ranges increase as the voltage is raised (**figure 5.23**). When no irradiation is applied, the MC-H⁺ form predominates, the current ranges are wider and the current values more unstable than when the SP form is predominant. This could be due to the decrease of the amount of positive charges on the surface, which probably brings a partial stabilisation of the current.

In both cases though, above 1 kV, the current becomes highly unstable and the EOF and the corresponding current could not be measured.

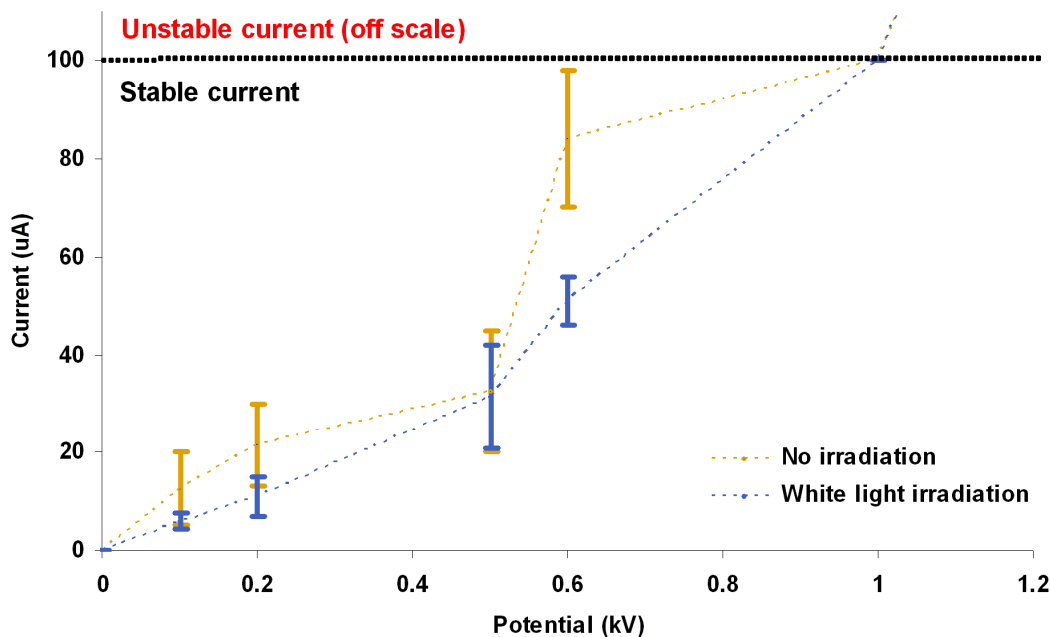


Figure 5.23: Graph showing the current increase as an effect of the application of an increasing potential both for the spiropyran acrylate monolith in the MC-H⁺ form (no irradiation) and for the monolith in the SP form (white light irradiation). Over 1 kV the current is extremely unstable.

Clearly these results show that, to some degree, the acrylate spiropyran monolith can function as a photodynamically controllable electro-osmotic pump (EOP).

While the system relies on the application of voltage to produce electroosmotic flow, the flow can then be modulated not only through increase/decrease of the voltage but simply by irradiating the column with white light which change the surface properties of the monolith, and alters the flow rate.

The synthesis of the acrylate spiropyran monolith and its characterisation in terms of EOF effect is the follow up of a recently submitted work by Walsh and al.³ In this work a styrene based monolith was synthesised by thermal polymerisation using vinyl SP (**Chapter 1**) as a monomer and divinylbenzene (DVB) as a cross-linking agent (**figure 5.24**).

In this case the SP presents a nitro group in the ortho position of the benzopyran ring and the monolith can be switched between a SP form (white light irradiation) and a MC form (UV light exposure) and the molecule is stable in both forms.

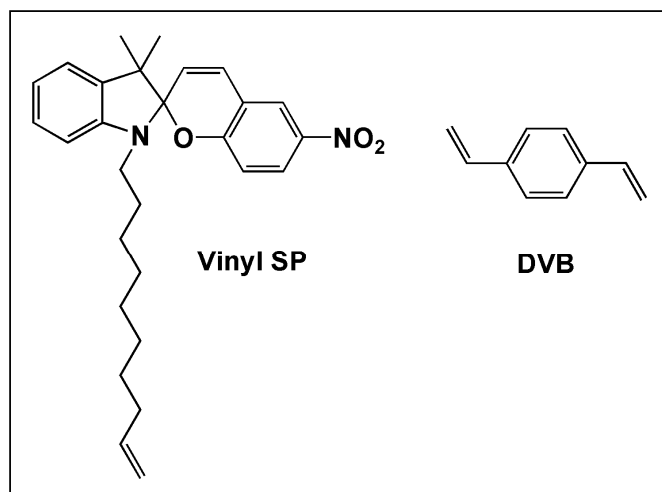


Figure 5.24: Structure of Vinyl SP monomer and DVB cross linker used for the spiropyran vinyl based monolith synthesis.

As in this work the monolith was encased on a microchip as described and the EOF measured by alternatively exposing the monolith to UV and visible light. Using 10^{-3} M HCl, EOF was produced even though the effect is of lower intensity and the recorded flows are in the nl range instead of the μ l range recorded for the acrylate spiropyran monolith.

In addition the EOF changes as a consequence of white or UV LEDs exposure can be detected only for voltages higher than 0.4 kV. From 0.5 kV to 1 kV the EOF produced from the spiropyran monomer in the two forms differs but it has been demonstrated to be higher for the SP form (60 to 150 nl min⁻¹) than for the MC (30 to 75 nl min⁻¹).

Irradiating the monolith with a white LEDs shifts the equilibrium in favour of the SP form and an increase in the EOF is observed while irradiation with UV LEDs pushes the equilibrium in favour of the MC form and the EOF is decreased by approx. 2-fold. What may be happening in this case is that because of the presence of the nitro group, the isomerisation of the merocyanine which, in this case, it is not only influenced by the light but also by the strong potential applied, is yielding different transoid isomers in which the charge is highly delocalised.

In contrast, in the SP form charges might find an affinity for the lone pair electron of the indoline nitrogen, providing localised region of charge density and thus induces a higher EOF than the MC form.

In general both the acrylate and styrene monoliths provide an example of EOPs, as they have been demonstrated to be polymeric structures which can act as electroosmotic pumps in the presence of an electrolyte and an external voltage, the flow can be modulated simply by external light irradiation.

The spiropyran functionalised acrylate monolith generates a much faster flow rate because of the stability of the MC-H⁺ form in the acid environment and the flow can be switched with the presence or the absence of white light.

5.6 Conclusions

These results suggest that we have achieved the first steps towards the creation of photoswitchable stationary phases that could be used for controlled accumulation and release of particular ions from a mixture. A column has been produced through the packing of spiropyran modified Si(10)SP microbeads in a microcapillary, using a monolithic polymer as a frit which enables a low pressure approach to be adopted. The SP-functionalised microbead column can be reversibly switched between inactive (non-ion binding) SP and active (ion-binding) MC forms using UV and visible light, enabling

certain ions to be retained and released under photonic control. The column is inherently self-indicating in terms of whether the inactive SP, active MC or ion-complexed MC-Zn²⁺ forms are present, suggesting that simple diagnostic measurements can be integrated into the system to determine how effectively it is functioning. Our group is actively collaborating with prof. Brett Paull and co-workers to further examine the behaviour of the column towards other ions using similar approaches, and apply the system to more complex sample mixtures to further characterise the interaction dynamics of the system.

In addition, an acrylate based spiropyran monolith has been synthesised and characterised in terms of photoswitchable EOF behaviour.

Under acidic conditions (10^{-3} M HCl), the spiropyran functionalised monolith surface is preferentially in the MC-H⁺ form, which can be readily converted to the SP form through exposure to white light.

When an external voltage is applied in the presence of 10^{-3} M HCl, EOF in the 0.7 μ l/min to 1.6 μ l/min range is generated. Under constant voltage, white light irradiation leads to a decrease in the EOF. Removal of the light source results in a flow increase. Clearly this spiropyran monolith can act as an electro-osmotic pump, in which the flow can be modulated through the presence or absence of light.

Furthermore it is possible to modulate the behaviour of packed micobead columns towards the binding of certain metal ions: UV-LED irradiation of the packed column turned it into an active binding state which upon complexation of the guest species produced a colour/spectral signal (i.e. the system is entirely self-indicating). White light irradiation was then used to reconvert the column to the original inactive form. This system can therefore be regarded as a photodynamic separation platform. The presence of spiropyran functionalised beads in a separation column allows the possibility of having two photodynamically interconvertible surfaces with different physical and chemical properties to be inter-switched.

Furthermore, accompanying colour/spectral changes mean that the system is inherently self-indicating.

Clearly adaptive materials with such properties have the potential to produce materials whose surface properties can be radically altered using an external stimulus (in this case

light). This in turn can dramatically change fundamental behaviour related to host-guest binding and effect electro-osmotic forces.

This ability to profoundly alter such properties using light has very significant implications for science as it could lead to the development of a control over column retention or liquid flow using light.

5.7 References

- (1) Scarmagnani, S.; Walsh, Z.; Paull, B.; Macka, M.; Diamond, D. *International Journal of Nanomanufacturing* **2010**, *5*, 38-52.
- (2) Scarmagnani, S.; Walsh, Z.; Slater, C.; Alhashimy, N.; Paull, B.; Macka, M.; Diamond, D. *Journal of Materials Chemistry* **2008**, *18*, 5063-5071.
- (3) Walsh, Z.; Scarmagnani, S.; Benito-Lopez, F.; Abele, S.; Nie, F.-Q.; Byrne, R.; Slater, C.; Diamond, D.; Paull, B.; Macka, M. *Analytica Chimica Acta* **2009**, *Submitted*.
- (4) Szilagyi, A.; Sumaru, K.; Sugiura, S.; Takagi, T.; Shinbo, T.; Zrinyi, M.; Kanamori, T. *Chemistry of Materials* **2007**, *19*, 2730-2732.
- (5) Rosario, R.; Gust, D.; Hayes, M.; Jahnke, F.; Springer, J.; Garcia, A. A. *Langmuir* **2002**, *18*, 8062-8069.
- (6) Chen, J. R.; Dulay, M. T.; Zare, R. N.; Svec, F.; Peters, E. *Anal. Chem.* **2000**, *72*, 1224-1227.
- (7) Okanda, F. M.; El Rassi, Z. *Electrophoresis* **2006**, *27*, 1020-1030.
- (8) Abele, S., Nie, F.-Q., Foret, F., Paull, B., Macka, M. *The Analyst* **2008**, *133*, 864-866.
- (9) Nie, F.-Q.; Macka, M.; Paull, B. *Lab on a Chip* **2007**, *7*, 1597-1599.

- (10) Kholmanskii, A. S.; Dyumaev, K. M. *Russian Chemical Reviews* **1987**, 136-151.
- (11) Diamond, D.; Hanratty, V. C. A. *Spreadsheet Applications in Chemistry using Microsoft Excel*; Wiley: New York, 1997.
- (12) Stitzel, S.; Byrne, R.; Diamond, D. *Journal of Materials Science* **2006**, *41*, 5841-5844.
- (13) Nie, F.-Q.; Macka, M.; Barron, L.; Connolly, D.; Kent, N.; Paull, B. *The Analyst* **2007**, *132*, 417-424.

**CONCLUSIONS
AND
FUTURE WORK**

6.1 Conclusions

Organic photochromic compounds such as spiropyrans are particularly interesting targets for the development of new approaches to sensing since they offer new routes to multi-functional materials that take advantage of their photo-reversible inter-conversion between thermodynamically stable states which have dramatically different physical and chemical properties. From our perspective, the ability to photo-control metal ion-binding, molecular recognition and polarity/charge is of particular interest.

Preliminary spectroscopic solution studies were successfully carried out in order to characterise SP-1 behaviour in different solvents and in the presence of different metal ions. The resulting data are a good reference for the evaluation of the behaviour of spiropyran derivative immobilised on different substrates, and in particular guideline for the characterisation of metal complex behaviour of the immobilised MC form.

In addition, simple approaches to perform reflectance measurements for the characterisation of the UV-vis spectroscopic properties of spiropyran immobilised on high light scattering microparticles, such as polystyrene were developed.

SPCOOH derivatives were immobilised on silica and polystyrene microbeads using different immobilisation strategies. These functionalised polymeric beads could reversibly switched between the colourless inactive spiropyran (SP) and highly coloured (purple) active merocyanine (MC) forms using low power light sources, such as light emitting diodes (LEDs). A UV-LED (375 nm) was used for the SP to MC conversion, and a white LED (430-760 nm) for the reverse MC to SP conversion. Interactions of the modified spiropyran microbeads with different metal ions were also evaluated. The investigations into the metal-ion binding behaviour of the functionalised microbeads showed that the immobilised MC undergoes strong spectroscopical and visual changes in the presence of Cu^{2+} while other metal ions, like Ca^{2+} do not cause any appreciable effect. On the other hand, functionalised silica microbeads exhibit particular sensitivity to both Cu^{2+} and Zn^{2+} , with different accompanying spectroscopic and visual responses in terms of colour change of the MC form for each ion type.

Furthermore, these interactions are photo-reversible, and the bead surface can be easily restored to the SP form by exposure to white light, with simultaneous release of the accumulated metal ions.

Subsequent exposure to UV light restores the MC active form and the binding/release cycle can be performed again.

Because of the accompanying colour/spectroscopic changes, the system is inherently self-indicating in terms of whether the active MC or inactive SP forms are present, and whether particular ions are bound to the MC form.

In principle, therefore, these functionalised beads could form the basis of a photoswitchable stationary phase to be incorporated into microscale devices for metal ion binding, detection and release: irradiation of the stationary phase with UV-LEDs causes retention of the guest ions due to the presence of the MC form, while subsequent exposure to white light LEDs causes release of guest species into the mobile phase and regeneration of the SP form.

Micro-fluidic chips are particularly attractive in biological and life sciences for analytical purposes because they provide a convenient small platform for rapid analysis and detection^{1,2}. The small characteristic dimensions of micro-fluidic devices results in extremely small internal volumes and high surface-to-volume ratios, which leads to improved heat and mass transfer rates. At this small scale, surface effects become dominant in fluid handling and surface properties play a crucial role in chip-based applications³.

In addition, continuous flow operation facilitates real-time measurements and consequently fast analysis protocols.

The incorporation of spiropyran derivatives or spiro-modified substrates into flow micro-systems opens up intriguing possibilities for creating stationary phases whose binding behaviour can be externally modulated using light.

We investigated this idea using two approaches.

In one case, the stationary phases were generated by packing spiropyran functionalised silica microbeads into polytetrafluoroethylene (PTFE)-coated fused silica capillaries (100 μm inner diameter) using a polymeric frit synthesised in-situ and preliminary results showing selective metal ion binding behaviour were demonstrated using reflectance spectroscopy.

In the second case, spiropyran compounds were used to create new monolithic stationary phases, using both a spiropyran monomer to synthesise a SP-derivatised monolith directly in silica capillaries, and a post-synthesis functionalisation strategy wherein the

spiropyran is immobilised on the monolith's inner surface after it has been formed in-situ.

These SP-modified stationary phases showed light-induced reversible ion-binding capability (functionalised microbeads) and light-modulated electroosmotic nanoflow (spiropyran monoliths).

When packed into a capillary, the MC functionalised microbeads surface exhibit an absorption band around 560 nm which shifts to 520 nm when Zn^{2+} is flushed through the column. The accumulated metal ions can be released by white LED irradiation, which restores the MC form back to the SP form. Then the cycle can be repeated again when the column is exposed to UV LED and the active MC form reappears. When other metal such as Ca^{2+} are injected no spectra shift is observed.

This packed column is an example of a photodynamic system that can be used for the retention, detection and release of metal ions passing through the capillary. Using light it is possible to modulate the column behaviour towards the binding of metal ions: irradiation of the column with UV LED turned the column into the active binding state which upon complexation of the guest species produces a spectral signal (i.e. the system is entirely self-indicating). Light irradiation was then used to reconvert to the original inactive SP form. This system can therefore be regarded as a photodynamic separation platform.

The last application discussed is the use of spiropyran to create monoliths which can generate a photoswitchable electro-osmotic flow (EOF). An acrylated spiropyran monomer was copolymerised with ethylene dimethacrylate cross-linker to synthesise a photochromic monolithic stationary phase, which in the presence of an acid can switch between an thermodynamically stable protonated MC form and a SP form as a consequence of white light irradiation. This polymeric phase was encased in a microfluidic chip and the effect of light on the electro-osmotic flow rate investigated. The spiropyran modified acrylate monolith produces different flow rates depending on the spiropyran state, and the flow can be simply controlled by alternating cycles of white light irradiation and non-irradiation. This effect is due to formation/disruption of the electrical double layer required for the efficient EOF generation.

The system was compared to a previously reported styrene based monolith encased on a similar microchip in which the electro-osmotic pump behaviour can be modulated using alternatively UV and white LEDs. It was found that the generated flow is lower when compared to the spiropyran functionalised acrylate based monolith and in which the UV light exposure seems to decrease the flow, probably because of the stabilisation of the molecule in a non-charged quinonic isomer.

The spiropyran functionalised acrylate based monolith can be regarded as a step towards the creation of a stationary phase in which the flow rate can be controlled using light.

6.2 Future work

Considering the photoswitchable ion retention and release behaviour of the spiropyran functionalised microbeads, improvement on the material side could probably be made in terms of sensing capability of our photoswitchable substrates in two directions:

- 1) increasing the concentration of photochromic sensing unit and
- 2) developing new and more selective spiropyran derivatives with increasing photostability.

In later 2008, a very interesting paper was published by Locklin and co-workers about colorimetric ion-sensors based on spiropyran polymeric brushes.

The research work involved the synthesis of polymer brushes in which a spiropyran methacrylate monomer is co-polymerised with methyl methacrylate from an activated silicon wafer⁴ (**figure 6.1**).

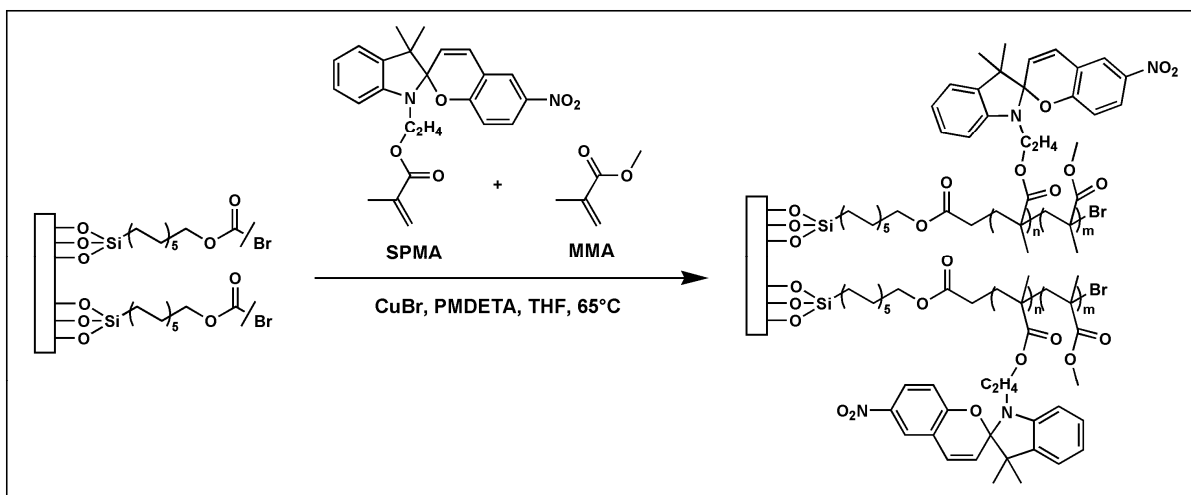


Figure 6.1: Surface initiated copolymerization of a spiropyran methacrylate derivative (SPMA) and methyl methacrylate (MMA).

Through a polymer grafting approach, the number of functional groups on the film surface can be highly enhanced through a three-dimensional arrangement of the polymer chains. The brush-like structured polymer allows a high density of active molecules in relatively small area, which increases the response of the sensing surface.

The copolymer is transparent to visible light but when irradiated with UV light, the SP converts to the MC form, which is characterised by an intense absorption band centred around 584 nm. When a series of metal ions is added to the film in the presence of the MC form, the different complexes can be easily discriminated with naked eye for most metal ions, as shown in the graph **figure 6.2**.

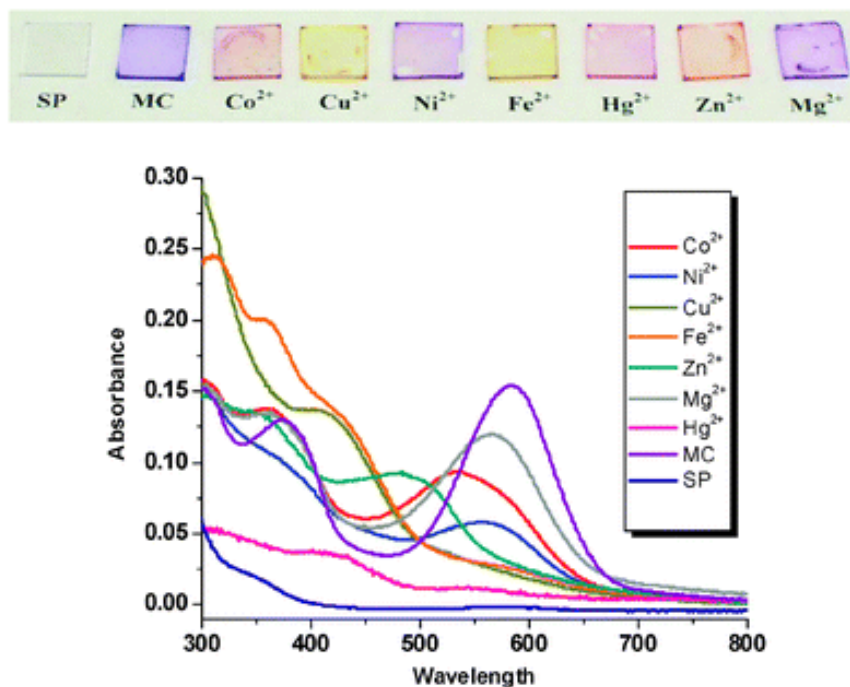


Figure 6.2: UV-Vis of polymer brush in the presence of different metal ions. Figure from Fries, K.; Samanta, S.; Orski, S.; Locklin, J. *Chemical Communications* **2008**, 6288-6290.

The metal complexation reaction is reversible and when the film is irradiated with visible light, the metal is expelled and the SP form is restored.

Polymer brushes have been demonstrated to be a very interesting approach to material functionalisation using spiropyran, though the dramatic increase in the photochromic unit density and rapid and reversible response to analytes.

On the other hand new spiropyran derivatives have been reported which show increasing selectivity towards certain metals, through for example the addition of crown ethers^{5,6} or by the synthesis of bis-spiropyran derivatives, which shows particular selectivity towards alkaline earth metal such as Ca²⁺ and Mg²⁺, which is eight times higher than the one achieved with a single spiropyran unit⁷.

In parallel, interest is increasing in the study of spironaphtooxazines, due to their ionochromism^{8,9} and improved photostability properties¹⁰.

A novel series of spirooxazine derivatives containing nitrogen heterocycles has been synthesized and analysed in various solutions and in polymers matrices; The new photochromic derivatives incorporated on PMMA films exhibit a remarkable fatigue

resistance: after 280 cycles performed by alternatively irradiating the film with UV and white light, the absorbance remained at 99.3% of its initial value, dropping only to 96.6% after 1000 cycles¹⁰.

The advances in the development of new methods for material functionalisation together with the synthesis of more selective and more thermally stable photochromic derivatives will lead to more efficient photoswitchable sensing platforms and will increase their practical uses in large scale minituarised sensor and analytical devices.

Switchable or adaptive surfaces that can be externally controlled at a molecular level, introduce the idea of a calibration-less sensing system as, through light irradiation, the state of the sensing unit can be changed between an active or passive state, enabling or inhibiting the capability to bind target molecules. Light-driven photoswitching is an important way to induce conformational transitions of molecules that can be used as a base for generating surfaces with switchable properties.

Research is also ongoing into the use of spirocyan functionalised beads and monoliths encased in capillary microsystem to achieve off-column detection of different species by switching the spirocyan with different LEDs between the SP and the MC form.

It was also found that organic species such as caffeine elute with different retention times depending on the spirocyan state as a consequence of non-specific affinity interactions. It is consequently possible to have two different light-switchable phases on the same separation column which can be used on demand¹¹.

For other guests, such as transition metal ions, the ion accumulation and release as a consequence of UV and white LEDs exposure of the columns has been achieved for Cu^{2+} , but further investigations are required as reproducibility has turned out to be a consistent issue¹¹. The evidence suggests a highly homogeneous means of irradiation with white light is required to allow a more complete and fast release of the ions along the entire length of the column.

As it has been demonstrated in this work, other properties such as polarity, wettability and surface charge can be photo-modulated, enlarging the number of possible application to switchable fluid movement, reversible swelling actuation and photoregulation of the electrochemical activity.

This ability to photo-regulate the electro-osmotic flow rate of a microcapillary system opens up the intriguing possibility of having a microfluidic system where liquid movement can be externally manipulated without the need for complex micro-valves. Improvements need to be made in terms of broadening the range of the operating flow, so that by the modulation of the light irradiation it would be possible to decrease the flow to a minimum value close to zero, and also increase it on demand towards the $\mu\text{l}/\text{min}^{-1}$ flow rate range.

At the moment using the acrylate based monolith, it is possible to generate a relatively high flow rate, from $0.8 \mu\text{l min}^{-1}$ to $1.6 \mu\text{l min}^{-1}$, which can be decreased using white light of an average 15%. However the flow cannot be totally “switched off”. With the styrene based spiropyran monolith, the flow generated is much slower, in the $\text{nl}/\text{min}^{-1}$ range and decreased almost to zero at a very low voltage, but it can't reach the relatively high flow rate in the $\mu\text{l min}^{-1}$ range obtained with the acrylate monolith mentioned above.

Further investigations are required using either new spiropyran monomers or perhaps copolymerised mixtures of these or other monolithic structures.

On the other hand, the existing systems, such as the acrylated spiropyran monolith, could be improved, for example, through a re-design of the microfluidic chip which would allow a more homogeneous light irradiation of the whole capillary, not as the present irradiation only at the bottom side of the chip.

The interesting aspect of all these works is how control of events at a molecular level, control bulk properties and the behaviour of platform using only external light irradiation from low power light sources such as LEDs.

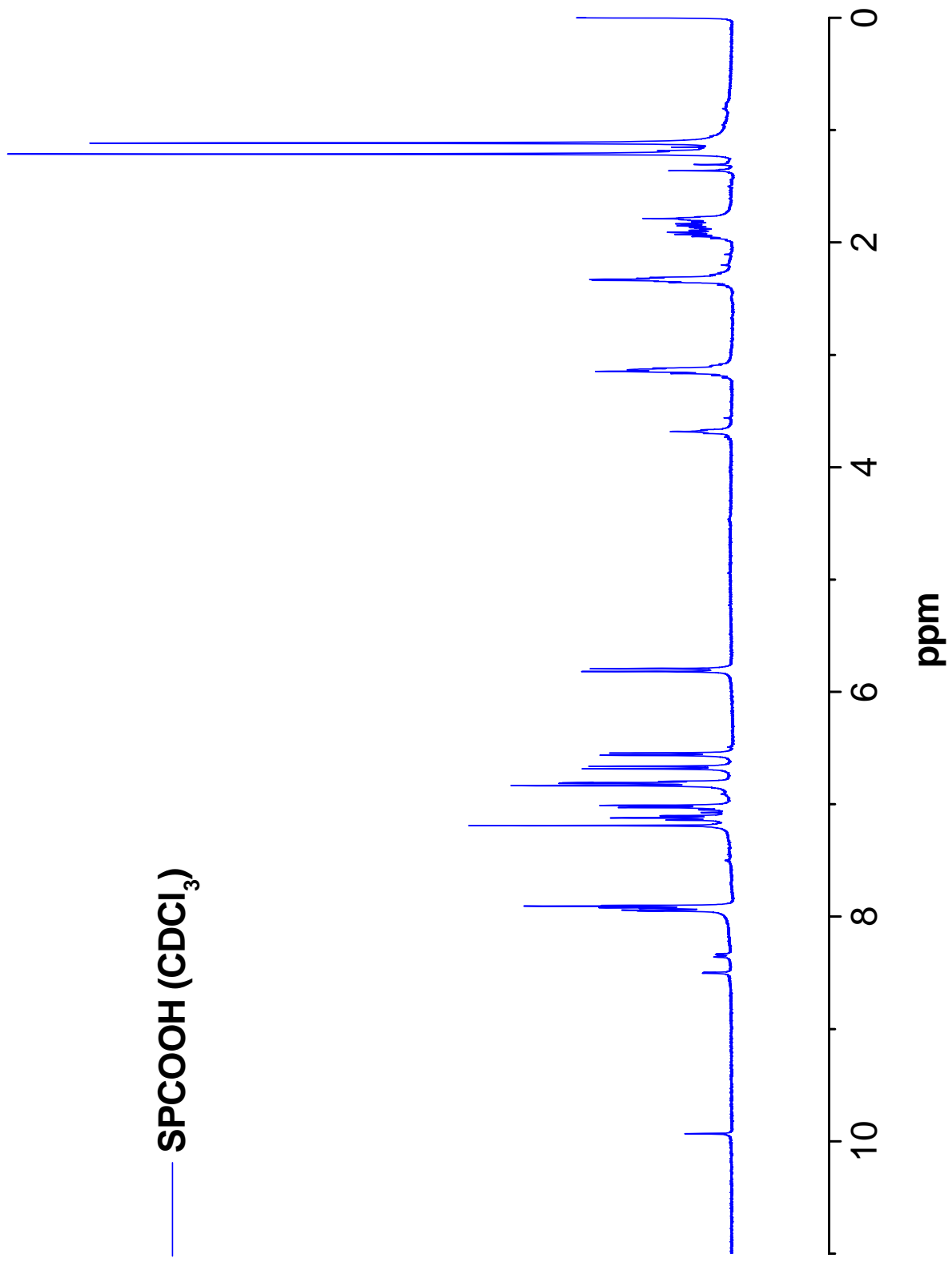
Further investigations and consistent improvements of the spiropyran based adaptive materials is undoubtedly necessary to capitalise on these effects, but the potential applications of these materials in microfluidics and other areas for a large number of potential applications are extremely promising.

6.3 References

- (1) West, J.; Becker, M.; Tombrink, S.; Manz, A. *Analytical Chemistry* **2008**, *80*, 4403-4419.
- (2) Yager, P.; Edwards, T.; Fu, E.; Helton, K.; Nelson, K.; Tam, M. R.; Weigl, B. H. *Nature* **2006**, *442*, 412-418.
- (3) Kim, S. H.; Yang, Y.; Kim, M.; Nam, S. W.; Lee, K. M.; Lee, N. Y.; Kim, Y. S.; Park, S. *Advanced Functional Materials* **2007**, *17*, 3493-3498.
- (4) Fries, K.; Samanta, S.; Orski, S.; Locklin, J. *Chemical Communications* **2008**, 6288-6290.
- (5) Sakamoto, H.; Takagaki, H.; Nakamura, M.; Kimura, K. *Analytical Chemistry* **2005**, *77*, 1999-2006.
- (6) Khairutdinov, R. F.; Hurst, J. K. *Langmuir* **2004**, *20*, 1781-1785.
- (7) Filley, J.; Ibrahim, M. A.; Nimlos, M. R.; Watt, A. S.; Blake, D. M. *Journal of Photochemistry and Photobiology A: Chemistry* **1998**, *117*, 193-198.
- (8) Minkovska, S.; Fedieva, M.; Jeliaskova, B.; Deligeorgiev, T. *Polyhedron* **2004**, *23*, 3147-3153.
- (9) Chernyshev, A. V.; Voloshin, N. A.; Raskita, I. M.; Metelitsa, A. V.; Minkin, V. I. *Journal of Photochemistry and Photobiology A: Chemistry* **2006**, *184*, 289-297.
- (10) Tan, T.-f.; Chen, P.-l.; Huang, H.-m.; Meng, J.-b. *Tetrahedron* **2005**, *61*, 8192-8198.
- (11) Walsh, Z., Dublin City University, 2010.

APPENDIX

— SPCOOH (CDCl₃)



Vinyl SP (CDCl₃)

